SUPPORTED BIOMIMETIC MEMBRANES TO STUDY THE SURFACE INTERACTIONS BETWEEN CANCER EXTRACELLULAR VESICLES AND HUMAN PRIMARY STEM CELLS

A Dissertation

Presented to the Faculty of the Graduate School

of Cornell University

In Partial Fulfillment of the Requirements for the Degree of

Doctor of Philosophy

by

Johana Uribe

December 2021

SUPPORTED BIOMIMETIC MEMBRANES TO STUDY THE SURFACE INTERACTIONS BETWEEN CANCER EXTRACELLULAR VESICLES AND HUMAN PRIMARY STEM CELLS

Johana Uribe, Ph.D.

Cornell University 2021

Cancer derived extracellular vesicles (cEVs) have been recognized as important modulators of intercellular communication within the tumor microenvironment[1, 2]. Two main cEV subpopulations, microvesicles (MVs) and exosomes (EXOs), facilitate the transfer of information between cancer and non-cancer cells, which has been determined to be a major factor contributing to cancer progression[3]. For instance, previous research showed that cEVs induce proangiogenic activity and myofibroblast differentiation in adipose derived stem cells (ADSCs)[4-6], further promoting their role in metastasis[7]. However, in most of the studies, the interactions leading to malignant outcomes induced by cEVs, remained unexplored. One limitation is the lack of techniques available to distinguish surface interactions from internalization to facilitate the investigation of these specific processes[8]. Towards that end, I present two biomimetic membrane models as tools to facilitate the isolation, study, and screening of blocking strategies of surface interactions between cEVs and ADSCs. These models are hybrid supported lipid bilayers (SLBs), a common biomimetic of cell membranes, but here, I am able to incorporate native components of cEVs and ADSC membranes into these SLBs. Their planar geometry enables the use of surface specific characterization techniques and

advanced microscopy for these studies.

First, I describe an cEV- SLB (EVSB) that incorporates cEV membrane material, working as an *in vitro* model of the cEV membrane that allows focused studies of cell interactions with this surface and its chemistry, isolated from effects of cEV cargo delivery. Using this system as a cell culture platform for ADSCs, we found that surface interactions between cEVs surface and ADSCs enhance cell viability, proliferation, adhesion, spreading, and proangiogenic activity, conditions that promote oncogenic activity.

In a second embodiment of this platform, I create an ADSCs- SLB (ASB), incorporating components of ADSC membrane, as a tool to study the initial EXO-cell interaction, binding. ASB integration with multi-electrode arrays (MEAs) allows recapitulation and dual detection, optical and electrical, of EXOs binding to ADSCs in a cell-free and label-free manner. Moreover, using these two sensing modes, anti-CD29 antibody was found to reduce EXOs binding to ADSCs, demonstrating the ability of this platform for therapeutic molecule screening and the potential of antibody treatment to mitigate outcomes of EXOs-ADSCs interactions that favor cancer progression. Lastly, these biomimetic membrane platforms are the first cell-free *in vitro* platforms for the recapitulation and study of surface interactions between cEVs and human primary stem cells compatible with scale-up and multiplexing.

BIOGRAPHICAL SKETCH

Johana Uribe was born and raised in Medellin, Colombia and moved to United States in 2006. Johana obtained an Associate degree in Engineering from Bunker Hill Community College at Boston, MA in December 2012 where she was awarded with an NSF REFLECT scholarship. She joined the Bioengineering undergraduate program at University of Massachusetts at Dartmouth in January 2013 and graduated summa cum laude in May 2015. While working in her undergraduate, Johana conducted research at Worcester Polytechnic Institute to develop an *in vitro* model for dystrophic calcification of cardiac valvular interstitial cells, and at The UMass Dartmouth Center for Innovation & Entrepreneurship on the production and purification of recombinant tetracycline repressor (TetR) protein. In 2015, Johana joined a doctorate program in biomedical engineering at Cornell University where she was awarded with a Sloan Foundation Fellowship. She conducted research on microenvironmental control of metastatic cellular energy production for over a year under the supervision of Dr. Cynthia Reinhart-King where she was awarded the NSF GRFP Fellowship. After the former laboratory moved to Vanderbilt University, Johana joined the Daniel Lab in the Department of Chemical and Biomolecular Engineering in November 2016. She explored the dynamic interactions between oncogenic extracellular vesicles and adipose derived stem cells using hybrid supported lipid bilayer platforms. She used these biomimetic membrane models as platforms to isolate and monitor surface interactions and their outcomes, and to investigate possible strategies to mitigate them and the subsequent cancer progression. In her PhD work, Johana integrated several techniques and technologies such as cell culture, western blot, ELISA, immunofluorescence, epifluorescence, and confocal microscopy, TEM, FRAP, TIRF, NTA, DLS, among others. She has since accepted a research postdoctoral position at King Abdullah University of Science and Technology (KAUST).

This work is dedicated to my loving family and husband. Thank you for all of your support and love during this PhD journey, I could not have done without your unconditional faith in me.

Especialmente le dedico este trabajo de doctorado a mis papás, por todo el esfuerzo que han hecho por nosotros y porque gracias a ellos he llegado hasta este lugar, que algún día parecía solo un sueño.

ACKNOWLEDGMENTS

I could not have come to the end of my PhD without the support and guidance of many individuals. First, I would like to acknowledge the members of my committee for their support and advice. Especially, my advisor, Dr. Susan Daniel, for giving me a new home during the challenging times when I did not have a lab, for offering me her support and research, professional, and personal guidance during these five years. Thanks to the Daniel Lab, current and former members, for the great research discussions, chisme time at the office, fun outings, for helping me troubleshot and learn new techniques, and for offering me a family in Ithaca; I would not have made it without such an amazing group. Particularly, I would like to acknowledge my girls, Ferra, Miriam, Tiffany, Miya, and Zeinab for being my support system, family, and for the many amazing times together; and Han-Yuan for all his advice and for believing every single lie/joke I told you. Special shutout to my abuela, Zeinab, for being my rock. We came, moved labs, and will leave Cornell as a pair, a pair of doctors! I could not have done it without you and all the amazing chisme we had these past six years.

Additionally, I am very thankful with many people at Cornell for their support during these six years. I want to thank Belinda Floyd for her advice and care during all these years especially during the lab moving and finishing/defense processes. In addition, I am very grateful with everyone at the DPE office and Hasbrouck as they have been a huge part of my experience at Cornell and an amazing family. Especially Jami Joyner and Julie Page for being always there and willing to help me, for teaching me to be an advocate and a mentor for our URM undergrads, and for letting me be part of

amazing communities. I also want to recognize the important role that my first friends in Ithaca had in my PhD journey: Josephine, Vienvi, and Mar. I could not have adjusted and learned to love Ithaca without the support and friendship.

Lastly, I would like to acknowledge my biggest support: God and my family. Thanks to God for allowing me to be here culminating one more of my dreams and to every member of my family for being my biggest fans, for their unconditional love and support during these years, for reminding me why I deserved to be here when I doubted myself, and for never stop believing in me. Definitely, I could not have done it without each one of them. To my parents, thank you for teaching me that perseverance and hard work have a good reward. I cannot even imagine coming to a new and unknown country with four kids to start from zero, thank you for your courage and sacrifices, so we could follow our dreams; this degree is also yours. Finally, specially thanks to Jeff, my loving husband, for your unconditional love and support especially during this past year of thesis writing. Thank you for dealing with me during the multiple writing crisis and bad mood, crying and frustration moments, for reassuring me that I could do this, and that things will get better, and for giving me courage, energy, and love to get to the end.

Finally, I would like to acknowledge my funding resources: the National Science Foundation Graduate Research Fellowship [Grant Number DGE-1650441), the Sloan Foundation [Grant number 70481], and King Abdullah University of Science and Technology grant OSR-2018-CRG7-3709.

TABLE OF CONTENTS

BIOGRAPHICAL SKETCH v
ACKNOWLEDGMENTS vii
LIST OF ABBREVIATIONS xvii
OUTLINE xx
1.INTERACTIONS BETWEEN EXTRACELLULAR VESICLES AND CELLS 25
1.1 Introduction 25
1.2. Role of adipose derived stem cells in cancer progression 28
1.3. Extracellular vesicles (EVs) 30
1.3.1 Subpopulations of EVs, microvesicles and exosomes 30
1.3.2. The role of EVs in cancer progression 32
1.3.3. EVs isolation and characterization 34
1.4. Molecular interactions between EVs and cells 39
1.4.1 EV targeting to cells 39
1.4.2. Mechanisms of interaction between EVs and target cells 41
1.5. Supported lipid bilayers as a cell membrane model system 42
1.6. Summary: 45
CHAPTER 2 47
2. FUNCTIONALIZATION OF SUPPORTED LIPID BILAYERS WITH ADHESION PROTEINS AND PEPTIDES FOR CELL CULTURE APPLICATIONS: A REVIEW 47
2.1. Acknowledgements 47
2.1.1. Individual acknowledgements 47
2.2. Abstract 48
2.3. Introduction 48
2.4. Supported lipid bilayer (SLBs) formation and characterization 51
2.4.1. Methods for the formation of SLBs 51
2.4.2. Characterization of SLBs 59
2.5. Biofunctionalization of SLBs for cell culture applications 64
2.5.1. Cell adhesion on SLBs 64
2.5.2. Functionalization of SLBs surface with adhesion peptides 65
2.5.3. Functionalization of SLBs' surface with adhesion proteins 72
2.6. Conclusions 82

CHAPTER 3 83
3.A SUPPORTED MEMBRANE PLATFORM TO ASSESS SURFACE INTERACTIONS BETWEEN EXTRACELLULAR VESICLES AND STROMAL CELLS. 83
3.1. Acknowledgments 83
3.1.1. Individual acknowledgments 83
3.1.2. Article acknowledgments 84
3.2. Abstract 84
3.3. Introduction 85
3.4. Materials and Methods 89
3.4.1. Cell culture 89
3.4.2. MVs and exosomes isolation 90
3.4.3. EVs size and concentration measurements 90
3.4.4. Transmission Electron Microscopy (TEM) 90
3.4.5. Western blot 91
3.4.6. Preparation of fusogenic liposomes 91
3.4.7. Formation of POPC/PEG-SLB and EVSB 91
3.4.8. Bicinchoninic acid assay (BCA) 92
3.4.9. Detection of EGFR in MV-EVSB 92
3.4.10. Detection of HSP70 and CD63 in exosome-EVSB 92
3.4.11. Visualizing EVSB formation by FRAP (Fluorescence Recovery after Photobleaching) 93
3.4.12. EV cargo tracking in EVSBs 93
3.4.13. ADSCs culture on EVSBs, POPC/PEG-SLB, and EZ-slides 93
3.4.14. Quantification of cell surface area and focal adhesions 93
3.4.15. Measurement of ADSC aspect ratio 94
3.4.16. Cell viability analysis using a LIVE/DEAD kit 94
3.4.17. Assessment of VEGF secretion by ADSCs 94
3.4.18. Statistical Analysis 95
3.5. Results and Discussion 95
3.5.1. Breast cancer cell EV isolation and characterization 95
3.5.2. Formation of EVSBs 98
3.5.3. Protein characterization in EVSBs 101
3.5.4. Cell spreading and adhesion of ADSCs on EVSBs 106

3.5.5. Cell Viability and angiogenic activity of ADSCs cultured on MV or exosome- EVSB 110
3.6. Conclusions 113
3.7. SUPPORTING INFORMATION 115
3.7.1. Experimental section 115
3.7.2. Results and Discussion 127
CHAPTER 4 135
4.DUAL MODE SENSING OF BINDING AND BLOCKING OF CANCER EXOSOMES TO BIOMIMETIC HUMAN PRIMARY STEM CELL SURFACES 135
4.1. Acknowledgments 135
4.1.1. Individual acknowledgements 136
4.1.2. Article acknowledgments 136
4.2. Abstract 137
4.3. Introduction 138
4.4. Materials and Methods 142
4.4.1. Cell Culture 142
4.4.2. Preparation of ADSC membrane blebs 143
4.4.3. cEXOs isolation and characterization 143
4.4.4. Characterization of cEXOs and ADSCs blebs 144
4.4.5. Preparation of glass slides for formation of supported bilayers 144
4.4.6. Polydimethylsiloxane (PDMS) well fabrication 144
4.4.7. Preparation of liposomes 145
4.4.8. Fluorescent labeling of liposomes, ADSCs blebs, and cEXOs 145
4.4.9 Formation of phosphatidylcholine supported lipid bilayers 146
4.4.10. Formation of ASB 146
4.4.11. Observing ASB formation and measuring diffusivity with fluorescence microscopy 146
4.4.12. Testing integrin β1/CD29, a native component of ADSCs membrane, presence in ASB 147
4.4.13. Binding of cEXOs to ASB 148
4.4.14. Blocking binding of cEXOs to ASB using Integrin β1/CD29 149
4.4.15. TIRFM Setting and Operation 149
4.4.16. Multi-electrode array Fabrication 149
4.4.17. Electrochemical Impedance Spectroscopy (EIS) 150
4.4.18. Assessment of VEGF secretion by ADSCs 151

4.4.19. Statistical Analysis 152
4.5. Results and discussion 152
4.5.1. ASB as an in vitro model of ADSC membrane 153
4.5.2. Formation and characterization of ASB 154
4.5.3. Detection of Integrin β1/CD29, a native component of ADSC membrane, in ASB 156
4.5.4. Optical detection of cEXOs binding to ASB 158
4.5.5. Blocking of Integrin β1/ CD29 reduces cEXOs binding to ASB 159
4.5.6. Electrical monitoring of cEXOs binding to ASB 161
4.5.7. Blocking of integrin β1 decreases cell proliferation and VEGF secretion by ADSCs in culture 166
4.6. Conclusions 168
4.7. Supporting information 171
4.7.1. Experimental Section 171
4.7.2 Results 175
File 4.S1. Proteomics Analysis of MDA-MB-231 derived cEXOs 177
CHAPTER 5 180
5.ELECTRICAL MONITORING OF CELL EPITHELIAL-TO-MESENCHYMAL TRANSITION INDUCED BY CANCER-DERIVED EXOSOMES 180
5.1 Acknowledgements 180
5.2. Abstract 181
5.3. Introduction 182
5.4. Experimental section 184
5.4.1. Cell Culture 184
5.4.2. Isolation and characterization of cEXOs 185
5.4.3. Treatment of MCF-10A cells with cEXOs 185
5.4.4. Cell fixation and lysis 185
5.4.5. Bicinchoninic acid assay (BCA) 186
5.4.6. Immunofluorescence 186
5.4.7. Antibodies 187
5.4.8. Western blot 187
5.4.9. Enzyme-linked immunosorbent assay (ELISA) 188
5.4.10. Confocal microscopy 188
5.4.11. Organic electrochemical transistor (OECT) fabrication 189

5.4.12. OECT operation 189
5.5. Results and discussion 190
5.5.1. Breast cancer-derived cEXOs lead to morphology changes in MCF-10A cells 190
5.5.2. Breast cancer-derived cEXOs induce EMT-like behavior in MCF-10A cells 193
5.5.3. Organic electrochemical transistors (OECTs) to monitor cell barrier integrity 197
5.5.4. cEXOs induce loss of barrier integrity, as a marker of EMT, in MCF-10A cells 199
5.6. Conclusions and future work 201
CHAPTER 6 203
6. CONCLUSIONS AND OUTLOOK 203
APPENDIX 1 214
1.HEPARIN BLOCKS BINDING OF ONCOGENIC EXTRACELLULAR VESICLES TO ADIPOSE DERIVED STEM CELLS 214
1. Introduction: 214
2. Materials and Methods 216
2.1. Blocking binding of cEVs to ASB using heparin 216
2.2. Assessment of VEGF secretion by ADSCs 216
3. Results and discussion 217
4. Conclusions 221
REFERENCES 223

LIST OF FIGURES

Figure 1.1. Cancer EVs biogenesis and biological outcomes of their interactions with stromal adipose derived stem cells (ADSCs). 32

Figure 1.2. Outcomes of interactions between stromal cells and cancer EVs in tumor progression. 34

Figure 1.3. Methods for EV isolation. 35

Figure 1.4. Physical properties and quantification of EVs. 38

Figure 1.5. Molecules involved in EV-cell contact and binding. 40

Figure 1.6. Mechanisms of interactions between EVs and target cells. 42

Figure 1.7. Formation of hybrid SLBs without and with cushion 44

Figure 2.1. Methods for preparation of supported lipid bilayers 53

Figure 2.2. Methods for characterization of SLBs. 63

Figure 2.3. Methods for SLB functionalization with adhesion peptides. 66

Figure 2.4. RGD functionalization of SLB as a cell culture for hMSCs. 68

Figure 2.5. Structure of clustered RGD-containing compound 69

Figure 2.6. SLB functionalization with IKVAV peptide. 71

Figure 2.7. E-Cad-ECD and N-Cad-ECD functionalized SLBs. 74

Figure 2.8. Schematics of ECM functionalized-SLBs and cell adhesion to them. 77

Figure 2.9. Functionalized SLBs as a mimic of the ECM. 80

Figure 3.1. Isolation and characterization of MDA-MB-231 derived EVs. 97

Figure 3.2. EVSBs formation and characterization. 101

Figure 3.3. Detection of EVs membrane components in EVSBs. 102

Figure 3.4. Cell surface area and focal adhesions of ADSCs cultured on different surfaces. 109

Figure 3.5. Viability and angiogenic activity of ADSCs on different surfaces. 111

Figure 3.S1. MVs and exosomes visualized by transmission electron microscopy (TEM). 127

Figure 3.S2. Formation of EVSBs visualized by fluorescence recovery after photobleaching (FRAP). 128

Figure 3.S3. Detection of extracellular vesicles membrane components in EVSBs. . 129

Figure 3.S4. Number of focal adhesions generated and cell area of ADSCs cultured on EVSBs normalized by EVSB protein content. 130

Figure 3.S5. Aspect ratio of ADSCs cultured on EVSBs, POPC/PEG-SLB, and EZ-slides. 130

Figure 3.S6. Secretion of VEGF by ADSCs normalized by EVSB protein content and number of viable cells. 131

Figure 3.S7. Expression of α-SMA, as a marker of myofibroblast transformation, on ADSCs cultured on EVSBs, POPC/PEG -SLB, and EZ-slides. 133

Figure 4.1. ASB formation and characterization. 157

Figure 4.2. Integrin β1/CD29 plays a role in cEXOs binding to ASBs 160

Figure 4.3. Electrical readouts support the role of integrin β1/CD29 in cEXOs binding to ASBs. 163

Figure 4.4. Blocking of integrin β1/CD29 decreases cell number and VEGF secretion by ADSCs treated with cEXOs. 167

Figure 4.S2. Surface components possibly involved in ADSCs-cEXO interactions. 176

Figure 4.S3. FRAP of ASB on PEDOT: PSS. 177

Figure 4.S4. Nyquist plots of cEXOs binding to ASB on PEDOT: PSS. 178

Figure 4.S5. Nyquist plots of C29 Ab-treated ASB on PEDOT: PSS. 178

Figure 4.S6. CD29 Ab treatment effect on ASB resistance. 179

Figure 5.1. Changes in morphology, epithelial, and mesenchymal markers in epithelial monolayer undergoing EMT induced by cEXOs treatment. 192

Figure 5.2. Morphology changes in MCF-10A treated with cEXOs. 193

Figure 5.3. EMT markers in MCF10A cells treated with cEXOs for 7 days. 194

Figure 5.4. EMT markers in MCF10A cells treated with cEXOs for 60 hours. 197

Figure 5.5. Schematic of OECT biosensor. 199

Figure 5.6. Electrical detection of decrease in barrier integrity of MCF-10A cells treated with cEXOs. 201

Figure A.1. Heparin blocks binding of EVs to ASB. 218

Figure A.2. Heparin decreases VEGF secretion and cell proliferation in ADSCs treated with breast cancer EVs. 220

LIST OF ABBREVIATIONS

ADSCs	Adipose Derived Stem Cell
AFM	Atomic Force Microscopy
ASB	ADSC-Derived Supported Bilayer
BCA	Bicinchoninic Acid Assay
Biotin DOPE	1,2-dioleoyl-sn-glycero-3-phosphoethanolamine
BM	Bicelle Method
BMI	Body Mass Index
BPE	Bovine Pituitary Extract
CD29 Ab	Anti-CD29 Antibody
CE	Counter Electrode
cEVs	Cancer Derived Extracellular Vesicles
cEXOs	Cancer Derived Exosomes
CM	Confocal Microscopy
Col	Collagen Type I
CP	Conducting Polymer
CPE	Constant Phase Element
D	Diffusion Coefficient
DBSA	Dodecylbenzenesulfonic Acid
DDT	Dichlorodiphenyltrichloroethane
dECM	Decellularized ECM
DLS	Dynamic Light Scattering
DOPC	1,2-dioleoyl-sn-glycero-3-phosphocholine
DP-NGPE	Dipalmitoyl-sn-glycero-3-phosphoethanolamine-N-(glutaryl)
DPPC	2-dipalmitoyl-sn-glycero-3-phosphocholine
dUC	Differential ultracentrifugation
E-cad-ECD	E-Cadherin Extracellular Domain
ECM	Extracellular Matrix
EEC	Equivalent Electrical Circuit
EGFR	Epidermal Growth Factor Receptor
EIS	Electrochemical Impedance Spectroscopy
ELS	Electrophoretic Light Scattering
EMT	Epithelial to Mesenchymal Transition
EVs	Extracellular Vesicles
EVSB	EVs-Derived Supported Bilayer
EXOs	Exosomes
FBS	Fetal Bovine Serum
FCS	Fluorescence Correlation Spectroscopy

FDA	Food And Drug Administration
FM	Fluorescence Microscopy
FN	Fibronectin
FRAP	Fluorescence Recovery After Photobleaching
FRET	Förster Resonance Energy Transfer
GAGs	Glycosaminoglycans
HEK-293t	Human Embryonic Kidney Cells
hMSCs	Human Mesenchymal Cells
HS	Heparan Sulfate
HSP70	70 Kd Heat Shock Protein
HSPGs	Heparan Sulfate Proteoglycans
Huh 7.5	Human Hepatocarcinoma Cells
HUVECs	Human Umbilical Vein Epithelial Cells
IA	Immunoaffinity
IGF	Insulin-Like Growth Factor
ISEV	International Society for Extracellular Vesicles
KAUST	King Abdullah University of Science and Technology
LB	Langmuir-Blodgett
LB/VF	Langmuir-Blodgett/Vesicle Fusion
LDE	Laser Doppler Electrophoresis
LS	Langmuir−Schaefer
MEAs	Multi-Electrode Arrays
MES	Embryonic Stem Cells
MF	Microfluidics
MVs	Microvesicles
MISEV	Minimal Information for Studies of Extracellular Vesicles
MMPs	Matrix Metalloproteinases
MVBs	Multivesicular Bodies
NSOM	Near-Field Scanning Optical Microscope
NT	No Treatment
NTA	Nanoparticle Tracking Analysis
NTA	Nitrilotriacetic Acid
NTU	Nanyang Technological University
OECTs	Organic Electrochemical Transistors
P2FM	Two-Photon Fluorescence Microscopy
PBS	Phosphate-Buffered Saline Solution
PDCs	Periosteum Derived Multipotent Cells
PDMS	Polydimethylsiloxane
PEDOT:PSS	Poly(3,4-Ethylenedioxythiophene) doped with poly (Styrene Sulfonate)

PEG	Polyethylene Glycol
PEG2000	Polyethyleneglycol-2000
POPC	1-Oleoyl-2-Palmitoyl-Sn-Glycero-3-Phosphocholine
PSo	Polystyrene
QCMD	Quartz Crystal Microbalance with Dissipation
R18	Octadecyl Rhodamine
RE	Reference Electrode
RGD	Arginylglycylaspartic Acid
RPS	Resistive Pulse Sensing
RT	Room Temperature
SALB	Solvent-Assisted Lipid Bilayer
SC	Spin Coating
SEC	Size Exclusion Chromatography
SEM	Scanning Electron Microscopy
SLBs	Supported Lipid Bilayers
SM	Sphingomyelin
SMCs	Vascular Smooth Muscle Cells
SPR	Surface Plasmon Resonance
SPT	Single Particle Tracking
SUVs	Small Unilamellar Vesicles
TBST	Tris-Buffered Saline and 0.1% Tween 20
TCEP	Tris(2-Carboxyethyl) Phosphine
TEAB	Triethylammonium Bicarbonate
TEM	Transmission Electron Microscopy
TGFβ	Transforming Growth Factor Beta
TIRF	Total Internal Reflection Fluorescence
TJ	Tight Junction
TME	Tumor Microenvironment
UF	Ultrafiltration
VEGF	Vascular Endothelial Growth Factor
VF	Vesicle Fusion
WB	Western Blot
WCL	Whole Cell Lysate
ZO-1	Zona Occludens I
α-SMA	Alpha Smooth Muscle Actin

OUTLINE

In the last decade, cancer derived extracellular vesicles (EVs) have gained in popularity among biomedical researchers as critical players in tumorigenesis and metastasis. EVs are highly involved in intercellular communication and act as "messengers" facilitating transfer of information between tumor and stromal cells, which often leads to outcomes in the recipient cells favoring cancer progression. Previous work has shown that interactions between adipose derived stem cells (ADSCs), an important cell type in the tumor microenvironment[7], and breast cancer cell-derived EVs induce proangiogenic activity and differentiation to myofibroblasts, a metastasis-favoring phenotype[4-6]. However, these interactions are not fully understood in part, due to a lack of techniques available to distinguish cell surface and vesicle interactions from internalization and cargo delivery. Towards this end, I have developed two hybrid supported lipid bilayers (SLBs) as biomimetic membrane models to facilitate the isolation, study, and screening of blocking strategies of EVs-ASDCs surface interactions.

To guide the research done in my PhD and its significance, the **first chapter** presents a general background on the biology of EVs and ADSCs, what is known about their interactions, and the importance of EVs on the tumor microenvironment and cancer progression. SLBs are the standard technique used in many areas of research to study cell membranes and their interactions with various proteins, pathogens, or molecules. Thus, the **second chapter** reviews the formation and characterization techniques for SLBs, and their functionalization with adhesion proteins and peptides for novel

applications as cell culture substrates.

In the **third chapter**, I describe the model I have generated that consists of a supported bilayer integrated with EV membrane components, called an EV supported bilayer (EVSB)[9]. This system allowed the isolation of the EVs surface, away from their cargo, to investigate the outcomes of their interactions with ADSCs. To do so, the EVSB was employed as a cell culture platform for ADSCs, and their cell adhesion, spreading, viability, VEGF secretion (as a sign of proangiogenic activity), and differentiation to myofibroblast were examined. Results showed that as ADSCs grew on a "cancer-like" surface, cell proliferation and viability, adhesion spreading, and proangiogenic activity were all enhanced, creating conditions that favor oncogenic activity and formation of pre-metastatic niches. Interestingly, cell differentiation was not enhanced when ADSCs were cultured on EVSBs.

Although the nature of the interactions between cancer EVs and ADSCs is not completely clear, it is known that receptor-mediated binding is the initial interaction between EVs and cells. This interaction is independent of the route EVs take to transport information into the cell. Therefore, understanding the mechanism of EV-cell binding and identifying strategies to block this interaction are essential to potentially stop the transfer of oncogenes from EVs to ADSCs and the associated malignant outcomes[10]. To the importance of understanding EVs cellular binding mechanisms and the absence of *in vitro* techniques to study them in isolation, I developed a hybrid supported biomimetic membrane derived from ADSC membrane components, called an ADSC-derived supported bilayer (ASB)[11]. In the **fourth chapter** of this dissertation, I used the ASB platform as an *in vitro* model of these stem cell membranes to detect and recapitulate

breast cancer EVs binding to ADSCs. This approach enabled me to isolate vesicle binding from downstream events, such as internalization and cargo delivery. Additionally, it allowed me to identify strategies to decrease EV binding and thus potentially prevent stem cells from adopting a pro-cancerous phenotype. The versatility of the ASB allowed its integration into multi-electrode arrays (MEAs) to allow optical and label-free electrical detection of EVs binding to ADSCs. We found that blocking the adipose stem cell surface receptor integrin β1 or heparan sulfate proteoglycans (HSPGs) on the surface of EVs using an anti-CD29 antibody or heparin respectively, successfully decreased EVs binding to ADSC. These results suggest that both cell and EV surface proteins are required for EVs binding to ADSCs. Using these same blocking strategies on EVs and cultured ADSCs caused a severe reduction in cell proliferation and VEGF upregulation, two outcomes of EV binding[9]. These *in vitro* results further validate our previous findings using the ASB and demonstrate that these two strategies have therapeutic potential to target EVs-mediated cancer progression.

The **fifth chapter** of this dissertation describes a work in progress on a project in collaboration with Owens lab at University of Cambridge in electrical monitoring of cell epithelial to mesenchymal transition (EMT) induced by breast cancer derived exosomes (EXOs), a subpopulation of EVs. EMT is a biological process and hallmark of cancer in which epithelial cells lose important markers and characteristics and gain those associated with mesenchymal cells. Previous evidence shows that EVs derived from different types of cancer, especially EXOs and their cargoes, induce cancer-associated EMT in epithelial cells, endowing them with migratory and invasive characteristics. Therefore, we investigate the ability of breast cancer cells-derived EXOs

to induce EMT-like behavior in breast epithelial. My work in this project is focused on using conventional biochemical techniques like immunofluorescence, western blot, and ELISA to detect EMT-like behavior as seen in my results in chapter 5. The Owens group focuses on the electrical monitoring of barrier integrity, as a sign of EMT transition, to validate the results found using conventional methods and offer a dual sensing system. *This project is under progress and all data presented in here is preliminary.* We aim to offer a label-free and convenient system to detect early changes associated with EMT in epithelial cells induced by cancer EVs as a tool with therapeutic potential to study strategies to block such mesenchymal transition. Finally, a closing **chapter six** offers a summary and conclusions of my thesis work and the future directions for the research conducted during my PhD.

Overall, my research contributes to the understanding of the interactions that occur between breast cancer derived EVs with breast epithelial cell and ADSCs. This approach offers a simplified *in vitro* system that enables the direct study of vesicle and cell membrane interactions, and by extension, strategies to block those interactions. In particular, I have focused on the surface interactions between EVs and ADSCs. The EVSB platform introduced in this work represents the first biomimetic EV membrane model used as a cell culture platform to study EVs surface interactions with stem cells. Similarly, the ASB platform represents the first cell-free, potentially label-free, biomimetic human primary stem cell membrane model to detect and study EV binding. Both systems facilitate the study and understanding of surface interactions between EVs and ADSCs and can be potentially used to develop therapeutics to limit EVs-ADSCs interactions and the outcomes associated to them. Furthermore, their versatility makes

them compatible with scale-up and multiplexing methods needed for drug development. Furthermore, these two models are not limited to the study of breast cancer EVs-ADSCs interactions; they can be used to investigate surface interactions across many different biological systems in which EVs lead to cellular changes and abnormalities that progress to disease.

CHAPTER 1

1.INTERACTIONS BETWEEN EXTRACELLULAR VESICLES AND CELLS

1.1 Introduction

Cancer is the second leading cause of death in The United States and the third one worldwide. However, 92% of cancer casualties are due to metastasis to a secondary site and not disease of the primary tumor[13]. Therefore, discovering mechanisms employed by cells that promote metastasis and subsequently developing strategies to stop such mechanisms will have vast impact on human health and are the main targets of cancer research today. Between the mechanisms known to promote cancer metastasis, tumor secreted factors such as cytokines, chemokines, and extracellular vesicles (EVs) have been recently highlighted[14]. In particular, EVs, small vesicles shed from cancer cells, have been implicated as important mediators of cellular communication and are suspected to play an important role in cancer invasion, progression, and metastasis[15, 16]. EVs, in general, are a heterogeneous group of membrane encapsulated particles secreted into the extracellular space by many eukaryotic cell types. In cancer, EVs production has been shown to be upregulated and correlated with cancer progression[17], but how EVs may regulate this progression is not fully understood.

EVs have received much attention in the last decade due to their capacity to exchange information between cells and to work as information vehicles between diseased and healthy cells[3]. In that manner, interactions between EVs and host cells have been shown to lead to modifications in the molecular makeup and phenotype of the recipient cell. In the case of cancer, cancer derived EVs are known to facilitate cell

transformation leading to angiogenesis, epithelial-to-mesenchymal transition (EMT), cancer aggression, and progression [1, 4-6, 18-20]. Studies have shown acquired proangiogenic activity and cell phenotype transformation when healthy cells were treated with cancer derived EVs[18]. For example, Song et al.[4] and Cho et al.[5] showed that breast cancer derived EVs influence adipose derived stem cell proangiogenic potential activation and transformation to myofibroblasts. In the same manner, it is thought that EVs carry critical inducers of EMT in the form of lipids, nucleic acids, and proteins[21]. For instance, Rahman et al[22]. showed that EVs derived from highly metastatic human lung cancer cells promoted EMT in in human bronchial epithelial cells. However, how interactions leading to such malignant outcomes occur at the molecular level, and how they may be initiated, is not always clear. We hypothesize that signals most certainly come from both the EV internal cargo as well as its membrane components.

Therefore, to understand disease progression promoted by EVs, it is essential to understand both the surface and internal cargo interactions occurring between EVs and cells. As there is an absence of techniques *in vivo* to study molecular and surface-level interactions between EVs and cells, our understanding is incomplete[23], yet this is the initiation of EVs' influence in the local microenvironment to favor metastasis. Towards this end, in this thesis work, I developed two platforms that will allow the study of i) the interactions between EV surface and cells and how that influences cell behavior and will work as a cell culture platform, and ii) binding of EVs to cells and screening of strategies to block those interactions as a proof-of-concept device for development of cancer therapeutics. For i), I focused on how the cues coming from the surface of the EV influences the otherwise healthy cells, isolating surface cues from the impact of the EV

cargo and the mechanisms and factors favoring delivery of this cargo of it[24]. Then in ii), I describe a platform that allows the optical detection and study of binding of EVs to stromal cells and the possible factors/ proteins having a pivotal role in modulating this interaction. Additionally, label-free, electrical monitoring of EVs binding to cells is also facilitated by integrating this platform with an electrical device, multi-electrodes array. In this work, we chose to focus on investigating the interactions between highly metastatic human breast cancer cells, MDA-MB-231, derived EVs and human adipose derived stem cells, ADSCs, as one of the possible applications for our platforms. As stated before, it has been previously established that ADSCs treated with cancer derived EVs acquired proangiogenic potential and phenotype transformation to myofibroblasts[4, 5]. Hence, we generated a platform to investigate the molecular interactions leading to such malignant outcomes.

Our platforms consist of tunable *in vitro* EV/ADSCs surface models having planar geometry that mimics the membrane composition of EVs and ADSCs and allows the study of molecular interactions between EVs and ADSCs. These platforms are hybrid supported lipid bilayers (SLBs). SLBs are common model membrane systems used in many areas of research to understand biomolecular interactions with cell membranes[25-31]. SLBs can mimic the native configuration of the cell membrane, its protein and lipid content, and its two-dimensional fluidity; and so they have made good cell culture platforms to investigate cell interactions[30, 32]. In fact, chapter 2 of this work includes a complete review on SLBs surface functionalization using adhesion peptides and proteins and their applications in cell culture. Our group has furthered this important technology platform recently by developing methods to incorporate native plasma cell membrane

material that preserves the original orientation and function of the proteins from mammalian[33, 34] membranes. In this thesis, we leverage this work to tailor our supported bilayer platform to make "cancer-like" supported bilayers derived from EVs and ASDC-like supported bilayers from ASDCs blebs (membrane protrusions shed by mammalian cells) and we propose their use as an important tool to investigate interactions between EVs and ADSCs and for various applications. In addition, in a distinction from most prior studies in this field, we use microvesicles (MVs) and exosomes (EXOs) as two independent EVs populations to assess how both subtypes interact and influence ASDC biological behavior.

The tunability of our EVSB and ASB platforms allow us to study the outcome of any type of EV interaction with a desired kind of cell, opening the possibility of studying the effects of different types of cancer derived EVs on cells. As such, our platform will facilitate the investigation different diseases in which EVs play an important role, such as cardiovascular and metabolic diseases[16], neurodegenerative diseases[35], and cigarette smoke associated diseases[36]. Finally, this platform can be deployed to develop ways to disrupt deleterious surface interactions between EVs with recipient cells to avoid negative outcomes that lead to disease.

1.2. Role of adipose derived stem cells in cancer progression

Obesity has been established to be a risk factor for many types of cancer, most of which are more prevalent or specific to women including endometrial, gastric, colorectal, breast, ovarian, cervical, and thyroid cancer[37, 38]. As a matter of fact, excess body mass index (BMI) is related to increased risk of invasive cancer[39]. Therefore, research efforts have been focused on establishing the effect of obesity in adipose tissue behavior and

consequently in cancer development, invasiveness, and progression. Currently, it is thought that increased adiposity dysregulates the secretion of proinflammatory cytokines, chemokines, and adipokines contributing to cancer development[40]. The adipose tissue is a complex system with high endocrine activity and plasticity. It is mainly composed of immune cells, stromal vascular cells, adipocytes, and connective and nerve tissue matrices.

Adipose derived stem cells (ADSCs) are one of the types of stromal vascular cells forming the adipose tissue and are characterized by their high plasticity and ability to self-renew and differentiate into several cell lineages including cells that are essential in the formation of new vasculature promoting tumor proliferation, including fibroblasts and myofibroblasts[6, 7, 41-43]. ADSCs are an important cell group in the tumor microenvironment (TME) and have a critical role in tumor progression and aggressiveness due to their angiogenic, anti-apoptotic, and immunomodulatory properties[7, 41]. ADSCs are chemoattracted to solid tumors and secrete cytokines, growth factors, and inflammatory biomarkers such as VEGF, insulin-like growth factor (IGF), IL6, and transforming growth factor beta (TGβ1)[44]. Some of these secreted growth factors contribute to tumorigenesis by generating a TME with high levels of inflammation[45] and promoting angiogenesis to facilitate access of oxygen and nutrients to the tumor[44, 46]. Furthermore, TGFβ1 secreted by ADSCs contributes to an immunomodulatory effect[41, 47, 48] and increases ECM production and collagen organization leading to a fibrous TME. Therefore, several studies have shown that ADSCs can alter cancer properties by altering tumor cell behavior towards a more aggressive one (Figure 1.2)[49]. For example, Castro-Oropeza[39] et al. studied the effect of ADSCs in cervical cancer (HeLa) cells and found

that ASDCs promote cell migration, movement, angiogenesis, EMT, and malignant properties. In the same manner, Strong and colleagues[50] showed enhanced proliferation in breast cancer (MCF-7 and MDA-MB 231) cells when treated with ASDCs and an increased effect when ADSCs were derived from abdominal obese tissue. Interestingly, increased tumorigenesis is not just an effect of ADSCs in cancer cells, but it is the same case for the opposite interaction, cancer cells to ASDCs. In general, interactions between cancer cells, ADSCs, and peritumoral adipocytes lead to an increase in tumor aggressive behavior[51]. For instance, cancer cells promote ADSCs proangiogenic potential as well as their transformation into myofibroblasts, a highly contractile phenotype essential in tumorigenesis, to enrich the TME and the metastatic niche [52, 53]. Although the mechanism by which cancer cells lead to this differentiation is still not well understood, it is known that TGFβ is a key inducer of this process since it contains the contractile gene machinery that leads to myofibroblast differentiation in precursor cells [4, 5, 25, 53-56]. One method of transfer and activation of TGFβ and other growth factors from cancer cells to ADSCs, is through intracellular communication vehicles or EVs [54, 57].

1.3. Extracellular vesicles (EVs)

1.3.1 Subpopulations of EVs, microvesicles and exosomes

EVs are membrane encapsulated particles generated and secreted by several types of cancer and healthy cells with higher EVs secreted from cancer cells. Extensive research has shown the existence of two major EVs subtypes: exosomes (EXOs) and microvesicles (MVs) [1, 15, 16, 24, 58]. EXOs are membrane vesicles of endocytic origin that are generated from late endosomes and multivesicular bodies (MVBs) and secreted to the extracellular space by fusing with the plasma membrane (Figure 1.1) and thus may have a composition

that does not necessarily reflect the plasma membrane of the mother cell. EXOs are typically defined as a population subset of EVs, ranging 30 -120 nm in diameter and with some specific protein markers [59, 60]. The second type, MVs, are a more heterogeneous EV population, with a larger size range between 120 nm - 1μm in diameter[61]. MVs bud, and are directly shed, from the plasma membrane into the extracellular space, preserving native properties from the mother cell plasma membrane [15, 24] (Figure 1.1). EVs of both types contain an extensive variety of cargo and membrane components, which depends on the physiological condition in which they are produced and the type of cell from which they originate. Because of the endosomal nature, EXOs commonly express endocytic proteins like Alix, Tsg101, and flotillin, and membrane tetraspanins like CD9, CD63, and CD81. MV protein content is less generalized, and it depends on the mother cell generating it; however, integrins, selectins, and CD40 ligand have been highly associated with MVs[58]. In general, some of the main cargo varieties that have been identified in both types of EVs include miRNA, mRNA, DNA, proteins, lipids, oncogenes, and receptors[1, 62].

Most of the studies investigating outcomes of EV interactions with recipient cells are done using a general population of EVs rather than two individual (MVs and EXOs) subtypes[4, 5, 18]. This is in part due to the difficulty in defining subpopulations; however, it is reasonably well-established that there is a size cut-off that differentiates the broad class of EXOs from MVs and some specific markers that will differentiate between both types of EVs[63]. With this general distinction, MVs and EXOs have been shown to differ in biogenesis, cargo, lipid composition, surface makeup, and functions[58, 64].

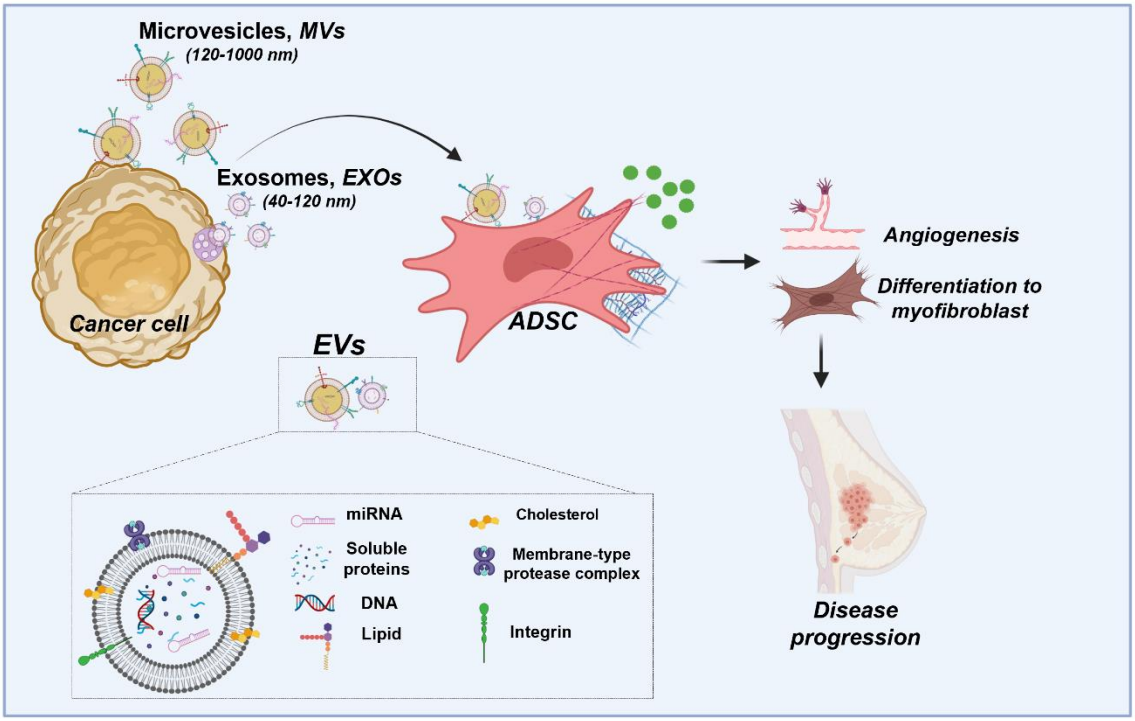

Figure 1.1. Cancer EVs biogenesis and biological outcomes of their interactions with stromal adipose derived stem cells (ADSCs). MVs are bud and shed into the extracellular space by the plasma membrane of cancer cells. EXOs are originated at multivesicular bodies (MVBs) and secreted to the extracellular space as MVBs fuse with the plasma membrane. Both EVs populations have a complex surface composition that aid their interactions with stromal cells. In the case of ADSCs, EVs have shown to cause high vascular endothelial growth factor, VEGF, secretion suggesting high proangiogenic activity, increment on fibers formation, and transformation to myofibroblasts, which favor cancer progression[4, 5].

Research findings also suggest that EXOs and MVs have different functions in cell-cell communication[65], and different intracellular routes with subsequent effects on healthy cells[65, 66]. Consequently, we decided to distinguish between these populations in some of our studies to test if EV subtypes interact differently with ADSCs and generate different biological outcomes.

1.3.2. The role of EVs in cancer progression

Tumors consist of malignant cells embedded in vasculature (tumor parenchyma), surrounded by nonmalignant cells (tumor stroma) like endothelial cells, myofibroblasts, fibroblasts, adipose cells, neoplastic cells, pericytes, connective tissue cells, immune

cells, and several stem and progenitor cells[67, 68]. The tumor stroma, tumor parenchyma, along with extracellular matrix (ECM), form the TME, a complicated signaling system that plays a pivotal role in tumorigenesis [48 69]. Crosstalk between cancer cells and stroma non-malignant cells within the TME, facilitated by EVs, promotes tumor formation and progression[70]. Cancer cell derived-EVs are known to contain oncogenic proteins and nucleic acids that stimulate and regulate angiogenesis, remodeling of the TME, apoptosis regulation, cell cycle, tumorigenesis, and metastasis[71-73]. Horizontal exchange of such material between cancer cells and neighboring and distant cells leads to significant molecular and phenotypic changes in the recipient cell, commonly favoring disease progression. In a study conducted by Fang et al.[74], transfer of miRNA-103 associated with EVs derived from hepatoma cells to human umbilical vein epithelial cells (HUVECs), contributed to tumor metastasis by increasing vascular permeability and promoting cell migration. Umezu et al.[75] presented evidence that miRNA-135 transferred from multiple myeloma cells derived-EVs to HUVECs enhanced angiogenesis under chronic hypoxia. In the context of breast cancer, Melo et al[76]. studied how miRNA-21 and miRNA-10b transferred from breast cancer cells-EVs (MDA-MB-231) to breast epithelial cells (MCF-10A) enhanced epithelial cells proliferation, viability, and tumorigenesis.

These are just a small set of several studies showing that cancer cell derived-EVs crosstalk with cancerous and healthy cells and enhance several cancer progression aspects such as angiogenesis[4, 5, 18, 77], EMT[21, 78], cancer immunosuppression[3, 79, 80], ECM remodeling[81-83], and contribution to a metastatic niche[84-86] as seen in Figure 1.2.

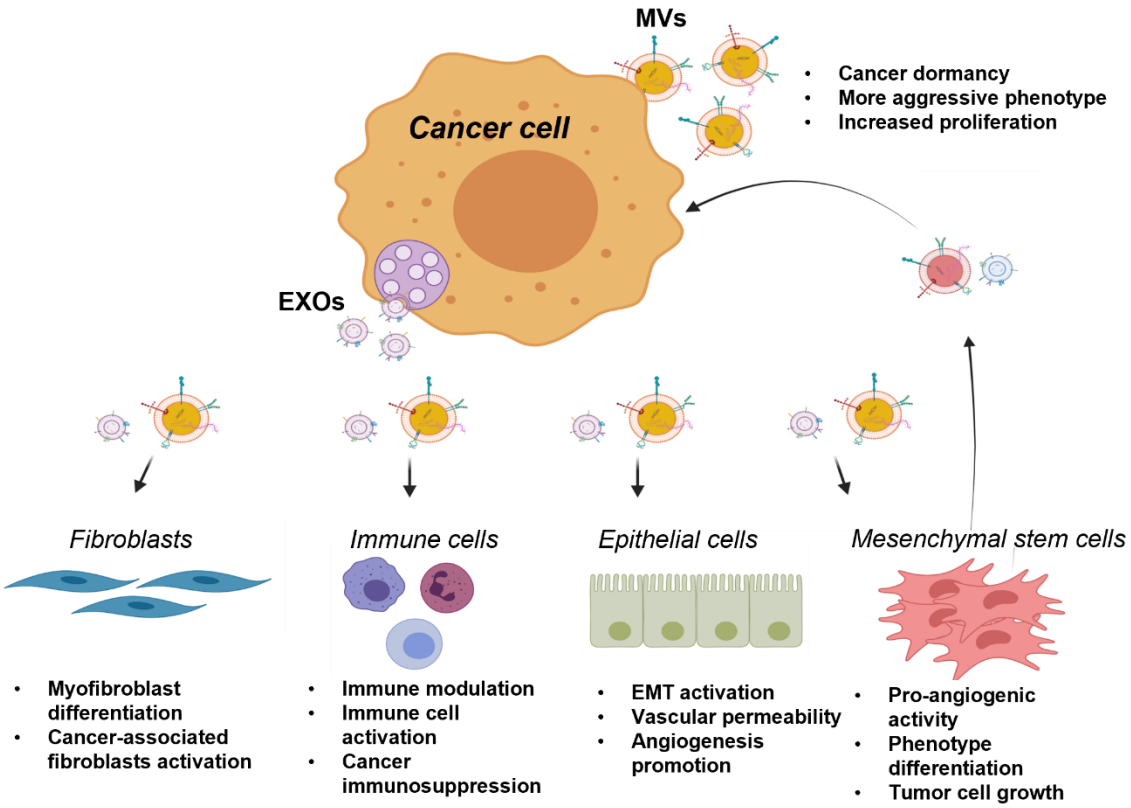

Figure 1.2. Outcomes of interactions between stromal cells and cancer EVs in tumor progression. Diagram of biogenesis of cancer MVs and EXOs and their effect when interacting with stromal cells. MVs are shed by the cancer cell plasma membrane and EXOs originate within the multivesicular bodies (MVB) and fuse with the plasma membrane to exit the cell into the extracellular space. Both types of cancer EVs get transfer between cancer cells and neighboring stromal cells like immune cells, fibroblasts, epithelial cells, and mesenchymal stem cells (and vice versa). This transfer of information via cancer EVs contributes to cancer progression in the TME through different mechanisms including but not limited to phenotype differentiation, immune modulation, cancer, immunosuppression, EMT, cancer dormancy, increased cancer aggressiveness, and angiogenesis[87]. *Created with BioRender.com*

1.3.3. EVs isolation and characterization

EVs are naturally secreted by most cell types as key players in intercellular communication. Therefore, no treatment is necessary to trigger EVs secretion by cells. However, recent studies have shown that isolation of EVs from *in vitro* cultured cells will potentially lead to not just isolation of EVs-associated RNA but to co-purification of RNAs derived from cell medium supplement like fetal bovine serum (FBS) and bovine pituitary extract (BPE). Despite the efforts done to eliminate this problem using non-

serum cell medium supplements, Auber et al[88]. showed that RNA contaminants derived from those supplements are still carried into the purified EVs.

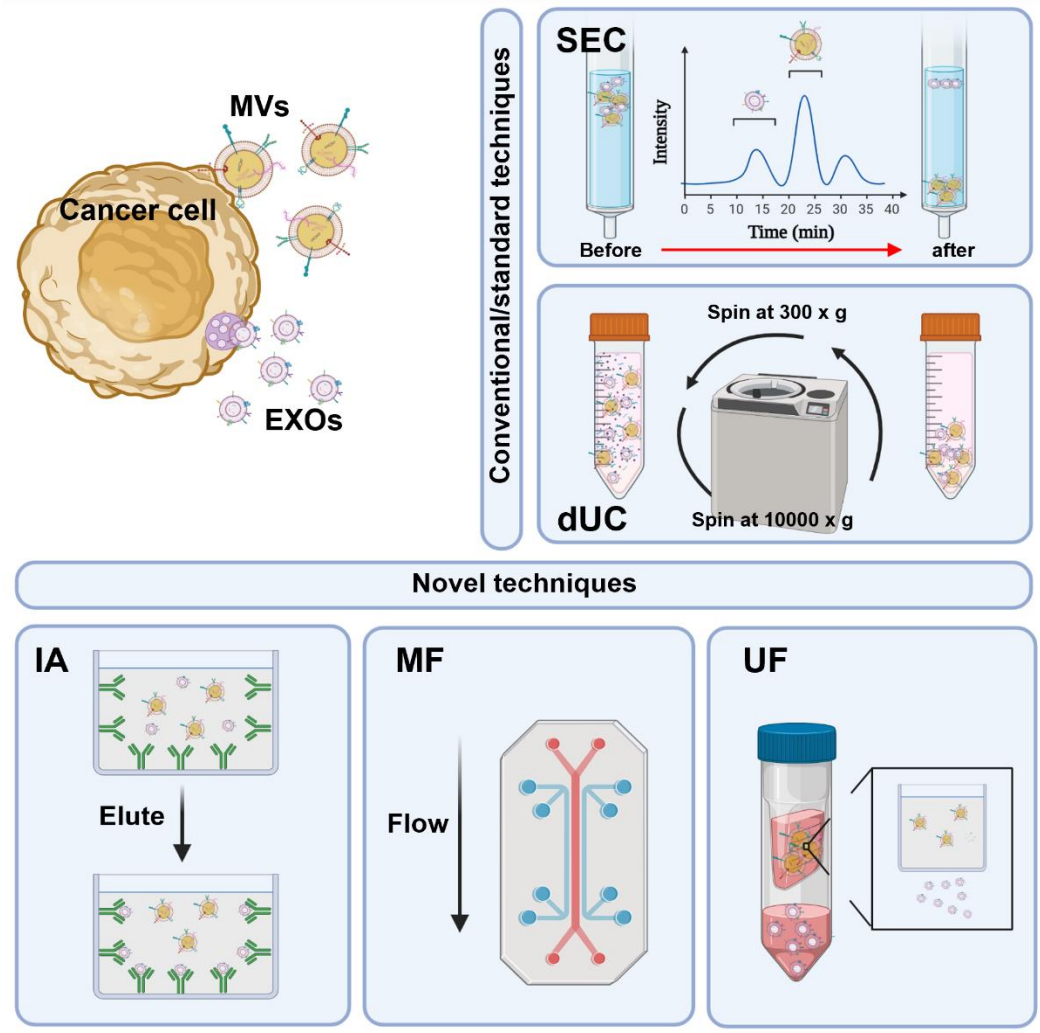

Figure 1.3. Methods for EV isolation. The standard methods for EV isolation based on their density and size are differential ultracentrifugation (dUC) and size exclusion chromatography (SEC) respectively. dUC uses a cycle of gradually increased velocity centrifugations to separate EVs, while SEC employs a porous filtration gel to elute bigger particles, MVs, followed by smaller ones, EXOs. Several novel techniques have been developed to isolated EVs including immunoaffinity (IA), microfluidics (MF), and ultrafiltration (UF). IA uses antibodies specific to EXOs surface to isolate and individual population of EVs; MF also uses antibodies that bind to a specific exosomal surface protein to isolate EXOs from MVs, and UF employs a nanopore size filter to create a filtrate rich in EVs of the desired size. Schematic adapted from *Sidhom et al*.[89].

Therefore, the standard procedure in EVs research is to use serum free cell medium or medium containing EXOs- depleted FBS to grow cells *in vitro* prior to EV isolation

(typically between 18-48 hours). Then, EVs are commonly isolated in two different subpopulations, MVs and EXOs, based on their differences in size, density, and immunoaffinity. Several methods have been developed towards this effort depending on the target characteristic (Figure 1.3).

To isolate and separate EVs populations based on their size, techniques including ultrafiltration[90], microfluidics[91], size-exclusion chromatography[92], and lab-on-chip technologies[93] are commonly used. For EVs density-based isolation, standard techniques include: ultracentrifugation[94], polymeric precipitation[95], and sucrose gradient[94]. Lastly, EVs isolation based on immunoaffinity can be performed by immunomagnetic beads separation[96] and immunoassays[97, 98]. Furthermore, a combination of several isolation techniques is a common approach to generate a larger yield of EVs. For instance, ultracentrifugation remains by far the most widely used EV isolation technique across the field, and it is usually performed along with filtration and several differential cycles of centrifugation (differential ultracentrifugation (dUC)). This combination of techniques has become the gold standard technique for EV isolation[99]. For our purposes, EVs were isolated and separated in two populations, MVs and EXOs, based on their density and size difference using dUC and filtration, as described in detail in chapter 3 and 4.

A full understanding of EVs, their working mechanisms, and their potential as important disease biomarkers relies on proper characterization of EV samples. It is essential to study and understand EV physical and compositional characteristics to fully exploit the potential of these nanoparticles as biomarkers, drug carriers, intracellular communication vehicles, among others. For instance, identification of EV surface and cargo composition is critical for the development of nanoparticles mimicking EV

functions or to simply understand their effect on promoting disease. In the same manner, to characterize individual subpopulations of EVs, MVs and EXOs, it is necessary to detect surface- and/or cargo- associated proteins specific to each subpopulation. Towards this end, Western Blot (WB) or immunoblotting is the most common technique to detect specific protein markers associated to MVs and EXOs. Tetraspanins are a family of proteins involved in several cell processes as cell adhesion, invasion, motility, and signaling. Tetraspanins CD9, CD63, and CD81 are highly expressed in EXOs and have become their main marker in WB[100]. Besides CD8, CD63, and CD81, Alix, an important protein in the formation of EXOs; and Flotillin, a protein that plays an essential role in membrane fusion, are widely used as EXOs markers in WB[101]. On the other side, to characterize MVs, membrane proteins of the mother cell are typically used as MVs markers since they directly bud from the plasma membrane of the mother cell. For instance, Grange and colleagues used CD105 as a marker of MVs derived from $CD105^+$ cancer stem cells[18]. Moreover, if a more comprehensive biological characterization of EVs is needed, lipid, protein, and nucleic acid content are usually assessed by lipidomic, proteomic, and transcriptome profiling. Towards this end, we offer a complete proteomics analysis of MDA-MB-231-derived EXOs including the detection of main exosomal markers (CD9, CD63, CD81, Flotillin, and ICAM-1) in chapter 4.

In the same manner, physical properties like morphology, size, concentration, and charge have crucial contributions to the function and working mechanism of EVs (Figure 1.4). For example, EV size[102] and charge have been shown to play a pivotal role in molecular interactions and internalization by cells[103]. Electron microscopy is the standard technique to image EVs and study their morphology while atomic force microscopy

(AFM)[104] is typically the gold standard to study EVs structure[105]. For EVs size measurements, Nanoparticle Tracking Analysis (NTA) and Dynamic Light Scattering (DLS) are the most commonly used methods[105]. Both techniques analyze the Brownian motion of EVs to find their size, but NTA measures the particle diffusion and DLS measures the changes in scattering intensity of the bulk sample. Although less common, high-resolution flow cytometry could also be used to measure the size of fluorescently labeled EVs[106]. NTA is also the traditional system used to measure EV particle concentration followed by Resistive Pulse Sensing (RPS) which uses the principles of the Coulter effect to measure EVs particle concentration and size [107]. To find EV charge,

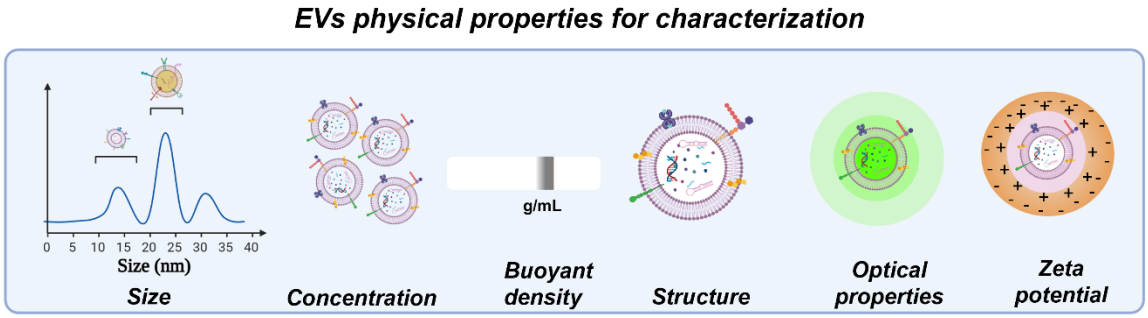

Figure 1.4. Physical properties and quantification of EVs. Size, concentration, density, structure, optical properties, and charge are the most studied physical properties of EVs. All these characteristics play an essential role in EVs function and interaction with cells[105].

Laser Doppler electrophoresis (LDE) and Electrophoretic Light Scattering (ELS) are widely used to find the Zeta potential of EVs, a measure of the surface potential that indicates surface charge and colloidal stability of EVs; RPS is also suitable to find EVs charge[108].

A complete characterization including both biophysical and compositional aspects will generate a deeper knowledge of EV origin and biological function[105]. EV characterization aspects required are determined by the information needed for the

particular study and by the minimal requirements established by The International Society for Extracellular Vesicles (ISEV) for published work. Due to the large increase in scientific publications involving EVs and their physiological and pathological roles in the past two decades, the ISEV established the Minimal Information for Studies of Extracellular Vesicles ("MISEV") guidelines in 2014 and an updated version in 2018[109]. The MISEV includes: a) a quantitative measure of the source of EVs such as the number of secreting cells, mass of tissue, or the volume of biofluid used; b) a measure of the abundance/density of EVs like total particle number or concentration, protein content, or lipid content; c) a test for the presence of proteins associated to EVs like immunoblotting to test specific markers of MVs and EXOs ; and d) a test for the presence of non-vesicular, co-isolated components such as immunoblotting for the detection of proteins contained in the cells as well as in MVs and EXOs, such as actin. All the guidelines dictated by MISEV were followed for the characterization of EVs in our work as seen in chapter 3 and 4.

1.4. Molecular interactions between EVs and cells

1.4.1 EV targeting to cells

One of the key features of EVs is their large and highly interactive surface area, compared to their volume. Their complex surface composition including, but not limited to, proteins, lipids, glycans, and proteins specific to the mother cell, play pivotal roles in EV surface interactions with components of the extracellular space[110]. EV surface composition mediates and facilitates many biological processes including EV motility, target cell recognition, contact and fusion to the targeted cells and cellular uptake of EVs. Both, EV surface composition and the origin of the mother cell, influences the types of

target cells for a specific kind of EV. Targeting of cells by EVs relies on cells having appropriate receptors for surface components to allow EV contact and binding (Figure 1.5). Since EV-cell interaction is a specific process, not all types of EVs interact with all types of cells. For instance, Lösche and colleagues showed that platelet-derived EVs interact with endothelial cells and macrophages but did not exhibit any interaction with neutrophils[111]. However, conversely, several groups have shown that neutrophil-derived EVs can interact with macrophages, endothelial cells, and platelets[112-114].

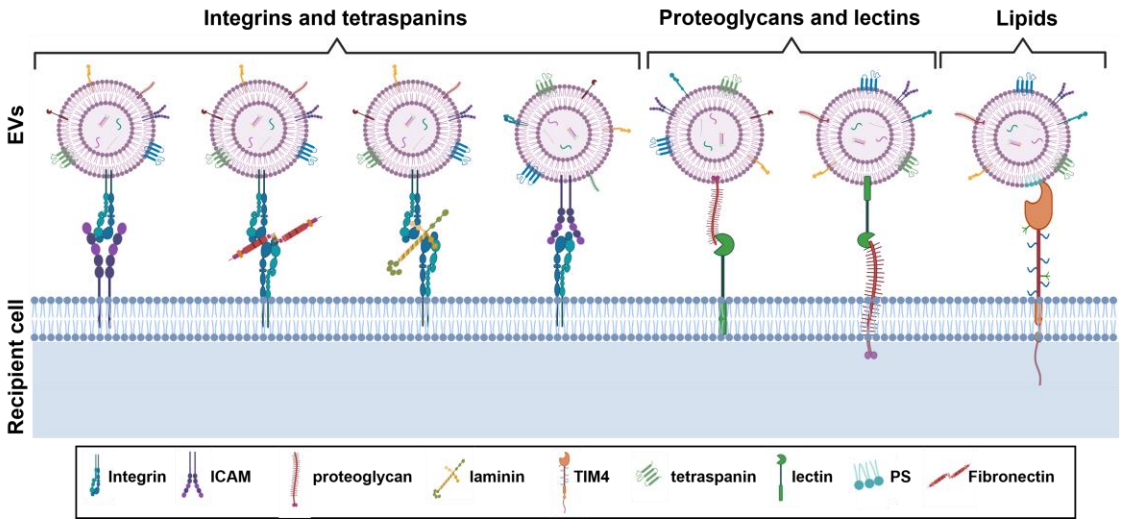

Figure 1.5. Molecules involved in EV-cell contact and binding. EVs surface components including integrins, proteoglycans, tetraspanins, adhesion proteins, ECM proteins, and lipids, mediate the contact and binding of EVs to target cells[115]. PS: Phosphatidylserine, TIM4: PS receptor, ICAM: intercellular adhesion proteins. *Created with BioRender.com*

The same pattern of specificity is observed *in vivo* where EVs from specific origins interact with different target tissues/cells. In a study done by Wiklander and colleagues, mice treated with EVs from different origins showed that melanoma derived EVs were mostly attracted to the GI-tract and lung areas while dendritic cells derived EVs mostly accumulated around the spleen[116].

1.4.2. Mechanisms of interaction between EVs and target cells

Several interactions between EVs and target cells have been established, mostly classified as direct interactions with the membrane or interactions mediated by a receptor in the membrane of target cells. The mechanisms of EV-target cell interactions have been studied and summarized by some thorough reviews[115, 117, 118]. However, they can be simplified in three main types: EVs attach to the surface or the target cells followed by: 1) direct fusion with the plasma membrane and release of EV cargo; 2) binding to a receptor and activation of signaling pathways and downstream response; and 3) EV internalization by several types of endocytosis and internal fusion with endocytic membranes and release of EV cargo into the cytoplasm (Figure 1.6)[110, 115, 119, 120]. Outcomes of such interactions differ from case to case depending on the origin of EVs, the nature of the interaction, and the type of target cell. In the case of cancer derived EVs, existent evidence shows that such interactions lead to disease characteristic behavior in the recipient cell[4, 9, 18, 20]. The surface composition of EVs influences the type of recipient cell to target, whereas the kind of interaction (1, 2 or 3 in Figure 1.6) taking place between the EV and the recipient cell, is mostly influenced by the surface composition of the targeted recipient cell[115]. For instance, pancreatic cancer derived EVs were successfully internalized by peritoneal exudate cells but their uptake was significantly lower when internalized by T-cells[121]. These findings suggest that EV-cell interactions are highly specific and depend on the right combination of ligand and receptor in EVs and target cells. Therefore, EVs might be able to interact and influence different types of cells but the mechanisms leading to it differ from cell to cell[19]. These questions are still open and an active area of research.

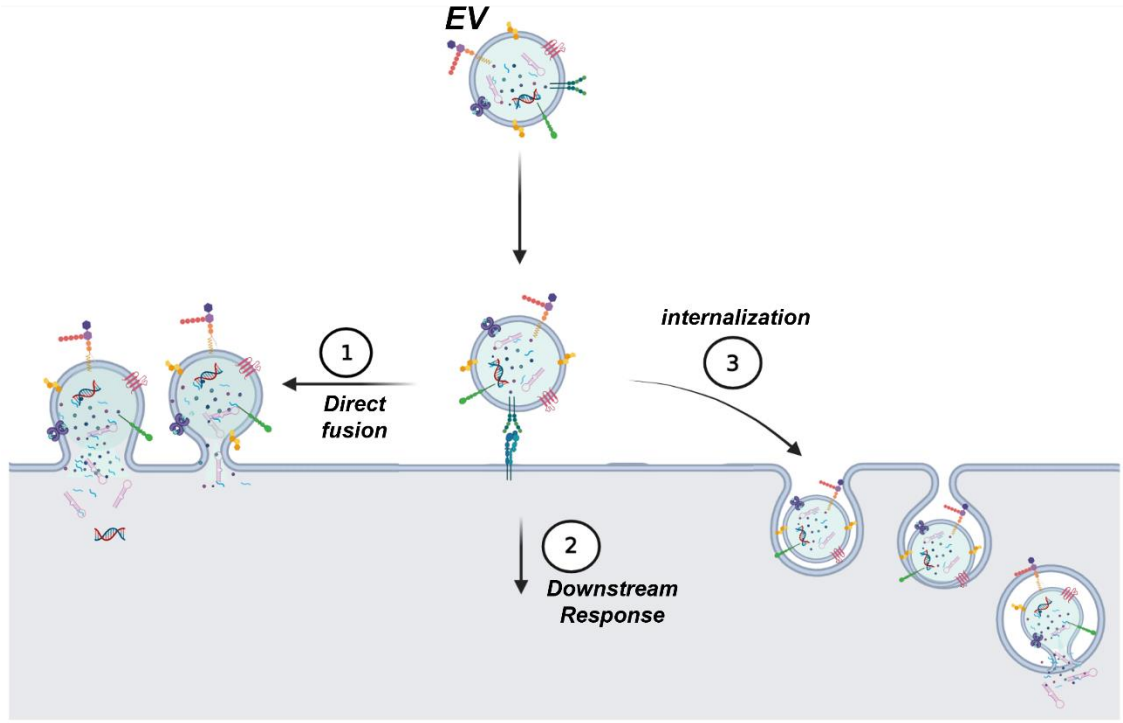

Figure 1.6. Mechanisms of interactions between EVs and target cells. After initial contact, there are three main routes employed by EVs to generate an effect on target cells. 1) EVs fuse directly with the plasma membrane of the target cells and release their cargo; 2) EVs generate a signaling response by interacting with surface components of the target cell, and 3) EVs are internalized by the target cell by several endocytosis pathways. *Created with BioRender.com*

1.5. Supported lipid bilayers as a cell membrane model system

Supported lipid bilayers (SLBs) are a gold standard cell membrane model system commonly used in several research fields to study the cell membrane, biomolecular interactions of their components, and biointeractions with external particles[122]. SLBs mimic the configuration of the cell membrane, harbor the hydrophobic phase to protect its constituents, and allow lateral diffusion of its lipid and protein constituents[33]. Their solid support and two-dimensional geometry allow the use of several characterization techniques described in detail in chapter 2[25]. SLBs are commonly formed on a solid

hydrophilic surface by several means: 1) the *fusion of vesicles*, 2) by transfer of sequential monolayers with the *Langmuir-Blodgett* technique, or 3) by a mixture of both techniques. However, several other techniques for formation of SLBs have been established and will be reviewed in detail in Chapter 2.

Although some of the formation techniques allow incorporation of proteins into the SLBs to better mimic the cell membrane, it is often a challenging process. One of the main issues is the small aqueous space between the solid support and the bilayer (~1.0-2.0 nm)[27, 123], which often is not enough to accommodate and allow mobility of the extracellular domain of some proteins, resulting on non-diffusivity in the plane of the membrane or in protein denature[124]. Towards that end, several groups have incorporated polymer cushions directly on the solid support to increase the water gap between the support and the bilayer and to allow the incorporation of transmembrane proteins with long cytoplasmic domains in a laterally mobile form[125, 126]. This polymer cushion provides stability through their linkage of the bilayer to the solid support and a soft support for the bilayer. Cellulose[127] and dextran[128] have been successfully used as cushions for SLBs but polyethylene glycol (PEG) functionalized with lipids or acyl chains is by far the most common polymer cushion used[26, 129]. Incorporation of PEG as a cushion is thought to create a larger lubricating water space, estimated to be between 5.0-10 nm depending on the length of PEG[130], between the support and bilayer to allow incorporation of transmembrane proteins. Besides creating a larger water space, PEG has an antifouling nature resulting in minimal interactions with proteins and lipids, within the bilayer[131, 132]. Another major challenge of protein incorporation into SLBs is the reconstitution of membrane proteins into vesicles can result in altered or denatured

proteins[133]. In this regard, our group has developed a technique to introduce membrane proteins into SLBs using cell membrane blebs to form hybrid SLBs (Figure 1.7).

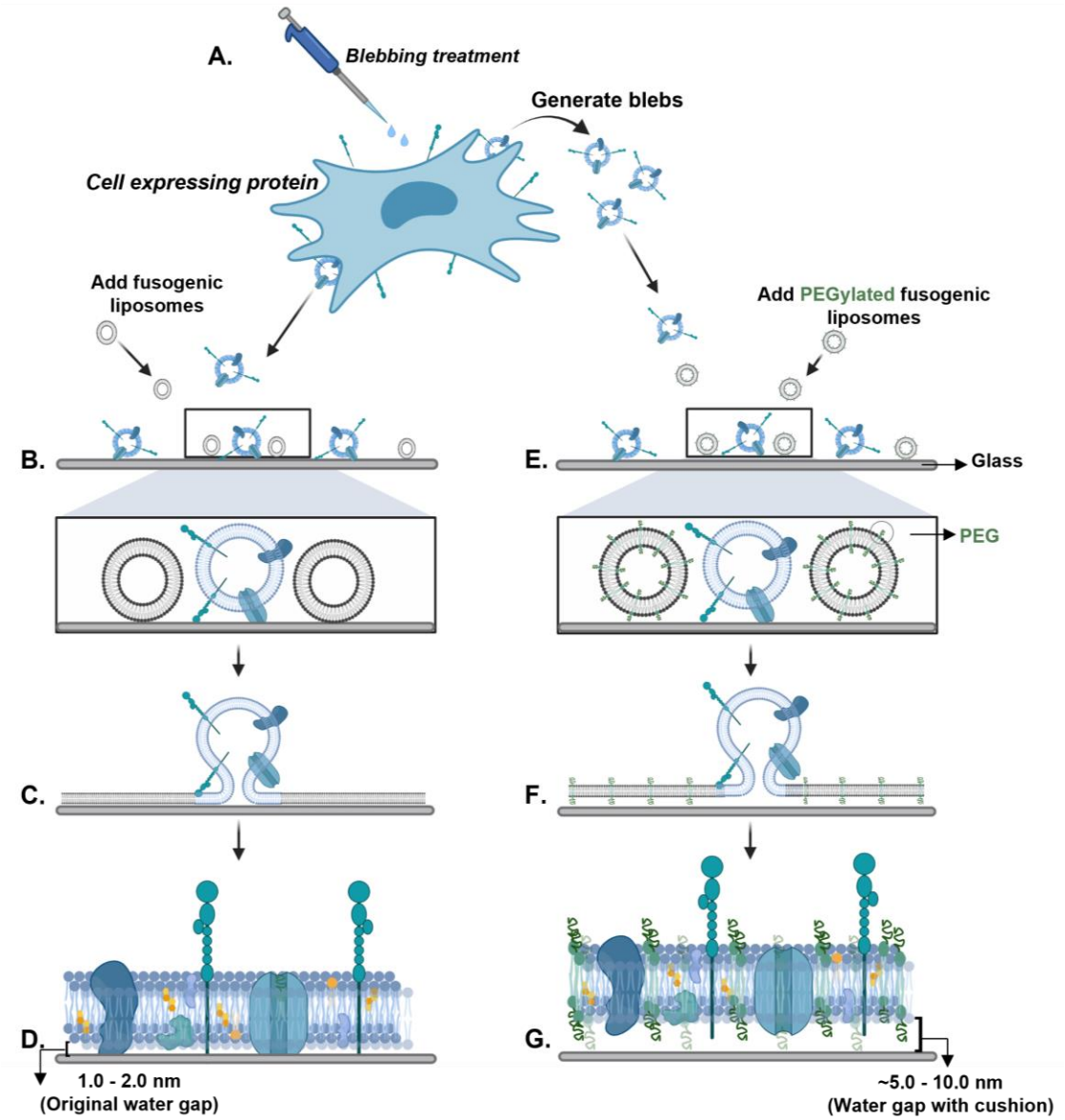

Figure 1.7. Formation of hybrid SLBs without and with cushion. A) Cell blebs are generated from the mother cell through chemical treatment. Blebs expressing native proteins of the mother cell are initially adsorbed into the glass support followed by addition of B) fusogenic liposomes or E) fusogenic PEGylated liposomes. Spontaneous rupture of liposomes (C) or PEGylated liposomes (F) induces rupture of blebs to form a SLB. D) SLB components are stuck to the glass, due to the small water gap, and are not mobile compared to G) where proteins are able to diffuse in the plane of the bilayer as a result of the extra lubricating water space created by the PEG cushion. *Created with BioRender.com*

Cell membrane blebs are proteoliposomes bud by the plasma membrane of the mother cell by chemical treatment. Blebs are adsorbed into a solid support and fused with the help of PEGylated liposomes via *vesicle fusion* to form a SLB that retains the membrane proteins from the mother cell membrane and have a larger water space between the bilayer and the support as seen in Figure 1.7 [33]. We have previously shown that our cell membrane bleb bilayer is a great biomimetic mammalian cell surface platform that preserves protein orientation, mobility, and activity under certain conditions[34]. Therefore, we used this technique to create systems to mimic the membrane of EVs and cell membrane of ADSCs for the rest of this work.

1.6. Summary:

Many types of eukaryotic cells produce EVs, but their secretion is upregulated during cancer. Two main EVs subpopulations include MVs, bud from the cancer cell plasma membrane and are typically between 120-1000 nm; and EXOs, ranging between 30 and 120 nm in diameter, are originated in the multivesicular bodies and as that fuse with the plasma membrane, EXOs are secreted into the extracellular space. Both EVs types have complex surface and cargo compositions including proteins, lipids, and nucleic acids. EVs play an important role in the tumor microenvironment (TME) facilitating intercellular communication between cells in the tumor and those in the stroma and on distal sites. That exchange of information between cells favors tumorigenesis and cancer progression in different ways including promotion of angiogenesis, EMT, and cancer immunosuppression. For instance, interactions between breast cancer EVs and ADSCs, an important cell type in the TME, and subsequent transfer of oncogenic information, induce upregulation of VEGF secretion in ADSCs and their

differentiation to myofibroblasts. Both outcomes highly favor tumorigenesis by contributing to a highly inflamed TME and to angiogenesis to promote tumor proliferation facilitating the access of nutrients and oxygen. The specific interactions between breast cancer EVs and ADSCs leading to those outcomes have not been understood, in part, due to the absence of techniques to study them and to decouple surface interactions from internalization or cargo delivery. Towards this end, in the next chapters, I will introduce two *in vitro* systems to facilitate the isolation, study, and screening of blocking strategies of surface interactions between EVs and ADSCs. SLBs are the standard membrane model system to study the cell plasma membrane and its interactions with external agents. Our group developed a method to integrate membrane proteins into SLBs using cell membrane blebs, proteoliposomes shed by the cell membrane, to form hybrid SLBs. Using this method, I made two hybrid SLBs platforms that incorporate membrane components of breast cancer EVs, both MVs and EXOs, and of ADSCs, making fine biomimetic membrane models of EVs and ADSCs membrane. Insights into their development and applications will be presented in chapters 3 and 4. Additionally, the next chapter reviews SLBs formation, characterization, and applications in cell culture, as the main system used in this body of work.

CHAPTER 2

2. FUNCTIONALIZATION OF SUPPORTED LIPID BILAYERS WITH ADHESION PROTEINS AND PEPTIDES FOR CELL CULTURE APPLICATIONS: A REVIEW

Johana Uribe[1], Miriam Huerta[2], and Susan Daniel[1,2]*

[1]Meinig School of Biomedical Engineering, Cornell University, Ithaca, NY.

[21]Robert Frederick Smith School of Chemical and Biomolecular Engineering, Cornell University, Ithaca, NY

2.1. Acknowledgements

This chapter is being prepared for publication. Johana Uribe is the first author, Susan Daniel is the corresponding author, and Miriam Huerta is a co-author.

2.1.1. Individual acknowledgements

JU: Determined the scope of the review, did literature research, and wrote the content of the review article. **MH:** discussed and edited manuscript. **SD:** advise on scope of the review, discussed and edited manuscript.

2.2. Abstract

The development of biofunctionalized substrates that support cell adhesion and growth is an ongoing effort in several fields including tissue engineering and drug development. Glass and polystyrene treated with ECM proteins, like fibronectin and collagen, or adhesion peptides, such as RGD and IKVAV, are the most common substrates for cell culture. Despite the value of these approaches, they have their limitations, as they do not fully recapitulate all of the characteristics of a cell's microenvironment. This can lead to altered morphology and non-physiologically relevant cell behavior[134]. Supported lipid bilayers (SLBs) have recently emerged as cell culture platforms with several applications including immunology[135], neurology[136], stem cell differentiation[137, 138], among others. SLBs are the standard cell membrane model and can mimic the native configuration and two-dimensional fluidity of the cell membrane, providing a better biomimetic model of the cell microenvironment[32]. Numerous techniques have been developed to biofunctionalize SLBs to better recapitulate the *in vivo* cell microenvironment and provide a more accurate cell culture system. Here, we review several studies and approaches used to functionalize SLBs with ECM adhesion proteins and adhesion peptides to study a wide range of cellular processes including neural cell adhesion[139], adherence junction formation[140], and stem cell differentiation[138].

2.3. Introduction

Creating biofunctionalized surfaces for cell culture systems is an ongoing area of research that is relevant to many applications including tissue engineering, regenerative medicine, cell-based diagnostics, and drug screening and development. The most

traditional and common systems used to adhere and support cell growth have been glass and polystyrene (PS) substrates. Glass was historically the first cell culture surface used at the beginning of the 20th century[141, 142]. Its broad availability, compatibility with solvents for easy cleaning and reuse, and transparency, made it the perfect candidate. For instance, experiments that advanced cell culture with the establishments of famous line cells like HeLa and CHO, were performed on glass vessels[141]. However, with the plastic boom of 1950s in many industrial areas, plastic, particularly PS, became a popular cell culture surface in many labs[143]. PS also offers great optical clarity, and it is widely available, and it is disposable and inexpensive. Because of these advantages and its compatibility with mass production, PS soon replaced glass and became the standard platform for cell culture[144]. Glass, on the other hand, is still the preferable choice for imaging since its low refractive index allows better image quality[145].

Although these mechanical and physical properties made glass and PS adequate candidates for cell culture, cell adhesion and growth are difficult in the native form of both materials since they are far from replicating the *in vivo* cell microenvironment consisting of an organized combination of extracellular matrix (ECM), physical properties, and mechanical support and applied forces[146, 147]. To overcome this drawback and in an effort to better represent the native cell microenvironment, biofunctionalization of PS and glass surfaces has been done using biological and synthetic materials able to improve cell attachment and spreading. The most common biological coatings include ECM proteins such as collagen, fibronectin, and laminin, and adhesion proteins like RGD; and synthetic coatings commonly include poly-lysine and poly-L-ornithine[148]. Although these treated platforms greatly favor cell adhesion and development, they still

lack the rich mechanical properties characteristic of the cell microenvironment leading often to physiologically irrelevant cell morphology and functions[134, 149].

Recently, SLBs have emerged as alternative cell culture systems that better mimic aspects of the *in vivo* cellular microenvironment and facilitate the study of processes occurring at the cell membrane interface. Complex processes such as cell adhesion, cell-cell and cell-ECM interactions and drug interactions have been studied using SLBs [150-153]. SLBs can mimic the native configuration of the cell membrane by recapitulating the membrane's protein and lipid content, two-dimensional fluidity, and the surrounding ECM that make up the cellular microenvironment. These biomimetic characteristics have made SLBs the standard model cell membrane system and an attractive cell culture platform in many areas of research [25-31]. In particular, SLBs have been crucial to study of specific cell-cell interactions within the immune system since the 1990s[27, 154]. Specifically, they have been used to reconstitute the immunological synapse[155], immune cell adhesion[156] and T-cell activation[135, 157]. In addition, SLBs have been used as a cell culture platform for studies of neuronal activation and synapse[30, 31], the cell-ECM microenvironment[151], mechanobiology[152, 158], stem cell adhesion and differentiation[137, 159], virus-cell fusion[160, 161], extracellular vesicle-cell interactions[9], and signaling studies[162]. The SLB system offers many advantages including: i) easy composition tunability, ii) complete control over the bilayer composition, iii) compatibility with several characterization and imaging techniques because of their planar geometry and rigid support, and iv) cell membrane lateral diffusivity, allowing mobility of the proteins present or functionalized on the surface of the bilayer mimicking native movement on the cell membrane. These unique characteristics make SLBs an ideal tool to study a diverse

range of membrane interactions at this interface. SLBs are also biocompatible because they are composed of zwitterionic lipids, which are nonfouling and resistant to the nonspecific adsorption of proteins and cells. Far from being a "disadvantage" of these systems, this aspect can be engineered to control the adsorption of proteins and attachment of cells to these platforms [32, 158, 163-168]. Towards this end, several research groups have modified SLBs nonfouling nature to enhance cell adhesion using different physiological and/or compositional strategies. In this review, we survey the main techniques used for the formation and characterization of SLBs. We also present the techniques implemented to biofunctionalize the surface of SLBs with adhesion proteins and peptides and their applications as cell culture platforms in different research areas.

2.4. Supported lipid bilayer (SLBs) formation and characterization

2.4.1. Methods for the formation of SLBs

Supported lipid bilayers coupled to solid supports are formed in one of three ways: vesicle fusion [169], Langmuir Blodgett/Langmuir Schafer[165, 170], or a combination of the previous two techniques: Langmuir-Blodgett/vesicle fusion[169]. In addition to these standard approaches, alternative methods to form SLBs on solid supports include using lipid/detergent mixed micelles[171-173], a droplet interface bilayer method, a solvent-assisted lipid bilayer (SALB) technique, and bicelle fusion [174].

2.4.1.1. Vesicle fusion technique

Vesicle fusion (VF) was first introduced as a technique to form SLBs 30 years ago by Brian and McConnell[175] and Kalb et al.[176]. VF is considered the simplest SLB formation technique and is based on the idea that when vesicles encounter a clean hydrophilic support, they fuse spontaneously and form a supported bilayer[25, 170, 175, 177].

Small unilamellar vesicles (SUVs) of pure lipid composition or proteoliposomes between 20 to 100 nm[178] are prepared by the desired method and used as the starting material. SUVs are usually prepared by extruding a lipid solution through a polycarbonate membrane with pores <100 nm at high pressure[165, 179]. However, other methods such as sonication and ultracentrifugation of lipid solutions[180] and variation of pH[181] have been successfully used to form them. The prepared bulk solution of SUVs is then added onto a clean hydrophilic surface (glass, quartz, or mica), where the vesicles adsorb, rupture and fuse with another one to form a continuous bilayer; unruptured SUVs are washed out with a buffer (Figure 2.1a)[170, 173, 175, 182, 183]. Although there are some gaps on the understanding of SLB formation via SUVs fusion, it is thought that after a critical concentration (θ_c) of SUVs are adsorbed onto the support, an initial vesicle fuses spontaneously with the support forming a SLB patch. Other SUVs interact with the active or energetically unfavorable edge of that SLB patch and fuse with it to form a continuous bilayer[25, 182]. Interactions between SUVs and their subsequent fusion to form a continuous bilayer depend on different conditions, such as their size, composition, and electrical charge[25, 165, 182], as well as the properties of the surface used as a support and the temperature[184, 185]. Various strategies can be used to enhance the fusion of SUVs to the surface such as the addition of fusogenic compounds like polyethylene glycol (PEG)[9, 186] and creating osmotic pressure through the SUV membrane[165, 182, 185].

VF is an easy and accessible technique that enables high-quality SLBs to be generated using simple equipment. It is also a very versatile technique allowing the SUV's lipid composition to be tuned to fit the desired experimental specifications[165, 173, 182]. This adaptability has made VF the base method to form multilayer supported lipid

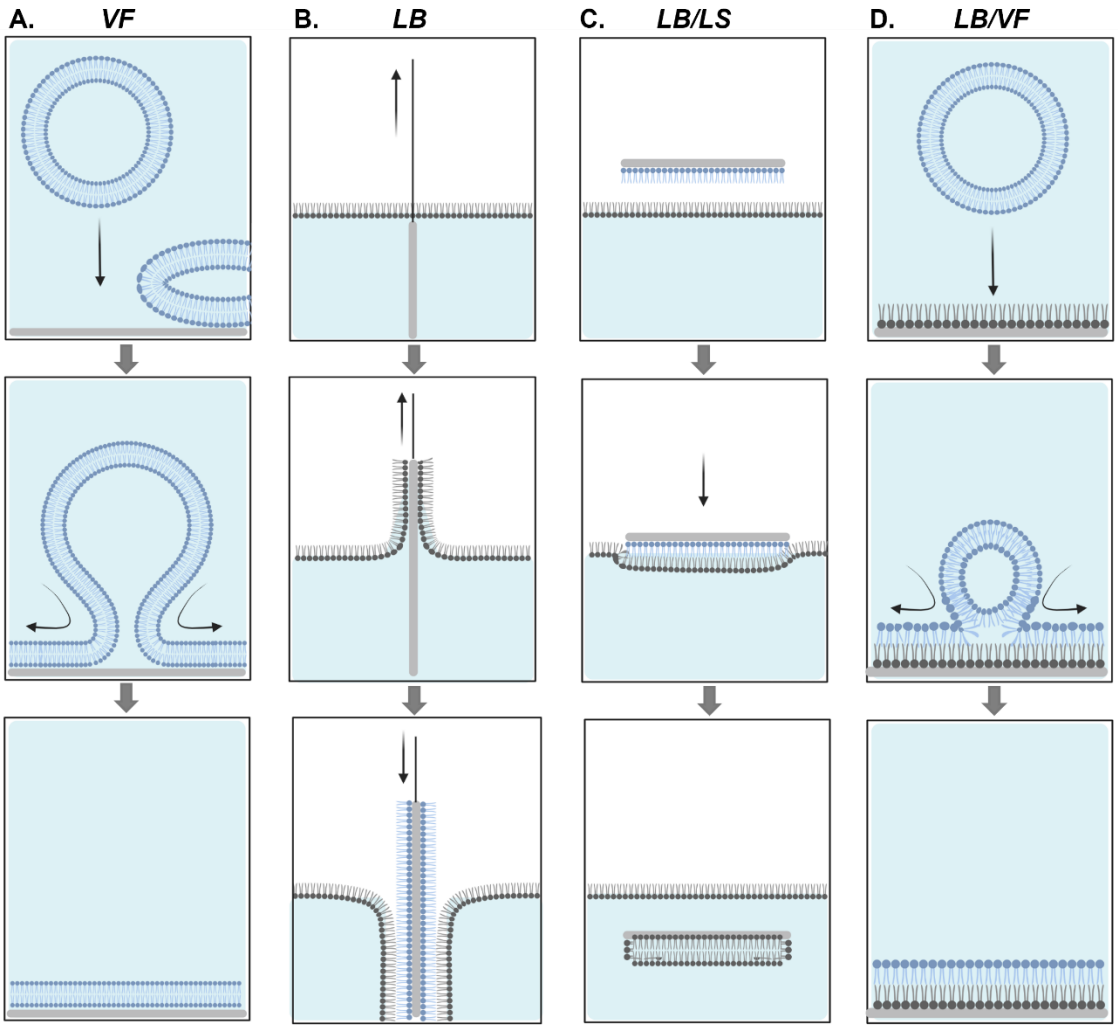

Figure 2.1. Methods for preparation of supported lipid bilayers. A) In the vesicle fusion (VF) method, vesicles are adsorbed onto a support, where they rupture and form a bilayer spontaneously. VF is the simplest and most common method to form SLBs but is not useful preparing asymmetric bilayers. B) In the Langmuir-Blodgett (LB) method, the solid substrate is drawn through a monolayer of one lipid A (blue) and pushed through a second layer of lipid B (gray) producing an asymmetric layer. C) In the Langmuir-Blodgett/Langmuir-Schaeffer (LB/LS) method, formed monolayers are transferred to a solid substrate in consecutive operations. D) LB/VF method allows asymmetric bilayers to be made in situ and are ideal for conducting measurements on SLBs immediately after preparation. Adapted from Sanderson et al.[187]. *Created with BioRender.com*

membranes[169, 188, 189] and complex SLB systems[182]. For instance, hybrid SLBs which are composed of supported bilayers containing lipids and cellular membrane components, are complex SLBs that closely mimic the native cell membrane of the originating species and are formed using the VF method[9, 34, 190]. Moreover, polymer-supported bilayers,[170]

formed by SUV fusion on a polymer-treated surface, make excellent cell culture systems where the polymer works as a cushion between the SLB and the solid support allowing lateral mobility of proteins[131, 191]. In the same manner, complex SLBs needed to study SLB-live cell interactions are commonly generated using the VF method and functionalized using different strategies such as biotinylation[192, 193], thiol maleimide covalent coupling[140, 193], and protein incorporation[177, 193] .

One of the original drawbacks of the VF method was the inability to visualize and study domains within the bilayer, such as lipid rafts and protein clusters, using epifluorescence microscopy due to their small size and difficulty to detect [170]. However, techniques like atomic force microscopy (AFM), fluorescence recovery after photobleaching (FRAP), and total internal reflection fluorescence microscopy (TIFRM) can be utilized to overcome those challenges due to their high optical resolution. Another disadvantage of using the VF technique to form SBLs is the inability to control the orientation of the proteins within the supported bilayer[170] and the difficulty in making asymmetric bilayers containing two different membrane layers[183].

2.4.1.2. Langmuir-Blodgett technique

The Langmuir-Blodgett (LB) was historically the first technique developed to form SLBs. Developed by Irving Langmuir and Katharine Blodgett in 1919[194], this technique allows the transfer of a fatty acid monolayer at the air-water interface onto a solid substrate. This technique was not adapted to form SLBs until Tamm and McConnell did so in 1985[27]. The LB technique results in the formation of stacked layers of amphiphilic molecules such as lipids. Because of their innate properties, these molecules self-organize in the air-water interface to minimize free energy and form a monolayer

with headgroups immersed in the liquid phase and tail groups facing the air or gas phase, known as a Langmuir film[195]. Using a Langmuir trough filled with a subphase (water or buffer), the monolayer is transferred from the air-water interface to a hydrophilic substrate (glass, quartz, mica, silicon dioxide, silicon wafers, or thin sections of metals). The transfer is done by dipping a hydrophilic slide into the subphase or buffer and retracting it slowly, while the surface pressure is kept constant by compressing the remaining part of the monolayer. During this process, the hydrophilic headgroups of the monolayer interact with the hydrophilic surface, transferring the monolayer to a solid support[195, 196]. To form a SLB, a second monolayer is transferred by submerging the substrate into the subphase and repeating the process, as seen in Figure 2.1b. Therefore, multilayers can be built by successive transfers of monolayers onto a substrate[165, 182]. The LB technique is often used to transfer the first or LB monolayer, and the outer monolayer is transferred to the substrate by a technique known as the **Langmuir−Schaefer (LS) technique**. Vincent Schafer and Irving Langmuir first introduced the LS technique to form pepsin and urease monolayers[197]. This technique is similar to the LB method, but the substrate is submerged in the subphase in a parallel orientation to the air-water interface for deposition of the monolayer. This is in contrast to the perpendicular orientation used in LB technique. Because of the substrate orientation during monolayer transfer, the LS method is also known as horizontal deposition[196, 198]. The LS technique is frequently used to deposit the outer monolayer to form a SLB, as shown in Figure 2.1c.

The LB/LB and LB/LS techniques are commonly used to form asymmetrical SLBs since the composition of both monolayers is not necessarily identical. The ability to form asymmetrical SLBs is the main advantage of these methods in comparison to the

VF technique since membrane asymmetry is an important property of cells. Furthermore, this technique allows control over the thickness and molecular organization of the SLB. However, the LB/LB and LB/LS techniques are not without their limitations. As evidenced by Tamm and McConnell's[27] pioneering work using LB, one of the main disadvantages of this method is the difficulty of incorporating transmembrane proteins into the monolayers. This is because part of the monolayers is exposed to the air-water interface before monolayer transfer onto the substrate and this exposure can lead to the irreversible denaturing of membrane proteins.

2.4.1.3. Langmuir-Blodgett/vesicle fusion technique

The Langmuir-Blodgett/vesicle fusion (LB/VF) technique, which combines the LB and VF methods, was first used to form an SLB on a quartz supported LB monolayer [176]. The inner first supported monolayer is formed first using the LB method by transferring a lipid monolayer from the water-air interface to a hydrophilic substrate. Then, using the VF method, unilamellar vesicles added to the dry LB monolayer fuse, forming the outer or second layer of the SLB (Figure 2.1d). The LB/VF technique offers the following advantages over the LB and VF methods: i) incorporation of transmembrane proteins, by integrating them into the lipid vesicles, in the SLB[199-201], ii) creation of asymmetric bilayers[202], iii) and the formation of each monolayer from different compositions[165, 203]. In addition, the lateral diffusion of integrated transmembrane proteins in the SLB can be increased by adding a polymer cushion between the bilayer and the substrate, like in VF[131, 204, 205].

2.4.1.4. Emerging techniques for SLB formation

Although VF, LB, and variations on these methods are the most common techniques used to form SLBs, several promising methods to form SLBs have been developed including spin coating, solvent exchange, and bicelle-based approaches. Mennicke and Salditt[206] first introduced **spin coating (SC)** in 2002 as a method to create stacks of more than two SLBs, which is not possible with any of the previously mentioned techniques. To make SLBs, a lipid mixture dissolved in an organic and volatile solvent is deposited and spread onto a clean substrate on a spin coater. Next, it is accelerated to a desired rotational speed (usually 1000-3000 rpm) to remove the solvent and generate a dry lipid film that is then hydrated with the preferred buffer[126, 170, 207]. The main advantage of the SC technique is the ability to form highly oriented stacks of up to 30 bilayers[196, 206]. Since SC is still a new technique, integrating proteins into the SLB using this method has only been done with peptides and short membrane proteins mixed with the initial lipid composition[208, 209]. Additionally, Mashaghi and Van Oijen combined VF and SC and fused proteoliposomes containing membrane proteins on a SC-produced SLB[129].

Solvent-assisted lipid bilayer **(SALB)** is based on the solvent-exchange concept, which shows that as the solvent of a phospholipid mixture is exchanged from isopropanol to water, the phospholipids have a series of phase transitions from inverted micelles to lamellar phase vesicles leading to the formation of a SLB[210, 211]. The **SALB** technique was first introduced by Tabaei et al[212] in 2015 to easily form SLBs on silicon dioxide and gold. In their method, lipid mixtures in a water-miscible organic solvent (preferably isopropanol) on a solid substrate, are changed to an aqueous buffer in a single solvent exchange step forming a SLB[174, 212]. The main advantages of SALB are: i) simple

experimental preparation, since lipids are dissolved in an organic solvent, ii) the ability to use several types of substrates and lipids, and iii) the simplicity of the equipment needed[174, 213, 214]. The main disadvantage of the SALB method is the need for extensive washing of the SLB after formation to assure complete removal of the organic solvent (isopropanol) used initially [174, 211]. Moreover, incorporating membrane proteins into the SLBs using the SALB method is also challenging; the organic solvent-water mixture used during solvent exchange can lead to protein denaturation[174, 215].

The **bicelle method (BM)** was first introduced by Zeineldin et al. in 2006 to form supported and suspended lipid bilayers on flat and nanotextured silicon substrates[216]. In this procedure, a dry film of lipids is hydrated using a buffer followed by a series of freeze-thaw-vortex mixing cycles[174, 217]. Several groups have demonstrated the successful formation of SLBs using bicelle mixtures of both long and short-chain phospholipids[174, 216-218]. One of the advantages of using the BM is the ability to form SLBs with high cholesterol concentrations[219]. Jackman et al. showed that bicelles containing up to 40 mol% cholesterol formed homogeneous and complete SLBs; formation of SLBs with this high amount of cholesterol using conventional methods like VF is very challenging[220]. Furthermore, since bicelles are ideal environments to host membrane proteins[221, 222], the formation of SLBs with incorporated membrane proteins is a great advantage of BM[214]. To form SLBs using BM requires only simple laboratory equipment, such as a vortex and a sonicator. Moreover, SLBs can be formed using very low concentrations of lipids, or typically 10-fold less than the lipid concentration needed to form SLBs by VF[174, 217]. In the field BM is a new technique that shows great potential as a simple, cost effective and adaptable method to form SLBs.

2.4.2. Characterization of SLBs

One of the main advantages of the SLB system is the compatibility that their 2D geometry and solid support offer with several characterization tools. Fluidity and surface coverage are the main characteristics of SLBs since they are fundamental qualities of a strong cell membrane biomimetic model. The most common methods to characterize the SLB surface coverage and fluidity are fluorescence microscopy, quartz crystal microbalance with dissipation (QCM-D), atomic force microscopy (AFM), and surface plasmon resonance (SPR).

2.4.2.1. Surface coverage

SLBs surface coverage is commonly assessed using several types of fluorescence microscopy (FM). Simple techniques such as epifluorescence microscopy allow visualization of the integrity of the bilayer through imaging fluorescent moieties that are incorporated in the lipids or proteins used to generate the bilayer (Figure 2.2a). Higher-resolution FM techniques like near-field scanning optical microscope, Förster resonance energy transfer, and total internal reflection fluorescence (TIRF) have all been used to study the integrity of SLBs. These imaging techniques have also been used to examine more in-depth features of SLBs, including protein interactions[223], microdomains[224], lipid asymmetry[202, 225], and lateral diffusion of single proteins within the bilayer[226]. Additionally, research groups have previously characterized the lipid bilayer phases of an SLB using confocal microscopy[227] and two-photon fluorescence microscopy to examine the texture/surface of lipid bilayer domains[228]. Fluorescence microscopy also allows one to determine the lateral diffusion of a formed SLB, which is an essential feature of a good bilayer. Fluorescence recovery after photobleaching (FRAP) and fluorescence correlation

spectroscopy are two types of microscopies that have been used towards this end.

High-resolution FM techniques, such as near-field scanning optical microscope facilitate the visualization of small surface defects in a bilayer. Atomic force microscopy (AFM) has become the standard technique to study the nanoscale structure of SLBs, allowing the detection of surface defects on the order of 10 to 500 nm[196]. The basic principle behind AFM is a sharp nanoscale tip attached to a cantilever forms a spring to scan the surface of an SLB (Figure 2.2b). When the tip is in contact with the SLB, the cantilever bends, and the deflection is captured by a laser diode and a split photodetector. This deflection event is sensitively measured in piconewtons, and it is measured as a tip-SLB interacting force. AFM generate 3D images of the SLB surface for further analysis. Thus, this technique offers the measurement of a SLB's physical and mechanical properties at high spatial resolution and images surface defects at the nanoscale. AFM also can provide analysis of SLB interactions with detergents, peptides, proteins, drugs, and nanoparticles. Excellent reviews on the characterization of SLBs by AFM are available by El Kirat et al.[198] and Dufrêne and Lee[229].

In the last two decades, quartz crystal microbalance with dissipation (QCM-D) has become a standard technique to characterize SLBs[230]. This technique is used to verify their formation and assess bilayer quality, mass, and thickness. QCM-D can also provide information about SLB interactions with external components, such as nanoparticles [231]. QCM-D characterization of SLBs is usually paired up with an optical tool to visualize the formed SLB. QCM-D uses a quartz crystal sensor located between two electrodes excited by an electric field generating oscillatory movements[213]. Frequency and dissipation measurements from the oscillating sensor are generated, providing readouts on the

mechanical properties of the SLB such as mass, thickness, and viscoelasticity (Figure 2.2c)[173].

Surface plasmon resonance is another technique that provides real-time detection of SLB formation and interactions between the formed bilayer and external agents. Its basic principle is to measure the changes in the refractive index at the surface of a gold sensor as interactions between two agents are happening. One of the agents (*e.g.* a ligand) is immobilized on the surface of a gold sensor; the other agent (the analyte) is flowed in excess over the surface to allow binding[232]. Measurements generated by SPR allow the study of SLB formation, bilayer thickness, and membrane binding kinetics.

A combination of the methods described above can provide a complete characterization of SLBs. Parkkila and colleagues[233] used SPR and QCM to characterize SLBs originating from synthetic lipids on silicon dioxide surfaces. This strategy allowed them to assess the thickness, refractive indices, linear dispersion coefficient, and critical biophysical details of the SLB with great accuracy. Similarly, a combination of optical and analytical tools facilitates the improved analysis of the SLB formation process. AFM, QCM-D, and ellipsometry were used in combination by Richter et al.[234] to characterize the formation of synthetic SLBs on mica and provided a detailed picture of the mechanisms of lipid vesicle deposition. Using these methods, the authors obtained the kinetics of SLB formation (QCM-D), the overall quality, stability, and mobility of small regions of the SLB (AFM), and the total dry mass or desorption of lipids (ellipsometry).

2.4.2.2. Fluidity and lateral diffusion

The plasma membrane is a highly dynamic region in which integral-membrane proteins and lipids are continuously moving laterally. The appropriate localization and

lateral mobility of proteins within the membrane is partly determined by the fluidity of the membrane. One of the key features of a SLB is the retention of this membrane fluidity. Fluorescence recovery after photobleaching (FRAP) and fluorescence correlation spectroscopy (FCS) are techniques used to study SLB fluidity by assessing the mobility and lateral diffusion of membrane constituents. For both techniques, lipids or proteins forming the SLB are fluorescently labeled to enable SLB imaging by FM. FRAP employs a laser beam to photobleach a small area of the fluorescent bilayer, and the fluorescence recovery is monitored over time. In a fluid bilayer, fluorescently labeled components outside of the photobleached area will laterally diffuse through the membrane and restore fluorescence to the previously photobleached spot. That time-dependent fluorescence recovery data is used to find the diffusion coefficient (D) of the fluorescent tracer used (Figure 2.2d) [235]. Because of its simplicity, noninvasiveness, and compatibility with a wide range of FM tools, FRAP is the standard technique used to assess the lateral diffusivity of SLBs. FCS coupled with fluorescence microscopy is widely used to study molecular diffusion in SLBs as well. FCS focuses on small volumes (1 μm^3) of fluorescently labeled particles in the SLB, analyzes how the fluorescence intensity fluctuates in that specific area, and records measurements with high temporal resolution (Figure 2.2e). Using statistical analysis to measure the changes in fluorescence intensity over time, the diffusion coefficient (D, $\mu m^2/s$) of the fluorescent tracer can be obtained[236].

To study lateral diffusion of individual proteins, single-particle tracking (SPT) coupled with TIRF is a frequently used approach. Images obtained by TIRF are analyzed using specialized software to find the location of each fluorescent molecule (Figure 2.2f).

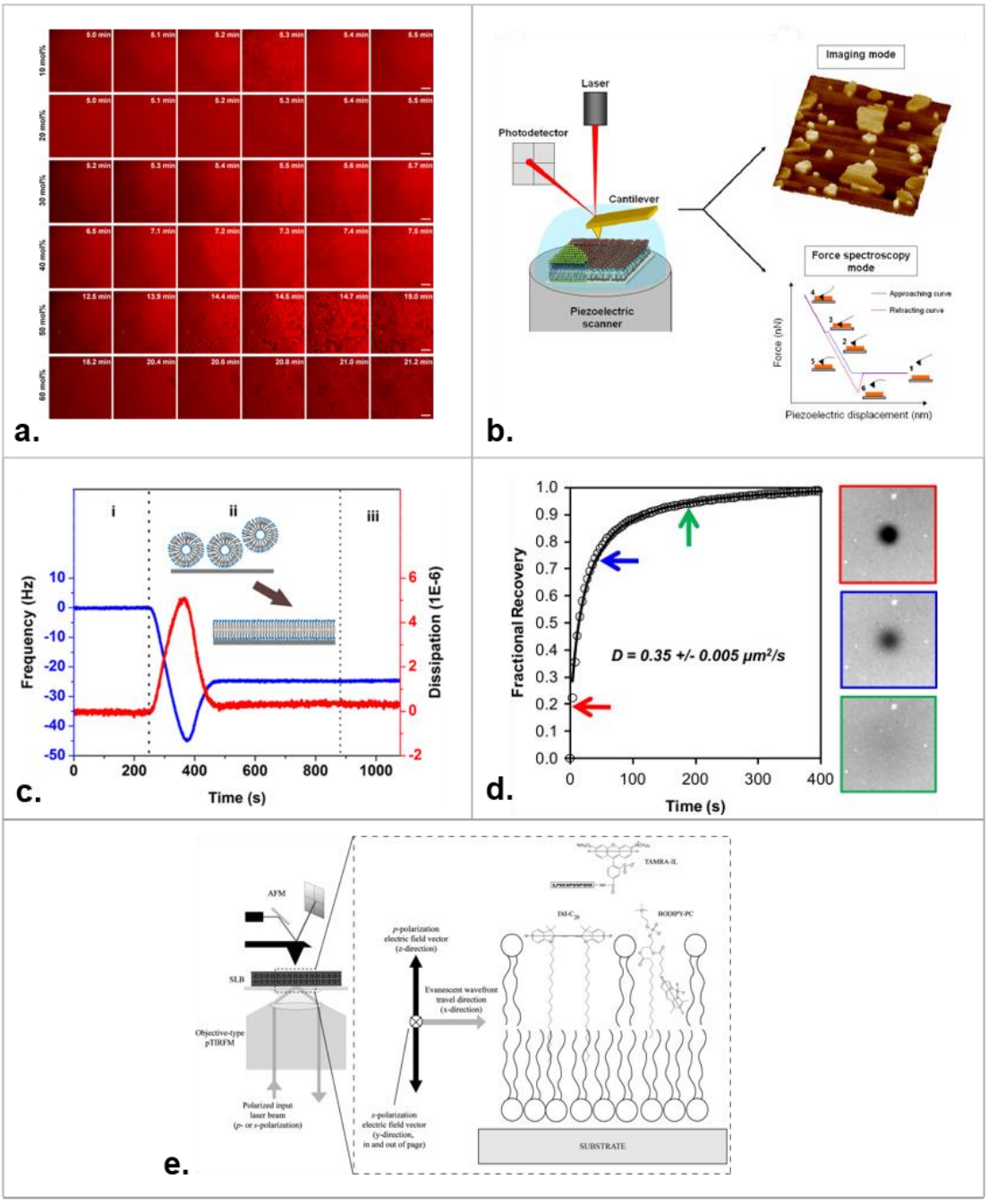

Figure 2.2. Methods for characterization of SLBs. A) Fluorescence microscopy (FM). Visualization of SLB formation from 10-60 mol % cholesterol-rich bicellar mixtures[219]. B) Atomic Force Microscopy (AFM). Schematic of AFM set-up with two modes: imaging and force microscopy. A 3D plot of Dipalmitoylphosphatidylcholine/Sphingomyelin (SM)/Cholesterol (Chol) 2:1:1 (mol/mol/mol) supported bilayer is presented as well as a typical force curve generated from a SLB[237]. C) Quartz crystal microbalance with dissipation (QCM-D); Representative frequency (blue) and dissipation (red) shifts during the formation of a DOPC-SLB on a silica surface at pH 7.4[238]. D) FRAP; fAPN supported bilayer characterization and mobility by FRAP. R18 fluorescence recovery after photobleaching in a fAPN supported bilayer. The images correspond to the times for each color-coded arrow on the plot. The data are fit to the

curve (black line) to obtain the diffusion coefficient[239]. E) TIRFM/AFM coupled for characterization of SLB and study of protein-membrane interactions[240].

Then single-molecule positions across the frames are linked, generating a molecular track for each molecule/protein studied[241]. SPT has been previously used to find the lateral diffusivity of lipids as well. For more in-depth information about these techniques, two reviews by Macháň et al.[236]. and Rose et al.[241] compare the three standard techniques used to study lateral diffusion in SLBs: FRAP, FCS, and SPT.

2.5. Biofunctionalization of SLBs for cell culture applications

2.5.1. Cell adhesion on SLBs

Cell adhesion is an important biological process by which cells contact other cells or extracellular matrix (ECM) components via protein complexes. Cell adhesion is an essential process that affects cell function, regulation, differentiation, migration, and communication[242]. Changes in cell adhesion are associated with disease progression for several pathologies, including cancer[243] and atherosclerosis,[244] making it an important process study in biomedical research today [245].

Most mammalian cells grown *in vitro* are anchorage-dependent, requiring strong attachment to a substrate for survival and proliferation[246]. The development of substrates that facilitate cell attachment and adhesion is therefore imperative in mammalian cell culture. Supported lipid bilayers have been recently gaining traction as cell culture platforms[32, 158, 247]. It was initially observed that SLBs generated from reconstituted lipids, such as POPC, are not a favorable substrate for cell culture because phosphocholine-containing lipids are zwitterionic, inert, and lack surface moieties essential for cell adhesion. As a result, cells are incapable of creating strong adhesions to these platforms[32, 158, 163-167]. Several strategies have been developed to modify SLBs to facilitate cell

adhesion, spreading and proliferation. We will review the most common SLB-based cell culture systems in the following section.

2.5.2. Functionalization of SLBs surface with adhesion peptides

The standard method used to functionalize the surface of SLBs for cell culture involves incorporating cell adhesion peptides into the bilayers themselves. The tri-amino acid sequence, arginylglycylaspartic acid (RGD), is the major integrin-binding domain mainly present within the ECM protein, fibronectin[248]. Due to its mediating role in cell adhesion to the ECM and its ability to bind multiple integrins, RGD has become the main adhesion peptide motif used to promote and control cell attachment to different biomaterials[249]. Additionally, RGD synthesis is a simple and low-cost process, and its orientation and density can be easily controlled. For instance, RGD has been previously utilized to functionalize SLBs surface and allow cell adhesion for different cell culture/tissue engineering purposes. Different techniques have been employed to incorporate cell-adhesive peptide ligands *(i.e., RGD ligands)* into the SLB surface to bind integrin receptors on the surface of cells and promote cell attachment (Figure 2.3).

The most common method consists of adding free adhesion peptides (ligands) to the lipid solution used to make the SLB, resulting in lipid vesicles with linked adehsion peptide ligands[166, 250]. As the adhesion peptide-liposomes are adsorbed onto the surface, they fuse spontaneously and form an adhesion peptide-SLB once a critical threshold of adsorption is reached. Adhesion peptides also can be linked to the SLB via additional proteins, such as Annexin 5 (Anx5). Anx5 is known to self-assemble into highly ordered 2-D lattices on the surface of SLBs, where they can serve as tethering and support posts for smaller cell adhesion peptides. Regardless of the approach used, SLB

functionalization itself can be closely monitored using QCM-D[166, 251] and AFM,[252] and successful adhesion and spreading of cells on RGD-SLBs has been achieved by several groups for different research applications[250, 252].

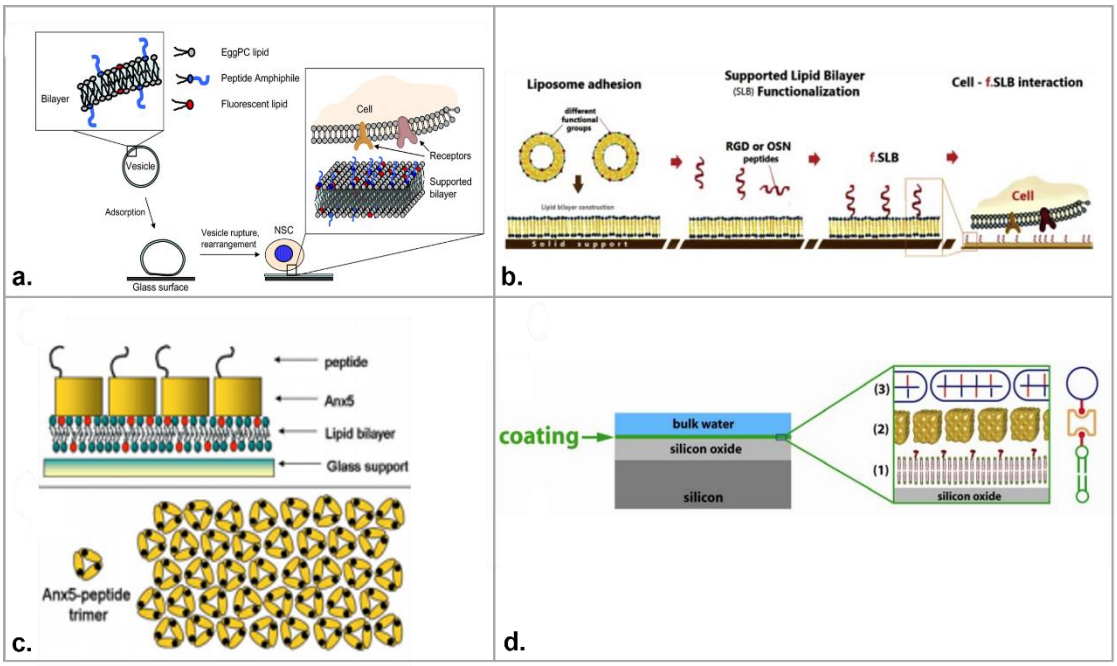

Figure 2.3. Methods for SLB functionalization with adhesion peptides. a) Schematic representation of the method used to create peptide-functionalized surfaces for studying adhesion of neural stem cells. Peptide amphiphiles were formed conjugating a hydrophobic 'tail' moiety to the N-terminus of the RGD peptide via an intermediate PEG spacer consisting of two ethylene-oxide units[250]. b) SLBs functionalized with bioactive molecules, RGD and Osteocalcin (OSN), to evaluate cell surface interactions via QCM-D[251]. c) Scheme of cell culture platform based on a 2D matrix of Anx5-RGD and Anx5-IKVAV on a SLB. The top is the side view of Anx5-peptide protein complexes self-assembled in a 2D matrix over a SLB. Peptides are exposed to the aqueous solution. The bottom shows a top-down view of a closely packed assembly of Anx5-trimers[253]. d) Schematic of SLB containing 2% of biotinylated lipids (1) coated with streptavidin (2) which binds to the SLB by biotin anchors. The RGD-containing biotinylated peptide is bound on top of the streptavidin layer (3)[139].

For example, Koçer and Jonkheijm prepared synthetic SLBs composed of 1,2-dioleoyl-*sn*-glycero-3-phosphocholine (DOPC), 1,2-dipalmitoyl-sn-glycero-3-phosphocholine (DPPC) and 1,2-dioleoyl-*sn*-glycero-3- phosphoethanolamine (Biotin DOPE), and biotinylated RGD peptides. Neutravidin, a biotin-binding protein, was used

to link biotinylated RGD peptides to the Biotin-SLB to form an RGD-SLB (Figure 2.4). The resulting platform was used to study human mesenchymal stem cell (hMSC) adhesion and differentiation. Using this platform to culture these cells, they found that both ligand (RGD) density and mobility significantly affected aspects of the hMSC's osteogenic differentiation, such as cell morphology and adhesion[254]. The results of this study, along with others, suggest that engineering of ligand presentation in SLBs has the potential to greatly influence stem cell behavior[159, 250, 254]. For better engineering of these platforms, it is imperative to consider fundamental properties of the RGD-SLB affecting cell adhesion, including ligand (RGD peptide) concentration and mobility.

Focal adhesions are organized integrin-containing assemblies that link the cell to the ECM, via ligands, and directly influence cell signaling and downstream responses involved in cell adhesion, migration, and differentiation[255]. One of the aspects interfering in the maturation of cellular contacts to form focal adhesions is thought to be ligand concentration and mobility[138, 254, 256, 257]. Because of the versatility of SLBs and the ability to control ligand presentation on them, they have been previously utilized towards a better understanding of the role that ligand (adhesion peptide) density and mobility have on cell adhesion and spreading[258, 259]. For instance, Sandrin and colleagues functionalized a SLB with a clustered RGD-containing ligand to find the optimal ligand concentration to trigger human embryonic kidney cells (HEK 293t) cell adhesion and spreading on a fluid substrate, SLB. The clustered-RGD compound consisted of a cyclic decapeptide scaffold with two functional domains: a clustered ligand domain for cell targeting via integrin recognition and a lipid surface anchoring domain (Figure 2.5) to facilitate its incorporation into the POPC derived SLB.

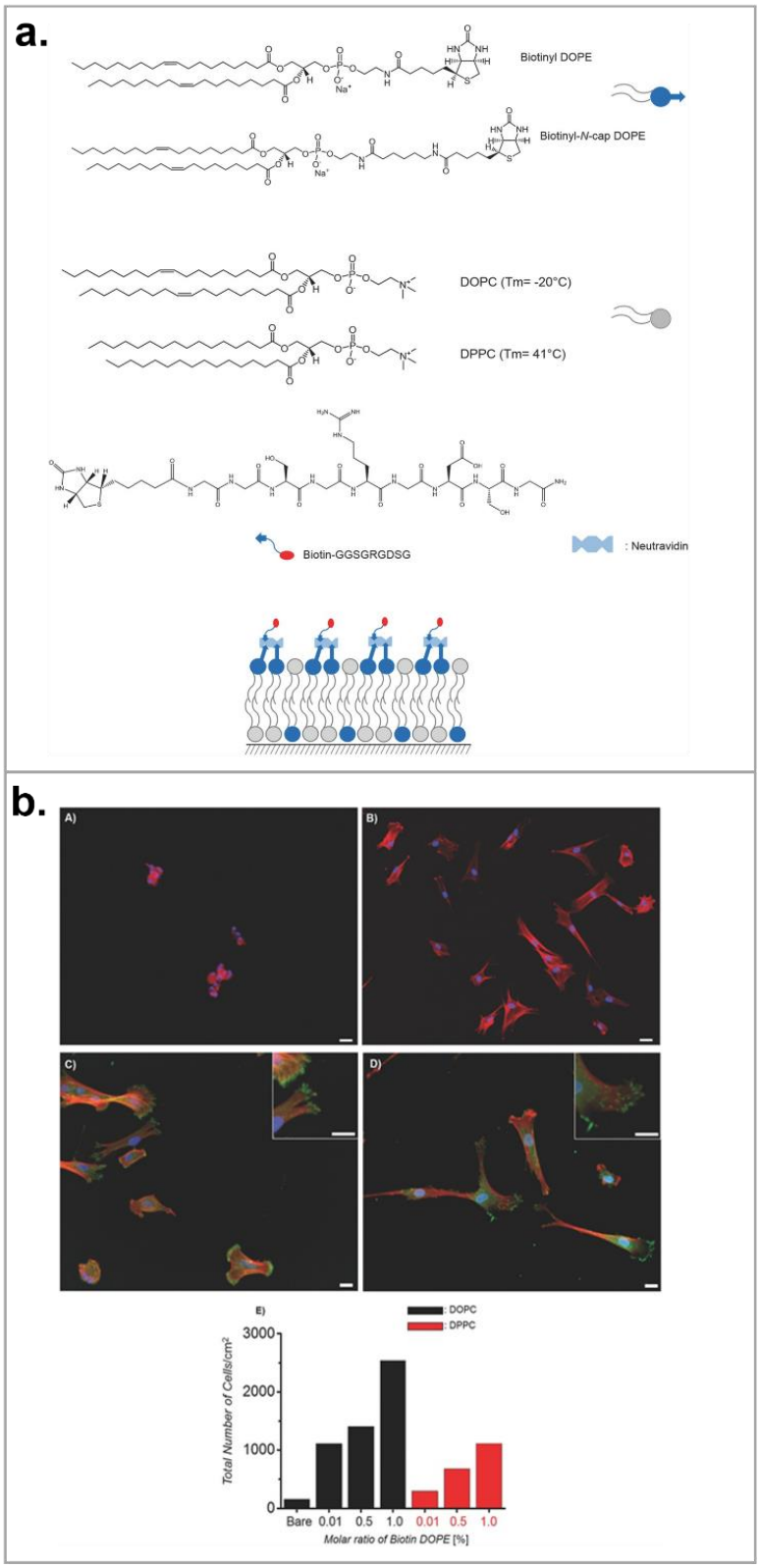

Figure 2.4. RGD functionalization of SLB as a cell culture for hMSCs. a) Schematic of RGD-functionalized-SLB with lipids and RGD peptide chemical structures. The amount of RGD ligand

on the surface of SLB was varied by tuning the molar concentration of biotinylated functional lipids. b) hMSCs adhesion after 17 hrs on A) non-treated DOPC-SLB and B) FBS treated glass. Vinculin staining after C) 17 hrs on 1 mol% biotinyl DOPE-SLB presenting RGD peptide ligands, D) 24 hrs on 1 mol% biotinyl-N-cap-DOPE – SLB presenting RGD peptide. Actin is red, vinculin is green, and nucleus in blue. E) Number of adhered cells per surface area after 17 hrs on RGD presenting DOPC and DPPC-SLBs for each percentage mol% of biotin DOPE and for non-treated SLBs[254].

HEK 293t cells were cultured on the RGD-SLBs of varying molar ratios of the clustered-RGD compound (from 0.01% to 5%). Results suggest that concentrations between 1430 ligands/ μm^2 and 14300 ligands/μm^2 were ideal for cell adhesion and spreading, respectively, on a fluid substrate SLB[252].

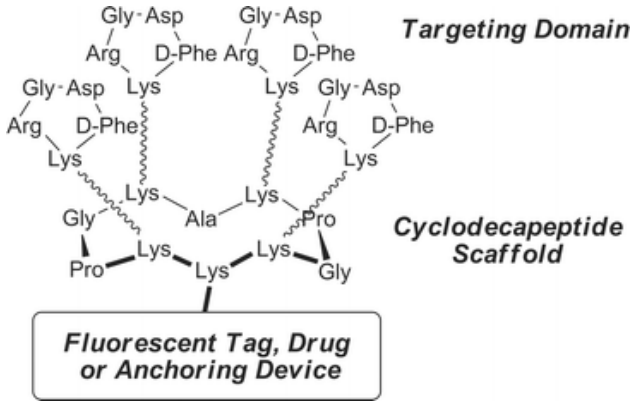

Figure 2.5. Structure of clustered RGD-containing compound[252].

Studies on the effect of ligand mobility on cell adhesion were done using two RGD peptide (ligand) functionalized-SLBs, of differing viscosities, as cell culture platforms for C2C12 mouse myoblast[247]. The different viscosities of the RGD-SLBs were obtained by manipulating the lipid composition of the bilayers; they resulted in largely distinct ligand (RGD) mobilities in the bilayers. In another experiment one SLB composed of DOPC (fluid phase) and another of DPPC (gel phase) were functionalized with equal density of RGD peptide ligand via neutravidin-biotin coupling, as previously explained[254]. C2C12 cells showed adhesion to both RGD-SLBs with cells forming more

stable integrin binding and focal adhesions in the most viscous RGD-SLB (DPPC, D = 0.1 μm^2 /s) compared to the least viscous RGD-SLB (DOPC, D = 3.6 μm^2 /s). These findings show that RGD ligand mobility, indicated by the diffusion coefficient (D), sensed by the cells via the focal adhesion molecular clutch (actin-talin-integrin-fibronectin), greatly influences cell signaling response, cell adhesion, migration, and differentiation[247]. The use of this system as a fluid tissue biomimetic model will allow the study of cell mechanotransduction and signaling responses in tissues that are viscoelastic by nature.

Although RGD is the most common cell-adhesive peptide used to functionalize SLBs and promote cell adhesion for different research purposes, IKVAV has been also employed as an adhesion peptide/ligand to favor cell attachment on SLBs. IKVAV is a pentamer peptide found in the α chain of laminin (an ECM protein) and it is actively involved in several biological functions including cell adhesion, neurite outgrowth, stem cell proliferation, and tumor growth. It is widely used in neuronal research to promote the differentiation of neural progenitor cells AHP to neurons and sustain neuron adhesion and growth[260]. Svedhem and colleagues designed a method to functionalize POPC derived SLBs *in situ* using an IKVAV-containing peptide to induce stem cell adhesion. Briefly, POPC-SLBs were treated with maleimido-terminated phospholipids to facilitate their covalent coupling to the cysteine at the C-terminal of the IKVAV adhesion peptide and to a VKAIV scrambled sequence (as a negative control)[167].

These platforms were then employed by Thid et al. as a cell culture substrate to study AHP adhesion and growth and the specificity of IKVAV ligand-AHP interactions (Figure 2.6).

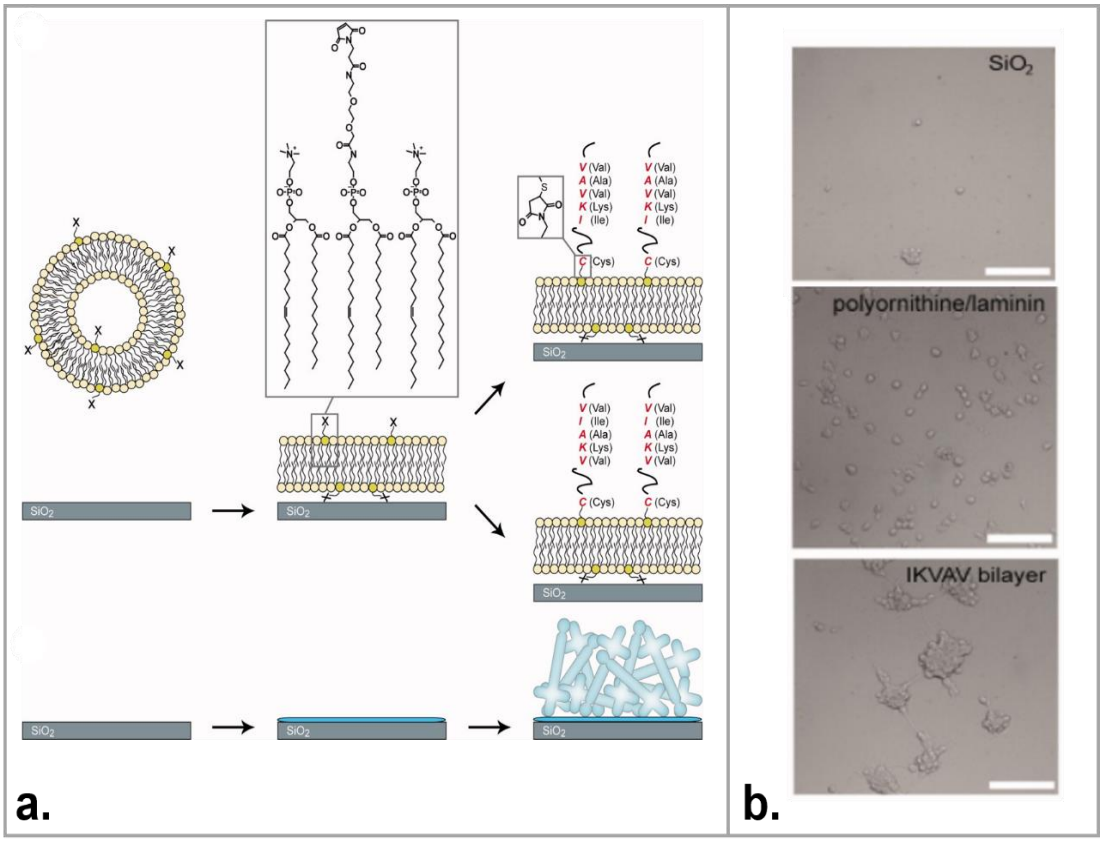

Figure 2.6. SLB functionalization with IKVAV peptide. a) Schematic of SLB surface modifications. (Top) SLB formed from Maleimido-EG_2-POPE doped POPC vesicles on SiO_2. The bilayer was functionalized with cysteine-terminated peptides, 19-mer IKVAV or 19-mer VKAIV (scrambled sequence as negative control), via thiol-maleimide coupling. (Bottom) SiO_2 coated with polyornithine and laminin was used as a control substrate for attachment of AHP cells. b) Images of AHP cells after 8 days of culture on IKVAV-SLB, SiO_2, and polyornithine/laminin SiO_2 [136]. Scale bar is 100 μm.

AHP successfully attached and spread on IKVAV-SLBs but did not differentiate, suggesting a specific interaction between IKVAV ligand and its receptor in the surface of AHPs[136]. Similarly, Bérat and colleagues functionalized DOPC- and DOPS-SLBs with RGD and IKVAV containing peptides and used them as cell adhesion platforms. RGD and IKVAV peptides were selectively linked to annexin A5 allowing homogeneous surface functionalization of the SLB. Both platforms, Anx5-RGD-SLB and Anx5-IKVAV-SLB, successfully promoted specific cell adhesion of human saphenous vein

endothelial cells (HSVEs) and mouse embryonic stem cells (MES) respectively[253].

2.5.3. Functionalization of SLBs' surface with adhesion proteins

2.5.3.1. Cell-cell adhesion proteins

E-cadherin and N-cadherin are important cell to cell adhesion proteins located in adherence junctions; structures formed between cells that act as adhesion zippers[261]. Cadherins form calcium-dependent, homophilic bounds with other cadherins at adjacent cells allowing cell to cell adhesion and communication[262]. SLBs have been employed as models to recapitulate and study the formation of E-cadherin- and N-cadherin-based adherence junctions. For example, Biswas and colleagues used functionalized SLBs with E-cadherin peptides to reconstitute and study E-cadherin-based adherens junction formation in MKN-28 Callisaurus epithelial cells. In culture, MKN-28 cells typically form packed colonies that synthesize high concentrations of E-cadherin and other important proteins in cell-cell adhesion. To make E-cadherin containing SLBs, DOPC- and DPPC-derived SLBs were prepared via the vesicle fusion method and functionalized with the E-cadherin extracellular domain (E-cad-ECD) via kinetic-controlled Ni-nitrilotriacetic acid (NTA)-poly-His chelation (Figure 2.7a). The E-cad-SLB was then used as a cell culture substrate for MKN-28 cells to analyze their behavior and E-cadherin adherens junction formation on E-cad-ECD-functionalized-SLBs offering different E-cadherin mobilities, fluid (DOPC-E-cad-ECD-SLB) and gel phase (DPPC-E-cad-ECD-SLB). Results showed formation of E-cadherin adherens junctions in both E-cad-ECD-SLBs (fluid and gel phase) with higher E-cad enrichment and more stable adhesion interactions being achieved in substrates with low mobility of E-cadherin, less fluid bilayers (DPPC). This system facilitated the study of E-cadherin clustering and adherens

nction formation and its mechanisms[140].

N-cadherin plays an essential role in the formation of cell-cell junctions contributing to the formation of tissues. It is one of the few adhesion proteins expressed in skeletal cells and it is thought to influence the development of cartilage and bone. Moreover, N-cadherin highly influences chondro and osteogenic differentiation of mesenchymal stem cells. In order to study the role of N-cadherin and cell-cell junctions in cell primary adults periosteum derived multipotent cells (PDCs) differentiation and tissue generation, Evans et al.[263] used N-cadherin functionalized SLBs as a cell culture platform for PDCs. A DOPC-SLB was functionalized with N-cadherin extracellular domain via NTA-poly-His chelation (Figure 2.7b). PDC cells, found to express junctional proteins ZO-1 (*zona occludens I)* and N-cadherin, were seeded on the N-cadherin-SLB and on N-cadherin functionalized glass, for comparison. Cells cultured on N-cadherin-SLBs showed attachment, aggregation, and down-regulation in N-cadherin, ZO-1 and Periostin (osteoblast factor). In addition, transcription of gene markers associated with early lineage commitment (adipo, chondro, and osteogenic phenotypes) and mesenchymal condensation (gathering of mesenchymal cells prior to differentiation) were significantly downregulated on PDCs cultured on N-cadherin-SLB while hyaluronic acid was upregulated. These results suggest that PDCs cultured on N-cadherin-SLBs form successful cell-cell junctions and enter a precondensation state and do not differentiate to a final fate. Furthermore, N-cadherin-SLB mimics the *in vivo* environment in a better fashion than glass or tissue cultured polystyrene making a better cell culture platform for PDCs. Lastly, the authors presented this system as a potential tissue patterning platform to guide and control stem cell lineage commitment and cell fate.

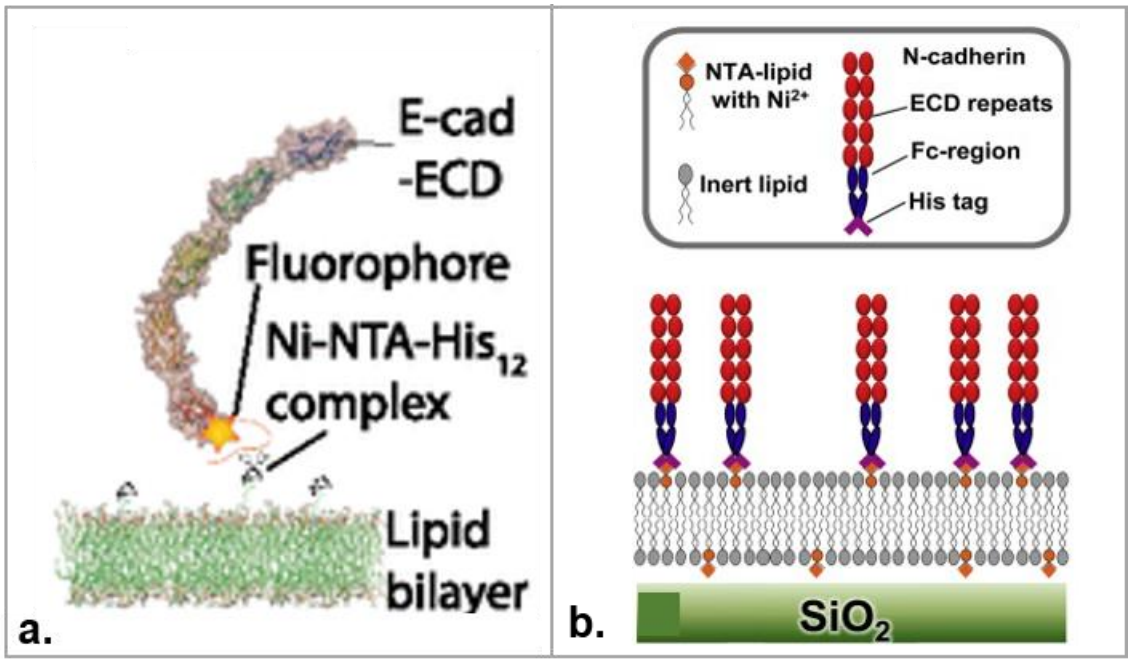

Figure 2.7. E-Cad-ECD and N-Cad-ECD functionalized SLBs. a) Schematic of E-cad-ECD bound to SLB via Ni-NTA interaction and relative position of the fluorophore on the crystal structure on the E-cad ECD[140]. b) Schematic of the SLB functionalized with N-cad ECD by Evans et al.[263]

2.5.3.2. ECM proteins

Besides providing structural support for cells and tissues, the extracellular matrix (ECM) is a group of proteins that plays an essential role in cell signaling and, consequently, in the regulation of several cellular processes. For example, cell-ECM interactions generate cell signals that influence several cell functions, including cell morphology, adhesion, proliferation, migration, and differentiation. These cell-ECM interactions are mediated by transmembrane protein receptors, like integrins, that act as "bridges" to connect the cell cytosol proteins with ECM proteins. This cell-ECM contact allows bi-directional signaling exchange and triggers a downstream response that influences cellular behavior and fate[264]. Abnormalities and dysregulation of these cell-ECM interactions are associated with several pathogenesis and diseases, including

cancer, diabetes, osteoarthritis, and chronic wound healing[265]. Therefore, due to the importance of cell-ECM interactions, it is imperative to study and understand them to develop biomaterials and cell culture substrates that properly mimic the *in vivo* cell microenvironment and to find therapeutic applications.

SLBs functionalized with ECM proteins have become an attractive *in vitro* model system for cell culture to mimic and study cell-ECM interactions. Huang et al.[266] pioneered this field working with type I collagen (Col)- functionalized SLB as a cell culture platform. Synthetic SLBs derived from a mixture of POPC and DP-NGPE (dipalmitoyl-sn-glycero-3-phosphoethanolamine-N-(glutaryl)) were formed on SiO_2 substrates via the vesicle fusion method. DP-NGPE carries a free carboxylic acid that allows chemical modifications to convert NHS -ester groups by EDC/sNHS treatment. The NHS-ester groups bind to the ε-amino group side chains of lysine residues on type I collagen allowing direct attachment to the bilayer generating a collagen-SLB (Figure 2.8a). In addition, collagen type-I surface coverage, molecular orientation, and conformation were controlled by tuning the percentage of DP-NGPE used (0 to 40%) to form the SLB. The collagen's functionalization process and molecular properties in the SLB were characterized using QCM-D, AFM, and FRAP. Vascular Smooth Muscle Cells (SMCs) cultured on collagen-SLB showed successful attachment and spreading compared to SMCs cultured on plane synthetic SLBs (Figure 2.8b). These results showed that the collagen-SLB system makes a fine biomimetic strategy and cell culture platform for the study of cell -ECM interactions. Moreover, using a SLB as a base system, instead of rigid support like glass, allows a better recapitulation of the cell microenvironment like collagen type I-lipids interactions happening *in vivo* required for many biological

processes.

Fibronectin (FN) -collagen interactions, via specific binding domains, play an important role in the organization of the ECM structure and in cell behavior[267]. For instance, cell attachment to collagen, usually mediated by FN, is critical in subsequent cellular processes like spreading, proliferation, and differentiation. During *in vitro* culture, as a mechanism to adapt to the environment, cells remodel the culture surface secrete ECM proteins for optimal adhesion and growth[268]. Because of the importance of FN, collagen, and FN-collagen interactions in cell behavior, Huang and colleagues conjugated collagen and/or FN on SLBs and study cell response to it as a cell culture system. As done in the previous study, a synthetic SLB was made using a mixture of POPC and 20% NGPE and EDC/sNHS treated to allow amine group binding from ECM proteins. The activated NHS-NGPE-SLB and oxygen plasma pretreated polystyrene (PSo), as a control, were functionalized with direct addition of collagen type I, FN, or a layer of collagen followed by a layer of FN (Figure 2.8c). Formation of resultant ECM-SLBs was characterized using standard techniques like QCM-D for protein adsorption and collagen-FN interactions and by FRAP for bilayer mobility and diffusivity. To test their efficacy as cell culture platforms, NIH 3T3 fibroblasts were cultured on ECM-SLBs as well as on ECM-PSo, for comparison. Their results showed successful adhesion of cells to all ECM-SLBs with significantly increased cell adhesion and spreading on FN-SLB and Col/FN-SLB than on the rest of the substrates (Figure 2.8d). Additionally, it was observed that cells on Col-PSo secreted significantly more FN and laminin than cells on Col-SLBs, showing that cells secrete ECM proteins to remodel the culture microenvironment when cultured on rigid substrates, like PSo, towards more *in vivo*

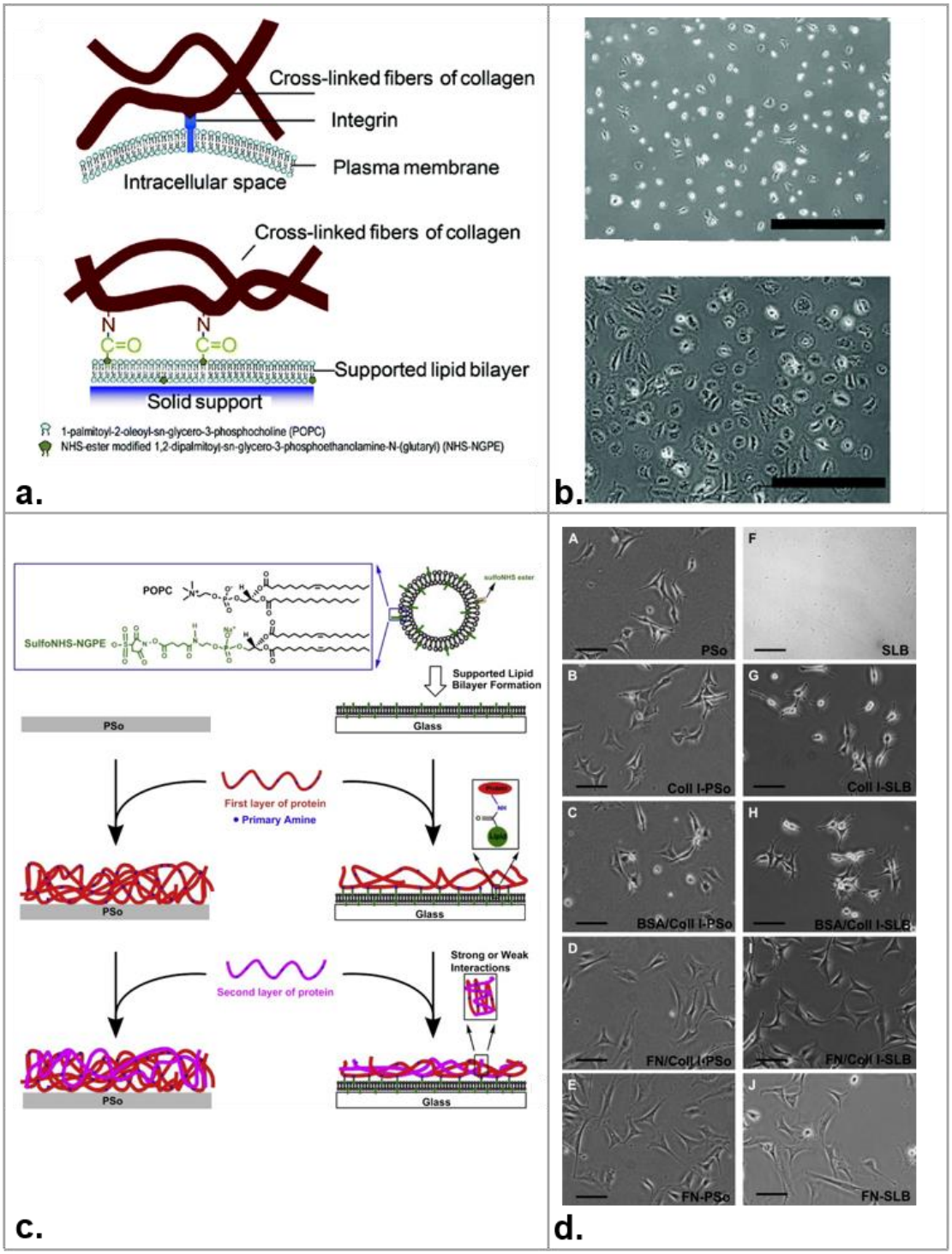

Figure 2.8. Schematics of ECM functionalized-SLBs and cell adhesion to them. a) schematic of mimetic collagen binding strategy based on integrins in cells. Top, cells bind to collagen fibers via integrins; bottom, collagen fibers are chemically conjugated to SLBs. The olive pentagons are the NHS-ester groups of DP-NGPE, and the blue ones are POPC headgroups. b) Smooth muscle cells (A10 cells) adhesion on SLBs activated with 20% NHS-DP-NGPE without collagen (top)

or functionalized with collagen type I (bottom)[266]. c) schematic of functionalization process for PSo (negative control) and SLBs to study the response of 3T3 fibroblasts to the different substrates. d) Images of 3T3 fibroblasts after 6 hrs of culture on: PSo, Coll I-PSo, BSA/Coll I-PSo, FN/Coll I-PSo, and FN-PSo (A, B, C, D, and E) and on SLB, Coll I-SLB, BSA/Coll I-SLB, FN/Coll I-SLB, and FN-SLB (F, G, H, I, and J)[269]. All scale bars are 100 μm.

conditions compared to when cultured on fluid substrates, like SLBs. In conclusion, their results suggest that ECM-SLBs make a fine system to study specific protein-cell and cell-materials interactions.

Cho group at NTU (Nanyang Technological University) Singapore has added several contributions to this field. In their first study, they used ECM functionalized SLBs, as low rigidity cell culture platforms, to mimic the mechanical properties of soft tissues.[152] Towards this end, they made SLBs from a mixture of DOPC and varying percentages of DP-NGPE using the SALB formation method and functionalized them with collagen and FN via amine coupling, as previously done[270]. QCM-D characterization of the bilayers showed 10-20% of DP-NGPE to be the optimal percentage to show a homogeneous distribution of collagen and FN on SLBs. Effective use of collagen and FN- functionalized SLBs as cell culture platforms were shown by the successful growth of human hepatocarcinoma cells (Huh 7.5) on both bilayers. Additionally, cells cultured on collagen/FN-SLBs showed lower spread and higher circularity than those cultured on glass. This behavior is expected of cells on low rigidity substrates, which shows that collagen/FN-SLBs are good mimetic models for low rigidity surfaces like soft tissues. Furthermore, collagen and FN-SLBs with higher densities of proteins showed higher cell adhesion and spreading, suggesting that cell adhesion efficacy depends on protein density. Importantly, FRAP experiments were done on the collagen/FN-SLBs after cell seeding showed retention of lateral mobility on collagen and FN functionalized bilayers

with a small reduction in diffusivity to have final diffusion coefficients of 1.4 ± 0.1 $\mu m^2 s^{-1}$ and 2.0 ± 0.1, for FN and collagen-SLBs, respectively. Lateral translocation of collagen and FN on the bilayers was observed by forming of protein enrichment and depletion areas underneath and around the cells, respectively. This phenomenon was mediated and controlled by the diffusivity of collagen/FN functionalized-SLBs. Due to the tunability of rigidity on the collagen/FN-SLBs and its success as a soft tissue mimic, the authors proposed their use as a system to study gene expression and differentiation of stem cells and study cell adhesion in very low-rigidity tissues such as neuronal. Moreover, this group utilizes the same platforms to study and compare the biological activity of both ECM proteins on a SLB versus on SiO_2/glass[32] (Figure 2.9a and 2.9b).

For SiO_2 functionalization, collagen, FN, and Col/FN were nonspecifically adsorbed onto the surface. QCM-D characterization of both processes showed that FN and collagen have more stable interactions and higher structural flexibility on SLBs than on SiO_2/glass. Huh 7.5 cells cultured on collagen, FN, and collagen/FN-SLBs showed higher proliferation and metabolic activity than their counterparts cultured on rigid surfaces, glass and SiO_2 (Figure 2.9c). These results suggest the presence of more efficient and stable adhesion interactions between cells and FN and/or collagen-SLB than those on glass/SiO_2 surfaces showing that SLBs mimic the native microenvironment better than rigid substrates like glass and SiO_2. Decellularized ECM (dECM) has been highly used as a natural 3D scaffold for numerous tissue engineering and biomedical applications. It conserves the native 3D structure of the ECM and supports cellular functions, including cell adhesion, proliferation, and survival.

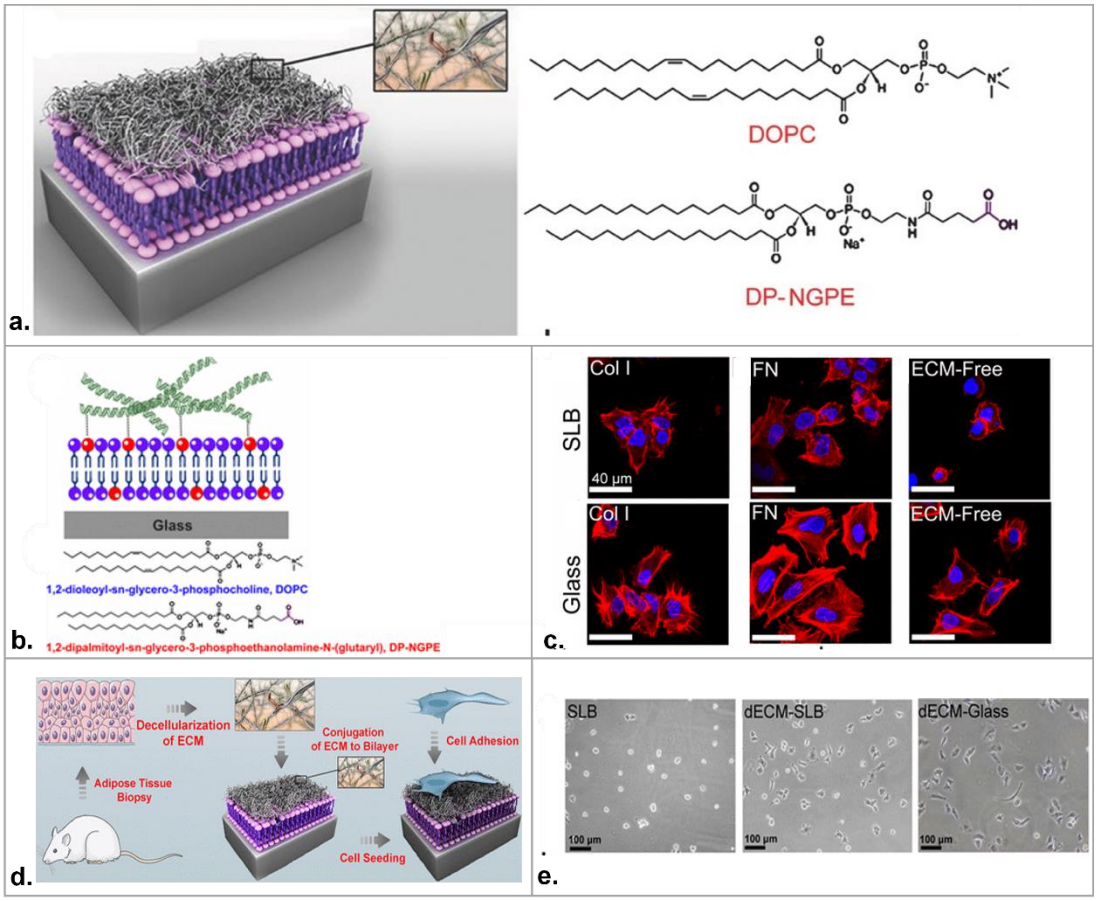

Figure 2.9. Functionalized SLBs as a mimic of the ECM. a) schematic of collagen type I bound to SLB via amine coupling and chemical structures of lipids used to make the SLBs[54]. b) schematic of SLBs functionalized with ECM molecules via covalent bonding to lipids with reactive headgroups and chemical structures of SLBs lipids. c) confocal images of one day plated Huh 7.5 cells on Col I and FN- functionalized SLBs and glass, and on non-functionalized SLBs and glass. F-actin is red, and nuclei are blue. Scale bars are 40 µm[75]. d) schematic of steps involved in preparation of functionalized SLBs using dECM components. e) Brightfield images of Huh 7.5 cells on non-treated SLBs, dECM-SLB, and dECM-glass after 24 hours. Observe morphology of cells on non-treated SLB is rounded, while those on DECM- SLB and -glass showed more spread cells[187].

Towards the development of a better biomimetic platform that resembles the ECM, Vafaei et al.[271] functionalized SLBs with dECM components (Figure 2.9d). The SLB was made from a mixture of DOPC and 20% DP-NGPE by the SALB formation method, as in their previous work. To generate dECM components, a biopsy from murine adipose tissue went through sequential treatments with organic solvents and enzymatic digestion

to facilitate fat removal and cell detachment. Characterization of the tissue after treatment showed successful decellularization. Scanning Electron Microscopy (SEM) images and DNA quantification showed no remaining cells, 2% remaining DNA, and an organized collagen fibers structure on the treated tissue. In addition, the analyses showed that collagen and GAGs (glycosaminoglycans) levels were enriched and conserved, respectively, on the decellularized tissue. Next, the dECM was solubilized via acid treatment, its proteins were attached to the activated SLB by amine groups (in the proteins) - carboxylic acid (in DP-NGPE) covalent bonding as previously done. dECM-SLB was characterized by QCM-D, FRAP, and immunofluorescence microscopy. Results showed the formation of a soft protein layer on the SLB where the ECM proteins conserve their natural flexibility, a uniform fluorescence signal across the SLB from collagen and FN staining, and retention of lateral fluidity in the SLB after functionalization. Furthermore, the potential of the dECM-SLB as a cell culture substrate was studied seeding Huh 7.5 cells on it and allowing cell adhesion for 24 hrs. Cells were grown on the dECM-SLB showed significantly higher adhesion and spreading than cells on non-treated SLBs, and comparable behavior to cells on ECM-glass (Figure 2.9e). These results indicate that functionalization of SLB using dECM components facilitates specific cell adhesion mediated by cell-ECM interactions. The biological function of ECM proteins in SLBs was compared to those on glass by analyzing cell viability, proliferation, and metabolism markers after 3 days of culture on both substrates. There was not a significant difference in those cell functions on both substrates suggesting that the biological activity of ECM proteins functionalized on SLBs is conserved. In summary, ECM-functionalized SLBs not only provide mechanical support to cells but

also facilitate exchange of signals between cells and substrate important in regulation of many cellular functions. The dECM-SLB is a great model to study the native ECM in biological scenarios where ECM-mediated responses are imperative.

2.6. Conclusions

The unique characteristics of SLBs such as fluidity, fouling resistance, biocompatibility, and versatility make them great scaffolds for cell culture with potential biomedical applications. Although their nature is non-fouling and resistant to protein and cell adhesion, several strategies have been developed to overcome this aspect. Moreover, the flexibility of SLBs functionalization methods opens the possibilities for diverse uses. Here, we showed how diverse techniques allowed the successful cell adhesion, spreading, and in some cases, differentiation. These platforms will facilitate the study of fundamental cell biology mechanisms such as cell adhesion, stem cell behavior and differentiation, cell-cell, cell-ligand, cell-ECM, and cell-substrate interactions. Functionalized SLBs could contribute towards the design and development of biomaterials for tissue engineering. Because this is a very dynamic area, we do not have doubt that the future SLB functionalization methods as well as applications will be as creative as the ones we reviewed in this paper.

CHAPTER 3

3.A SUPPORTED MEMBRANE PLATFORM TO ASSESS SURFACE INTERACTIONS BETWEEN EXTRACELLULAR VESICLES AND STROMAL CELLS.

Johana Uribe[1], Han-Yuan Liu[2], Zeinab Mohamed[1], Aaron E. Chiou[1], Claudia Fischbach[1,2], and Susan Daniel[1,2]*

[1]Meinig School of Biomedical Engineering, Cornell University, Ithaca, NY.

[2]School of Chemical and Biomolecular Engineering, Cornell University, Ithaca, NY.

3.1. Acknowledgments

This chapter was published in its entirety including the SI section in "A supported Membrane Platform to Assess Surface Interactions between Extracellular Vesicles and Stromal Cells" in ACS Biomaterials Science & Engineering. Johana Uribe is the first author, Susan Daniel is the corresponding author, and the co-authors include Han-Yuan Liu, Zeinab Mohamed, Aaron E. Chiou, and Claudia Fischbach.

3.1.1. Individual acknowledgments

JU: conceived the idea presented in this paper, designed, and performed all the experiments, data analysis and interpretation, drafted and edited the manuscript and made the figures. **HYL:** data interpretation, research advise, manuscript editing. **ZM:** acquisition of TEM images of MVs and exosomes. **AEC:** trained and advised JU in MVs isolation and ADSCs culture. **CF:** oversaw the project, results interpretation, manuscript

writing and editing. **SD:** conceived the idea presented in this paper, oversaw the project, results interpretation, manuscript writing and editing. All authors discussed the results and commented on the manuscript.

3.1.2. Article acknowledgments

This work was supported by the Memorial Sloan Kettering Cancer Center [grant number (MKSCC) BD520101]; the Center on the Physics of Cancer Metabolism [Award Number 1U54CA210184-01] from the National Cancer Institute; the National Science Foundation Graduate Research Fellowship [Grant Number DGE-1650441), and the Sloan Foundation [Grant number 70481]. Any opinions, findings, and conclusions or recommendations expressed in this material are those of the author(s) and do not necessarily reflect the views of any of the funding institutions. *This work made use of the Cornell Center for Materials Research Facilities supported by the National Science Foundation under Award Number DMR-1719875.*

3.2. Abstract

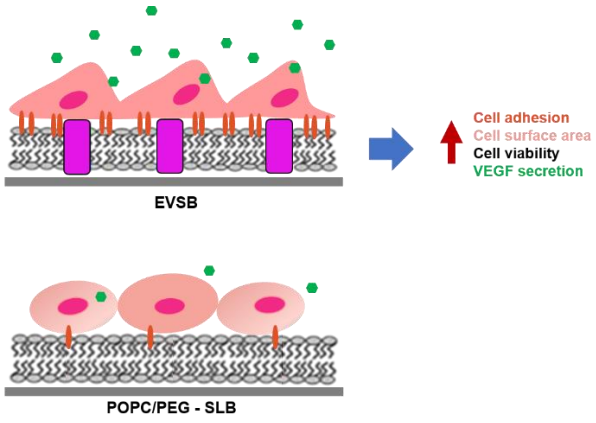

TOC Figure. Graphical abstract

Extracellular vesicles (EVs) are membrane encapsulated particles secreted by eukaryotic cells that stimulate cell communication and horizontal cargo exchange. EV interactions with stromal cells can result in molecular changes in the recipient cell, and in some cases, lead to disease progression. However, mechanisms leading to those changes are poorly understood. Few model systems are available for studying the outcomes of surface interactions of the EV membrane with stromal cells. Here, we created a hybrid supported bilayer incorporating EV membrane material, called an extracellular vesicle supported bilayer, EVSB. Using EVSBs, we investigated the surface interactions between breast cancer EVs and adipose-derived stem cells (ADSCs) by culturing ADSCs on EVSBs and analyzing cell adhesion, spreading, viability, VEGF secretion, and myofibroblast differentiation. Results show that cell viability, adhesion, spreading, and proangiogenic activity were enhanced, conditions that promote oncogenic activity, but cell differentiation was not. This model system could be used to develop therapeutic strategies to limit EV-ADSC interactions and proangiogenic conditions. Lastly, this model system is not limited to the study of cancer but can be used to study surface interactions between EVs from any origin and any target cell to investigate EV mechanisms leading to cellular changes in other diseases.

3.3. Introduction

Extracellular vesicles, EVs, are membrane encapsulated particles secreted by many eukaryotic cell types [1, 272]. There are two major EV subtypes: exosomes, ranging between 30 -120 nm in diameter, which originate from late endosomes and are secreted when multivesicular bodies fuse with the plasma membrane; and microvesicles (MVs), ranging between 100 -1000 nm in diameter, which directly bud from the plasma

membrane [1, 15, 16, 24, 58]. Both types of EVs contain an extensive variety of biomolecules on their membrane surfaces and internal cargo contents including nucleic acids, proteins, lipids, oncogenes, and receptors [1, 62]. However, their specific surface composition and cargo contents depend on the physiological condition in which they are produced and the type of cell and location from which they originate.

Due to their important role in cell communication, EVs have gained a great deal of attention for their potential role as disease spreading agents. EVs work as " messenger vehicles" between cells, facilitating intercellular communication by horizontal transfer of cargo [3]. Their interactions with host cells have been correlated to modifications in molecular makeup and behavior of the recipient cell[4, 5, 18] and promotion of disease progression in cancer[70, 77, 273-275], infectious diseases[276], neurodegenerative diseases[274], metabolic diseases[16], inflammatory diseases[277], and several other human diseases[278]. In the context of cancer, Grange et al. showed that lung endothelial cells acquired an activated angiogenic function after treatment with EVs derived from CD105-positive tumor-initiating renal cancer stem cells[18]. Additionally, Song et al.[4] and Cho et al.[5] showed that EVs derived from MDA-MB-231 breast cancer cells influence adipose derived stem cell (ADSC) proangiogenic activity and transformation to myofibroblasts when EVs were added in the cell culture media.

How the interactions between EVs and stromal cells leading to disease progression occurs at the molecular level is not clear. Cues most certainly come from both the EV membrane components, as well as the internal cargo, but specific mechanisms to deliver information from EVs to stromal cells are poorly understood. This is due, in part, to the absence of techniques available to investigate interactions between

EVs and stromal cells. In particular, few systems exist to study the initial surface-level interactions, though this is the first point at which EVs begin to influence the local microenvironment to favor disease progression [23]. Surface interactions are the "first touch" between EVs and cells, so understanding this interaction better to disarm it would potentially lead to highly impactful treatment options that reduce disease progression by both disrupting the specific surface interactions, but also potentially disrupting the ability to deliver the cargo as well.

To fill this need, we developed an *in vitro* EV surface model that allows us to isolate and study the influence of EV surface components on stromal cell behavior. This platform is a hybrid supported lipid bilayer (SLB) known as an extracellular vesicle supported bilayer (EVSB). SLBs are a common model membrane system used in many areas of research to understand biomolecular interactions with cell membranes[25-31] and have found utility as cell culture platforms to investigate various types of cell interactions using simple reconstituted bilayer lipid compositions[30, 32, 158]. SLBs can mimic the native configuration of the cell membrane. Importantly, their 2D geometry and stability make them compatible with many surface characterization tools and optical microscopy. Our group has advanced this important technology platform recently by developing methods to incorporate native plasma cell membrane material that preserves the original orientation and function of the membrane proteins from mammalian[33, 34] and bacterial[190] membranes. Here, we leverage this work to tailor our platform to make "cancer EV-like" supported bilayers derived from EVs. Importantly, here the EVSB mimics just the surface of the EV type and eliminates the possibility of EV uptake and cargo delivery, allowing

us a convenient way to isolate the surface effects from these other factors and study how those surface moieties affect cell behavior.

In the specific case of ADSCs, their exposure to EVs derived from breast cancer cells have been correlated to elevated proangiogenic activity and transformation to myofibroblasts[4, 5]. To isolate and study how the surface interactions between EVs and ADSCs contribute to these biological outcomes, we made EVSBs from MDA-MB-231 derived EVs and used them as cell culture platforms to investigate the effect of EV membrane components on ADSC adhesion, spreading, viability, proangiogenic potential, and phenotype differentiation. In a distinction from most prior studies in this field, we use MVs and exosomes as two independent populations to assess how both subtypes influence stromal cell behavior.

It is important to note that outcomes of EV interactions with stromal cells, in the studies cited above [4, 5, 18], were assessed for a general population of EVs. This is in part due to the difficulty in defining subpopulations; however, it is reasonably well-established now that there is a size cut-off that differentiates the broad class of exosomes from MVs[63]. They have been shown to also differ in biogenesis, cargo, and surface makeup[58, 64]. Research findings suggest that they have different functions in cell-cell communication[65], and different intracellular routes with subsequent effects on cells[65, 66]. Therefore, we separated these populations to test if their surface compositions differentially influence interactions with ADSCs and subsequent biological outcomes.

We show here that ADSCs cultured on both types of EVSB lead to enhanced cell survival, adhesion, spreading, and proangiogenic activity, but did not lead to ADSC differentiation to myofibroblasts in either case. MV-derived bilayers had a slightly

stronger effect than the exosome-derived bilayers. Knowing that these outcomes are observable in our platform, it opens up future studies of the EV-ADSC surface interactions with an eye towards the development of strategies to disrupt or block such interactions and thus limit these biological outcomes and, ultimately, one avenue of promotion of cancer. On the other side, these results show that carefully tuned compositions of supported bilayers can influence cells cultured upon them and this could also lead to platforms that can be used to optimize tissue growth. As such, we note that our platform is not limited only to the study of EVs-stromal cells surface interactions in cancer progression, but it can be tuned to study nearly any cell type that generates vesicles from a membrane surface, for broader impact across many disease and infection processes.

As a last point, EVSB as a planar bilayer platform provides the understanding of local surface interactions between ASDCs and EV membranes, especially its proteins, in contact with the cells. Although this is a flat surface instead of the EVs natural spherical-like shape, EV membrane properties are mimicked by our model, and we will show that they reproduce known biological outcomes of these interactions. Thus, here we can decouple the shape factor from the observations we make. Future studies will focus on understanding how EVs are uptaken and internalized by cells, a process influenced by EVs shape and size[279-281].

3.4. Materials and Methods

3.4.1. Cell culture

StemPro Human Adipose-Derived Stem Cells (ADSCs) were bought from ThermoFisher Scientific and cultured in ADSC growth media (Lonza). MDA-MB-231, highly

metastatic breast adenocarcinoma cells were bought from American Type Culture Collection (ATCC) and maintained in Dulbecco′s Modified Eagle′s Media, DMEM (Corning), complemented with 10% fetal bovine serum, FBS (Gibco), and 1% penicillin–streptomycin, P/S (Corning). All cultures were maintained in a humidified incubator (37°C and 5% CO_2).

3.4.2. MVs and exosomes isolation

MDA-MB-231 cells were cultured to 85% confluency and transferred to FBS-free media for 18-30 hours[282]. Media was collected, subjected to a series of centrifuge cycles, and filtered using a 0.22 μm Millipore Steriflip PVDF-filter (Millipore) to separate MVs and exosomes. Particles retained by the filter, MV fraction, were resuspended in 0.5 mL of serum-free media and stored at 4°C. The remaining media was ultracentrifuged and the pellet, exosomes fraction, was resuspended in 0.5 mL of serum-free media and stored at 4°C. Procedure details are available at the SI materials and methods section.

3.4.3. EVs size and concentration measurements

EV size distribution was found using nanoparticle tracking analysis (NTA, Nanosight NS300, Malvern), dynamic light scattering (DLS, Zetasizer Nano ZS, Malvern), and transmission electron microscopy (TEM, Spirit). EV concentration was found using NTA as well. Procedure and equipment details are available at the SI Materials and Methods section.

3.4.4. Transmission Electron Microscopy (TEM)

To visualize EVs individual populations, freshly isolated EVs were imaged using FEI Tecnai-12 TEM (Spirit) at 120 kV at the Cornell Center for Materials Research. Samples

were loaded onto a 300-mesh carbon-coated copper grid and negatively stained with 1.5% uranyl acetate. Procedure and equipment details are available at the SI Materials and Methods section.

3.4.5. Western blot

40 µL MDA-MB-231 derived MVs, exosomes, and whole cell lysates (WCL) were loaded on a 4-12% Bis-Tris gel Bolt (Invitrogen), transferred onto a PVDF-membrane, blocked with 5% non-fat dry milk, incubated overnight at 4 ̊C with primary antibodies and with a secondary antibody for 1 hour. The membrane was imaged using a Western ECL detection kit (BioRad). Procedure details are available at the SI Materials and Methods section.

3.4.6. Preparation of fusogenic liposomes

Fusogenic liposomes consisting of 99.5% (mol/mol) POPC,1-Oleoyl-2-palmitoyl-sn-glycero-3-phosphocholine, and 0.5 (%mol/mol) PEG2000, 1,2-distearoyl-sn-glycero-3-phosphoethanolamine-N-[methoxy (polyethyleneglycol)-2000], were prepared. Procedure details are available at the SI Materials and Methods section.

3.4.7. Formation of POPC/PEG-SLB and EVSB

Polydimethylsiloxane, PDMS, wells were attached to previously cleaned glass slides. For POPC/PEG-SLB formation, fusogenic liposomes self-assemble on the coverslip using the well-established vesicle fusion method reported by our group [33, 34]. For EVSB, 100 µL of EVs were added to the well, incubated at room temperature for 8 minutes, and thoroughly rinsed with PBS to remove unabsorbed EVs. Formation of the EVSB was induced by addition of 70 µL of 1 mg/mL fusogenic liposomes, incubation for 20 min,

and gently rinsing with PBS to remove unruptured EVs. Procedure details are available at the SI Materials and Methods section.

3.4.8. Bicinchoninic acid assay (BCA)

Protein content of EVSBs was assessed by measuring the protein concentration of EVs samples used to create the EVSBs. It was performed using a QuantiPro BCA Assay Kit (Sigma-Aldrich) and following the manufacturer protocol. Procedure details are available at the SI Materials and Methods section.

3.4.9. Detection of EGFR in MV-EVSB

MV-EVSB, exosome-EVSB, and POPC/PEG-SLB were treated with primary anti-EGFR (R&D Systems) antibody, with Donkey Anti-Mouse IgG NorthernLights (R&D Systems) secondary antibody, and imaged using TIRFM (total internal reflection fluorescence microscopy) to detect presence or absence of EGFR on the surfaces. Procedure details are available at the SI Materials and Methods section.

3.4.10. Detection of HSP70 and CD63 in exosome-EVSB

The same procedure stated above for EGFR detection was followed to detect the presence or absence of HSP70 and CD63 in exosome-EVSB, MV-EVSB, and POPC/PEG-SLB using anti-HSP70 (R&D Systems) and anti-CD63 (R&D Systems) as primary antibodies and the same secondary antibody as stated above. Procedure details are available at the SI Materials and Methods section.

3.4.11. Visualizing EVSB formation by FRAP (Fluorescence Recovery after Photobleaching)

EVs previously labeled with Octadecyl Rhodamine, a membrane intercalating dye, were used to form EVSBs following the procedure in section 2.7. Fluorescently labeled EVs rupture was observed using an inverted Zeiss Axio Observer. Diffusivity and mobile fraction measurements were found using photobleaching experiments. Procedure details are available at the SI Materials and Methods section.

3.4.12. EV cargo tracking in EVSBs

EV cargo (mRNA) was labeled using ExoGlow-RNA EV Labeling Kit (System Biosciences). Labeled EVs were incubated on glass to image EVs cargo before EVSB formation. To image EV cargo after EVSB formation, labeled EVs were placed on glass followed by addition of liposomes as described above in section 2.7, then imaged with TIRFM to track EV cargo before and after EVSB formation. Procedure details are available at the SI materials and methods section.

3.4.13. ADSCs culture on EVSBs, POPC/PEG-SLB, and EZ-slides

ADSCs were seeded, 1.05 x10^4 cells/well, on four surfaces: MV-EVSB; exosome-EVSB; POPC/PEG-SLB as a negative control; and Millicell EZ slide (no bilayer present) as a positive control. These four surfaces were used for all of the subsequent cell studies.

3.4.14. Quantification of cell surface area and focal adhesions

After 24 of incubation, ADSCs seeded on the four surfaces were immunostained for vinculin and DAPI to detect the cell area, focal adhesions, and nuclei. Images were

captured using the inverted Zeiss Axio imaging system described in section 2.11. Procedure details are available at the SI Materials and Methods section.

3.4.15. Measurement of ADSC aspect ratio

Using ImageJ software, the length and width of each vinculin-stained cell was measured. To find the aspect ratio of each cell, the length: width ratio was determined. This measurement was done for all ADSCs cultured on EVSBs, POPC/PEG-SLB, and EZ-slides.

3.4.16. Cell viability analysis using a LIVE/DEAD kit

Viability of ADSCs on the four surfaces for day 1, 3, and 5 was assessed using a LIVE/DEAD imaging kit (ThermoFisher Scientific) following the manufacturer's protocol. Viable cells generate a green signal and dead cells generate a red one. Images were captured using 5X objective for day 1 and 20X for day 3 and 5 using the inverted Zeiss Axio Observer. Procedure details are available in the SI Materials and Methods section.

3.4.17. Assessment of VEGF secretion by ADSCs

As a measure of proangiogenic activity, VEGF secretion by ADSCs on the four surfaces was assessed using a Human VEGF DuoSet ELISA kit (R&D systems). Following the manufacturer's protocol, VEGF concentration was measured on four wells containing each a different cell culture substrate: MV-EVSB, Exo-EVSB, EZ-slides, and POPC, and ADSCs seeded on them. VEGF concentration was found for each well on day 1 and 4 after seeding. Three independent replicates of the experiment were performed. VEGF concentration secreted by ADSCs was normalized by the number of viable cells in day 4

(assuming all cells are viable in day 1) and by EVSB protein content on day 1 and 4.

3.4.18. Statistical Analysis

For all experiments performed in this study, variance analysis was performed using a t-test with unequal variances to find significant differences between substrates and conditions. All data was plotted using Microsoft Excel and it is presented as mean ± SD. For diffusivity measurements, FAs, cell area, viability assays, and VEGF secretion, 3 independent replicates of each experiment were done. Statistical significance levels were determined as follows: *$p \leq 0.05$, **$p \leq 0.01$, ***$p \leq 0.001$, ****$p \leq 0.0001$.

3.5. Results and Discussion

3.5.1. Breast cancer cell EV isolation and characterization

Isolation of EVs from MDA-MB-231 cells, as described in the Methods section, is summarized in Figure 3.1a. This procedure was optimized to yield two distinct populations of EVs, MVs and exosomes, to later test differences in cell response to the specific surface cues of each EV type. Isolated EV populations were characterized in a number of ways. First, particle size was measured for each type using dynamic light scattering (DLS) and nanoparticle tracking analysis (NTA). To further confirm the results, EVs were imaged using Transmission Electron Microscopy (TEM) as observed in Figure 3.1d and 3.S1. Sizes of MVs and exosomes found by NTA, DLS, and TEM are reported in table 1 and EV size profiles are shown in Figure 3.1b, 3.1c, and 3.1d. Reported EV sizes agree with standard literature designations in which MVs range between 120 - 1000 nm diameter, and exosomes range between 30 -120 nm diameter [1, 59-61]. NTA was also employed to obtain the concentration of MVs and exosomes and

found to be on average $1.62\times10^7 \pm 1.34 \times10^6$ MVs/mL and $4.77 \times10^7 \pm 1.78 \times10^6$ exosomes /mL, respectively. Concentration of MVs is consistently lower than exosomes for each batch, presumably because of retention of some MVs on the filter used during the isolation processes. However, the same concentration of EVs, $1.62\times10^7 \pm 1.34 \times10^6$ EVs/mL, was used during these experiments and formation of supported bilayers. Zeta potentials of MDA-MB-231 derived EVs have been previously reported in the literature to range between -12.7 mV to -9.0 mV for EVs between 60 nm to 450 nm in size[283, 284].

Besides differing in size, MVs and exosomes differ in surface composition. Exosomes are known to contain membrane proteins of endosomal origin called tetraspanins, such as CD63[285]. MVs, in contrast, preserve membrane proteins from the mother cell plasma membrane, such as epidermal growth factor receptor EGFR, which is overexpressed in MDA-MB231[286]. To reassure the presence of two distinct EV populations, Western blot was performed on MDA-MB-231 whole cell lysates (WCL), MV lysates, and exosome lysates to detect markers specific to each EV population. Samples were immunoblotted for CD63, as an exosomal marker, and EGFR, as a MV marker. Figure 3.1e shows a band detecting presence of CD63 in WCL and exosomes as expected. Note that the original CD63 band is smeared and it falls between 35 kDa and 65 kDa, which is normal, and attributed to heavy glycosylation[100, 287]. On the other side, EGFR, represented by a band around 175 kDa, is detected in WCL and MVs but not in exosomes, confirming that our isolation procedure can separate these populations.

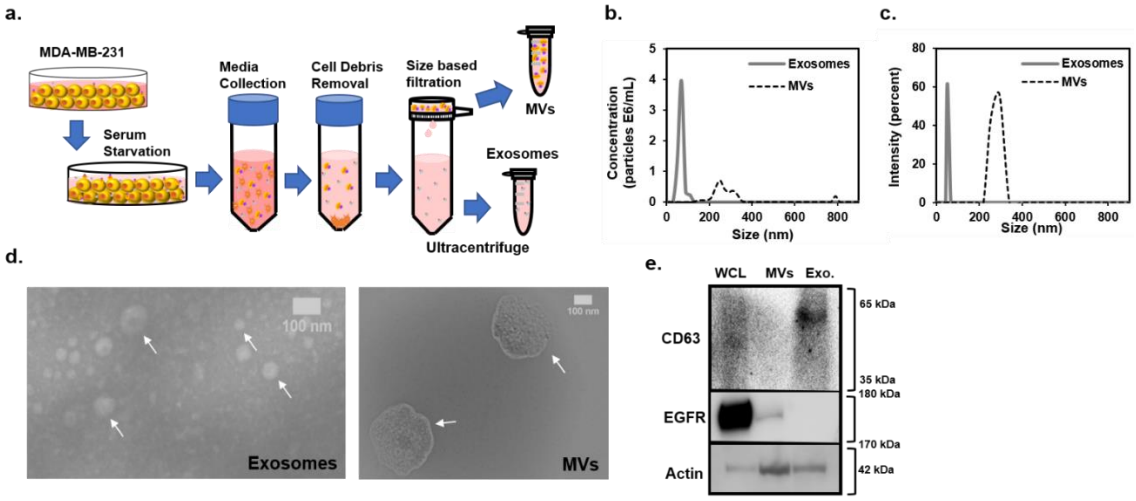

Figure 3.1. Isolation and characterization of MDA-MB-231 derived EVs. a) Isolation of MDA-MB-231 derived EVs through differential centrifugation, vacuum filtration, and ultracentrifugation. b) Size distribution of MVs and exosomes by NTA. c) Size distribution of MVs and exosomes by DLS. d) TEM images showing a population of exosomes on the left panel and one of MVs on the right panel, white arrows pointing at EVs. e) Western blot showing presence of EGFR in MVs and WCL, CD63 in exosomes and WCL, and actin in MVs, exosomes, and whole cell lysates (WCL).

Table 3.1. EVs Size Characterization by NTA, DLS, and TEM.

EV type	**Diameter (nm) by NTA**	**Diameter (nm) by DLS**	**Diameter (nm) by TEM**
MVs	286 ± 7.35	265 ± 3.34	263 ± 34.7
Exosomes	63.2 ± 5.82	51.4 ± 1.87	53.2 ± 19.9

Lastly, actin cytoskeleton is highly expressed in mammalian cells like MDA-MB-231[288]. MVs have also been shown to be actin positive and to have actin-ring structures[289, 290], and since maturation of multivesicular bodies to eventually generate exosomes is an actin guided process, exosomes are also actin positive[291, 292]. Therefore, WCL, MVs, and exosomes were immunoblotted for actin to assess the presence of particles in the three samples. Figure 3.1e shows an actin band at around 42 kDa

showing the expected results, presence in all three samples. These results taken together conclude that there is little cross contamination between these two EV populations. Given that we were able to achieve this degree of separation of populations, we proceeded to examine the differences between each type in the following studies.

3.5.2. Formation of EVSBs

EVSBs were made from MVs or exosomes using a modified protocol previously reported by our group to form proteinaceous bilayers[33, 34]. Briefly, MVs and exosomes previously labeled with a membrane-intercalating fluorophore, octadecyl rhodamine, R18, were incubated on a cleaned glass slide (Figure 2a). R18 was initially confined to exosomes and/or MVs. Next, unlabeled "fusogenic" liposomes were added to the well to induce rupture of EVs and spreading of R18 signal through the bilayer[34, 161]. This process mirrors what has been observed by us for other vesicle types, indicating that EVs also follow a similar rupture and relaxation process to form a planar bilayer[33]. After 40 min of incubation followed by PBS rinsing, a contiguous supported bilayer was formed and R18 signal uniformly spread out, diffusing freely within the planar bilayer surface. A time lapse video of this process can be found in the supplemental information 3.S1.

FRAP was utilized to determine mobility of R18 in the 2D plane of the supported bilayers. Using a laser beam, a 23 μm diameter spot was photobleached in the supported bilayers at time zero as indicated by the blue arrow on Figure 3.2b. Partial recovery of the photobleached spot in the bilayers is observed in Figure 3.2b at 108 sec, 217 sec, and 157 sec for exosome-EVSB MV-EVSB, and POPC/PEG-SLB respectively, indicated by the green arrows. Final recovery of the photobleached spot

is indicated by the orange arrow at around 900 sec. Color coded FRAP images presented in Figure 3.2c are micrographs of a supported bilayer at the corresponding time indicated by the color-coded arrows. The ability of EVSBs to recover confirms the formation of planar, mobile supported bilayers. Fluorescence recovery curves presented in Figure 3.2b were used to determine the Diffusion coefficient (D) and mobile fraction of EVSBs, and a control POPC/PEG-SLB, as described in the Methods section, and reported in table 3.2.

Table 3.2. Diffusion coefficient and mobile fraction of R18 in EVSBs.

Type of SLB	**Diffusion coefficient ($\mu m^2/s$)**	**Mobile Fraction**
MVs-EVSB	0.23 ± 0.071	0.94
Exosomes-EVSB	0.32 ± 0.033	0.94
POPC/PEG- SLB	0.49 ± 0.031	0.98

These data importantly show that the bilayer platforms that we generated are fluid over a scale of 20 microns and minimally free of defects, as noted by the very high mobile fraction (a low fraction would be indicative of a lack of unruptured vesicles that are not able to exchange with surrounding bilayer). Finally, comparing D values for all bilayers, we observe that both MV- and exosome- EVSBs are less fluid and diffusive than the POPC/PEG-SLB. These results are aligned with the expectation that the protein-laden SLBs would have lower diffusion coefficients due to obstacles that prevent lipid and protein diffusion[293].

Protein content of EVSBs from MVs and exosomes was assessed to allow cross comparison of our results between both types of EVSBs and to ensure the replication of

the same conditions between both types of EVSBs. To do so, the protein concentration on samples used to make EVSBs, $1.62\times10^{7} \pm 1.34 \times10^{6}$ EVs/mL, was found using a BCA protein assay. The protein content of MVs-EVSB was found to be 7.369 μg and 6.539 μg for exosomes-EVSB. Note that protein content of MVs-EVSB is slightly higher than that of exosomes-EVSB. However, the difference in protein content between the two EVSBs is not statistically significant as seen in Figure 3.2d.

Lastly, EV cargo was tracked before and after EVSB formation to ensure that no left-over cargo was present in the platform that could affect the results. EVSB, as a model of EVs surface, should contain just the components of EVs membrane and not their cargo after rupture and rinse. As EVs rupture, their cargo has two choices: it is either released to the bulk space (and so able to rinse away) or trapped underneath the created SLB. After being formed, EVSBs are thoroughly washed with PBS, to ensure any soluble EV cargo is removed. EV cargo was labeled using an RNA probe that crosses the EVs membrane and labels mRNA in the vesicles. Figure 3.2e and 3.2g displays presence of cargo (mRNA) of intact, adsorbed exosomes and MVs, respectively, as they are absorbed on the glass slide. After fusogenic liposome addition and subsequent rupture to form the EVSB, followed by copious PBS buffer washing, Figure 3.2f and 3.2h show no punctate fluorescence signal and therefore suggest no presence of EV cargo on either the exosome-EVSB or the MV-EVSB, respectively. Hence, any biological outcomes observed from interactions between EVSBs and ADSCs are most likely due to ADSCs interacting with EVs membrane constituents and not with their cargo.

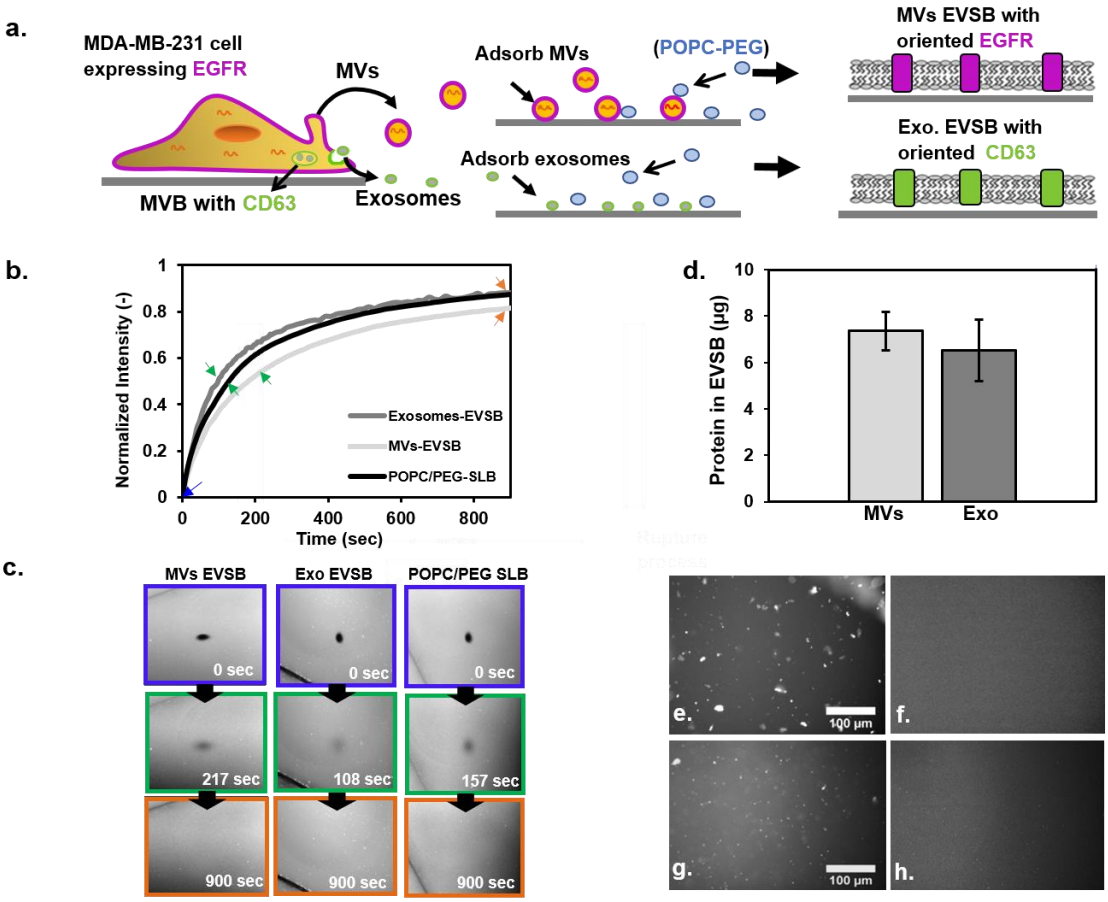

Figure 3.2. EVSBs formation and characterization. a) Diagram showing formation of MVs-EVSB and exosomes- EVSB. b) Profile of MVs- EVSB, exosomes-EVSB, and POPC/PEG-SLB fluorescence recovery after photo bleaching. c) Color coded pictures corresponding to the fluorescence recovery of the supported bilayers at the time indicated by the correspondent-colored arrow. d) protein content of EVSBs. e) Exosomes mRNA absorbed on glass. f) Exosomes mRNA after EVSB formation. g) MVs mRNA absorbed on glass. h) MVs mRNA after EVSB formation. n = 4, mean ± SD, *p ≤ 0.05, **p ≤ 0.01.

3.5.3. Protein characterization in EVSBs

3.5.3.1. Detection of EVs membrane components in EVSBs

Detection of HSP70 and CD63 presence in exosome-EVSBs. EVSBs are *in vitro* models of EV membranes and so must preserve components of the EV membrane to be useful. HSP70, a heat shock protein specific to, and highly expressed in exosomes[294, 295], and CD63, were utilized to verify the presence of native exosome surface components in exosome-EVSBs. Anti-HSP70 and anti-CD63 antibodies were employed as primary

antibodies and complemented with a fluorescent secondary antibody for HSP70 and CD63 fluorescent detection. Figure 3.3f and 3.S3c show exosome-EVSBs displaying specific binding and presence of HSP70 and CD63, suggesting that the generated EVSB preserves surface components similar to exosomes and that proteins in the bilayer conserve the same orientation as in exosomes derived from MDA-MB-231 cells[33], that is, the binding site for the antibody is facing towards the bulk phase. In contrast, Figure 3.3d and 3.3e, and 3.S3a and 3.S3b are controls to show no specific binding of CD63 and HSP70 to MV-EVSBs nor POPC/2k-SLBs. These results were expected since no CD63 nor HSP70 are present in POPC liposomes, nor in MV membranes.

Detection of EGFR presence in MV-EVSB. In the same manner, EGFR was used as a marker of MVs[20, 296, 297] and its binding and presence was tested on MV-EVSBs to assess the preservation of native MV surface components in the EVSB.

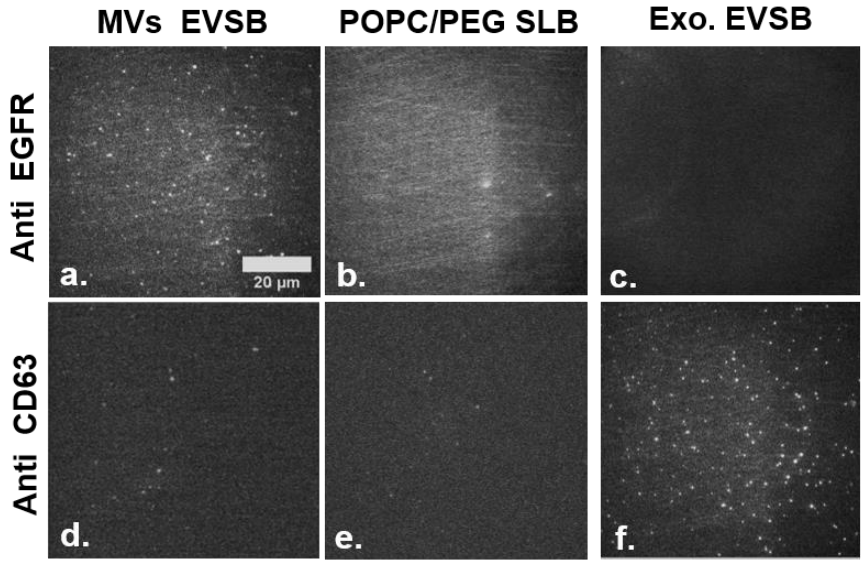

Figure 3.3. Detection of EVs membrane components in EVSBs. (a-c) EGFR detection on EVSBs. a) MVs- EVSB displays binding of EGFR, as a MVs native component. b) POPC/PEG-SLB (control) shows no binding of EGFR. c) Exosomes-EVSB (control) shows no specific binding of EGFR. **(d-f) CD63 detection in EVSB.** d) MVs- EVSB (control) shows not binding

of CD63. e) POPC/PEG-SLB (control) show no binding of CD63. f) Exosomes- EVSB shows specific binding of CD63, an exosome native component.

This experiment was conducted in the same manner as for exosomes but using a primary anti-EGFR antibody in conjunction with a fluorescent secondary antibody. Figure 3.3a shows a MV-EVSB displaying specific binding and presence of EGFR in the MV-EVSB. The results suggest that our MV-EVSB mimics the properties of cancer MVs in a planar platform containing these proteins and in the same orientation as MVs derived from MDA-MB-231 cells. Our results show that EGFR orientation in MVs is preserved in MV-EVSB because anti-EGFR antibody was able to bind to EGFR on the surface of MVs-EVSBs. Figure 3.3b and 3.3c are controls that show no specific binding to EGFR and no presence of it in exosome-EVSB and POPC/2k-SLB. These results are expected as EGFR is not an exosomal marker [20] and POPC liposomes do not contain any proteins such as EGFR. Note that presence of EGFR in exosome-EVSB, Figure 3.3c, and of CD63 and HSP70 on MV-EVSB, Figure 3.3d and 3.S3a, is negligible. These results reassure the presence of two different EVs populations, exosomes and MVs.

3.5.3.2. Protein orientation and mobility in EVSBs

Protein orientation. In previous work, our group has shown that supported lipid bilayers made directly from mammalian cell blebs[33, 34], bacterial outer membrane vesicles (OMVs)[190], and virus-like particles[298], preserve much of the complexity of the cell plasma membrane and preserve protein orientation and mobility. Moreover, it was shown that the rupture process of such nanoparticles (cell blebs, OMVs, and virus-like particles) forming supported bilayers results in primarily outward facing membrane proteins following a "parachute" mechanism of bleb rupture[33, 34], which is a similar behavior to a mechanism proposed in the literature[299], and corroborated by computational

simulations[300]. An enzymatic accessibility assay was conducted to find that the orientation of proteins in the supported bilayers made by our protocol results in the protein orientation matching the native state (outside facing up)[34, 190, 298]. Therefore, we believe that during EVSB formation, EVs will rupture following the same "parachute" mechanism that cell blebs and OMVs display, with membrane proteins predominantly facing outwards. To corroborate that our EVSBs also preserve EV membrane complexity and native protein orientation, we conducted antibody binding experiments, as described above. In the previous section (3.5.3.1.), immunolabeling was employed to detect the presence of native MVs membrane components (EGFR), and native exosomal membrane components (CD63 and HSP70). These tests also demonstrate the preservation of these proteins in their natural orientation in our EVSBs, by showing specific binding to the extracellular target.

Protein mobility. As mentioned above, figure 3.3a, 3.3f, and 3.S3c display the presence of EGFR on MVs-EVSB, and of CD63, and HSP70 on exosomes-EVSB. These proteins appear as bright punctuate clusters. Three main possibilities exist for this clustering we observe. First, the proteins in the EVSB, which originate from the EVs, may already be in a cluster within the EV before rupturing. Second, once EV ruptures and forms a planar patch, the protein within it interacts with the support and become immobilized at that point, thus they are unable to spread out radially from the rupture site. Third, the primary and secondary antibodies can link together multiple proteins, hindering their diffusion.

For the first possibility, there is no current information on aggregation of EGFR in MV membranes, nor on aggregation of CD63 and HSP70 in exosome membranes, so

we cannot rule out this possibility entirely. For the second possibility, we attempted to limit the interactions of proteins with the support by including PEG2000 spacers. Although these EVSBs exhibit full lipid mobility, the labeled proteins did not, presumably because the space between the bilayer and the glass was not enough to accommodate the cytosolic tails of EGFR, CD63, and HPS70. While a larger PEG molecular weight could have been used, we elected to use a short chain of PEG (MW of 2000) to limit its influence on the membrane surface presented to the cultured cells, as we expect PEG to be present on both sides of the liposome. It is of note that our results show that PEG2000 does not interfere with the ability of antibodies to bind to target proteins in the ESVBs. Thus, cells cultured on EVSBs should be able to interact with these species in the presence of PEG2000 as well. Our results suggest that the space generated between the bilayer and glass was not enough to allow the mobility of cytosolic tails in some proteins, but that this immobilization of proteins does not causes substantial changes to the protein structure facing the bulk solution since antibodies successfully bounded their target proteins (EGFR, CD63, and HSP70). For the last possibility, antibody binding and secondary labeling of those antibodies can also lead to reduced diffusion/immobilization due to linking of several proteins together that effectively increases the size of the diffusing entity. All things considered, we believe the most likely cause of the protein aggregation observed here is immobilization of proteins in our supported bilayer platform, but this is certainly a point of further investigation, and may be a combination of these possibilities.

3.5.4. Cell spreading and adhesion of ADSCs on EVSBs

In the past several years, SLBs have gained attention as potential cell culture platforms[32, 158, 247]. However, it has been observed that SLBs generated from reconstituted lipids, as POPC, are not a favorable substrate for cell culture. Because phosphocholine lipids are zwitterionic, inert, and lack surface moieties essential for cell adhesion, cells are incapable of creating strong adhesions on those surfaces[32, 158, 163-167]. To overcome this difficulty, several research groups have modified SLBs to enhance cell adherence with different approaches such as coating them with ECM proteins[32], incorporating RGD moieties [166], and modifying with in-situ peptides[167]. However, all these modified SLBs as cell culture platforms use a peripheral agent (antibody, peptide, ECM protein, etc.) external to the supported bilayer to aid cell growth and adhesion rather than an embedded, integrated component of the membrane; the lipids merely serving as an inert background, and not really serving the purpose of being true plasma membrane mimics.

As our goal is to isolate just the surface effects of the EVs on the behavior of cells, we endeavored to make bilayers that would more closely represent the surface of the native membranes from these vesicles. Here we showed that we can form hybrid bilayers, EVSB, derived from EVs. Then, we wanted to test if we could culture ADSCs on these surfaces and observe any differences in the cell morphological or biochemical behavior. To do so, ADSCs were cultured on four surfaces: MV-EVSB, exosome-EVSB, POPC/PEG-SLB, and EZ-slides. POPC/PEG-SLB was chosen as a negative control since cells should not adhere and grow on these substrates, as noted above [32]; and as a positive control, EZ-slides, were used, which allow cell adhesion and spreading. As a cell model, human ADSCs were used. These primary cells make an appropriate model for this study

as previous groups have shown that their interactions with MDA-MB-231 derived EVs may influence their phenotype and proangiogenic potential[4, 5]. Lastly, literature suggests the ADSCs play an important role in cancer metastasis and progression[7, 47, 301].

After 24 hours of incubation, ADSC adhesion and spreading were assessed by immunofluorescence detection of focal adhesions per cell and cell surface area respectively. Cells were fluorescently stained for vinculin, as a marker of focal adhesions, and DAPI to distinguish the cell nuclei. Vinculin is a cytoplasmic actin-binding protein highly expressed in focal adhesions and essential in cell-substrate adhesion[302, 303]. In addition, as it delineates the cytoskeleton, it allows measurements of cell surface area. Figure 3.4 shows fluorescence images of ADSCs cultured on the four surfaces, with red stain delineating the area of the cell and blue stain representing the nuclei.

Figure 3.4a indicates that ADSCs seeded onto a MV-EVSB, readily adhere to the bilayer leading to focal adhesion formation and elongation as suggested by a high cell aspect ratio of 2.57. In the same manner, ADSCs cultured on an exosome-EVSB (Figure 3.4b) adhere to the bilayer and spread with a slightly higher aspect ratio, 3.78, than cells on MVs-EVSB. As expected, ADSCs on POPC/PEG-SLBs (Figure 3.4d) generate fewer adhesions to the substrate compared to cells culture on EVSBs, and display low cell spreading on the substrate with a characteristic small aspect ratio of 1.09. This behavior may be attributed to a slow rearrangement of the cytoskeleton leading to incomplete spreading of cells on this bilayer, as has been described in the literature[247]. ADSCs cultured on EZ-slides (Figure 3.4c) adhere to the substrate and spread with a high aspect ratio of 3.71 as seen in Figure 3.S5. ADSCs exhibit similar adhesion behaviors on both EVSB types as ADSCs on EZ-slides with ADSCs on MV-EVSBs presenting increased

spreading and higher number of focal adhesions than ADSCs on exosome-EVSB. Individual focal adhesions images presented in Figure 3.4e-h were obtained from image processing of Figures 3.4a-d. The image processing technique used was an approach developed by Horzum et al. [304] using ImageJ software. It allows quantification of focal adhesions and its analysis as shown in Figure 3.4i-j. Moreover, data displayed in 3.S4a and 3.S4b is the data from Figure 3.4i and 3.4j, normalized by the total protein content of EVSBs. This normalization allows us to compare the effect that exosomes and MVs surface have on ADSCs spreading and focal adhesion formation independent of their different protein content. As presented in Figure 3.4i and 3.4j, ADSCs on MV-EVSBs spread more and form an increased number of focal adhesions per cell than ADSCs on exosome-EVSB and on POPC/2k-SLBs. The same trend is observed when cell area is normalized to EVSB protein content, whereas a different trend was noted when FA number is normalized to EVSB protein content, Figure 3.S4. In that case, number of FAs of ADSCs on both types of EVSBs are not significantly different.

Moreover, ADSCs on exosome-EVSBs spread more and formed an increased number of focal adhesions than cells on POPC/PEG-SLBs. As expected, ASDCs on EZ slides (i.e., soda lime silica glass coated with ECM proteins) spread readily and formed a high number of focal adhesions as these conditions enable optimal cell attachment and spreading. Lastly, ADSCs on POPC/PEG-SLBs display a round shape with decreased cell surface area and focal adhesion number per cell compared to ADSCs cultured on the other surfaces.

In general, our results show that ADSCs on EVSBs spread more and form more focal adhesions per cell than ADSCs on POPC/PEG-SLB. In addition, we showed that in

effect MV and exosome surfaces influence ADSC behavior in the same way, but MVs have a stronger influence than exosomes. We note here that one reason for the observed differences in spreading and focal adhesion formation can be differences in surface viscosity [247] but because the difference in diffusion coefficients across these samples is not large (factor of at most 2), we believe the effect we see here reflects the influence of the chemical composition of the supported bilayers.

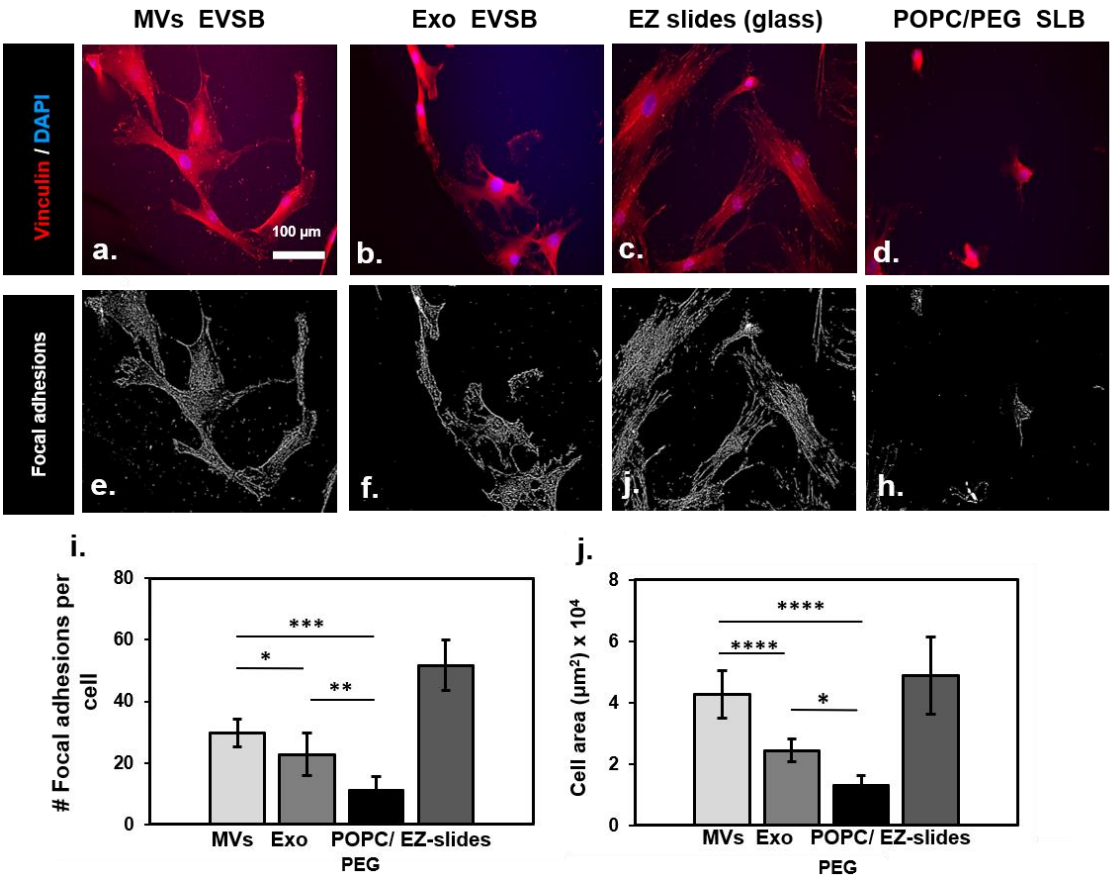

Figure 3.4. Cell surface area and focal adhesions of ADSCs cultured on different surfaces. (a-d) ADSCs on MVs-EVSB, exosomes- EVSB, EZ slides, and POPC/PEG-SLB. Vinculin (FAs) generates a red signal and DAPI (nuclei), a blue one. (e-h) Isolated focal adhesions obtained from images on the top (a-d). i) Quantitative analysis of number of focal adhesions per cell on all substrates. j) Quantitative analysis of cell surface area for ADSCs cultured on all substrates. n = 3, mean ± SD, *p ≤ 0.05, **p ≤ 0.01, and ***p≤0.001

3.5.5. Cell Viability and angiogenic activity of ADSCs cultured on MV or exosome-EVSB

For further investigation of biological activity of ADSCs on EVSBs, the viability of cells cultured on EVSBs was assessed and compared to the viability of cells seeded on EZ slides and on POPC/PEG-SLBs (Figure 3.5a) for day 1, 3, and 5 after seeding. Green signal represents live cells and red represents dead cells. As shown in the top row of Figure 3.5a, ADSCs on MV-EVSB reach about 95% confluency on day 5 and have a constant viability of around 91% on all examination days. The second row shows ADSCs on exosome-EVSB that reach around 85% confluency on day 5 and keep a constant behavior of around 92% viability on all days. ADSCs on EZ slides, third row, reach confluency of about 95% at day 5 and show constant viability of around 94% during all times. Lastly, ADSCs on a POPC/PEG-SLBs, fourth row, tend to form aggregates and display a round morphology with low aspect ratio as expected from previous literature reports. Cells reach about 50% confluency at day 5 and show constant viability of around 68% during all examination days. Our results suggest that modification of SLB surface composition with cancer EVs, generating EVSBs, contributed to a less fluid composition and to the preservation of some EVs membrane native proteins that allow cell attachment, cell spreading, and cell viability. Besides influencing adhesion, spreading, and viability, we hypothesized that EV components maintained in the EVSBs may trigger differences in cellular phenotype that may lead to altered production of proteins and growth factors. As mentioned before, it has been established that ADSC morphology and proangiogenic activity, indicated by high levels of VEGF secretion, are altered by addition of EVs to ADSCs culture [4, 5]; however, it is not known what drives these outcomes. Our aim was to

test the impact of the surface moieties of the EVs on these cellular activities using the EVSB platform, since this represents the first point of contact between ADSCs and EVs and an opportunity to change the microenvironment for eventual tumor growth.

Furthermore, with this platform we can isolate the surface effects from any effects of the cargo delivery. We note that the converse studies of cargo delivery are challenging due to the unknown entry pathway EVs take and the triggers that open the particle to deliver the contents inside the cell. Therefore, here we set out to assess first the role of the EV surface moieties on ADSCs and if there are any differences between MVs and exosomes. To do so, we measured VEGF secreted by ADSCs on the four test surfaces. VEGF was measured on day 1 and 4 after seeding to observe if VEGF secretion varies as a function of time. VEGF secretion by cells on all surfaces is similar on day 1. Figure 3.5c shows that ADSCs on MV-EVSB secreted nearly double

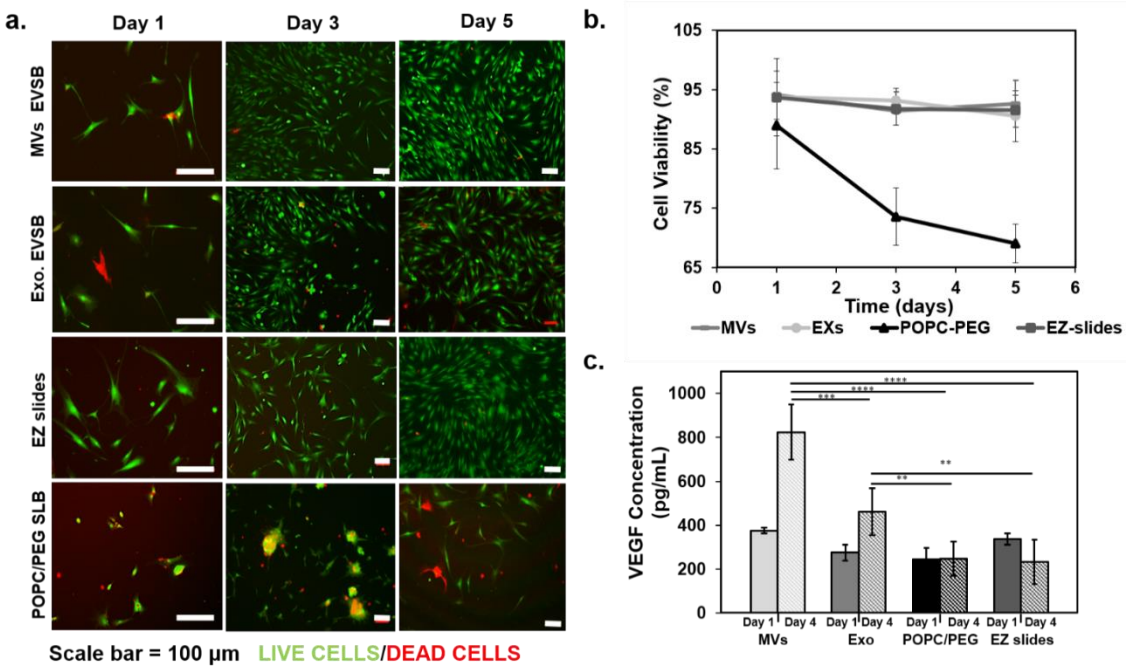

Figure 3.5. Viability and angiogenic activity of ADSCs on different surfaces. a) Top row displays viability of ADSCs seeded on MVs- EVSBs at day 1, 3, and 5 after cell seeding. Second row displays ADSCs on exosomes-EVSBs at day 1, 3, and 5. Third row displays ADSCs on EZ-

slides, and bottom row shows ADSCs on POPC/PEG-SLB at day 1, 3, and 5. Viable cells express green signal, and death cells originate red signal. b) Viability of cells on EVSBs and EZ slides is between 85% and 95% during all examination days, and cells on POPC/PEG-SLB have lower viability starting at 84% and decreasing to 67% from day 1 to 5. c) VEGF concentration secreted by ADSCs cultured on MVs derived EVSB, exosomes derived EV SB, POPC/PEG-SLB, and EZ slides on day 1 and 4 after cell seeding.

their VEGF secretion by day 4 compared to day 1 after seeding. In the same way, ADSCs on exosome-EVSB significantly increased their VEGF secretion by 50% on day 4 compared to day 1. In contrast, ADSCs on POPC/PEG-SLB did not show a significant difference between VEGF secreted on day 1 and 4. Finally, cells on EZ slides secreted significantly less VEGF on day 4 compared to day 1. That VEGF secretion levels decreased from day 1 to 4 in ADSCs on EZ-slides, contrary to the behavior in the rest of the culture surfaces where VEGF secretion increases over time, suggests that cell proangiogenic activity increases as a function of time on these other surfaces. However, VEGF secretion of ADSCs on MVs and exosomes-EVSBs is significantly higher than on ADSCs cultured on EZ slides and POPC/PEG-SLB at day 4, suggesting that cell proangiogenic activity increases not just as a function of time, but as ADSCs interact with EV surfaces.

In addition, our results showed preservation of an intact biological composition of EVSBs after four days of cell culturing. We can deduce that at least some of the cues for upregulating growth factor comes from the surface of the EVs themselves since cells on EV surfaces have a higher proangiogenic activity than cells on non-EV derived surfaces.

Data presented in Figure 3.5c was normalized by the protein content of EVSBs, Figure 5.S6a, and by the number of viable cells, Figure 3.S6b. These normalizations make the comparison of VEGF secretion of ADSCs on MV-EVSBs and exosome-EVSBs more

impartial since not just the EV concentration is considered but also the protein content and the number of viable cells in each EVSB. Normalized VEGF secretion of ADSCs on all surfaces maintains the same behavior as data presented in Figure 3.5c. These results suggest that the surfaces of EVs, with a higher impact from MVs, present cues that influence the receiving cell to promote growth factors and changes that support the microenvironment that can lead to new tumor growth.

Treatment of ADSCs with cancer EVs during cell culture results in myofibroblast differentiation compared to non-treated cells [4, 5]. Hence, we wanted to investigate the influence that EVs surface, represented by EVSB, have on promoting myofibroblast differentiation. To do so, ADSCs cultured on MV-EVSB, exosome-EVSB, POPC/PEG-SLB, and EZ-slides, grew for 3 days and were stained against alpha smooth muscle actin, α-SMA. α-SMA is a marker of myofibroblasts and was used to detect phenotypic changes on ADSCs to myofibroblast-like. Results presented in 3.S6 show that ADSCs on MV-EVSB and exosomes-EVSB do not express higher α-SMA than ADSCs on EZ-slides and/or POPC. Therefore, the interaction between EVs surface and ADSCs is not enough to trigger phenotype differentiation to myofibroblasts. We hypothesize then that phenotypic differentiation may result instead from the delivery of EVs cargo into ADSCs. This hypothesis will be further investigated in the future.

3.6. Conclusions

Using our EVSBs as models of EV surfaces, we were able to show that interactions between ADSCs and EV surfaces contribute to cell adhesion and spreading, proliferation, viability, and proangiogenic potential. Moreover, MV-EVSB influenced cell spreading and VEGF secretion significantly more than exosomes-EVSB. Since all

data was normalized by EVSBs content, we can say that those results were not necessarily due to different proteins levels in both EVs types EVSBs. However, we cannot rule out that size differences, and thus higher EV content (area) in the EVSB, between MVs and exosomes, could be a possible reason for MVs-EVSB to have stronger effects on cell spreading, adhesion, and proangiogenic activity than exosomes-EVSB.

We were able to show that rupture of EVs forms a homogeneous bilayer and no presence of EV cargo in the formed EVSB platform. Therefore, we suggest that the biological outcomes observed in ADSCs cultured on EVSBs are due to their interactions with EV membrane constituents and not a result of EV cargo. While it remains to be tested if the cargo delivery further enhances growth factor levels, we believe these platforms will be useful to defining the impact of the surface cues on cellular behavior and biological outcomes in various contexts. Furthermore, given that the interaction of the particle surface yields cellular impacts that promote conditions for oncogenic activity, this platform will be a useful tool for the development of strategies to limit these interactions for future therapeutic development.

Finally, the ability of our EVSB platform to be made with any type of EV allows us to study the outcome of any type of EV (used to make the EVSB) surface interaction with a desired kind of cell, opening the possibility of studying the effects of different types of cancer derived EVs on stromal cells and/or cancer cells that are cultured upon them. As such, our platform can facilitate the investigation different diseases in which EVs play an important role, such as cardiovascular and metabolic diseases[16], neurodegenerative diseases[35], and cigarette smoke associated diseases[36]. Finally, this platform can be deployed to develop ways to disrupt deleterious surface interactions

between MVs or exosomes with healthy cells to avoid negative outcomes that lead to disease progression.

3.7. SUPPORTING INFORMATION

3.7.1. Experimental Section

3.7.1.1. Cell Culture

StemPro human adipose-derived stem cells (ADSCs) were obtained from ThermoFisher Scientific (Rochester, NY) and cultured in ADSC growth media purchased from Lonza (Walkersville, MD). Experiments were performed with cells between passages 3 and 8. MDA-MB-231 cells, which are highly metastatic human adenocarcinoma cells, were purchased from ATCC (Manassas, VA) and maintained in Dulbecco's modified Eagle's media, DMEM, Corning (Corning, NY) supplemented with 10% fetal bovine serum, FBS, ThermoFisher (Waltham, MA) and 1% penicillin-streptomycin, P/S (Corning). For serum free media used for EVs isolation, MDA-MB-231 cells were maintained in DMEM media supplemented with 1% P/S. All cell cultures were maintained at 37°C and 5% CO_2 and media was changed every two days as recommended by manufacturers.

3.7.1.2. Preparation of Glass Slides for Formation of Supported Bilayers

Glass coverslips 25 x 25 mm, No. 1.5, VWR (Radnor, PA) were the rigid surfaces for supported lipid bilayers. They were cleaned by washing with 45 mL of 50% hydrogen peroxide, Sigma (St. Louis, MO) followed by 105 mL of 70% sulfuric acid, VWR (Radnor, PA) for 10 min. (Note: use extreme caution with this solution; highly oxidative). Coverslips were then rinsed for 30 min with generous amounts of deionized water generated by an Ultrapure water system, Siemens pureLab (Malvern, PA). Clean coverslips were stored in deionized water at room temperature until needed. For

formation of bilayers, coverslips were washed with deionized water and dried with high purity nitrogen gas before each use.

3.7.1.3. Polydimethylsiloxane (PDMS) Well Fabrication

A 10:1 ratio mix of Poly(dimethylsiloxane), PDMS, SYLGARD 184 (Ellsworth, ME) monomer and crosslinker was thoroughly stirred and degassed to make sure it was fully mixed. It was poured in a 100 mm petri dish and baked at 70 ̊C for 5 h. The cured PDMS sheet was cut in pieces to fit on top of a coverslip. Using a hole puncher, a circular hole of 1 cm diameter was made in each of the PDMS pieces to create a well when affixed to the coverslip. To ensure attachment of the PDMS to the clean coverslip, the well was placed in the oven at 65 ℃ for 10 min.

3.7.1.4. Preparation of Fusogenic Liposomes

1-Oleoyl-2-palmitoyl-sn-glycero-3-phosphocholine, POPC, Avanti Polar Lipids (Alabaster, AL) and 1,2-distearoyl-sn-glycero-3-phosphoethanolamine-N- [methoxy (polyethylene glycol)-2000], PEG2000-PE, Avanti Polar Lipids (Alabaster, AL) were used to create fusogenic liposomes. POPC/PEG liposomes were made with 99.5% (mol/mol) POPC and 0.5 %(mol/mol) PEG2000-PE. The lipid mixture was prepared by dissolving the powdered lipids in chloroform, Sigma (St. Louis, MO), adding appropriate ratios to a previously cleaned glass vial, and drying them with nitrogen gas followed by desiccation in a vacuum chamber for 3 h. The lipid film was resuspended in phosphate buffered saline, PBS, pH 7.4, to a final concentration of 1 mg/mL and stored at -20 ̊C overnight. After thawed, liposomes were extruded through a 100 nm membrane, Whatman (Maidstone, UK) and stored at 4 ̊C for up to two weeks.

3.7.1.5. MVs Isolation

MDA-MB-231 cells were cultured on a 150 cm^2 cell culture flask (Corning, NY) in 15 mL of DMEM media (Corning, NY) supplemented with 10% FBS and 1% P/S until they reached 75-85% confluency. To avoid the presence of serum-derived exosomes during EVs isolation, cells were incubated in serum-free DMEM supplemented with 1% P/S for 18-30 h. at 37°C and 5% CO_2. Media was collected and centrifuged at 280 x g for 12 min at 21 °C to remove cells, followed by a second centrifugation at 10000 x g for 25 min. at 21 °C to remove cell debris. The cleared media was vacuum filtered using a 0.22 μm Millipore Steriflip poly (vinylidene difluoride) (PVDF) filter, Millipore (Burlington, MA) to separate MVs and exosomes. The particles retained by the 0.22 μm filter (designated MV fraction) were resuspended in 0.5 μL of serum-free media and stored at 4°C. Remaining filtrate from the vacuum tube was stored at 4° C for subsequent isolation of exosome fraction (next section). Characterization of MVs was performed with NS300 NanoSight (Malvern, UK), Nano-ZS Zetasizer (Malvern, UK), and Transmission Electron Microscopy, TEM, FEI Tecnai-12 Spirit (Hillsboro, OR). All experiments were done with MVs within two days of isolation. To obtain MVs lysates further used for western blot detection of MV markers, MVs captured on the PVDF filter were resuspended in 100 μL of lysis buffer, RIPA buffer and Pierce proteinase inhibitor cocktail tablet, Thermo Fisher Scientific (Waltham, MA), and kept at -20° C until needed.

3.7.1.6. Exosome Isolation

Filtrate generated in the vacuum tube during MVs isolation was centrifuged for 5 min at 300 x g to eliminate any bigger particles and cell debris. Supernatant was transferred into ultracentrifuge tubes followed by ultracentrifugation at 100,000 x g at 4 °C for 4 h. The

generated exosome pellet was resuspended in 50 µL of serum-free media. Exosomes were kept at 4˚C until subsequent use. Characterization of exosomes was performed in the same way as MVs characterization. Exosomes sample preparation for Western blot was done following the same procedure as for MVs.

3.7.1.7. EVs Size and Concentration

NTA measures nanoparticles in suspension by analyzing Brownian motion tracking of particles and determining the corresponding the size of the translational diffusion diameter (hydrodynamic diameter) of each sphere/nanoparticle. The lower resolution limit of NTA depends on the scattered intensity of the particle and the sensitivity of the camera. Biological particles such as EVs have a refractive index of about 1.37-1.45 giving a lower limit of detection of around 30 nm[38]. For our study, NS300 Malvern was utilized. Using this equipment, particles between 30-800 nm can be measured with a concentration resolution of 10^6 to 10^9 particles/mL. In addition, EV size was also measured by dynamic light scattering (DLS, Zetasizer Nano ZS, Malvern), and transmission electron microscopy (TEM, FEI T12 Spirit, Tecnai). DLS measures the diffusion of particles in solution under Brownian motion using scattering of light and determines particle size distribution using the Stokes-Einstein relationship. Nano ZS (Malvern), the Zetasizer used for our study, has a particle size measurement range of 0.3 nm to 10 µm. Finally, TEM uses an electron beam to visualize particles and generate a highly magnified image of EVs. FEIT12 Spirit Tecnai TEM, the equipment used for our study, is capable of imaging particles as small as 0.20 nm.

3.7.1.8. Transmission Electron Microscopy (TEM)

Freshly isolated MVs and exosomes were visualized using a FEI Tecnai-12 Spirit TEM (Hillsboro, OR) at 120 kV at the Cornell Center for Materials Research. Samples were loaded onto a 300-mesh carbon-coated copper grid and negatively stained using 1.5% uranyl acetate.

3.7.1.9. Western Blot

Equal volume, 40 µL, of MVs lysate, exosomes lysate, and WCLs derived from MDA-MB-231 cells were loaded on a 4-12% bis-Tris gel Bolt, Invitrogen (Waltham, MA) and transferred onto a PVDF-membrane at 20V constant. Membranes were blocked with 5% nonfat dry milk in TBST (tris-buffered saline and Tween20) and incubated overnight at 4˚C with primary antibodies in TBST for the appropriate target protein. After washing, membranes were incubated with secondary antibody in TBST for one 1 h. at room temperature and imaged using a Western ECL detection kit, BioRad (Hercules, CA) on a ChemiDoc XRS, BioRad (Hercules, CA) imaging system. Primary antibodies used were: 0.8 µg/mL CD63, ab193349, Abcam (Cambridge, MA), 1:1000 EGFR, 2232, Cell Signaling Technology (Danvers, MA), and 0.20 µg/mL Actin, AF4000, R&D Systems (Minneapolis, MN). Secondary antibodies used were: 1:2500 Goat Anti-mouse (HRP), ab6789, Abcam (Cambridge, MA) for CD63, 1:2500 Goat Anti-Rabbit IgG H&L (HRP), ab205718, Abcam (Cambridge, MA) for EGFR, 1:1000 and Sheep IgG HRP-conjugated Antibody, HAF016, R&D systems (Minneapolis, MN) for actin.

3.7.1.10. Fluorescent Labeling of Liposomes and EVs

To visualize the formation of supported bilayers, liposomes were fluorescently labeled with a membrane-intercalating fluorophore, octadecyl rhodamine (R18). 1 µL of 0.1

mg/mL R18, Molecular Probes (Eugene, OR) was incubated with 100 µL of liposomes, sonicated, Model # BD2500A-DTH, VWR (Radnor, PA) for 30 min, and the unincorporated fluorophore was removed using a G25 spin column, GE Healthcare (Pittsburgh, PA). The same procedure was followed to label exosomes and MVs, using 100 µL of each of the samples.

3.7.1.11. Formation of Phosphatidylcholine Supported Lipid Bilayers

Supported lipid bilayers, SLB, self-assemble on a clean coverslip using the well-established vesicle fusion method as shown previously[33, 34]. 100 µL of 1.0 mg/mL of POPC/PEG were added into a well and incubated for 20 min. at room temperature. Wells were thoroughly washed with phosphate buffered saline, PBS, to remove excess lipid vesicles remaining in the bulk phase after bilayer formation. This surface was used as a negative control surface for ADSC culture.

3.7.1.12. Formation of MVs- or Exosome- EVSBs

For EVSB formation, 100 µL of MVs (concentration 1.623×10^7 MVs/mL) solution were added to the a PDMS well and incubated at room temperature for 7 min. The well was thoroughly rinsed with phosphate-buffered saline, PBS, to remove unabsorbed MVs. Formation of the bilayer was induced by addition of 70 µL of 1 mg/mL POPC/PEG into the well and incubated for 20 min at room temperature followed by rinsing with PBS. The same procedure was followed to form an exosome - EVSB, using 100 µL of exosomes (concentration 1.623×10^7 exosomes/mL). Millicel EZ- glass slides (Millipore, Burlington, MA) were utilized as a positive control surface for ADSC cell culture.

3.7.1.13. Detection of Epidermal Growth Factor Receptor (EGFR) in MVs- EVSB

MV- EVSB were incubated in 70 µL of 20% normal goat serum, GS, Thermo Fisher Scientific (Waltham, MA) for 30 min for nonspecific binding blocking. The well was washed with phosphate-buffered saline, PBS, and incubated in 70 µL of µg/mL EGFR, aa 746-750 deletion, R&D Systems, (Minneapolis, MN) for 2 h. at room temperature. The well was incubated in 70 µL of 1:2000 Donkey Anti-Mouse IgG NorthernLights R&D Systems, (Minneapolis, MN) secondary antibody for one hour at room temperature and imaged using total internal reflection fluorescence microscopy (TIRFM) to detect the presence or absence of EGFR on MVs-EVSB. The same procedure was repeated with a POPC/PEG-SLB and an exosome- EVSB as negative controls to show no specific EGFR binding.

3.7.1.14. Detection of HSP70 and CD63 in Exosome- EVSB

The same procedure stated above for EGFR detection in MVs-EVSB was followed for detecting the presence of HSP70 and CD63 in exosomes-EVSB. Antibodies used were: 20 µg/mL Human/Mouse/Rat HSP70/HSPA1A Antibody, R&D Systems (Minneapolis, MN) and 20 µg/mL Human CD63, R&D Systems, (Minneapolis, MN) as primary antibodies and 1:2000 Donkey Anti-Mouse IgG NorthernLights R&D Systems, (Minneapolis, MN) as secondary antibody.

3.7.1.15. EVSB Formation and Diffusivity by Fluorescence Recovery After Photobleaching (FRAP)

Fluorescently labeled EV rupture was observed using an inverted Zeiss Axio observer.Z1 microscope with α Plan-Apochromat objectives, a Hamamatsu EM-CCD camera, Image EM, model C9100- 13 (Bridgewater, NJ), and a X-Cite 120 microscope light source,

Lumen Dynamics Group Inc. (Ontario, Canada). To accumulate the fluorescence emitted by the fluorophores (R18), an ET MCH/TR filter cube, 49008, c106274, Chromatech Inc. (Canton, MI) was utilized. Labeled EVs were first incubated on the coverslips as described above, followed by addition and incubation of POPC/PEG vesicles (unlabeled) to rupture them. Formation of EVSBs was recorded and full rupture observed as shown in the Figure S2, supplemental movies, further corroborated by FRAP and additional techniques.

Diffusivity and mobile fraction measurements were carried out using photobleaching experiments. Using a 4.7 mW 488 nm krypton/argon laser, a 23 μm spot was photobleached for 300 ms followed by 40 min (30 sec intervals) of recovery of the photobleached spot. The fluorescence intensity of the photobleached spot was determined by subtracting the background from a reference spot that was unbleached and normalizing to each image captured to the maximum difference between the initial photobleached spot and the original intensity of that area. Using MATLAB, the spot recovery data was fit into a Bessel function model by the method of Soumpasis[34] to extract the half time to recovery, $t^{1/2}$. The following equation was used, $D = w2 /4t^{1/2}$ (Eq. S1), to determine the diffusion coefficient (D) for each bilayer type, where *w* is the full width at half-maximum of the Gaussian profile of the focused beam. The mobile fraction was determined by the final intensity over the initial intensity of the bleached area.

3.7.1.16. EVs Cargo Tracking in EVSBs

EVs cargo messenger RNA (mRNA) was labeled using an ExoGlow-RNA EV labeling kit, System Biosciences (Palo Alto, CA) and following the manufacturer's protocol. The Labeled MVs and exosomes were placed and adsorbed on PDMS wells to image EVs

cargo prior to EVSB formation. To image EV cargo after EVSB formation, the labeled MVs and exosomes were placed on a PDMS well followed by the addition of POPC/PEG to aid EVs rupture. Images of EV cargo before and after EVSB formation was carried out using total internal reflection fluorescence microscopy, TIRFM.

3.7.1.17. Bicinchoninic Acid Assay (BCA)

To measure the protein content of EVSBs, a BCA assay was performed to find the protein concentration on the EV samples used to prepared EVSBs. The assay was performed using a QuantiPro BCA assay kit, Sigma-Aldrich (St. Louis, MO) and following the manufacturer's protocol. MilliQ water was used as a blank for the BCA assay, and MVs and exosomes samples of varying dilutions were prepared and used as unknown protein concentration samples. A Corning 96 well plate with flat bottom, Sigma-Aldrich (St. Louis, MO) was used to conduct the BCA assay. 150 µL of BSA protein standards, blanks, or EVs unknown concentration samples were added in each of the wells. The same volume, 150 µL, of BCA working reagent were added to each of the wells containing standards, blank, or unknown EVs sample. Replicates were done for all the samples. Using the standard curve and the A_{562} obtained for each of the EVs samples, the protein concentration in MVs and exosomes was determined.

3.7.1.18. ADSCs Culture on EVSBs and on POPC/PEG- SLBs

ADSCs were seeded at a density of 1.05 x 10^4 cells/well on each of the following substrates. MVs-EVSB, exosome-EVSB, POPC/PEG-SLB, as a negative control, and Millicell EZ slide (no bilayer present) as a positive control. Four replicates of the experiment were performed.

3.7.1.19. Quantification of Cell Surface Area and Focal Adhesions (FAs)

ADSCs seeded on the four platforms were incubated for 24 h. at 37 ̊C and 5% CO_2 prior to cell imaging. Cells were fixed using a solution of 3.7% formaldehyde, Sigma-Aldrich (St. Louis, MO) and were incubated with 20% normal goat serum, GS, Thermo Fisher Scientific (Waltham, MA) for 30 min. to block unspecific binding. Cells were then incubated with 1:300 anti-vinculin antibody, Sigma-Aldrich (Waltham, MA) overnight at 4 ̊C to label cell focal adhesions, FAs ,and cell area. Cells were incubated with secondary Donkey Anti-Mouse IgG NorthernLights antibody, R&D Systems (Minneapolis, MN) at room temperature in the dark for 1 h. for detection of vinculin and with 6-diamidino-2-phenylindole (DAPI) SouthernBiotech (Birmingham, AL), for detection of cell nuclei. Cells were then imaged using the inverted Zeiss Axio imaging system stayed before. For each of the substrates, 45 images of the cells were taken with a 20X objective and analysis of focal adhesions and cell area were completed using ImageJ. Images were taken in frames where individual cells could be identified to allow the quantification of cell area and FAs. A total of 180 images, from 4 replicates, were obtained and analyzed for cells in each of the substrates. Quantitative analysis of focal adhesions was done following a protocol developed by Horzum et al.[304].

3.7.1.20. Cell Viability Analysis Using a LIVE/DEAD Kit

Viability of ADSCs cultured on the four platforms was assessed using LIVE/DEAD imaging kit obtained from Thermo Scientific (Pittsburgh, PA). ADSCs were cultured on the substrates and grown for 5 days with viability assessments done on days 1, 3, and 5. Following the manufacturer's protocol, the content of the green (live) vial was transferred into the red (dead) vial and gently mixed to create a 2x stock solution. Cells were

incubated with the generated 2x solution for 15 min. at room temperature and fluorescent images were captured. Using a 5x objective in the inverted Zeiss Axio observer stated before, 15 images were captured on each of the days for each of the substrates. Since the experiment was performed 3 times, 45 images were analyzed for each of the substrates on each of the examination days. Calcein is converted to a fluorescent molecule, green, when it interacts with viable cells, and EthD-1, which reacts with the nuclei content of dead cells, generated a red signal.

3.7.1.21. Assessment of Vascular Endothelial Growth Factor (VEGF) Secretion by ADSCs

To assess the proangiogenic activity of ADSCs, represented by VEGF secretion levels, VEGF concentration secreted by ADSCs cultured on the fourth different substrates was assessed on day 1 and day 4 after seeding. VEGF secretion levels were measured using a human VEGF DuoSet ELISA kit, R&D systems (Minneapolis, MN) according to the manufacturer's protocol. A standard curve was obtained by measuring the intensity of known VEGF concentrations. Using this formula, VEGF concentrations secreted by ADSCs in each of the four substrates were found by the intensity emitted by the samples. Three replicates of the experiment were performed. VEGF concentration secreted by cells on the four substrates were normalized by the number of viable cells in day 4 and by EVSB protein content in day 1 and 4.

3.7.1.22. Detection of Alpha Smooth Muscle Actin (α-SMA) in ADSCs on EVSBs

To investigate in ADSCs undergo myofibroblast transformation when seeded on EVSBs, levels of alpha smooth muscle actin, α-SMA, a marker or myofibroblasts, were measured on ADSCs on the four substrates. ADSCs cultured of EVSBs, POPC/PEG -

SLB, and EZ-slides were fixed 7 days after seeded. Cells were incubated in 20% goat serum, ThermoFisher Scientific (Waltham, MA) and 0.1% Triton X, VWR (Radnor, PA) for unspecific blocking and cell permeabilization. Cells were incubated with 15 µg/mL anti-α-SMA antibody, R&D Systems (Minneapolis, MN) overnight at 4°C. Secondary Donkey Anti-Mouse IgG NortherLights, R&D Systems (Minneapolis, MN) was incubated with cells at room temperature in the dark for 1 hour for the detection of α-SMA. To detect cell nuclei, 6-diamidino-2-phenylindole (DAPI, SouthernBiotech, Birmingham, AL) was incubated with the cells. Cells were then imaged using the inverted Zeiss Axio imaging system. Using a 20x objective, 20 images of cells in each of the substrates were captured and analysis of α-SMA fluorescence intensity was done using ImageJ. Captured images were taken of individual cells to distinguish α-SMA fibers in cells.

3.7.1.23. Statistical Analysis

For all experiments performed in this study, variance analysis was performed using a *t*-test with unequal variances to find significant differences between substrates and conditions. All data was plotted using Microsoft Excel, and it was presented as mean ± standard deviation (SD). For FAs and cell area experiment, three replicates were performed; hence, ADSCs on 16 wells were analyzed. For cell viability assays, three replicates of the experiment were done; hence, ADSCs in 12 wells were analyzed. VEGF secretion level experiment was performed 3 times, so 12 wells were analyzed for the experiment. Statistical significance levels were determined as follows: $*p \leq 0.05$, $**p \leq 0.01$, $***p \leq 0.001$, $****p \leq 0.0001$.

3.7.2. Results and Discussion

3.7.2.1. Visualization of MVs and Exosomes Using Transmission Electron Microscopy (TEM)

Populations of MVs and exosomes derived from MDA-MB-231 cells were isolated following the protocol presented in Section 3.S1. To visualize the size, dispersion, and morphology difference between both EV subtypes, transmission electron microscopy (TEM) was employed. Images of MVs and exosomes can be observed in Figure 3.S1. Note that exosomes tend to aggregate and are a more homogeneous and less disperse population than MVs. Size characterization of both EVs populations is presented in Table 3.1 in the main manuscript and agrees with the standard literature designations[1].

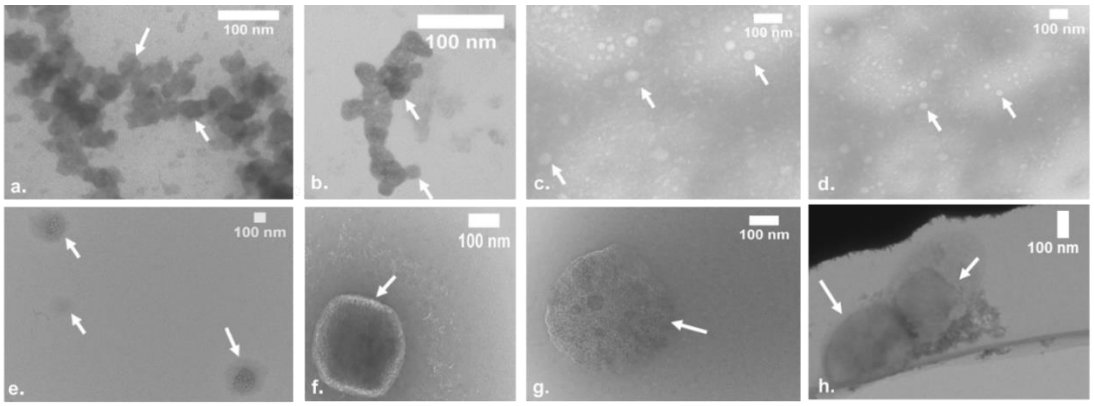

Figure 3.S1. MVs and exosomes visualized by transmission electron microscopy (TEM). (a-d) TEM images of exosomes populations. (e-h) TEM images displaying populations of microvesicles. White arrows point at MVs and exosomes. Note that populations of exosomes are more homogeneous than MVs populations.

3.7.2.2. Visualization of EVSB Formation

EVSBs from MVs and exosomes were made following the protocol explained in Section 3.S1. To allow visualization of the formation process, EVs used to generate the EVSB were labeled with octadecyl rhodamine (R18). Videos 3.S1a and 3.S1b show the formation of a MVs-EVSB and an exosomes-EVSB captured by FRAP. Note that R18-

labeled MVs initially looked like punctuate white dots on the glass slide at 0 sec, after addition of fusogenic liposomes (POPC/PEG) at 1 sec, the MVs start rupturing and the R18 is diffusing in the plane. This process continues until the end of video at 13 sec, when a formed bilayer can be observed. A more homogeneous bilayer is formed after 20 min. of incubation and thoroughly washing process. The upper left scratch is made to aid the focus of the bilayer in the Z plane. The same procedure was followed to form an exosome-EVSB.

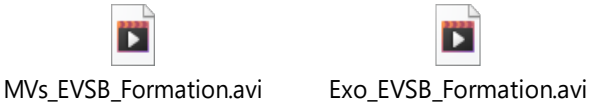

Figure 3.S2. Formation of EVSBs visualized by fluorescence recovery after photobleaching (FRAP). (S1a) MVs-EVSB formation. R18-labeled MVs were adsorbed on a previously cleaned glass. POPC/PEG liposomes were added to aid MVs rupture and formation of a bilayer. (S1b) Exosomes-EVSB formation. R18-labeled exosomes were adsorbed on a previously cleaned glass. POPC/PEG liposomes were added to aid exosomes rupture and formation of a bilayer.

3.7.2.3. Detection of HSP70 Presence in Exosome-EVSBs

As in vitro models of exosome membrane, exosome-EVSB must preserve components of the exosomal membrane. HSP70 is a heat shock protein highly expressed in exosomes lumen and membrane [294, 295]. HSP70 presence was detected in exosome-EVSB to verify the presence of native exosomal membrane components in our generated exosomes-EVSB. A primary anti-HSP70 antibody and a secondary Northern Lights fluorescent antibodies were used for HSP70 detection. Figure 3.S3 shows the presence of HSP70 in an exosome-EVSB (Figure 3.S3c), and the absence of HSP70 in MVs-EVSB and POPC/PEG-SLB, in figure 3.S3a and 3.S3b respectively. These results suggest that the generated exosome-EVSB preserves surface components similar to exosomes and

that proteins in the bilayer keep the same orientation as in exosomes [33] since the binding site for the antibody is facing toward the bulk and not the glass.

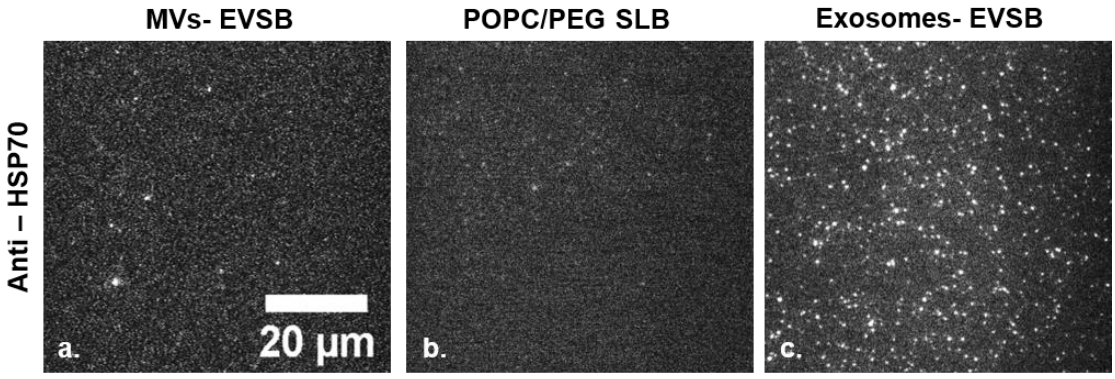

Figure 3.S3. Detection of extracellular vesicles membrane components in EVSBs. (a-c) HSP70 detection on EVSBs. (a) MVs- EVSB (control) treated with both primary and secondary antibody, not specific binding detected since HSP70 is not a marker of MVs. (b) POPC/PEG-SLB (control) to show no specific binding when treated with primary and secondary antibodies for HSP70. (c) Exosome-EVSB treated with primary and secondary antibodies. Specific binding and expression of HSP70 shows that exosome- EVSB preserve native components of exosomal membrane.

3.7.2.4. ADSCs Spreading and Adhesion Normalized by EVSBs Protein Contents

As seen in Figure 3.4i and 3.4j, ADSCs cultured on MVs-EVSB have a significantly higher cell area and generated focal adhesions than ADSCs cultured on exosomes-EVSB. To investigate if these results are caused by the difference in protein contents between both types of EVSBs, the data presented in Figure 3.4i and 3.4j was normalized by each EVSB protein content and Figure 3.S4a and 3.S4b show the resultant data. This normalization allows the comparison of the effect that MVs and exosomes membrane have on ADSCs spreading and attachment independent of their different protein content. Figure 3.S4b shows that after normalization, ADSCs cultured on MVs-EVSB still show significantly higher cell area than cells cultured on exosome-EVSB. However, in the case of focal adhesions, Figure 3.S4a shows that after normalization, the number of FAs per cell between both types of EVSBs is not significantly different.

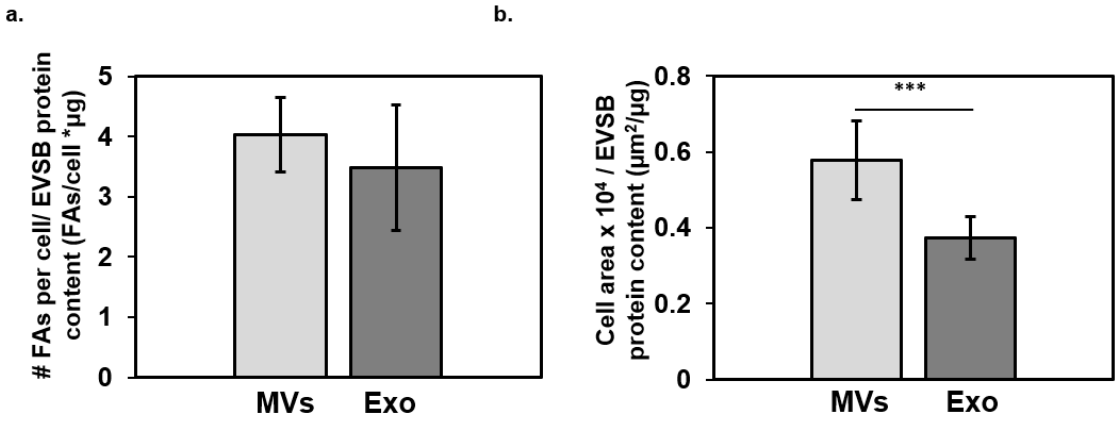

Figure 3.S4. Number of focal adhesions generated and cell area of ADSCs cultured on EVSBs normalized by EVSB protein content. (a) data presented in Figure 4i, number of focal adhesions per cell, normalized by EVSB protein content. Note that after normalization, there is not a significant difference between the number of FAs generated by ADSCs on MVs-EVSB compared to the number of FAs generated by ADSCs on exosomes-EVSB. (b) data presented in Figure 4j, cell area, normalized by EVSB protein content. In this case, after normalization, ADSCs on MVs-EVSB still display significantly higher cell area than ADSCs on exosomes - EVSB. *n = 4 ***p≤0.001*

3.7.2.5. Aspect Ratio of ADSCs Cultured on EVSBs

As mentioned in the main manuscript in the section of cell spreading and adhesion of ADSCs on EVSBs, one of the differences between ADSCs cultured on exosome-EVSB compared to ADSCs cultured on MV-EVSB, is that cells on exosome-EVSB displayed higher aspect ratio than cells on MV-EVSB, as shown in Figure 3.S5.

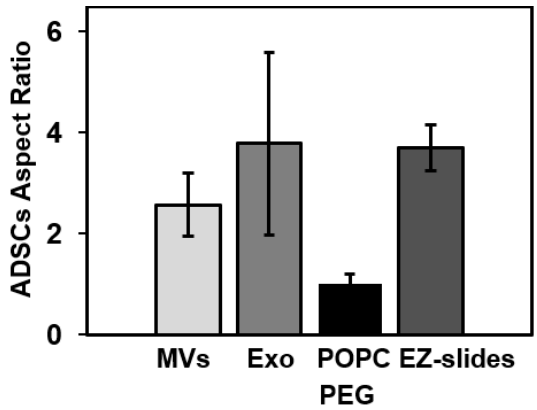

Figure 3.S5. Aspect ratio of ADSCs cultured on EVSBs, POPC/PEG-SLB, and EZ-slides. Aspect ratio of cells on different surfaces as measured using ImageJ software.

Aspect ratios of ADSCs cultured on EZ-slides and exosome-EVSB is similar. Lastly, ADSCs cultured on POPC/PEG-SLB presented the lowest aspect ratio compared to ADCs cultured on all other substrates.

3.7.2.6. ADSCs Secretion of VEGF Normalized by EVSB Protein Content and Number of Viable Cells

In the same manner as in Section 3.7.2.4., data obtained for VEGF concentration secreted by ADSCs on EVSBs (Figure 3.5c) was normalized by EVSBs protein contents and by number of viable cells. These normalizations were done to investigate if the effect of EVs membrane on ADSCs secretion of VEGF and proangiogenic activity was influenced by the protein content of each EVSB of by the number of viable cells in each of the substrates. Figure 3.S6a shows that the trend presented by the data in Figure 3.5c was conserved when the data was normalized. That is the ADSCs on MV-EVSB secreted higher VEGF concentration than ADSCs on exosomes-EVSB on day 4 independent of the EVSB protein content or the number of viable cells on the substrate.

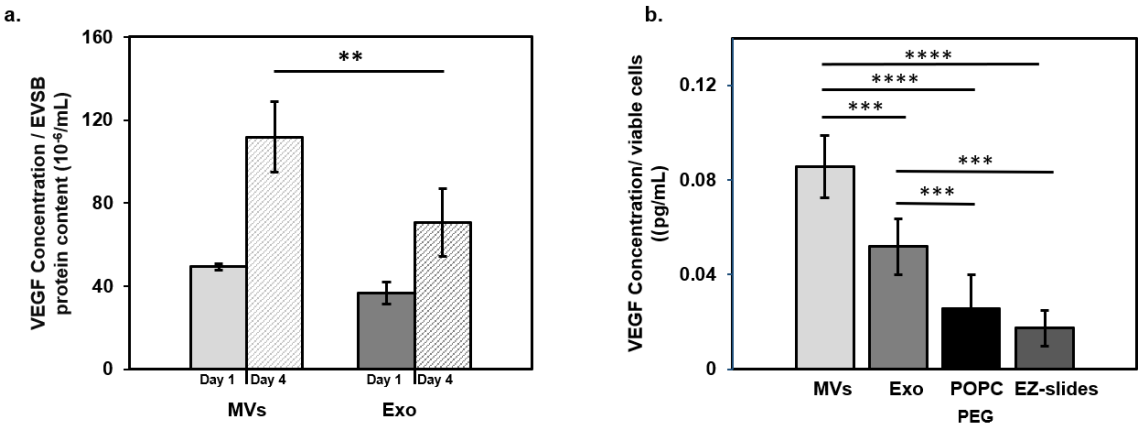

Figure 3.S6. Secretion of VEGF by ADSCs normalized by EVSB protein content and number of viable cells. VEGF concentration secreted by ADSCs cultured on MVs- EVSB, exosomes- EVSB, POPC/PEG- SLB, and EZ slides was measured by ELISA and displayed on Figure 5c. a) VEGF concentration secreted by ADSCs on EVSBs on day 1 and 4 normalized by EVSB protein content. b) VEGF concentration secreted by ADSCs on EVSBs, POPC/PEG-SLB,

and EZ-slides on day 4 normalized by number of viable cells in each substrate. We assume that 100% of cells on the substrates were viable at day 1, hence normalization was done just for day 4. *p ≤ 0.05, **p ≤ 0.01, ***p≤0.001, and ****p≤0.0001.

3.7.2.7. Effect of EVSBs on ADSCs Differentiation to Myofibroblasts

Previous studies suggested that ADSCs have the potential to act as a tumor promoter for various types of cancer, supporting disease progression, invasiveness, and metastasis [48]. This potential is thought to be developed through the activation of different signaling pathways resultant from ADSCs interactions with the microenvironment. Among the possible mechanisms leading to ADSCs potential as a cancer promoter, interactions with the tumor microenvironment and with oncogenic EVs are the most studied in the field today[42, 48].

In the case of ADSCs interactions with oncogenic EVs, it has been shown that treatment of ADSCs with breast cancer derived EVs leads to ADSCs transformation to myofibroblast phenotype[4, 5]. Myofibroblasts are highly contractile cells with high levels or stress fibers and alpha smooth muscle actin (α-SMA)[43 305, 306]. In the case of normal tissue repair, this transformation is beneficial for tissue healing and repair. However, in the case of cancer, this transformation to myofibroblasts, leads to fibrosis, tissue stiffening, and generation of a metastatic niche[4, 43, 301].

We showed that ADSCs grown on EVSBs produce higher VEGF levels than cells cultured on glass and POPC/PEG-SLBs. These results suggest that interactions between ADSCs and EVs membrane led to proangiogenic activity, represented by high levels of VEGF secretion. In the same manner, we wanted to investigate if ADSCs interactions with EV membranes by being cultured on EVSBs was a trigger for ADSCs transformation to myofibroblasts. To do so, ADSCs were cultured on MV- and exosome-EVSBs, EZ-

slides, and POPC/PEG -SLB. After seven days of culture, cells were subjected to immunofluorescent staining for α-SMA as a marker of myofibroblasts.

Figure 3.S7a, 3.S7b, S7c, and 3.S7d, showed ADSCs on MV-EVSB, exosome-EVSB, EZ-slides, and POPC/PEG -SLB respectively expressing α-SMA, red signal, and DAPI (nuclei), blue signal. Figure 3.S7e displays the quantitative data of α-SMA fluorescence intensity in ADSCs culture on different substrates. Observe that α-SMA fluorescence intensity is similar and low for ADSCs cultured on EVSBs and POPC/PEG-SLB, and it is significantly higher on ADSCs cultured on EZ-slides. In the same manner, Figure 3.S7f shows the data of Figure 3.S7e normalized by the protein content of EVSBs. Note that α-SMA intensity levels on ADSCs cultured on MV -EVSBs is not significantly higher than α-SMA levels on ADSCs cultured on exosome-EVSBs.

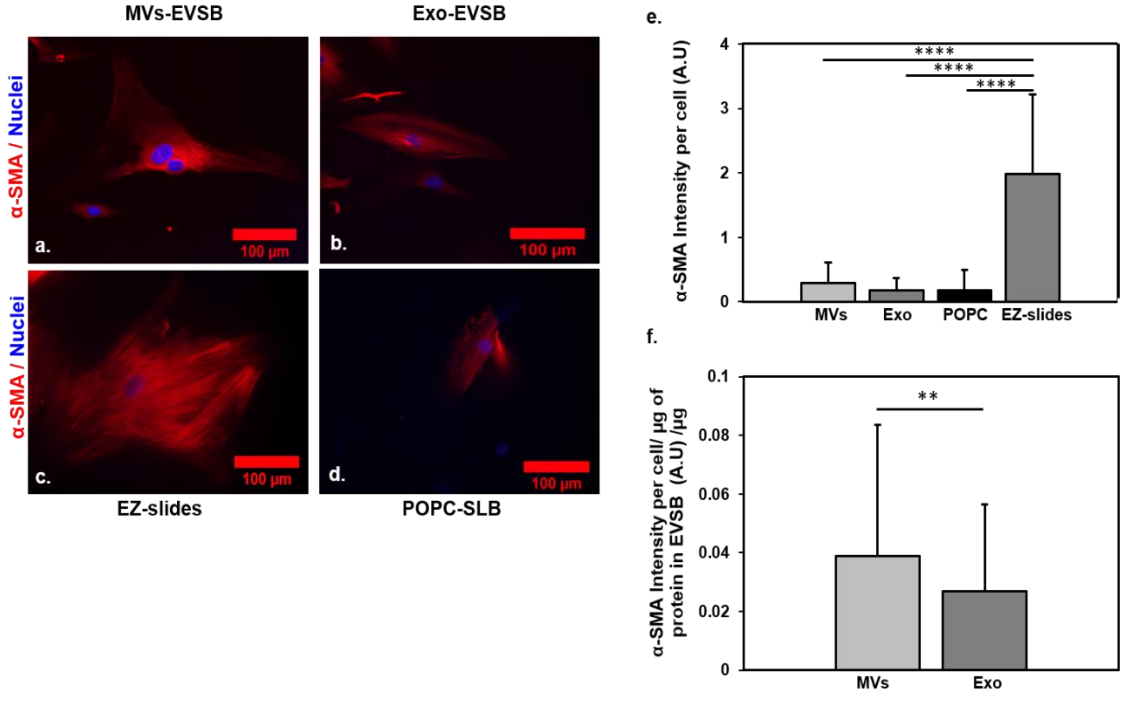

Figure 3.S7. Expression of α-SMA, as a marker of myofibroblast transformation, on ADSCs cultured on EVSBs, POPC/PEG -SLB, and EZ-slides. (a- d) ADSCs cultured on MVs- EVSB,

exosomes-EVSB, EZ-slides, and POPC/PEG - SLB were immunoassayed for α smooth muscle actin (α-SMA), red signal, and for DAPI, blue signal, seven days after seeding. (e) Quantitative data for α-SMA fluorescence intensity of ADSCs on different substrates. (f) Data from (e) normalized by protein contents of EVSBs. *n=3. Mean ±SD. *p ≤ 0.05, **p ≤ 0.01, ***p≤0.001, and ****p≤0.0001*

These results suggest that interactions between ADSCs and EV membranes, by being cultured on EVSBs, do not lead to myofibroblast transformation. This leads us to the conclusion that myofibroblast transformation of ADSCs treated with EVs that has been observed in the past, may be due to the EVs cargo delivery into ADSCs and not a result of the surface interactions.

CHAPTER 4

4. DUAL MODE SENSING OF BINDING AND BLOCKING OF CANCER EXOSOMES TO BIOMIMETIC HUMAN PRIMARY STEM CELL SURFACES

Johana Uribe[1], Walther C. Traberg[2], Adel Hama[3], Victor Druet[3], Zeinab Mohamed[1], Amanda Ooi[3], Anna-Maria Pappa[4,2], Miriam Huerta[5], Sahika Inal[3], Róisín M. Owens[2], and Susan Daniel[1,5] *

[1]Meinig School of Biomedical Engineering, Cornell University, Ithaca, NY, United States.

[2]Department of Chemical Engineering and Biotechnology, University of Cambridge, Cambridge, United Kingdom.

[3]Biological and Environmental Sciences and Engineering Division, King Abdullah University of Science and Technology (KAUST), Thuwal, Kingdom of Saudi Arabia.

[4]Department of Biomedical Engineering, Khalifa University of Science and Technology, Abu Dhabi, United Arab Emirates.

[5]School of Chemical and Biomolecular Engineering, Cornell University, Ithaca, NY, United States.

4.1. Acknowledgments

This chapter was published in its entirety including the SI section in "Dual Mode Sensing of Binding and Blocking of Cancer Exosomes to Biomimetic Human Primary Stem Cell Surfaces" in ACS Biomaterials Science & Engineering on November 22nd, 2021. Johana Uribe is the first author, Susan Daniel is the corresponding author, and the

co-authors include Walther C. Traberg, Adel Hama, Victor Druet, Zeinab Mohamed, Amanda Ooi, Anna-Maria Pappa, Miriam Huerta, Sahika Inal, and Roisin M. Owens.

4.1.1. Individual acknowledgements

JU: conceived the presented idea; cEXOs and ADSCs blebs isolation and characterization; ASB formation and characterization by FRAP, cEXOs binding/blocking by TIRFM; cell culture and VEGF assessment experiments; data analysis and interpretation; and drafted the manuscript and designed the figures. **WT:** ASB-MEA formation and characterization by EIS, cEXOs binding/blocking by electrical means, data analysis, and manuscript writing and edition. **AH:** cEXOs proteomics analysis. **VD:** MEA fabrication. **ZM:** TEM imaging acquisition. **AO:** cEXOs proteomics analysis. **AMP:** Electrical data analysis, modelling, and interpretation; optimization of EEC models to fit data for Rm extraction. **MH:** ADSCs blebs size characterization, manuscript writing and editing. **SI:** Oversaw the project, coordinated cEXOs proteomic analysis and device fabrication. **RO:** Oversaw the project, coordinated electrical experiments performance, data analysis, and interpretation. **SD:** conceived the presented idea, oversaw the project, results interpretation, manuscript writing and editing. All authors discussed the results and commented on the manuscript.

4.1.2. Article acknowledgments

We wish to acknowledge Zixuan Henry Lu for his assistance with the electrical measurements, Achilleas Savva for his assistance with the EEC modelling, and Anil Koklu for his assistance in MAE design and fabrication. This work was supported by the National Science Foundation Graduate Research Fellowship [Grant Number DGE-

1650441), and the Sloan Foundation (Grant number 70481) to J.U. and a research grant from King Abdullah University of Science and Technology under contract OSR-2018-CRG7-3709 to S.I., R.M.O, and S.D. W.T. acknowledges funding from the Cambridge Trust. *This work was performed in part at the Cornell NanoScale Facility, an NNCI member supported by NSF Grant NNCI-2025233.* Any opinions, findings, and conclusions or recommendations expressed in this material are those of the author(s) and do not necessarily reflect the views of any of the funding institutions.

4.2. Abstract

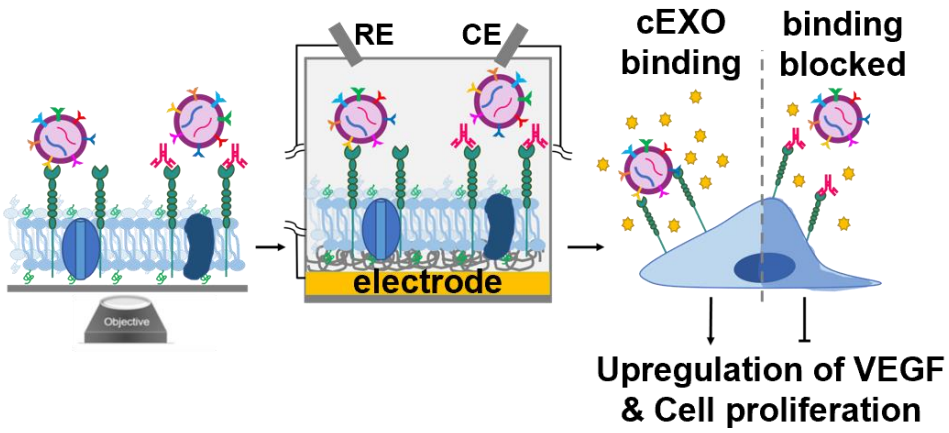

TOC Figure. Graphical abstract

Cancer derived exosomes (cEXOs) facilitate transfer of information between tumor and human primary stromal cells, favoring cancer progression. Although the mechanisms used during this information exchange are still not completely understood, it is known that binding is the initial contact established between cEXOs and cells. Hence, studying binding and finding strategies to block it is of great therapeutic value. However,

such studies are challenging for a variety of reasons, including the need for human primary cell culture, the difficulty in decoupling and isolating binding from internalization and cargo delivery, and the lack of techniques to detect these specific interactions. In this work, we created a supported biomimetic stem cell membrane incorporating membrane components from human primary adipose derived stem cells (ADSCs). We formed the supported membrane on glass and on multi-electrode arrays (MEAs) to offer the dual option of optical or electrical detection of cEXOs binding to the membrane surface. Using our platform, we show that cEXOs bind to the stem cell membrane and that binding is blocked when an antibody to integrin β1, a component of ADSCs surface, is exposed to the membrane surface prior to cEXOs. To test the biological outcome of blocking this interaction, we first confirm that adding cEXOs to cultured ADSCs leads to upregulation of VEGF, a measure of proangiogenic activity. Next, when ADSCs are first blocked with anti-integrin β1and then exposed to cEXOs, the upregulation of proangiogenic activity and cell proliferation are significantly reduced. This biomimetic membrane platform is the first cell-free, label-free, *in vitro* platform for the recapitulation and study of cEXO binding to human primary stem cells with potential in therapeutic molecule screening as it is compatible with scale-up and multiplexing.

4.3. Introduction

Cui and colleagues recently showed that cancer derived extracellular vesicles (cEVs) transfer miR-630 to fibroblasts promoting their differentiation to carcinoma-associated fibroblasts and ovarian cancer invasion and metastasis[10]. Similarly, several others have implicated cEVs in cancer development and progression in other types of cancers[3, 18, 70]. In particular, a subset of cEVs called exosomes (cEXOs), are known to

mediate transfer of information between cells within the tumor and distal sites contributing to tumor growth and formation of pre-metastatic niches[307, 308]. For instance, interactions with breast cancer derived cEXOs induced pro-angiogenic behavior, indicated by upregulation of vascular endothelial growth factor (VEGF) in adipose-derived stem cells (ADSCs) and their subsequent differentiation to myofibroblasts[4, 5]. Both outcomes favor tumorigenesis by promoting tumor vasculature formation and high levels of inflammation at the tumor microenvironment (TME), respectively[7, 45, 48]. Therefore, hindering interactions between cEXOs and healthy cells is expected to reduce these types of negative outcomes and possibly mitigate the progression of cancer.

Blocking specific interactions as a route to inhibit the transfer of information between cEXOs and cells and subsequent outcomes is an important emerging avenue for cancer therapeutics. However, given the complexity of the plasma membrane surface and all the possible targets for cEXOs to bind to and deliver their message, screening for such interactions is a challenge that could benefit from new ways to mimic the surfaces and interactions between the cell plasma membrane and cEXOs, as well as technologies to read out these interactions. These types of screening studies are complicated because the molecular interactions between cEXOs and cells are specific to each type of cEXO-cell pair and are determined by the surface composition of both entities[115, 119, 309]. All possible cEXO-target cell interactions are expected to be begin by surface contact that involves binding of at least two surface components, one from the cEXO surface and one from the cell plasma membrane[115, 119]. Subsequently, cEXOs can take different routes for transfer of information including: binding-induced activation of signaling pathways at the plasma surface that leads to downstream cellular responses, cellular internalization via various

endocytosis pathways that leads to delivery of contents to various organelles, and direct fusion with the cell plasma membrane that leads to direct release of information into the cytosol[115, 119 110]. Of note, however, is that a common theme among the different routes is that *binding* is the initial interaction where cEXOs begin to influence the local microenvironment to promote tumorigenesis and cancer progression. Being able to assess binding isolated from these subsequent biological processes, and with an easy readout that can be scaled up to integrate technologies for high throughput screening to identify effective blocking agents, is a current need in the field. To create a model system to study and visualize cEXO-cell binding, we report here a planar and tunable *in vitro* ADSC plasma membrane model system that allows us to study the interactions of cEXOs and ADSCs and to test potential binding blockers using both optical and electrical readout of binding interactions, isolating the membrane interaction without the complexity of the whole cell. Our platform's central element is a hybrid supported lipid bilayer (SLB) incorporating native ADSC membrane components derived from plasma membrane blebs from human primary stem cells. We refer to this element as an Adipose derived stem cell supported bilayer (ASB).

SLBs are employed in several research fields as cell membrane models [25-27, 165, 310, 311] and have been used as cell culture platforms[9, 30, 32], and as tools to investigate interactions at the cell membrane interface including cell-cell interactions[28] and cell-particles interactions [9, 30, 32, 158] and strategies to inhibit virus binding[312, 313]. In the past, our group has expanded SLB platform molecular complexity by developing methods to integrate native components from cell membranes that preserve the natural function and orientation of the proteins in mammalian cell membranes [33, 34]. Here, we adapted these

methods to create a stem cell supported bilayer from human primary stem cells that maintains much of the authenticity of the plasma membrane of ADSCs, preserving native constituents, molecular complexity, and lateral diffusivity of the membrane. Because this platform is a representative mimic of the plasma membrane that is free of the dynamism of live cells, it is useful for isolating and focusing on cEXO binding and blocking without competing effects of cEXO uptake and cargo delivery. Here we demonstrate using ASBs combined with two different sensing modalities to assess binding/blocking in one example of this application.

The versatility of our "native-like" lipid bilayer platform to be formed on surfaces compatible with multiple sensing modes, allows us to use both optical and label-free electrical means to readout membrane-related events. For example, glass surfaces enable optical techniques like fluorescence recovery after photobleaching (FRAP) for bilayer fluidity characterization[9, 32-34, 196, 235], and total internal reflection fluorescence microscopy (TIRFM) to detect interactions such as nanoparticle binding[314-317] and blocking virus binding[312, 313]. Moreover, given the practicality of label-free methods for screening applications, we create these bilayers on customized bioelectronic sensors, to electrically monitor molecular events at the cell membrane[318, 319].

Using these sensing modes, we validate the detection of cEXO binding to ASBs, and subsequent blocking by an antibody to integrin β1/CD29 on the surface of ADSCs. First, using fluorescence microscopy on glass surfaces. Secondly, using electrochemical impedance spectroscopy (EIS) via poly(3,4-ethylenedioxythiophene) doped with poly (styrene sulfonate), PEDOT:PSS-based devices for sensitive measuring of the ASB frequency-dependent impedance.

PEDOT:PSS is a conducting polymer which acts as a cushioned interface between the electrode and the ASB; mimicking an *in vivo*-like environment, and enables direct electronic signal transduction for sensing biological events with excellent sensitivity[320]. PEDOT:PSS-coated electrodes have previously been used to detect the open/close state of transmembrane proteins in an SLB[318]. The addition of an insulating layer between these electrodes, here the ASB, alters the impedance characteristics of the system, and the resistance and capacitance properties of this layer can be extracted using equivalent electrical circuit (EEC) modelling[321]. When cEXOs bind or are blocked by antibodies, these changes can be detected in the ASB resistance and used for label-free detection of binding interactions, which we demonstrate with the same antibodies used in the fluorescence study. Finally, as a means to corroborate our platform's results, in the context of live cells, we show that this antibody blocking strategy stops the upregulation of VEGF and cell proliferation in ADSCs that are direct outcomes of cEXO-ADSCs surface interactions. This result supports that blocking cEXO binding is a potential therapeutic strategy and validates the utility of this ASB sensing platform in finding successful targets that reduce cEXO binding and reduce proangiogenic outcomes when applied to cells.

4.4. Materials and Methods

4.4.1. Cell Culture

StemPro Human Adipose-Derived Stem Cells (ADSCs) were obtained from ThermoFisher Scientific (Rochester, NY) and cultured in ADSC growth medium kit purchased from Lonza (Walkersville, MD). Experiments were performed with cells between passages 1 and 6. MDA-MB-231 cells, highly metastatic human

adenocarcinoma cells, were purchased from American Type Culture Collection, ATCC (Manassas, VA) and maintained in Dulbecco′s Modified Eagle′s Medium, DMEM, Corning (Corning, NY) supplemented with 10% fetal bovine serum (FBS) ThermoFisher (Waltham, MA) and 1% penicillin–streptomycin (P/S) Invitrogen, (Carlsbad, CA). For serum free medium used for cEXO isolation, MDA-MB-231 cells were maintained in DMEM medium supplemented with 1% P/S. Experiments were performed with cells between passages 1 and 8 after received. All cell cultures were maintained at 37°C and 5% CO_2 and the media were changed every two to three days as recommended by manufacturers.

4.4.2. Preparation of ADSC membrane blebs

Cell blebbing was performed through chemical induction. ADSCs were seeded in 10 cm culture dishes (Corning, NY) at a density of 1.2 x 10^5 cells/mL. After 72 hours of incubation at 37 ˚C and 5% CO_2 or until they reached 85% confluency, cells were washed with Giant Plasma Membrane Vesicle (GPMV) buffer (2 mM $CaCl_2$, 10 mM HEPES, and 150 mM NaCl) at pH 7.4. Cells were then incubated in 4 mL of blebbing buffer (25 mM formaldehyde, FA, (Sigma, St. Louis, MO) and 2 mM Dichlorodiphenyltrichloroethane, DDT, (Sigma, St. Louis, MO) in GPMV buffer) on a rocker for one hour at room temperature and for one hour at 37 ˚ C. Blebs were then transferred to a falcon tube and incubated on ice for 25 minutes. Supernatant was transferred to a new tube and stored at 4 ˚ C for up to two weeks.

4.4.3. cEXOs isolation and characterization

cEXOs derived from MDA-MB-231 breast cancer cells were used for this study. Detailed

isolation and characterization procedure are found in SI experimental procedures section.

4.4.4. Characterization of cEXOs and ADSCs blebs

ADSCs blebs and cEXOs size were measured by nanoparticle tracking analysis (NTA), dynamic light scattering (DLS) and further corroborated using transmission electron microscopy (TEM). Laser Doppler electrophoresis respectively (LDE) was used to measure the zeta potential of both nanoparticles. Finally, bicinchoninic acid assay (BCA) and NTA were used to find particle concentration and protein content, respectively. Experimental procedure for characterization methods is reported in SI experimental procedures section.

4.4.5. Preparation of glass slides for formation of supported bilayers

Glass coverslips 25 x 25 mm, No. 1.5, VWR (Radnor, PA) were used as a rigid surface for supported lipid bilayers. They were cleaned by piranha washing consisting of 45 mL of 50% hydrogen peroxide (Sigma, St. Louis, MO) followed by 105 mL of 70% sulfuric acid, VWR (Radnor, PA) for 10 minutes (Note: use extreme caution with this solution; highly oxidative). Then, coverslips were rinsed for 30 min with generous amounts of deionized water generated by an Ultrapure water system, Siemens pureLab (Malvern, PA). Clean coverslips were stored in deionized water at room temperature until needed. Immediately prior to the formation of bilayers, coverslips were rinsed with deionized water and dried with high purity nitrogen gas.

4.4.6. Polydimethylsiloxane (PDMS) well fabrication

A 10:1 ratio mix of PDMS, SYLGARD 184 (Ellsworth, ME) monomer and crosslinker

was thoroughly stirred, degassed, and poured in a 100 mm petri dish and baked at 70˚C for 5 hours. The cured PDMS sheet was cut into pieces to fit on top of a coverslip. A circular hole of 1 cm diameter, using a 1 cm hole puncher, was made in each PDMS piece to create a well when affixed to the coverslip. To ensure attachment of the PDMS to the clean coverslip, the well was placed in the oven at 65 ℃ for 10 minutes.

4.4.7. Preparation of liposomes

1-Oleoyl-2-palmitoyl-sn-glycero-3-phosphocholine, POPC, Avanti Polar Lipids (Alabaster, AL) and 1,2-distearoyl-sn-glycero-3-phosphoethanolamine-N- [methoxy (polyethylene glycol)-2000], PEG2000-PE, Avanti Polar Lipids (Alabaster, AL) were used to create liposomes. POPC-PEG2k liposomes were made with 99.5% (mol/mol) POPC and 0.5 (%mol/mol) PEG2000. The lipid mixture was prepared by adding appropriate ratios to a previously cleaned glass vial and drying them with nitrogen gas, followed by desiccation in a vacuum chamber for 3 hours. The lipid film was resuspended in phosphate-buffered saline solution (PBS) pH 7.4 to a final concentration of 2 mg/mL and stored at -20˚C overnight. After thawed, liposomes were extruded through a 100 nm membrane 12 times, Whatman (Maidstone, UK), and kept at 4˚C for up to two weeks.

4.4.8. Fluorescent labeling of liposomes, ADSCs blebs, and cEXOs

To visualize the formation of supported bilayers and for diffusivity measurements using fluorescence recovery after photobleaching (FRAP), liposomes were fluorescently labeled with a membrane intercalating fluorophore, Octadecyl Rhodamine (R18). 2 µL of 0.1 mg/mL R18 (Molecular Probes, Eugene, OR) were incubated with 100 µL of liposomes, sonicated (Model # BD2500A-DTH; VWR) for 30 min, and the

unincorporated fluorophore was removed using a G25 spin column (GE Healthcare, Pittsburgh, PA). The same procedure was followed to label ADSCs blebs and cEXOs, using 100 μL of each sample.

4.4.9 Formation of phosphatidylcholine supported lipid bilayers

Supported lipid bilayers (SLBs) self-assemble on a clean coverslip using the well-established vesicle fusion method as shown previously [33, 34]. 100 μL of a 2.0 mg/mL liposome solution (POPC-PEG 2k) were added into a well and incubated for 20 minutes at room temperature. Wells were thoroughly washed with PBS pH 7.4 to remove excess lipid vesicles remaining in the bulk phase after bilayer formation. This surface was used as a negative control surface.

4.4.10. Formation of ASB

For ASB formation, 100 μl of ADSC membrane blebs (2.48×10^8 blebs/mL) in GPMV buffer were added to a PDMS well and incubated at room temperature for ~10 min. Then, the well was thoroughly rinsed with PBS pH 7.4 to remove unabsorbed blebs. Formation of the bilayer was induced by adding 100 μL of 2 mg/mL POPC-PEG2k into the well and incubation for 20 min at room temperature followed by rinsing with PBS.

4.4.11. Observing ASB formation and measuring diffusivity with fluorescence microscopy

The rupture of fluorescently labeled ADSC blebs was observed using an inverted Zeiss Axio Observer.Z1 microscope with α Plan-Apochromat objectives, a Hamamatsu EM-CCD camera (Image EM, model C9100- 13, Bridgewater, NJ), and a X-Cite 120

microscope light source (Lumen Dynamics Group Inc., Canada). To accumulate the fluorescence emitted by the fluorophores (R18), an ET MCH/TR filter cube (49008, c106274, Chromatech Inc.) was used. Labeled ADSCs blebs were first incubated on the coverslips or PEDOT:PSS-coated coverslips as described above, followed by addition and incubation of POPC-PEG2k vesicles (unlabeled) to rupture them. The process was recorded with the camera and complete rupture observed as shown in the supplemental movie, further corroborated by FRAP and additional techniques.

Diffusivity and mobile fraction measurements were carried out using photobleaching experiments. Using a 4.7 mW 488 nm krypton/argon laser, a 25 μm spot was photobleached for 300 ms followed by 40 min (30 s intervals) of recovery of the photobleached spot. The fluorescence intensity of the photobleached spot was determined by subtracting the background from a reference spot that was unbleached and normalizing to each image captured to the maximum difference between the initial photobleached spot and the initial intensity of that area. Using MATLAB, the intensity recovery data was fit into a Bessel function model using the Soumpasis[34] method to extract the half time to recovery, $t_{1/2.}$ The following equation was used, Eq. 4.1: $D = w^2 /4\ t_{1/2}$, to determine the diffusion coefficient (D) for each bilayer type, where *w* is the full width at half-maximum of the Gaussian profile of the focused beam. The mobile fraction was determined by the final intensity over the initial intensity of the bleached area.

4.4.12. Testing integrin β1/CD29, a native component of ADSCs membrane, presence in ASB

ASB was formed as stated above. After washing the residual POPC-PEG2k vesicles

away with PBS, 70 uL of 20% normal goat serum (GS, ThermoFisher Scientific (Waltham, MA)) was added to the well and incubated for 30 min at room temperature. The well was thoroughly washed with PBS one more time to remove GS excess. 100 µL of 1:100 anti-integrin β1/CD29 antibody solution (MAB1778, R&D Systems, Minneapolis, MN) was added to the well and incubated for 2 hours at room temperature. The well was thoroughly washed with PBS to remove excess primary antibody and incubated with 100 µL of 1:2000 Donkey Anti-Mouse IgG NorthernLights (NL009, R&D Systems, Minneapolis, MN) conjugate antibody for one hour at room temperature in the dark. After, the bilayer was washed one last time with PBS to remove excess secondary antibody, then was imaged using total internal reflection fluorescence microscopy (TIRFM) to detect specific binding of integrinβ1/CD29 antibody to ASB. As a negative control, an ASB was treated just with the secondary conjugated antibody to show nonspecific binding of integrinβ1/CD29 to the ASB with the absence of the primary antibody. Additionally, treatment with both antibodies as done with the first condition was repeated with a POPC-PEG2k SLB (no ADSC material) as a negative control to show nonspecific binding of integrinβ1/CD29.

4.4.13. Binding of cEXOs to ASB

ASB was formed as stated above and blocked using 70 uL of 20% normal GS for 30 min at room temperature to prevent nonspecific binding. After thoroughly washing the well with PBS to remove excess GS, 100 uL of R18 labeled cEXOs were added to the ASB and incubated for 30 min in the dark to allow binding. Finally, the well was thoroughly washed with PBS to rinse unbound vesicles. Binding of cEXOs to ASB was imaged using TIRFM and quantified by ImageJ software.

4.4.14. Blocking binding of cEXOs to ASB using Integrin β1/CD29

An ASB was incubated with 100 uL of 20% normal GS for 30 min at room temperature, followed by a thorough wash with PBS to remove excess GS. 100 µL of 1:100 anti-integrin β1/CD29 were added to the well and incubated for 2 hours at room temperature. The well was thoroughly washed with PBS to remove the primary antibody, followed by incubation with 100 uL of R18 labeled cEXOs at room temperature for 30 minutes to allow binding. The ASB was washed with PBS to rinse unbound cEXOs and images were captured using TIRFM.

4.4.15. TIRFM Setting and Operation

Total Internal Reflection Fluorescence Microscopy (TIRFM) was conducted on an inverted Zeiss Axio Observer.Z1 microscope with an α Plan-Apochromat 100× objective; 488 nm and 561 nm wavelength from solid-state lasers were used to excite the samples. A Laser TIRF 3 slider (Carl Zeiss, Inc., Oberkochen, Germany) was used to adjust the angle of incidence at approximately 68.2° generating an evanescent wave at 100 nm and total internal reflection. The excitation light was filtered by a Semrock LF488-B-ZHE filter cube and sent to the electron multiplying CCD camera (ImageEM C9100-13, Hamamatsu).

4.4.16. Multi-electrode array Fabrication

Multi-electrode arrays (MEAs) were fabricated using an established photolithography process on 4-inch glass wafers. The wafers were cleaned using a piranha (H_2O_2:H_2SO_4, ratio 1:3–4) bath, washed with water and cleaned with O_2 plasma (Nanoplas DSB 6000). The electrode areas were defined using standard photolithography steps. To perform the

lift-off step, the wafers were coated with a photoresist bilayer consisting of LOR 5B (Microchem) and S1813 (Shipley) and exposed to UV light using the EVG 6200 mask alignment system and developed using MF319 developer. A 10 nm layer of Cr and a 100 nm layer of Au were deposited using magnetron sputtering (Equipment Support Company Ltd. ESCRD4) and lifted using appropriate solvents. After the lift-off step, the first Parylene C layer was vaporized to a thickness of 1.7 μm using a SCS Labcoater 2 with Silane as an adhesion promoter. A second Parylene C layer was vaporized to act as the sacrificial layer for polymer film patterning. A layer of AZ9260 was spun cast and developed using AZ developer as a mask for reactive ion etching (Oxford Instruments Plasmalab 100–ICP 380) which was used to expose the device channels and pads for polymer deposition. Each chip consists of four circular electrodes of 500 μm in diameter (0.00196 cm^2).

4.4.17. Electrochemical Impedance Spectroscopy (EIS)

EIS was utilized as a label-free approach to assess cEXO binding capabilities. ASBs were formed on PEDOT:PSS-coated MEAs and cEXOs binding and blocking experiments were carried out in the same manner as described for glass substrates in 2.18 and 2.19. ASBs were prepared fresh on the devices and were stable for 48 hours, meaning device performance did not decrease during this time nor did the membrane resistance change. A potentiostat (Autolab PGSTAT128N) equipped with a frequency response analysis module was used to record impedance spectra at the frequency range between 100 KHz – 0.1 Hz. Commercially available Ag/AgCl and platinum mesh were used as reference and counter electrodes, respectively. The PEDOT:PSS-coated Au MEAs were used as the working electrodes. The PEDOT:PSS solution contained 95% v/v Clevios PH 1000

(Heraeus), 5% v/v ethylene glycol (Sigma-Aldrich), 0.002% v/v 4-dodecylbenzenesulfonic acid (Sigma-Aldrich), and 1% v/v (3-glycidyloxypropyl) trimethyoxysilane (Sigma-Aldrich). PEDOT:PSS was spin coated onto MEAs (dried under nitrogen and treated with oxygen plasma for 2 min just prior to use) at 3,000 rpm for 35 s and baked at 140 °C for 1 h. A glass cloning cylinder was glued onto the MEA using PDMS to act as a well. The electrodes were circular, 500 μm in diameter, and thus, the active electrochemical area was 0.00196 cm^2. The applied AC voltage was 0.01 V and a DC voltage of 0 V versus open circuit potential. All measurements were taken in 1X PBS buffer contained in a glass well attached to the MEAs. To monitor cEXOs binding, we took EIS measurements on individual electrodes after each step as follows: (1) bare PEDOT:PSS electrodes, (2) ASB formed on top, (3) after incubation with anti-CD29 antibody, in the case of blocking, and (4) after addition of cEXOs. Nova software was then used for data analysis and electrical equivalent circuit (EEC) modeling to extract the membrane resistance values.

4.4.18. Assessment of VEGF secretion by ADSCs

ADSCs were seeded on a Millicell EZ-slide (Millipore, Burlington, MA) at a density of 8 x 10^4 cells/well. After 48 hours, ADSCs were changed to 2% FBS media to slow down cell proliferation and incubated overnight at 37 °C and 5% CO_2. Each well had a different treatment, as follows: negative control with no treatment (NT), ADSCs treated with 40 μg of cEXOs, ADSCs incubated with 20 μg/mL of anti-integrin β1/CD29 antibody (MAB 2253Z, Millipore, Burlington, MA) for two hours at 37°C followed by addition of 40 μg of cEXOs, and ADSCs treated with 10 ng/mL of TGFβ1 (ThemoFisher Scientific, Waltham, MA). Cell media was changed every other day along each of the treatments. In

addition, 100 µL of media from each well were removed on days 0, 2, and 5 and stored at -20°C for VEGF-ELISA assay. As a measure of proangiogenic activity, VEGF secretion by ADSCs in all mentioned conditions was assessed using a Human VEGF DuoSet ELISA kit (R&D Systems, Minneapolis, MN) following the manufacturer's protocol. VEGF concentration was normalized by the number of alive cells in each condition. The number of alive cells was assessed for each well/treatment on days 2 and 5 by staining cells nuclei using Hoechst (ThermoFisher Scientific, Waltham, MA) and getting the average number of cells in 30 frames per well in images acquired by an inverted Zeiss Axio Observer. Z1 microscope with α Plan-Apochromat objectives, a Hamamatsu EM-CCD camera, Image EM, model C9100- 13 (Bridgewater, NJ), and an X-Cite 120 microscope light source, Lumen Dynamics Group Inc. (Ontario, Canada). Four independent replicates of the experiment were performed.

4.4.19. Statistical Analysis

For all experiments performed in this study, variance analysis was performed using a *t*-test with unequal variances to find significant differences between substrates and conditions. All data were plotted and analyzed using Microsoft Excel, and it is presented as mean ± SE. Statistical significance levels were determined as follows: *$p \leq 0.05$, **$p \leq 0.01$, ***$p \leq 0.001$, ****$p \leq 0.0001$.

4.5. Results and Discussion

Overview. Here, we present the use of ADSCs-derived SLB (ASB) to facilitate the studies of cancer cEXOs-ADSCs binding and blocking strategies. First, we use optical means to characterize the formation of an ASB and binding of cEXOs, followed by

screening the potential of blocking β1/CD29 with a specific antibody to reduce cEXOs binding. Next, these results are repeated using a label-free electrical approach. Lastly, to corroborate the results obtained using our cell-free ASB platform, we used a cell culture assay to investigate the effect of blocking integrin β1 in the surface of ADSCs for the prevention of cEXOs binding and show that this stops the upregulation of VEGF secretion and cell proliferation, which are direct outcomes of cEXOs and ADSCs binding[5, 9].

4.5.1. ASB as an in vitro model of ADSC membrane

We chose to study ADSCs because they are an important cell group in the tumor microenvironment (TME) with a critical role in cancer progression and aggressiveness[7, 41]. In particular, ADSCs secrete inflammatory biomarkers, such as VEGF, that promote angiogenesis and a **TME w**ith high levels of inflammation, fostering tumorigenesis[44, 45]. Notably, surface interactions between cEXOs and ADSCs, are known to stimulate VEGF secretion in ADSCs contributing to their angiogenic potential[9]. Because of these malignant implications, it is imperative to study cEXOs-ADSCs binding and to find treatments to block it as a mean to decrease ADSCs angiogenic properties. Towards this end, we developed a tool to study cEXO-ADSC binding by replicating it in an *in vitro* setting using an ADSCs-membrane model, ASB.

To recapitulate the membrane of ADSCs in the ASB, we incorporated native components of the cell membrane into a SLB using ADSCs membrane blebs[33, 34]. Cell blebs are proteoliposomes that protrude and bud from the cell surface and retain the lipid and protein composition of the mother cell membrane[34]. Here, ADSCs membrane blebs were obtained by chemical treatment and characterized by several techniques. Size was

obtained by complementary methods such as nanoparticle tracking analysis (NTA), dynamic light scattering (DLS), and transmission electron microscopy (TEM). Concentration was determined also by NTA. Total protein concentration was determined by bicinchoninic acid assay (BCA). Finally, laser Doppler electrophoresis was used to assess their zeta potential. The size of the blebs found by the three methods were highly comparable ranging between 214 ± 22.8 nm (NTA) and 232 ± 39.3 nm (TEM), and zeta potential of membrane blebs in GPMV buffer was 14.3±1.22 –mV; these are both in the range of values reported in the literature[34, 284, 322].

cEXOs were isolated from breast cancer cells (MDA-MB-231) and characterized in the same manner as cell blebs. cEXOs isolation and characterization is described in detail in the supporting information section. Our average cEXOs size, 109 ± 12.3 nm, agreed with reported values in literature in which their diameters range between 30-120 nm[1, 59-61]. A complete characterization of cell blebs and cEXOs is reported in Table 4.1 and Figure 4.S1.

Table 4.1. Characterization of cEXOs and ADSC cell blebs

Particle	Diameter Size by NTA (nm)	Diameter Size by DLS (nm)	Diameter Size by TEM (nm)	Zeta potential (-mV)	Concentration (particles/mL)	Protein content (µg/mL)
cEXOs	93.9 ± 22.2	116 ± 11.9	118 ± 28.3	10.3±0.41	$2.26 \times 10^8 \pm 9.21 \times 10^7$	638 ± 11.9
ADSCs blebs	214 ± 22.8	229 ± 33.6	232 ± 39.3	14.3±1.22	$6.25 \times 10^8 \pm 5.70 \times 10^7$	$1.23 \times 10^3 \pm 89.2$

4.5.2. Formation and characterization of ASB

ASBs were produced from membrane blebs from ADSCs using a protocol previously established by our group to form proteinaceous bilayers from mammalian

cells (Figure 4.1a)[33]. In brief, cell membrane blebs labeled with octadecyl rhodamine (R18) a membrane-intercalating fluorophore, were incubated, and adsorbed on a cleaned glass slide. The fluorophore, R18, was initially confined to cell blebs and visualized as bright dots, as shown in the left image of the fluorescence images (Figure 4.1a). Next, fusogenic POPC-PEG2k liposomes were added to the well to induce rupture of blebs and spreading of R18 signal through the bilayer, as seen in the middle image of the fluorescence images[34, 161]. After 30 min of incubation followed by thorough PBS rinsing, a contiguous supported bilayer was formed and R18 signal from blebs uniformly spread out, diffusing freely within the planar bilayer surface as seen in the right fluorescence image. The dark scratch in the lower right (Figure 4.1a and 4.1b) of microscopy images was made to assess focus at the z-plane of the bilayer during image acquisition. The formation of an ASB can be found in Video 4.S1.

Lateral diffusion of components within the cell membrane is a fundamental process involved in many biological functions including binding and fusion of external particles[323 236, 241, 324]. For proper mimicking of ADSCs plasma membrane, ASB should retain the fluidity of the cell membrane since it allows diffusion within its 2D plane[241], influences binding-avidity[325], and facilitates lateral rearrangement of ligands to optimize binding[326]. We assessed the diffusivity of octadecyl rhodamine (R18) in the 2D plane of ASB using Fluorescence Recovery After Photobleaching (FRAP). Using a laser beam, a 22 μm diameter circle was photobleached in the bilayer at time zero as indicated by an arrow in the fluorescence recovery graph in Figure 4.1c and as shown in the top fluorescence image in Figure 4.1b. Partial recovery of the photobleached circle can be visualized in Figure 4.1b and 4.1c at around 350 sec for ASB. Lastly, final recovery

of the photobleached circle was achieved at about 1600 sec for ASB as shown in the fluorescence recovery graph in Figure 4.1c and in the bottom fluorescence image in Figure 4.1b. The ability of the ASB to undergo fluorescence recovery and its resultant high mobile fraction value of 90% and above validates the formation of a diffusive and mobile supported bilayer, minimally free of defects. Fluorescence recovery curves (Figure 4.1c) formed as described in the experimental section and used to determine the diffusion coefficient (D) of ASB and a control POPC/PEG-2k SLB are reported in Figure 4.1d. ASB was found to be less diffusive (D: 0.297 ± 0.035 $\mu m^2/s$) than POPC/PEG-2k SLB (D: 0.486 ± 0.096 $\mu m^2/s$). These results were expected since POPC/PEG-2k SLB contains only lipids and ASB consists of not just lipids, but also ADSCs membrane proteins from ADSCs blebs, which have been established to reduce diffusion within the bilayer[293]. Therefore, ASB conserves the characteristic fluidity properties of cell membranes.

4.5.3. Detection of Integrin β1/CD29, a native component of ADSC membrane, in ASB

To recapitulate the cell membrane of ADSCs, ASBs should retain its native components. Integrin β1 is a protein highly expressed in the plasma membrane of ADSCs and is implicated in several biological functions including cell adhesion, wound repair, tumor directed angiogenesis, and tumor cell growth[327, 328]. ASB, as an *in vitro* model of ADSC membranes, should preserve this component. Here, we confirmed the presence of integrin β1 in the ASB using immunofluorescence with an-anti integrin β1/CD29 antibody, directed to recognize the extracellular portion of this transmembrane protein. We then labeled with a fluorescent secondary antibody for

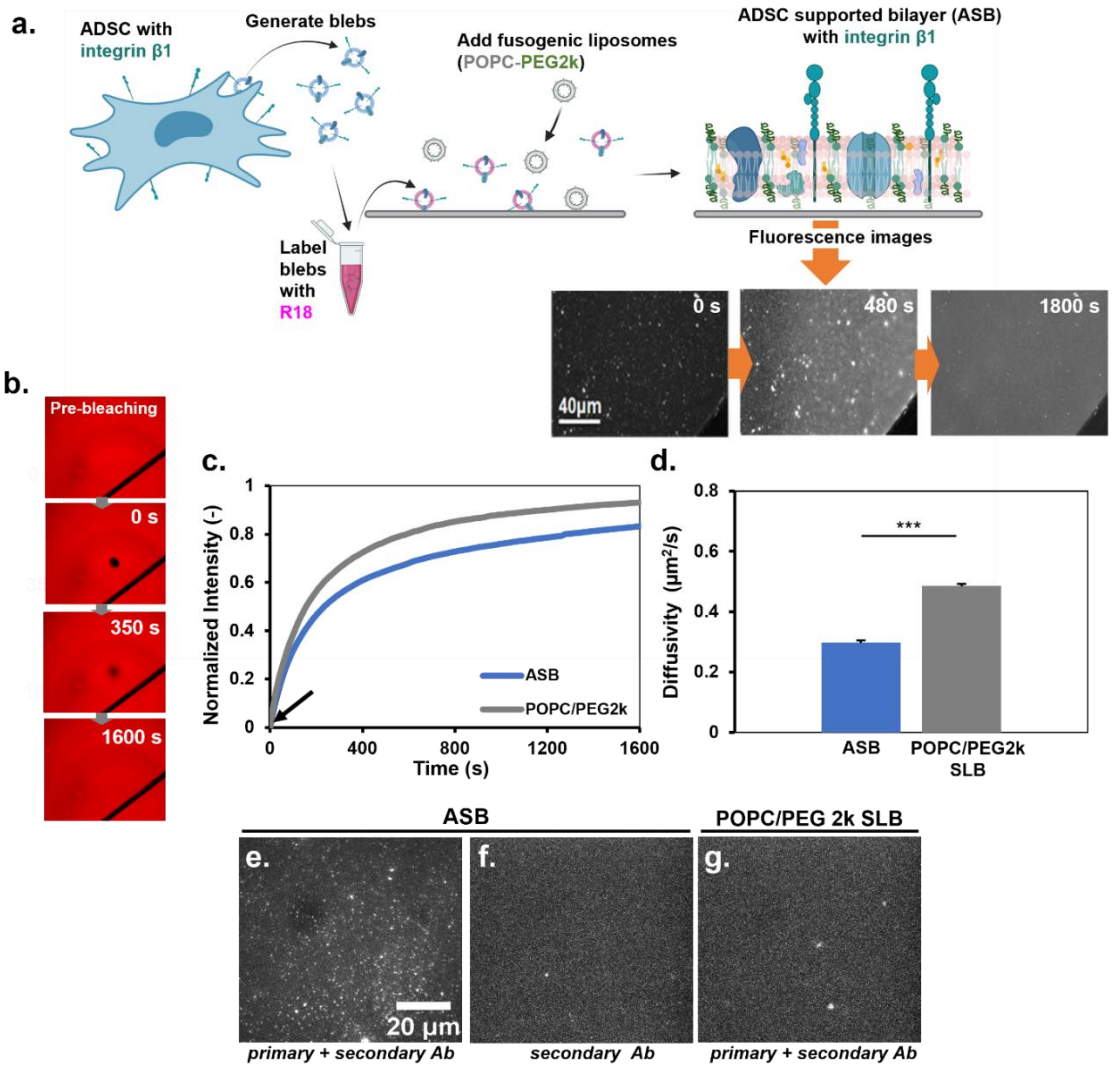

Figure 4.1. ASB formation and characterization. a) Diagram and fluorescence images of ASB formation. *Created with BioRender.com.* b) Pictures depicting pre-bleached, photobleached, partially recovered, and completely recovered ASB. c) ASB fluorescence recovery after photobleaching curve. d) Coefficient of diffusivity of ASB and POPC/PEG2k SLB. e) TIRF microscopy images of ASB treated with CD29/integrin β1 antibody shows specific binding of CD29/integrin β1 to ASB and its presence in it. f) Absence of CD29/integrin β1 in ASB treated with secondary antibody in the absence of primary antibody. g) Absence of CD29/integrin β1 in POPC/PEG2k-SLB. N = 4, mean ± SE, ***$p \leq 0.001$.

integrin β1 detected using TIRFM. Figure 4.1e depicts the bright spots associated with binding and presence of integrin β1 in an ASB. Furthermore, given that the antibodies bound to the appropriate epitope that faces away from the membrane, it suggests that

the orientation of the integrins is also intact. This result agrees with our previous observations for protein orientation where the extracellular portions face the bulk phase after bleb rupture[33, 34]. To reassure that our results were specific and not reflective of nonspecific adsorption, we used two negative controls shown in Figure 4.1f and 4.1g. Figure 4.1f depicts an ASB treated with conjugated secondary antibody in absence of primary antibody. Since the secondary antibody label is specific for the primary antibody[329], absence of the latter led to lack of detection of integrin β1/CD29 in the ASB. Moreover, in Figure 4.1g, a POPC/PEG2k-SLB is treated with primary and secondary antibodies, and no presence of integrin β1 is detected since it is a synthetic and inert bilayer that does not contain adhesion molecules like integrins. Collectively, these results suggest that our ASB preserves native membrane components, making it a good platform to study cEXOs interactions with ADSCs.

4.5.4. Optical detection of cEXOs binding to ASB

Independent of the route taken by cEXOs after initial contact with the cell membrane, binding is a common initial step for all mechanisms. Therefore, targeting it as a way to universally inhibit these malignant outcomes of cEXO-cell interactions is a strategy with high therapeutic potential. To detect binding to the ASB platform, R18-fluorescently labeled cEXOs were incubated with an ASB, and their initial interactions were captured using TIRFM and reported in Video 4.S2. We observed cEXOs binding to the ASB within 3 min of contact, with some of them being stably bound and some others binding and detaching from the ASB. Images captured by TIRFM after 30 additional minutes of incubation, show that cEXOs remained attached to ASBs (Figure 4.2a) suggesting a stable binding, however further experiments must be performed to confirm

that. In contrast, Figure 4.2c shows a negligible amount of cEXOs binding to POPC/PEG2k-SLB as expected since POPC/PEG2k-SLBs are inert, non-fouling surfaces, and do not contain adhesion proteins to mediate binding. It also suggests that in the ASB, the cEXOs binding specificity comes from the ADSCs membrane components that come from the blebs.

4.5.5. Blocking of Integrin β1/ CD29 reduces cEXOs binding to ASB

Binding between cEXO and ADSCs is known to be mediated by at least two proteins, one on the surface of each entity. Since it is established that integrins, including β1, α3, and α5 have been involved in binding of different types of EXOs to recipient cells[330, 331], we suspect that integrin β1, present on our ASB, could be one of the proteins involved in cEXO-ADSC binding. Figure 4.S2a, an schematic of the EXOs-cell surface interactions previously established[115], shows that integrins on the surface of the target cell potentially bind to ICAM and/or ECM proteins (fibronectin, laminin and collagen) on the EXOs surface[115]. To confirm the presence of those ligands on the surface of breast cancer cEXOs that will facilitate binding to integrin β1 on the surface of ADSCs, we performed a proteomics analysis available on File 4.S1. Figure 4.S2b shows several integrin β1 ligands on the surface of cEXOs including ICAM1, fibronectin, laminin, and collagen subunits, among others. Therefore, we decided to focus on investigating the role of integrin β1 in ADSCs membrane, on cEXOs-ADSCs binding, specifically the ability to block that binding by antibodies directed against integrin β1.

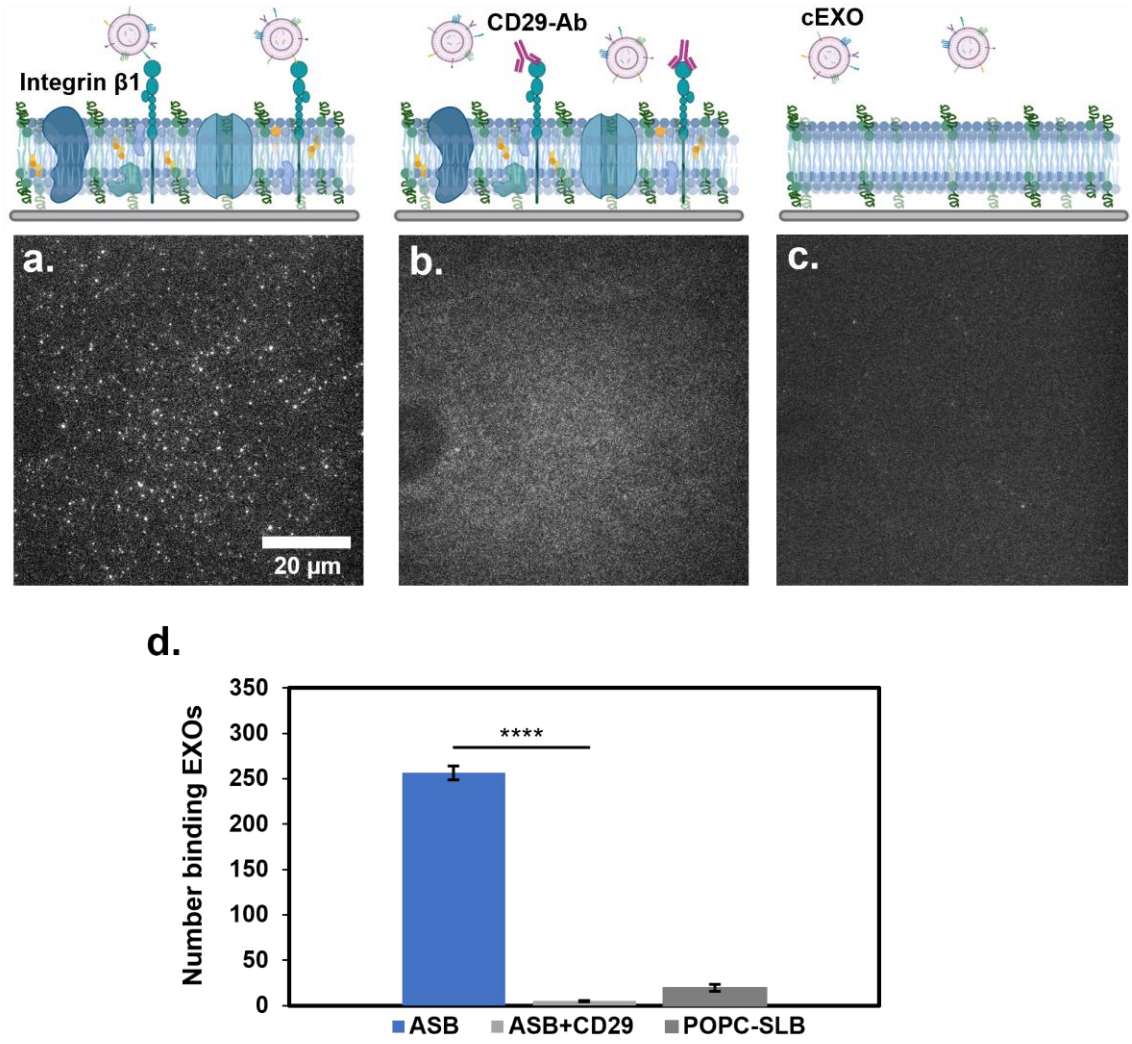

Figure 4.2. Integrin β1/CD29 plays a role in cEXOs binding to ASBs. TIRFM images of cEXOs binding to a) ASB with no treatment. b) ASBs treated with CD29/integrin β1 antibody. c) POPC/PEG2k SLB. d) Quantification of cEXOs bound to ASBs, non-treated and treated with integrin β1/CD29 antibody, and POPC/PEG2k SLB after 30 min incubation. *Created with BioRender.com.* N = 3, mean ± SE, ****$p \leq 0.0001$.

To examine the potential of blocking integrin β1 as a strategy to decrease cEXO binding, the surface of the ASB was treated with an anti-integrin β1/CD29 primary antibody (referred as CD29 Ab here) prior to incubation with cEXOs. Following the same procedure previously stated, treatment of the ASB with CD29 Ab resulted in significantly reduced binding compared to cEXOs binding to the untreated ASB, Figure 4.2b and 4.2a

respectively. Additionally, as seen in figure 4.2d, the number of cEXOs binding to the CD29 Ab-treated ASB is significantly less than cEXOs bound to untreated ASB, and similar to the number of cEXOs binding to the POPC/PEG2k-SLB. These results indicate that integrin β1 plays a specific role in cEXO-ADSCs binding, recapitulated in ASB, and its blockage decreases attachment of cEXOs to ASB.

A convenient aspect of our platform is that ASBs are free of maintenance required for live cells, simplifying that aspect of assay and drug screening development. Furthermore, we can focus on binding, isolated from cEXOs internalization by cells, to target that conserved aspect of cEXO-cell interactions. We demonstrated that ASB is a functional *in vitro* ADSC cell membrane model able to detect cEXOs binding using optical approaches and can be leveraged to develop strategies to block it. A great advantage of SLBs is their high amenability to scale up, through rapid functionalization and patterning of surfaces and integration of microfluidic and electrical components. Toward this end, we coupled the ASB with an electrical device forming a bioelectronic platform to allow label-free and sensitive detection of cEXOs binding.

4.5.6. Electrical monitoring of cEXOs binding to ASB

By coupling the ASBs with MEAs we can probe changes in the electrical signals resulting from modifications of the membrane properties associated with the binding of cEXOs. We have previously demonstrated the capability of electrical methods for monitoring biological events at the cell plasma membrane[318, 332, 333]. This led us to integrate ASBs with poly(3,4-ethylenedioxythiophene) doped with poly(styrene sulfonate) (PEDOT:PSS) -based MEAs (Figure 4.3a) for electrical sensing of cEXOs binding to ASB using EIS. PEDOT:PSS has overall low impedance and can hence be

ideal for biological sensing applications. Additionally, PEDOT:PSS films modified with silane based crosslinkers swell in aqueous biological environments and act as a hydrogel-like cushioned support well suited for cell - cell membrane integration while preserving mechanical and electrical properties[334-336]. This more native-like environment ensures transmembrane protein functionality by facilitating their free lateral movement in the membrane[332].

ASB lipid membranes were successfully formed on PEDOT:PSS transducers and initially characterized using FRAP to reassure the formation of a proper bilayer to the electrical transducer. Results in Figure 4.S3 show FRAP images and fluorescence recovery of an ASB on PEDOT:PSS after 400 sec suggesting successful formation of a diffusive lipid bilayer on PEDOT:PSS. The reported coefficient of diffusivity of ASB on PEDOT:PSS (0.500 ± 0.022 $\mu m^2/s$) is slightly higher than on glass (D: 0.297 ± 0.035 μm2/s), and we hypothesize that this increase in diffusivity is due to the ability of PEDOT:PSS to act as a cushion for the ASB, as it has been previously observed for other hybrid-SLBs formed on polyelectrolyte cushions[337].

EIS measurements of ASBs formed on PEDOT: PSS-coated electrodes were performed for the electrical monitoring of the bilayer formation too. Here, the impedance magnitude, Z, as a function of frequency, is captured in the Bode plot shown in Figure 4.3b and 4.3c and Figure 4.S5 and 4.S6, and the fitted resistance values were used as figures of merit. The magnitude of the calculated membrane resistance relates to the membrane ion permeability and has thus been successfully used in similar setups as a figure of the membrane “leakiness” or the membrane “integrity”. For example, we have shown in the past that membrane binding events result in an increase in the membrane

resistance whereas membrane events that could potentially result in membrane "leakiness" (i.e., disruption, pore formation, ion channel opening) result in a decrease in the calculated resistance values. EEC model was fitted to the raw impedance as illustrated in the Nyquist plot of Figure 4.S4b, allowing extraction of the membrane resistance (R_m) using the EEC. R_m was calculated for ASB and for ASB with integrin β1 blocking (*ASB+CD29*), and again after the addition of cEXOs (*+cEXOs*) for each condition.

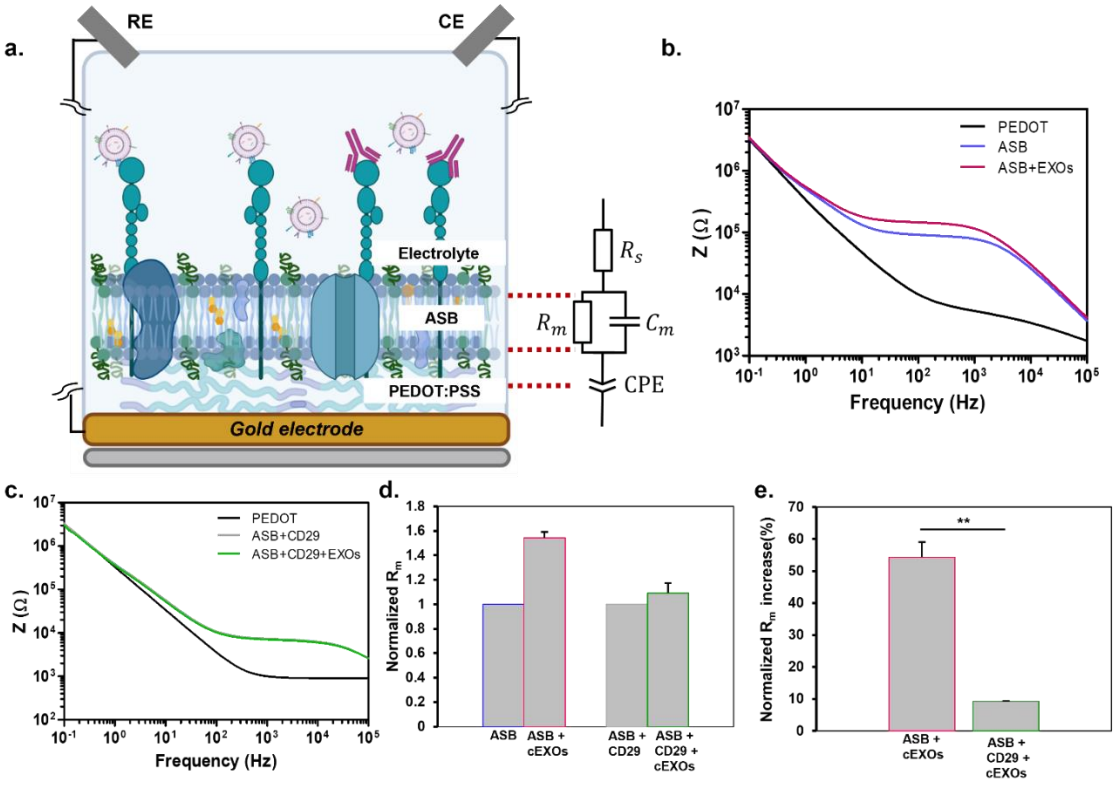

Figure 4.3. Electrical readouts support the role of integrin β1/CD29 in cEXOs binding to ASBs. a) Experimental setup showing ASB formed on top of PEDOT:PSS-coated Au electrode. RE: Reference electrode, CE: Counter electrode. The EEC is shown with R_s being the solvent/electrolyte PBS 1X, R_m and C_m being the membrane resistance and capacitance, respectively, and the PEDOT:PSS modeled as a constant phase element (CPE), *Created with BioRender.com.* b) Bode plot of cEXOs binding to the ASB. c) Bode plot of cEXOs binding to the CD29 Ab-treated ASB. (d). R_m normalized to the ASB prior to cEXO binding showing ASB + cEXOs in the absence and presence of CD29 Ab treatment. e) Comparison of the normalized percentage increase in R_m between the ASB + cEXOs addition and between the ASB+CD29+cEXOs addition as defined by equation 2. N= 5, mean ± SE, **p ≤ 0.01.

The experimental protocol was carried out using multiple single MEAs for each

condition to control for MEA batch-to-batch variability. Measurements were taken from multiple electrodes within the same MEA (i.e., of the same ASB) for each condition to control for electrode-to-electrode variability and to ensure that measurements were only collected from electrodes where there was good coverage of the ASB. ASB sealing quality was assessed based on the increase in impedance compared to the bare PEDOT:PSS impedance, as observed in the Nyquist and Bode plots (see Figure 4.S4-5) and as determined from the increase in the derived R_m value. It was typical to achieve a 25-50% success rate of electrodes whose R_m reflected a tightly-sealed lipid bilayer. The calculated R_m values were normalized for each measurement due to the variability in absolute R_m between MEAs, which ranged between 0.01 and 1.02 kΩ cm^2. This range in R_m values was likely caused by small differences in the ASBs, as the MEAs are very sensitive to defects found in the bilayer. These values are comparable to values obtained from similar setups that used mammalian cell-derived SLBs. To address this variation, R_m normalization was performed to assess the relative change in magnitude of R_m before and after cEXOs binding for each condition (Figure 4.3d). This allows cEXOs binding to be inferred from changes in R_m, essentially rendering R_m a function of the abundance cEXOs binding to the membrane and allows comparison across multiple experiments performed on different MEAs regardless of the baseline R_m obtained. In the case of the CD29 Ab condition, the R_m of the ASB after treatment with CD29 Ab was used as a reference for cEXOs binding. The addition of anti-CD29 Ab to the ASB resulted in a small increase in R_m ~14% (from 0.010 to 0.011 kΩ cm^2) (Figure 4.S6).

The relative change in normalized R_m, ΔR_m, is defined as:

Eq. 4.2 $$\Delta R_m = \frac{R_{m,cEXO} - R_{m,ASB^*}}{R_{m,ASB^*}}$$

Where R_{m,ASB^*} is either ASB or ASB+CD29, we can calculate the relative change in R_m before and after cEXO binding. The results presented here are an average of these. The addition of cEXOs caused an average increase in normalized R_m of ~54% and ~9% for the non-treated and anti-CD29 Ab-treated conditions, respectively (Figure 4.3e). These results align with the ones from the optical experiments and provide further proof that blocking integrin β1 receptors with anti-CD29 Ab reduces cEXO binding to the ASB.

In summary, using our ASB platform with optical and electrical analytical approaches, we were able to detect cEXOs binding and to verify the mediating role of integrin β1 on it. Fluorescence/label-based methods are more established in this field and in this study, and we confirmed the fluorescence data with the novel electrical data and demonstrated the capability of detecting cEXOs binding in a label-free manner for the first time. Further analysis to compare the two techniques is part of our future work as it will require us to establish a more thorough understanding of the EIS data, such that we can tune the sensitivity of the devices to quantitatively assess cEXOs binding events.

To validate our results obtained by both sensing methods (optical and electrical), we investigated the biological outcome of blocking integrin β1 in ADSCs in an *in vitro* cell setting. However, the utility of this platform is only promising if the results obtained here translate to changes in biological outcomes. To assess this, we next carry out the same studies in cell culture and measure changes in pro-angiogenic behavior to determine if the binding we block here leads to a reduction in negative outcomes.

4.5.7. Blocking of integrin β1 decreases cell proliferation and VEGF secretion by ADSCs in culture

We previously used an *in vitro* cEXO-membrane platform (EVSB) to isolate interactions between cEXOs surface and ADSCs and found proangiogenic markers including upregulation of VEGF and cell proliferation to be a direct outcome[9]. Therefore, to validate the mediating role of integrin β1 in cEXOs-ASDCs binding, found in the previous sections, we investigated its influence on VEGF and cell proliferation upregulation, as binding outcomes. Towards this end, we conducted an *in vitro* assay to assess the number of alive cells and concentration of VEGF secreted by ADSCs treated with cEXOs in the presence and absence of CD29 Ab (anti-CD29 antibody), as a blocking treatment for integrin β1, in ADSCs.

ADSCs grown to 80% confluency were treated during 5 days with four conditions: 40 μg of cEXOs (cEXOs), CD29 Ab followed by cEXOs (CD29), transforming growth factor beta (TGFβ) as a positive control, and no treatment (NT) as a negative control (Figure 4.4d). ADSCs with no treatment (NT) were expected to secrete less VEGF than the treated counterparts[5, 9]. Conversely, ADSCs treated with TGFβ were expected to show increased VEGF secretion since TGFβ plays a key role in VEGF regulation and induction of proangiogenic factors[338-340]. Secreted VEGF concentration per cell for all conditions was assessed by ELISA assay at days 2 and 5 of treatment. For easier data interpretation, results displayed in Figure 4.4a and 4.4b represent VEGF secretion per cell for all conditions normalized by the no treatment (NT_2) values on day 2. Therefore, NT_2 values were used as a baseline to analyze VEGF concentration by ADSCs.

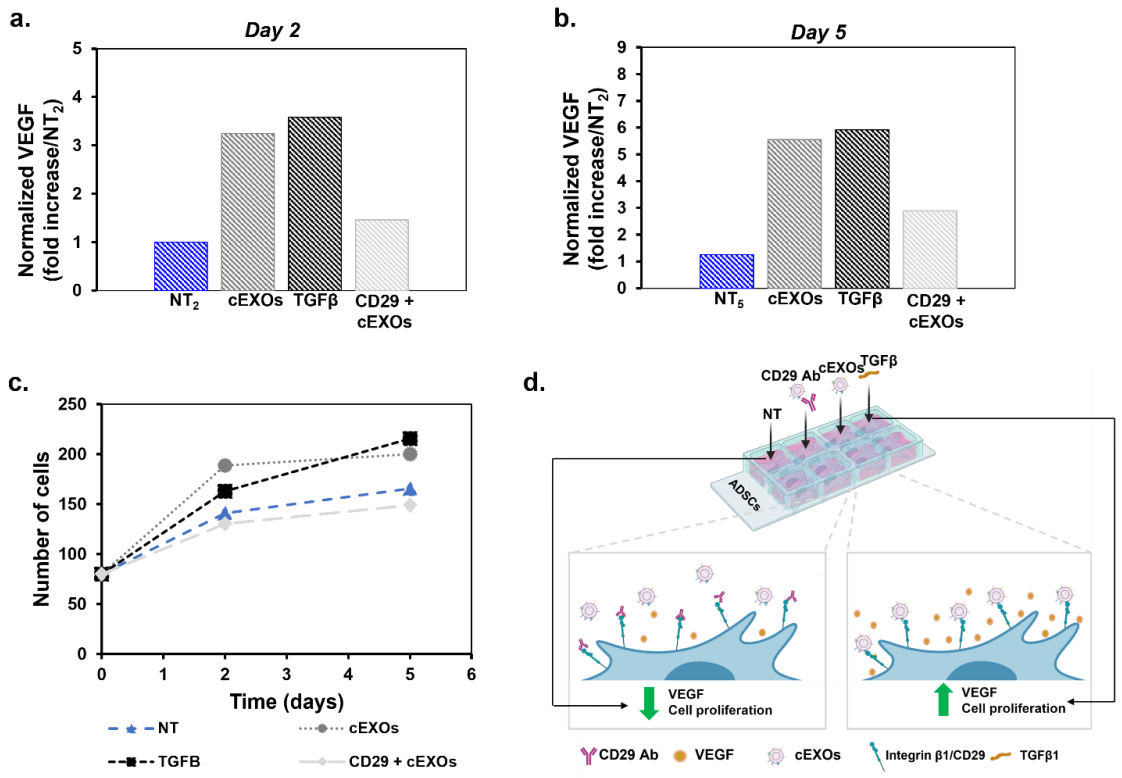

Figure 4.4. Blocking of integrin β1/CD29 decreases cell number and VEGF secretion by ADSCs treated with cEXOs. a) Normalized secreted VEGF concentration by ADSCs for all four conditions: NT, CD29 Ab +cEXOs, cEXOs, and TGFβ on day 2 and b) on day 5 of treatment. VEGF secretion for all conditions was normalized by VEGF concentration at no treatment (NT_2) on day 2. c) Number of alive ADSCs at days 0, 2, and 5 of treatment for the same conditions as in (a). d) Schematic representation of experiment done on section 3.6 of ADSC-cEXOs leading to upregulation of VEGF secretion and cell proliferation on ADSCs; and inhibition of ASDC-cEXOs binding and decrease in those outcomes by blocking integrin β1 with CD29 Ab. *Created with BioRender.com.* N = 3.

As expected, VEGF secretion is significantly upregulated in ADSCs treated with cEXOs and with TGFβ compared to the NT counterparts for both days. Results displayed in Figure 4.4a show that cells treated with cEXOs and TGFβ for two days secreted approximately 3 and 4 times more VEGF than NT_2 cells. Interestingly, ADSCs treated with CD29 Ab, previous to cEXOs addition, secreted similar VEGF concentration as NT_2 cells. The same behavior was observed on day 5 of treatment where cells treated with cEXOs and TGFβ secreted around 6 times more VEGF than NT_2 and NT_5 cells, and cells treated with CD29 Ab secreted just 2 times more VEGF than N_2 and N_5 cells. As

expected, VEGF quantity was slightly higher on day 5 than on day 2, for all conditions as shown in Figure 4.4b. These results indicate that blocking integrin β1 in ADSCs prevent the pro-angiogenic activity, indicated by upregulation of VEGF observed in ADSCs treated with cEXOs (Figure 4.4d).

Since cell proliferation is also influenced by cEXOs binding to ADSCs, we counted the number of alive cells under the same conditions. As seen in Figure 4.4c, treating ADSCs with cEXOs and TGFβ leads to a higher number of alive cells than NT, as we previously reported. Conversely, a decrease on cell number was observed with CD29 Ab treatment before cEXOs addition. Given these results, it suggests that integrin β1 plays an important role in cEXO-ADSC binding and blocking it is a strategy with therapeutic potential to decrease pro-angiogenic activity that occurs from VEGF upregulation and proliferation of ADSCs in the tumor microenvironment.

4.6. Conclusions

We have successfully generated an ASB platform that conserves lateral fluidity and presence of integrin β1, important characteristics of ADSCs surface, making an adequate *in vitro* model of human primary ADSC plasma membrane. Using this system, we were able to replicate cEXO binding, isolating it from subsequent cEXO internalization and cargo delivery, in a cell-free manner. The planar nature of the stem cell membrane model renders it amenable to surface sensitive techniques, optical and electrical, which hold potential for extracting valuable information regarding cEXOs binding and function that would otherwise remain elusive to cell-based systems and its complementary analytical techniques. This geometry facilitated the integration of the ASB to a PEDOT:PSS-based MEA and detection of cEXO binding using optical

(TIRFM) and electrical (EIS) techniques, allowing visualization and label-free monitoring of such interaction. Moreover, we showed a significant decrease of cEXO binding to the ASB with anti-CD29 Ab treatment (as a mean to block integrin β1) with both optical and electrical readouts. These results suggest that integrin β1 receptors were bound to CD29 Ab and not available to interact with cEXOs, supporting our initial hypothesis that integrin β1 facilitates cEXO binding to ADSCs. Likewise, treatment of cultured ADSCs with CD29 Ab prior to cEXO addition led to a small change in VEGF secretion and cell proliferation, both processes highly upregulated in ADSCs treated with cEXOs in the absence of CD29Ab. This validates our results obtained with the ASB showing the ability of CD29 Ab to reduce cEXOs binding to ADSCs and its malignant outcomes, and it further corroborates an important role of integrin β1/ CD29 on cEXOs-ADSCs binding.

Moreover, the detection of low levels of remaining cEXOs-ASB binding and some increase in VEGF secretion and cell proliferation in ADSCs despite CD29 blocking, suggests the involvement of other molecules in this binding. This possibility opens a new avenue to use our ASB system and study the role of other ADSCs and cEXOs surface components in cEXOs-ADSC binding and find strategies to inhibit it through drug screening. The proteomics analysis available in the SI offers several cEXOs surface molecules, including possible ligands for integrin β1, that can be further analyzed. Furthermore, our ASB will facilitate the study of cEXOs binding kinetics and the mechanisms behind it to further attain its complete inhibition along its malignant outcomes.

Here we showed how our ASB platform allows the recapitulation of human primary ADSCs plasma membrane and the monitoring of cEXOs binding in a simpler manner than the available conventional methods such as optical tweezers[8] and immunofluorescence[341]. Although previous groups have used native cell membrane models to screen virus binding inhibitors[312, 313], to the best of our knowledge, we are the first study to propose the use of biomimetic membrane models incorporating native components of human mammalian cells to screen strategies to block EXOs binding to cells. Our system offers several advantages including: (i) it is free of the dynamic complexity of cells; (ii) it does not need the aseptic conditions required in cell culture; (iii) reduces the need for extensive human primary ADSCs culture which are highly sensitive, not widely available, and have a limited number of cell culture passages allowed before they differentiate; and (iv) the ability to use complementary analytic techniques like TIRFM and EIS, for visual detection in real time and for label-free and sensitive electrical monitoring of cEXOs binding/blocking, respectively. This versatility makes the ASB an excellent option for screening potential therapeutic molecules as it is compatible with scale-up and multiplexing, with the option to be label-free. Therefore, multiple testing conditions can be screened using ASBs originated from a single batch of human primary cells. Lastly, the ASB can be tuned to generate model systems of the plasma membrane of different types of cells to investigate their binding to diverse types of EXOs. This model will facilitate the study of different types of cancer and other diseases for which the prognosis is worsened as communication between diseased and healthy cells progresses via EXOs [3, 5, 274, 275, 342]. Our platform will make then a great tool for drug discovery and the development of treatments and therapeutics to mitigate the

strong effect that cEXOs have on tumorigenesis and metastasis.

4.7. SUPPORTING INFORMATION

4.7.1. Experimental Section

4.7.1.1. cEXOs isolation

MDA-MB-231 cells were cultured on a 150 cm^2 cell culture flask (Corning, NY) in 15 mL of complete media until they reached 75-85% confluency. To avoid the presence of serum-derived EXOs during isolation, cells were incubated in serum-free media for 18-48 hours at 37°C and 5% CO_2. Media was collected and centrifuged at 280 x g for 12 min at 21 ̊C to remove cells, followed by a second centrifugation at 10000 x g for 25 minutes at 21 ̊C to remove cell debris. The cleared media was vacuum filtered using a 0.22 μm Millipore Steriflip PVDF-filter, (Millipore, Burlington, MA) to separate bigger particles from exosomes. The filtrate generated in the vacuum tubes was transferred to ultracentrifuge tubes followed by ultracentrifugation at 100,000 x g at 4 ̊C for 4 hours. The cEXO pellet was resuspended in 1 mL of PBS pH 7.4 supplemented with 1% P/S. cEXOs were kept at 4 ̊C until needed. To obtain exosomes lysates further used for protein quantification by Bicinchoninic acid assay (BCA), the cEXOs pellet was resuspended in 200 uL of lysis buffer, RIPA buffer and Pierce proteinase inhibitor cocktail tablet, Thermo Fisher Scientific (Waltham, MA) and kept at -20̊C until needed. All experiments were done with exosomes within five days of isolation.

4.7.1.2. Characterization of cEXOs and adipose derived stem cell blebs: size

Adipose derived stem cells (ADSCs) blebs and cEXOs size and concentration were found by nanoparticle tracking analysis (NTA). NTA measures nanoparticles in suspension by analyzing Brownian motion and finding the size of the translational diffusion diameter

(hydrodynamic diameter) of each sphere/nanoparticle. The lower resolution limit of NTA depends on the scattered intensity of the particle and the sensitivity of the camera. Biological particles such as cEXOs have a refractive index of about 1.37-1.45 giving a lower limit of detection of around 30 nm[38]. For our study, NS300 Malvern was utilized. Using this equipment, particles between 30-800 nm can be measured and concentration resolution is 10^6 to 10^9 particles/ml.

Additionally, cEXOs and ADSCs blebs size and zeta potential were found by dynamic light scattering, DLS, and laser Doppler electrophoresis respectively, LDE. DLS measures the diffusion of particles in solution under Brownian motion and obtains particle size distribution using the Stokes-Einstein relationship. Nano ZS, Malvern, the Zetasizer used for our study, has a measurement range of 0.3 nm to 10 μm for particle size measurement. Finally, LDE finds the surface charge of particles in suspension or zeta potential by measuring the movement of the charged particle in an applied electric field using the Doppler principle. The Nano ZS used for this study can measure the zeta potential of particles ranging between 3.8 nm and 100 μm in diameter and has no limits for zeta potential value.

4.7.1.3. Transmission Electron Microscopy (TEM)

Size and morphology of ADSCs blebs and cEXOs was further corroborated using transmission electron microscopy (TEM). TEM uses an electron beam to visualize particles and generate a highly magnified image of cEXOs and blebs. FEIT12 Spirit Tecnai TEM, the equipment used for our study, is capable of imaging particles as small as 0.20 nm.

Briefly, freshly isolated cEXOs and ADSCs blebs were visualized using FEI

Tecnai-12 Spirit TEM (Hillsboro, OR) at 120 kV at the Cornell Center for Materials Research. Samples were loaded onto a 300-mesh carbon-coated copper grid and negatively stained with 1.5% uranyl acetate.

4.7.1.4. Characterization of cEXOs and ADSCs blebs: protein concentration

A Bicinchoninic acid assay (BCA) assay was performed to find the protein concentration of cEXOs and ADSCs blebs. The assay was performed using a QuantiPro BCA Assay Kit (Sigma-Aldrich, St. Louis, MO) and following the manufacturer's protocol. PBS was used as a blank for the BCA assay, and cEXOs and blebs of varying dilutions were prepared and used as unknown protein concentration samples. 150 µL of BSA protein standards, blanks, or unknown concentration of cEXOs samples were added in each PORVAIR 96 well plate wells with flat bottom (Porvair, UK). The same volume, 150 µL, of BCA working reagent was added to each well, containing standards, blank, or unknown concentration samples. Replicates were done for all the samples. Using the standard curve and the A_{562} obtained for each of the samples, the protein concentration of cEXOs and ADSCs was determined.

4.7.1.5. Isolation and extraction of exosomal proteins for single-pot, solid-phase-enhanced sample preparation (SP3) for mass spectrometry analysis

After isolation of cEXOs, previously described, total proteins were then extracted using the RIPA lysis buffer supplemented with 1X Halt protease and phosphatase inhibitor cocktail, ThermoFisher Scientific (Waltham, MA) after which the exosomal protein sample was processed using the SP3 protocol as previously described[343]. Briefly, 100 g of exosomal protein were reduced with 10 mM of TCEP (tris(2-carboxyethyl) phosphine) at 55 °C for an hour followed by alkylation of the reduced disulfides with 17 mM of

iodoacetamide at room temperature in the dark for 30 mins. The alkylation reaction was subsequently quenched with 5 mM of DTT by incubating at room temperature for 15 mins. The SP3 beads, GE Lifesciences (Chicago, IL) were added to the protein sample at a bead/protein ratio of 10:1 (w/w) and were mixed by pipetting. Absolute ethanol was then added to the protein-beads mixture at a final concentration of 50 % (v/v) and incubated at room temperature for 5 mins to induce protein binding to the beads. Using a magnetic rack, the protein sample bound to the SP3 beads was washed thrice with 80 % ethanol, after which the protein was digested overnight at 37 °C in trypsin digestion solution (1:25 (w/w) trypsin to protein ratio in 100 mM Triethylammonium bicarbonate, TEAB). After digestion, the peptide sample was recovered from the beads by centrifuging at 20 000 x *g* for 1 min at 24 °C followed by elution on the magnetic rack. The peptide sample was processed by KAUST Bioscience Core Lab for mass spectrometry analysis.

4.7.2 Results

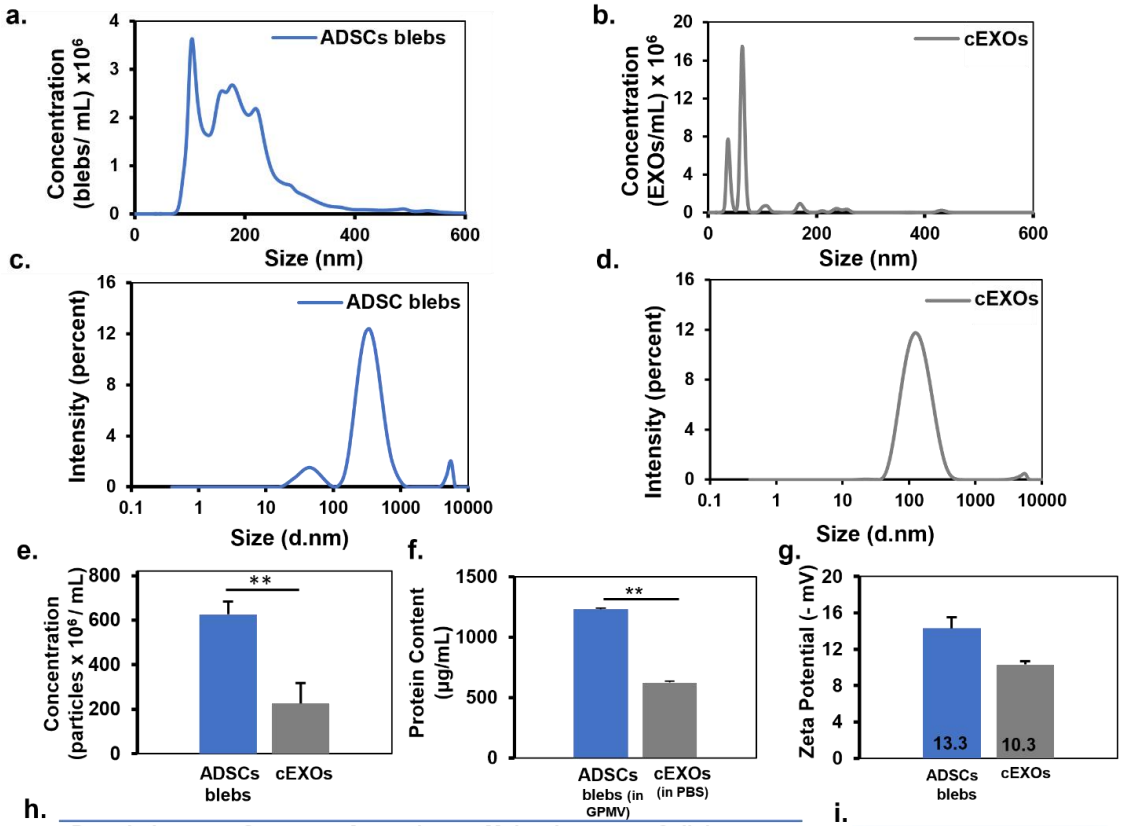

Description	Gene	Accession	Molecular function	Cellular location
Flotillin-1	FLOT1	O75955	protein binding	cytoskeleton; endosome; membrane
CD9 antigen	CD9	P21926	protein binding	cell surface; membrane
CD81 antigen	CD81	P60033	protein binding; receptor activity	membrane
CD63 antigen	CD63	P08962	protein binding	cell surface; endosome; extracellular; membrane;
Intercellular adhesion molecule	ICAM1	P05362	protein binding; receptor and signal transducer activity	cell surface; membrane

Figure 4.S1. Characterization of ADSCs blebs and cEXOs. Size distribution of ADSCs membrane blebs by a) NTA and by c) DLS. Size distribution of cEXOs by b) NTA and by d) DLS. Particle concentration of ADSCs blebs and cEXOs by e) NTA and protein concentration by f) BCA. g) Zeta potential of ADSCs blebs and cEXOs using laser Doppler electrophoresis. h) exosomal markers detected in cEXOs sample by proteomics analysis in File S1. i) TEM images of ADSCs cell blebs (top) and cEXOs (bottom).

a.

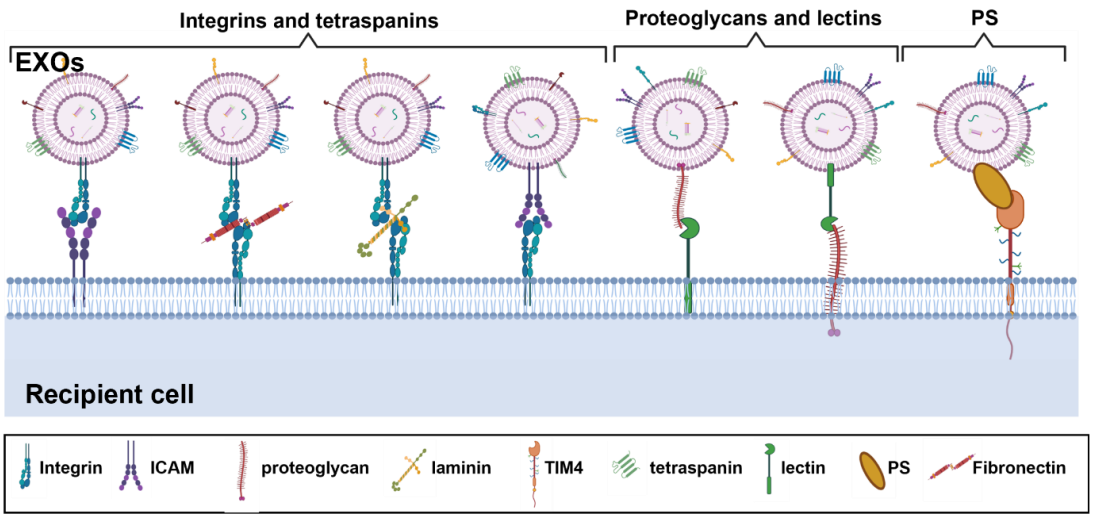

b.

Description	Gene	Accession	Molecular function	Cellular component
Intercellular adhesion molecule 1	ICAM1	P05362	protein binding; receptor activity; signal transducer activity	cell surface; membrane
Fibronectin	FN1	P02751	enzyme regulator activity; protein binding	membrane; organelle lumen
Laminin subunits:				
α3, **α4,** **α5,** **γ2,** **β2,** **β3**	LAMA3, LAMA4, LAMA5, LAMC2, LAMB2, LAMB3	Q16787-2, Q16363, O15230, Q13753-1, P55268, Q13751	catalytic activity; motor activity; protein binding; structural molecule activity	Extracellular Membrane; nucleus

c.

Description	Gene	Accession	Molecular function	Cellular component
Integrin subunits:				
α2, **α3,** **α5,** **αV,** **α6,** **β1,** **β4,** **β5**	ITGA2 ITGA3 ITGA5 ITGAV ITGA6 ITGB1 ITGB4 ITGB5	P05556-1, P16144-1 P18084 P26006 P23229-1 P17301 P06756 P08648	enzyme regulator activity; metal ion binding; protein binding; receptor activity; signal transducer activity; transporter activity	Membrane; nucleus; cell surface; cytoplasm; cytosol; endosome; Golgi

Figure 4.S2. Surface components possibly involved in ADSCs-cEXO interactions. a) Schematic of EVs and cell surface components that mediate the binding of EVs to target cells[115]; PS: Phosphatidylserine, TIM4: PS receptor, ICAM: intercellular adhesion proteins. *Created with BioRender.com* Possible ligands in the surface of MDA-MB-231- derived cEXOs to bind integrin β1 in the surface of ADSCs directly (b), or indirectly (c) using an ECM protein as an intermediating binding agent as seen in the third and fourth configuration in a.

File 4.S1. Proteomics Analysis of MDA-MB-231 derived cEXOs

MDA-MB-231_cEXOs_proteome.xlsx

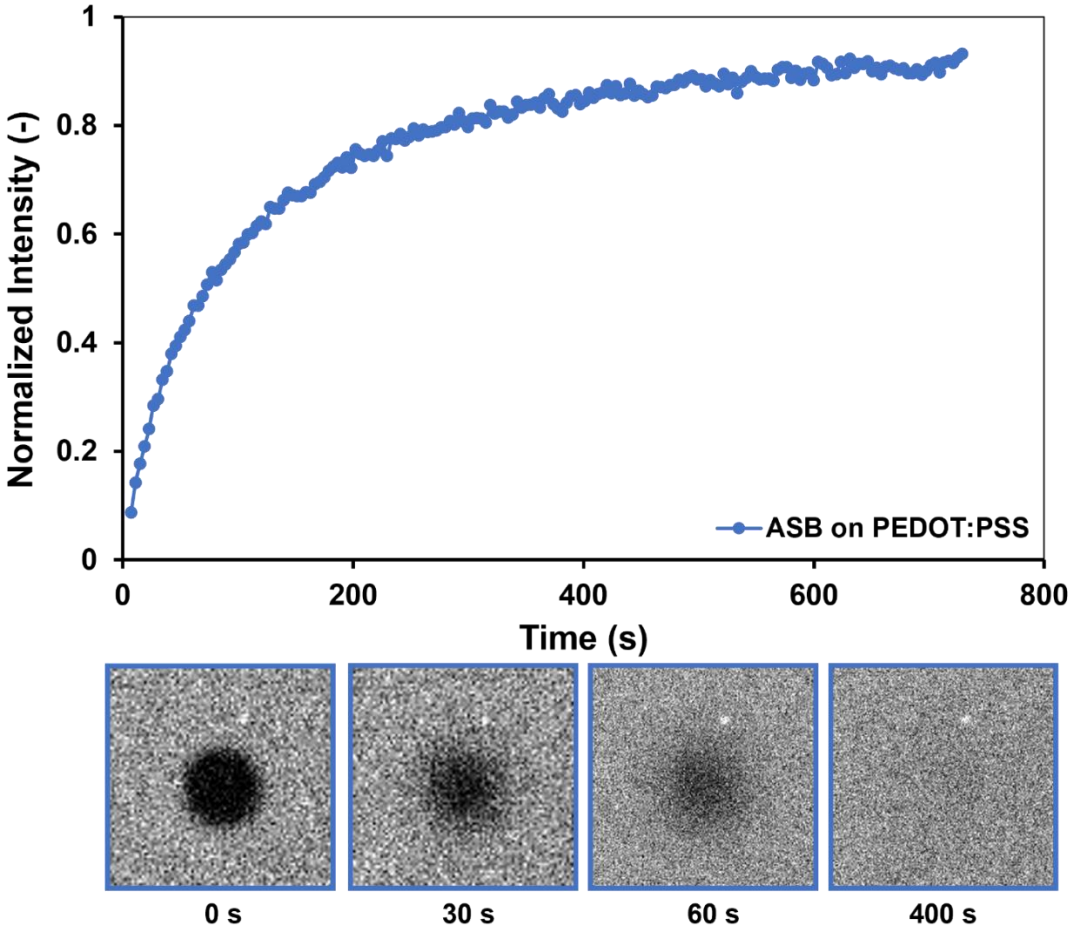

Figure 4.S3. FRAP of ASB on PEDOT: PSS. Fluorescence recovery after photo bleaching curve for ASB on PEDOT: PSS and pictures depicting photobleached, initial recover, partial recover, and completely recovered ASB. D = 0.50 ± 0.02 μm^2/s, MF=0.99 ± 0.03.

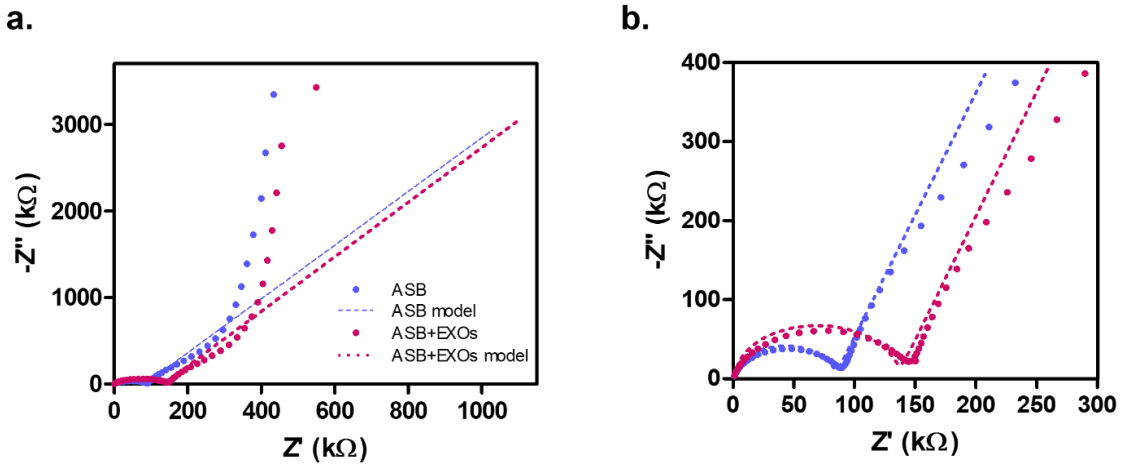

Figure 4.S4. Nyquist plots of cEXOs binding to ASB on PEDOT: PSS. S4b shows a zoomed in view of S4a. The capacitance of bare PEDOT: PSS is $C_{m,PEDOT:PSS} = 1.09\ nF\ cm^2$. Nyquist plots showing the EEC model fitted to the raw impedance data. Membrane resistance values are extracted from this model. This data complements the Bode plots presented in Figure 3b (main text) and is further evidence that cEXOs binding results in a detectable electrical change.

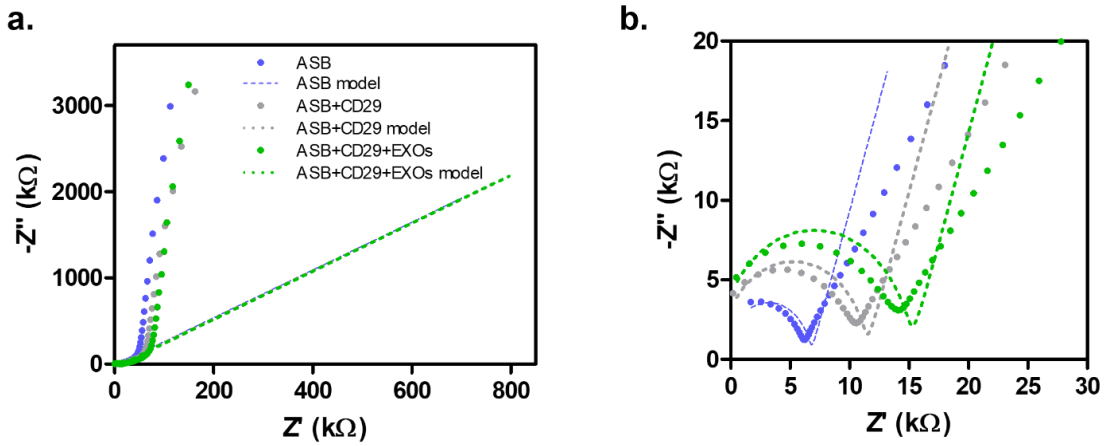

Figure 4.S5. Nyquist plots of C29 Ab-treated ASB on PEDOT: PSS. S5b shows a zoomed in view of S5a. Nyquist plot of the ASB after treatment with anti-CD29 antibody and after cEXO addition. This data complements the Bode plots presented in Figure 3c (main text) and is further evidence that blocking CD29 results in decreased cEXOs binding as detectable by electrical change.

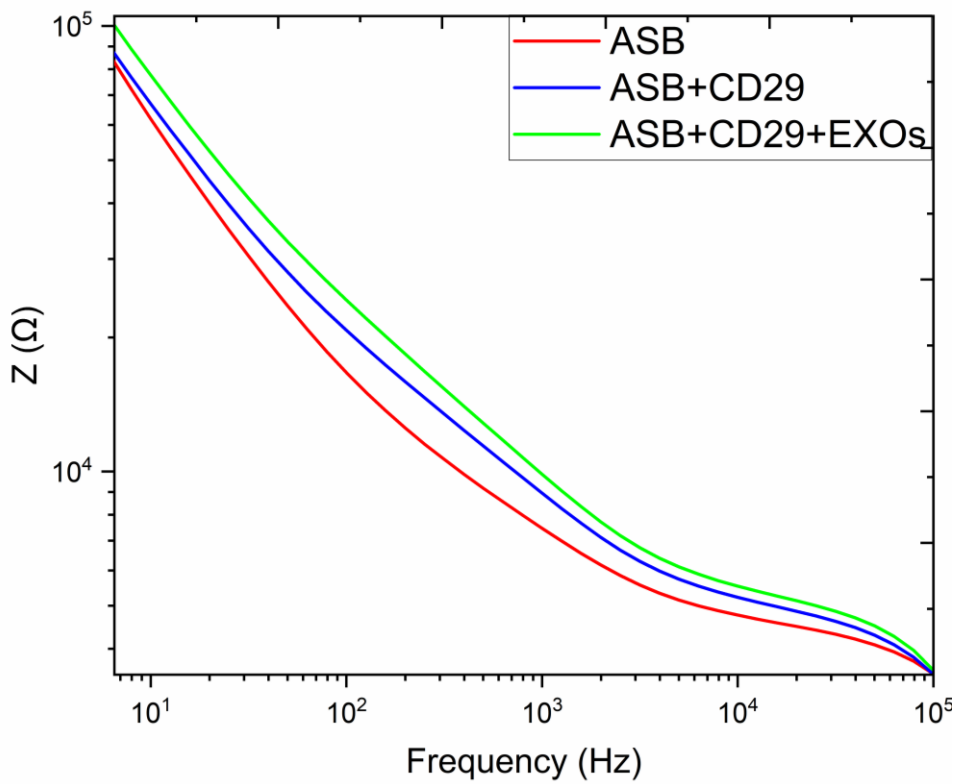

Figure 4.S6. CD29 Ab treatment effect on ASB resistance. Treatment of the ASB with anti-CD29 antibody resulted in a small change in membrane resistance.

Video 4.S1. Formation of ASB using FRAP

ASB_formation.zvi_Ch0.avi

Video 4.S2. Interactions of cEXOs and ASB using TIRFM

EXOs_ASB_2.avi

CHAPTER 5

5. ELECTRICAL MONITORING OF CELL EPITHELIAL-TO-MESENCHYMAL TRANSITION INDUCED BY CANCER-DERIVED EXOSOMES

Walther C. Traberg,[1*] Johana Uribe,[2] Adel Hama,[3] Miriam Huerta,[4] Victor Druet,[3] Anna-Maria Pappa,[1] Susan Daniel,[2,4] Sahika Inal,[3] and Róisín M. Owens[1]

[1]Department of Chemical Engineering and Biotechnology, University of Cambridge, CB3 0AS Cambridge, UK

[2]Meinig School of Biomedical Engineering, Cornell University, Ithaca, NY, United States.

[3]Biological and Environmental Sciences and Engineering Division, King Abdullah University of Science and Technology (KAUST), Thuwal 23955−6900, Saudi Arabia

[4]Department of Chemical and Biomolecular Engineering, Cornell University, 14850, Ithaca NY, USA

5.1 Acknowledgements

This study is in progress. All data included in this section is preliminary and under optimization. Johana Uribe and the Cornell team oversee EMT detection using biochemical techniques, and Walther C. Traberg ,Adel-Hama, and the Cambridge and KAUST teams are in charge of device fabrication and electrical experiments.

Walther C. Traberg is the first author, Róisín M. Owens is the corresponding author, and co-authors include Johana Uribe, Adel Hama, Miriam Huerta, Victor Druet, Ana-Maria Pappa, Susan Daniel, and Sahika Inal.

5.2. Abstract

Cancer derived exosomes (cEXOs) have been reported to favor tumorigenesis and metastasis owing to their ability to transmit oncogenes. One of their mechanisms to contribute to metastasis is thought to be the induction of epithelial-to-mesenchymal transition (EMT), a hallmark of cancer, characterized by the loss of barrier integrity and function, loss of epithelial proteins, and gain of mesenchymal markers, in barrier tissue-forming cells. In this work, we aim to investigate the ability of breast cancer cells (MDA-MB-231) derived cEXOs to induce EMT in non-tumorigenic breast epithelial cells (MCF-10A). We first show that breast cEXOs induce an EMT-like behavior in breast epithelial cells indicated by changes to cell morphology, loss of epithelial markers, and gain of mesenchymal ones, characteristic of the transformation using conventional techniques: immunofluorescence, western blot, and ELISA. However, these current techniques for investigating the spatial and temporal aspects of EMT are long and tedious and lack the ability to obtain quantitative data in real time. Hence, we describe a system to use organic electrochemical transistors (OECTs) based on the conducting polymer poly(3,4-ethylenedioxythiophene): poly(styrenesulfonate) (PEDOT:PSS) as cell culture substrates for MCF-10A cells to facilitate, optical and electrical, real-time monitoring of EMT. To do so, ongoing studies will be focused on electrically monitoring the changes in barrier integrity of MCF-10A monolayers treated with cEXOs on OECTs, gaining a truly quantitative insight into cEXOs-induced EMT with higher temporal resolution than conventional, orthogonal methods. This complement of optical and electrical readouts will provide invaluable information for developing strategies that may inhibit cEXOs interactions with epithelial cell monolayers thereby preventing cEXO-induced EMT with

implications for preventing cancer progression and metastasis.

5.3. Introduction

Epithelial to Mesenchymal Transition (EMT) is a reversible biological process in which cells lose epithelial characteristics, including cell-cell adhesion and baso-apical polarity, and acquire mesenchymal traits. In embryonic development, EMT is a fundamental cellular process for organogenesis, stem cell differentiation, induction of pluripotency, and wound healing[344]. However, in adults, EMT has been mostly associated with chronic fibrosis and disease states, including cancer. For instance, cells that undergo EMT show several changes in their cytoskeleton and secrete more ECM components acquiring migratory and invasive properties characteristic of metastatic cells[345]. The loss of epithelial properties in cells during EMT is characterized by a decreased expression in E-cadherin, an epithelial surface marker, and loss of barrier integrity. On the opposite, cells undergoing mesenchymal transformation present an increased expression of mesenchymal markers, including N-cadherin, vimentin, alpha-smooth muscle actin (α-SMA), fibronectin, and EMT- associated transcription factors[346].

Cancer-derived exosomes (cEXOs) are membrane encapsulated vesicles produced by cancer cells, originated in multivesicular bodies, and secreted into the extracellular space. They facilitate communication between cells within the tumor microenvironment (TME) and are known to influence tumorigenesis and cancer progression. One of the mechanisms used by cEXOs to facilitate cancer metastasis [21, 347] is the modulation of EMT, characterized by the loss of barrier function in barrier tissue-forming cells.

The limited methods available to investigate cEXOs interactions with cells, often optical, lack the ability to obtain quantitative data in real time[8, 9, 348, 349]. In order to create new ways to study these interactions, we have developed a bioelectronic platform consisting of complex biological systems coupled to organic electronic devices based on the conducting polymer poly(3,4-ethylenedioxythiophene):poly(styrenesulfonate)(PEDOT:PSS) that facilitate quantitative real-time monitoring of biological interactions[318] and detection of cell damage at early stages with high sensitivity[350]. The optical transparency of our PEDOT: PSS-based devices provides the unique advantage of dual transduction increasing the credibility of our platform and enriching the biological information obtained. Moreover, their compatibility with microfabrication methods allows for high throughput studies. Thus, in this study, we aim to elucidate and monitor the ability of cEXOs to induce EMT and to disturb barrier integrity as a precursor of metastasis, using our bioelectronic platform.

Here, we used conventional biochemical techniques to show that cancer-derived cEXOs induce EMT-like behavior in non-tumorigenic breast epithelial cells. Signs of the generated EMT-like behavior includes changes in cell morphology, loss of apico-basal polarity, reorganization of cytoskeleton proteins like F-actin, decreased expression of E-cadherin, and increased expression in N-cadherin. An important feature of EMT process is the disorganization of cell junctions and the consequential loss of lateral cell-cell adhesion, which leads to increased motility and invasiveness, favoring a metastatic phenotype. In ongoing studies by our collaborators, organic electrochemical transistors (OECTs) based on PEDOT: PSS conductive polymer will be used to monitor the loss of the barrier integrity, as a sign if EMT, of the cell monolayer in real time. This electrical

monitor strategy will give us a complete insight into the cEXO-induced EMT with quantitative data and higher temporal resolution than the conventional methods used above. Additionally, immunofluorescence of barrier-forming adherent junction proteins and EMT markers will be performed on the OECTs to complement the electrical data and show the ability of this system to allow simultaneous electrical and optical monitoring of barrier integrity. This combination of optical and electrical measurements of cEXOs interactions with epithelial cell monolayers will provide essential information for developing new strategies to inhibit them. Thus, this innovative system offers the possibility to study novel ways to prevent cancer metastasis induced by cEXOs and to facilitate rapid and large-scale drug screening compared to conventional methods.

5.4. Experimental section

5.4.1. Cell Culture

Mammary non-tumorigenic epithelial cells (MCF-10A) were purchased from American Type Culture Collection, ATCC (Manassas, VA) and cultured in MEGMTM epithelial cell growth medium bulletKit from Lonza (Walkersville, MD) supplemented with 100 ng/mL cholera toxin, Sigma (St. Louis, MO) and 1% penicillin–streptomycin (P/S) Invitrogen, (Carlsbad, CA). Experiments were performed with cells between passages 1 and 8 received. To slow down cell proliferation during cEXOs treatment, MCF-10A cells were cultured on a growth medium in the absence of bovine pituitary extract (BPE, BPE-free medium), one of the growth supplements included in the MEGMTM bulletKit. MDA-MB-231 cells, highly metastatic human adenocarcinoma cells, were purchased from American Type Culture Collection, ATCC and maintained in Dulbecco′s Modified Eagle′s Medium, DMEM, Corning (Corning, NY) supplemented with 10% fetal bovine

serum (FBS) ThermoFisher (Waltham, MA) and 1% P/S, Invitrogen. For serum-free medium used for cEXOs isolation, MDA-MB-231 cells were maintained in DMEM medium supplemented with 1% P/S. Experiments were performed with cells between passages 1 and 8 after being received. All cell cultures were maintained at 37°C, 5% CO_2, and the media were changed every two to three days as recommended by manufacturers.

5.4.2. Isolation and characterization of cEXOs

Exosomes derived from MDA-MB-231 cells were isolated and characterized as previously established in chapter 3 and chapter 4.

5.4.3. Treatment of MCF-10A cells with cEXOs

MCF-10A cells were seeded on Millicell EZ-slides, Millipore (Burlington, MA), at a density of 68,000 cells/cm^2. As 90-95% confluency was reached, cells on 3 of the wells were fixed (initial time), and the other 3 wells undergo different treatments: 50-100 µg of cEXOs, 5-10 ng/mL TGFβ1, ThermoFisher Scientific (Waltham, MA), and a negative control well with no treatment, all in BPE-free medium. Media was changed and treatments were repeated every 12 h for 48, 60, and 96 h, and 7 days. Cells were fixed at the final time of the experiment and stored at 4°C for subsequent immunofluorescence (IF). For ELISA and western blot, the same procedure was followed, but cells were lysed and stored at -20° C until needed.

5.4.4. Cell fixation and lysis

For IF, MCF-10A cells were fixed with ice cold 99% acetone, Alfa Aesar (Haverhill, MA) at initial and final treatment time. Cells incubated at -20 °C for 5 min, followed by

washing 3X with phosphate-buffered saline, PBS (1.37 M NaCl, 27 mM KCl, 100 mM Na_2HPO_4, and 18 mM $KH_2PO_4$50 at pH 7.4) and stored in PBS at 4°C until needed. For western blot and ELISA, MCF-10A cells were lysed (at initial and final time of treatment) in ice-cold RIPA buffer (ThermoFisher Scientific) plus proteinase inhibitor cocktail, Pierce (Sigma), scraped using a pipette tip, collected, and stored at -80°C until needed. Lysed samples were thawed at 37 °C for one min, vortexed for 3 min, and centrifuged at 14,000 rpm for 5 min. Bicinchoninic acid assay (BCA) assay was done in all samples to determine protein concentration.

5.4.5. Bicinchoninic acid assay (BCA)

BCA assay was performed using a QuantiPro BCA Assay Kit (Sigma) and following the manufacturer protocol. BSA was used as a protein standard, PBS as a blank, and MCF10-A samples with varying treatments were used as unknown protein concentration samples. The assay was conducted in a Corning 96-well plate with a flat bottom (Sigma) using 150 µL of standard, blank, or unknown concentration samples and 150 µL of BCA working reagent in each well. Protein concentration was determined using a standard curve and the A_{562} obtained for each of the MCF-10A samples.

5.4.6. Immunofluorescence

Previously fixed MCF-10A were incubated in 1% bovine serum albumin, BSA (Sigma) in PBS for one hour at room temperature (RT) to block non-specific binding. Then, cells were incubated with 1:300 primary antibodies followed by incubation with 1:1000 secondary antibodies, at 37°C for one hour for each antibody. Samples on EZ-slides were mounted with SlowFade antifade mountant with DAPI (Life Technologies, Carlsbad,

CA) to preserve the fluorescent samples. Images were captured with a Zeiss Axio Observer Z1 LSM 710 confocal microscope.

5.4.7. Antibodies

For immunofluorescence, the following primary antibodies were used: E-cadherin (24E10) Rabbit monoclonal, (Cell Signaling, Danvers, MA); N-cadherin (13A9) Mouse monoclonal (Cell Signaling); Vimentin (D21H3) Rabbit monoclonal (Cell Signaling); α-SMA (MAB1420) Human/Mouse/Rat monoclonal (R&D Systems, Minneapolis, MN). Secondary antibodies: Donkey anti-Rabbit IgG (H+L) Alexa Fluor 488-conjugated antibody (Life Technologies) and Donkey Anti-Mouse IgG NorthernLights antibody (R&D Systems). For western blot, primary antibodies used include the ones used for IF and Actin, (AF4000), Sheep polyclonal (R&D Systems) antibody. Secondary antibodies: Donkey Anti-Sheep IgG HRP-conjugated antibody (R&D Systems); Goat Anti-IgG Mouse Polyclonal Antibody HRP-conjugated antibody (Rockland Immunochemicals, Pottstown, PA); and Donkey Anti-IgG Rabbit Polyclonal Antibody HRP-conjugated antibody (Rockland Immunochemicals).

5.4.8. Western blot

Equal volume (35 µL) and protein content of cell lysates from section 3.4 were mixed with NuPAGE LDS sample buffer and sample reducing agent (Life Technologies), loaded on a 4-12% Bis-Tris gel Bolt (Life Technologies), and transferred onto an immobilon-P PVDF-membrane (Sigma) at 20V constant. Membranes were blocked for an hour with 5% non-fat dry milk in TBST (tris-buffered saline and 0.1% Tween 20) at RT and incubated overnight and rocking at 4 ̊C with primary antibodies specific to the

target protein. After thorough washing with 1% non-fat dry milk in TBST, membranes were incubated with secondary antibody for one hour and rocking at room temperature. Membranes were imaged using a Western ECL detection kit (BioRad, Hercules, CA) on a ChemiDoc XRS (BioRad) imaging system. The concentrations for antibodies used were 1:1000 and 1: 2500 for primary and secondary, respectively.

5.4.9. Enzyme-linked immunosorbent assay (ELISA)

To investigate the expression of epithelial marker E-cadherin, and mesenchymal marker N-cadherin, in MCF-10A cells before and after treatment, ELISA assay was done for both proteins. Following the manufacturer's protocol, Human E-Cadherin and N-cadherin DuoSet ELISA kits (R&D Systems) were utilized to measure the concentration of both cadherins in MCF-10A lysates for 0 and 7 days of treatment. Absorbance at 450 nm, as recommended, was measured for all samples, and the concentration of both cadherins was found using the absorbance and concentration of the protein standards and the absorbance of the unknown concentration samples. E- and N-cadherin protein concentration present in MCF-10A lysates were normalized by the total protein concentration at each time point to reassure those values were not influenced by the amount of protein or number of cells in each condition.

5.4.10. Confocal microscopy

IF images were captured by confocal (LSM 710) inverted Zeiss Axio Observer. Z1 microscopes (Zeiss, Oberkochen, Germany) with α Plan-Apochromat objectives and an Andor SIM camera (Andor, Belfast, UK). A 63x oil immersion objective was used to capture the images.

5.4.11. Organic electrochemical transistor (OECT) fabrication

Fabrication of OECTs was done as previously reported[351, 352]. In brief, gold source and drain contacts were patterned on a previously cleaned glass slide (75 mm x 25 mm) using photolithography, followed by thermal evaporation and lift-off. The patterns were designed using Chrome mask and Mask Aligner. A S1813 photoresist, Kayaku Advanced Materials, Inc. (Westborough, MA), was spin-coated at 3000 rpm during 30 seconds on the glass, and microposit MF-26A was employed as a developer. Evaporation of 5 nm of chromium and 100 nm of gold was achieved followed by lifting-off the photoresist in an acetone bath in sonication for one hour, leaving only the gold source and drain contacts on the substrate. A PEDOT: PSS channel and a gate with dimensions (50 x 50 μm^2 x 460 nm thick) and (1 x 1 mm^2) respectively, were patterned by a perylene peel-off method previously described[353, 354]. The conducting polymer (CP) preparation consisted of: PEDOT: PSS, Heraeus, Clevios PH 1000 (Leverkusen, Germany) plus 0.25 mL of ethylene glycol (Sigma-Aldrich), 0.5 µL of 4-dodecylbenzenesulfonic acid (DBSA), and 10 mg of 3-glycidoxypropyltrimethoxysilane (GOPS), for each ml of PEDOT:PSS. After CP deposition, the device was baked at 140 °C for one hour under atmospheric conditions. The cell growth area was defined by polydimethylsiloxane (PDMS) wells of 0.9 cm diameter and 0.64 cm^2 area.

5.4.12. OECT operation

Experiments were performed at 37 °C, 5% CO_2 in an XL multi-SI humidified incubator, PeCon GmbH (Erbach, Germany), mounted on a Axio Observer Z. microscope, Carl Zeiss (Oberkochen, Germany). The following parameters were used for experiments: V_{DS} = −0.2 V, V_{GS} = 0.3 V, V_{GS} on time = 2 s, off time = 28 s. All

experiments were done with voltages under 0.5 V to avoid cell membrane damaging previously associated with higher ones. OECT data was acquired using a 2612 Source Meter SMU, Keithley (Cleveland, OH) and customized LabView software.

5.5. Results and discussion

Overview: Cancer-derived exosomes, cEXOs, are recognized as molecular vehicles that carry messages from tumor and transformed cells to healthy ones and are thought to deliver signals to induce EMT in healthy endothelial cells[78]. It has been previously shown that intensive treatment, every 3 hours of mammary epithelial cells with extracellular vesicles from the plasma of women with breast cancer promotes transient EMT-like behavior[355]. As previously established, we aim to monitor the effect of breast cancer cEXOs on MCF-10A (mammary non-tumorigenic epithelial cells) barrier integrity as a sign of EMT induction using OECTs. However, first, we focused on elucidating the ability of cEXOs to induce EMT-like behavior in MCF-10A cells using conventional techniques like western blot, ELISA, and immunofluorescence, followed by electrical monitoring.

5.5.1. Breast cancer-derived cEXOs lead to morphology changes in MCF-10A cells

cEXOs were isolated from MDA-MB-231, highly metastatic adenocarcinoma breast cancer cells, as previously done and presented in chapter 3. Size, Zeta potential, particle concentration, total protein concentration, and proteomic characterization of cEXOs is found in chapter 4.

It is known that as non-tumorous breast epithelial cells, MCF-10A, reach high confluency, they acquired a cobblestone epithelial morphology, apicobasal polarity, and

are bound via cell-cell junctions forming an impermeable barrier[356, 357]. As MCF-10As reached this stage and formed a homogenous monolayer, they were treated with various cEXOs dosages for different periods of time to obtain the optimal conditions to induce EMT. Two control conditions were also implemented, a negative one, consisting of cells with no treatment; and a positive control where cells undergo treatment with 5 ng/mL transforming growth factor beta, TGFβ, to also induce EMT. The TGFβ signaling pathway is a key player in EMT process and commonly used to induce EMT in epithelial cells in culture[358, 359]. Figure 5.1 schematized the changes that cells undergo during EMT process, expected to be triggered by cEXOs and TGFβ treatment of MCF-10A cells.

Initially, to assess the ability of cEXOs to trigger morphology changes in MCF-10A monolayer, cells were treated with cEXOs and TGFβ (100 μg and 5 ng/mL, respectively) every 24 hours for 6 days and Figure 5.2 displays images captured on day 7, 24 hours after the last treatment. Cells under no treatment (left panel) conserve the cobblestone morphology and organized F-actin cytoskeleton characteristic of healthy epithelial cells observed in Figure 5.1a. Cells under treatment with cEXOs (middle panel) exhibit a less organized cobblestone morphology with loss of apico-basal polarity and a disorganized cytoskeleton characteristic of cells undergoing mesenchymal transition as

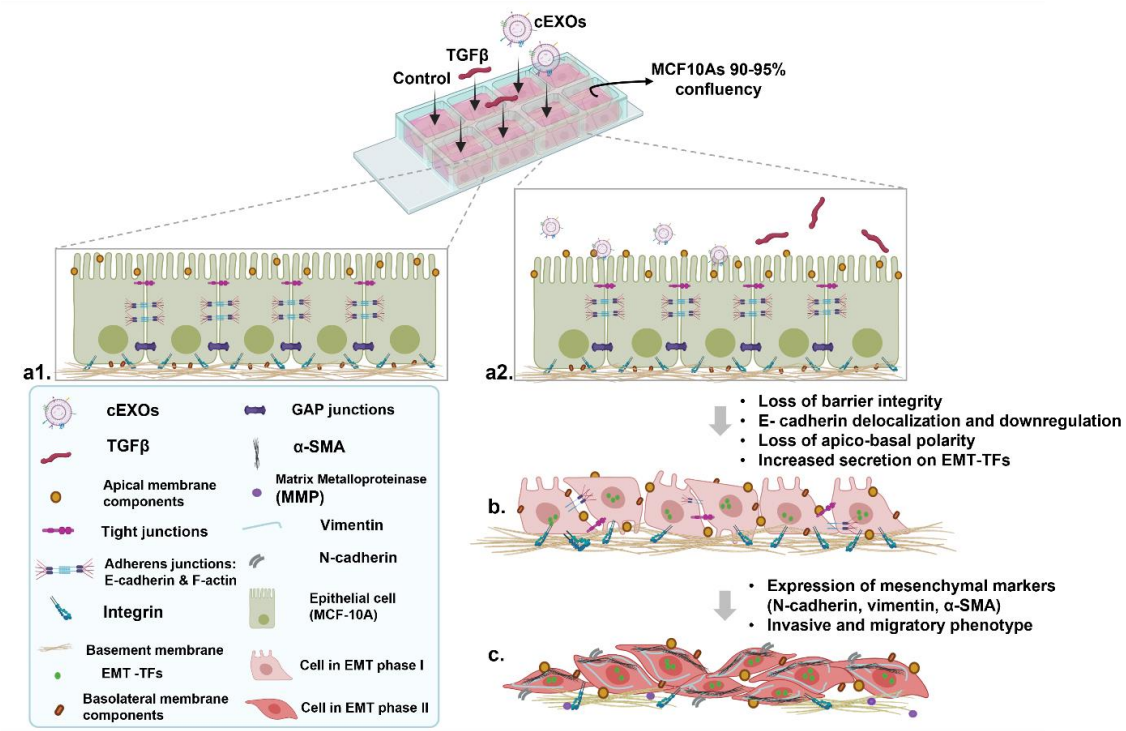

Figure 5.1. Changes in morphology, epithelial, and mesenchymal markers in epithelial monolayer undergoing EMT induced by cEXOs treatment. a) Polarized epithelial cells joined by tight, GAP, and adherens junctions, involving E-cadherin and F-actin, forming a homogeneous monolayer. b) after cEXOs and/or TGFβ stimuli, cells secrete higher levels of EMT-associated transcription factors (EMT-TFs) causing disorganization of cell junctions with lower E-cadherin expression resulting in loss of apico-basal polarity and barrier integrity. c) Further stimulation leads to disorganization of the cytoskeleton, expression of mesenchymal markers such as vimentin, α-SMA, N-cadherin, and secretion of matrix metalloproteinases (MMPs) leading to dissolution of basement membrane extracellular matrix resulting in cell transformation to an invasive and migratory phenotype. *Created with BioRender.com* and adapted from Vaquero et al.[360]

seen in Figure 5.1b and 5.1c. Moreover, cells treated with TGFβ (right panel) reveal morphology changes similar to the cEXOs-treated counterparts but with less pronounced changes possibly caused by treatment with low concentration of TGFβ. As morphology changes were observed in cells treated with cEXOs, changes in epithelial and mesenchymal standard markers, E- and N-cadherin induced by cEXOs treatment were investigated using a variety of conventional biochemical methods.

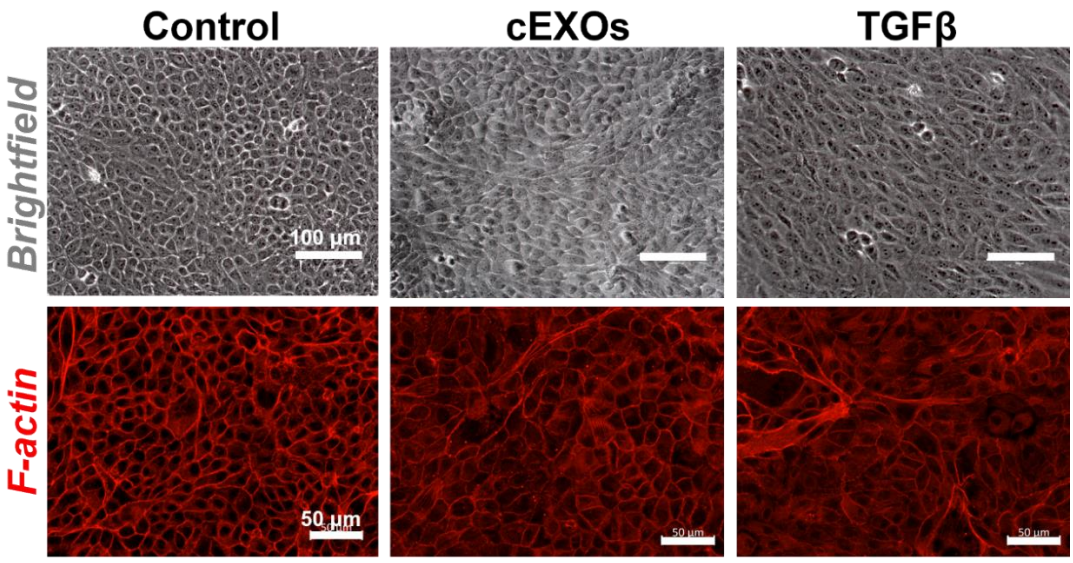

Figure 5.2. Morphology changes in MCF-10A treated with cEXOs. Images of MCF-10A cells with no treatment, treated with 100 µg of cEXOs, and with TGFβ on day 7 of treatment; left, middle, and right panel, respectively. Top row displays brightfield images and bottom row, F-actin images of two different areas for each condition. Note cobblestone morphology on cells in control condition, and loss of polarity and acquisition of mesenchymal-like morphology and disorganized cytoskeleton (F-actin) on cells under cEXOs and TGFβ treatment.

5.5.2. Breast cancer-derived cEXOs induce EMT-like behavior in MCF-10A cells

MCF-10A cells forming a monolayer were treated with 50 µg of cEXOs and 5 ng/mL TGFβ every 24 hours for 6 days followed by E-cadherin and N-cadherin immunostaining, as epithelial and mesenchymal markers, respectively. Figure 5.3a top row shows reduced E-cadherin expression, labeled in green, on cells treated with cEXOs and TGFβ (middle and right panel) compared to no-treated cells (left panel). Besides intensity, the localization of E-cadherin also differs among the conditions. Control cells show the typical localization of E-cadherin in adherents junctions around the cells forming a honeycomb pattern,[361] but it is delocalized in cells treated with TGFβ and cEXOs. This behavior is expected in cells undergoing mesenchymal transformation as decrease in cell junction organization is one of its main characteristics[362]. Moreover,

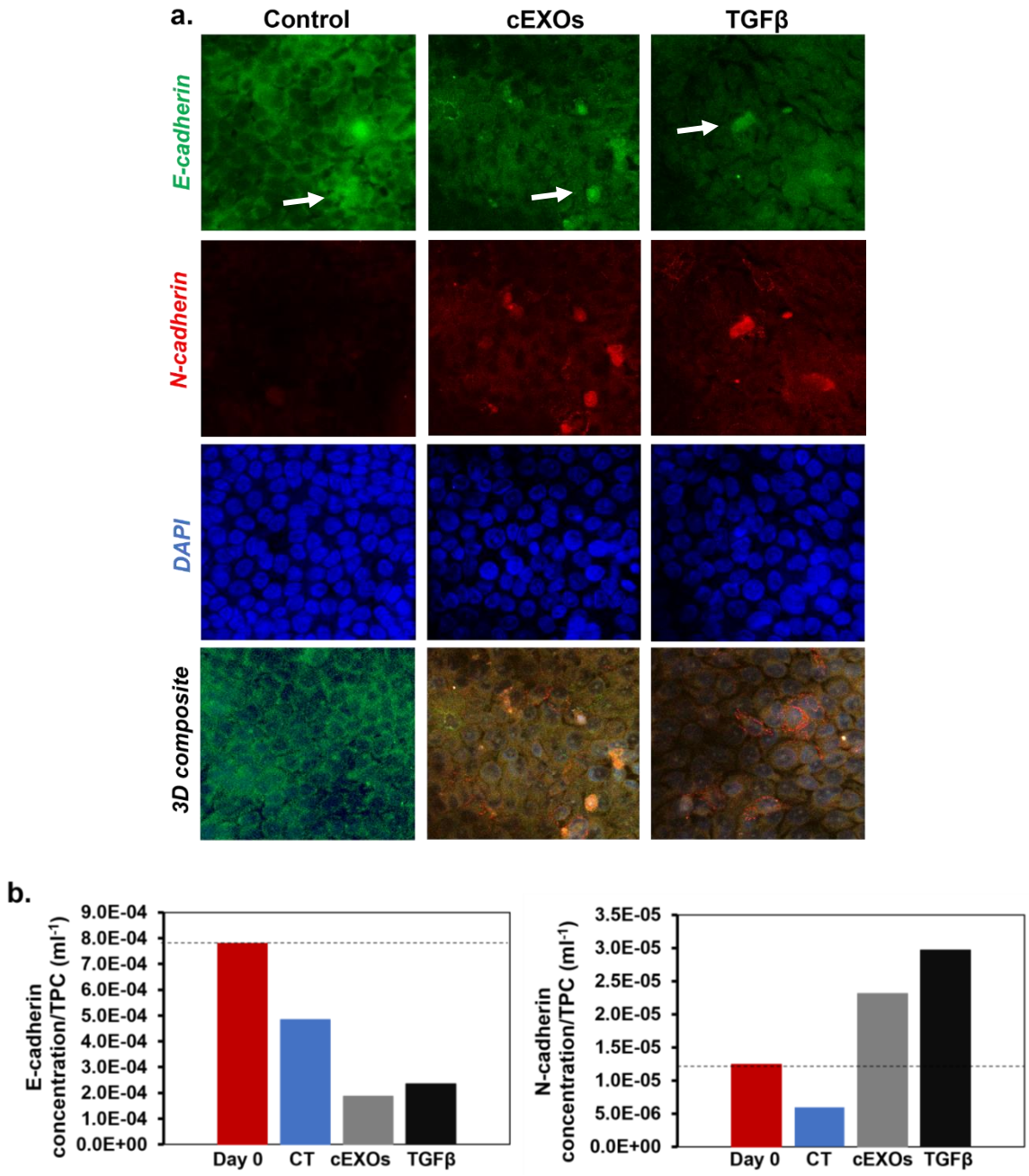

Figure 5.3. EMT markers in MCF10A cells treated with cEXOs for 7 days. a) Immunofluorescence of E-cadherin (green), N-cadherin (red), and nuclei (blue), and integration of all in a 3D composite on MCF-10A monolayer with no treatment (left column), treated with 100 μg of cEXOs (middle column), or with 5 ng/mL TGFβ (right column) every 24 hours for 7 days. White arrows indicate dome-like structures formed by cells at high confluency. b) ELISA quantitation of E-cadherin (left) and N-cadherin (right) in MCF-10A cells on day 7 of treatment. Dashed line indicates initial concentration. CT: control (non-treated MCF-10A cells).

images in the second row of Figure 5.3a show higher expression of N-cadherin on cells treated with cEXOs and TGFβ compared to no-treated cells. N-cadherin, a hallmark of EMT, is expressed around the membrane of mesenchymal and transformed cells[363], as seen in cEXOs- and TGFβ- treated cells. Lastly, images of the cell nuclei in the third row show a reduced number of nuclei in cEXOs -treated cells compared to the other two conditions. We hypothesize that treatment with cEXOs resulted in increased cell proliferation, as seen in other epithelial cells[364], leading to cell over confluency and subsequent detachment of some cells from the substrate. Moreover, in all three conditions, cells still formed dome-like structures, indicated by white arrows, characteristic of breast epithelial cells with high confluency. Lastly, images in the bottom row show 3D composites integrating E-cadherin, N-cadherin, and DAPI in all treatment conditions. Note that control cells show a cobblestone morphology with high expression of E-cadherin and none of N-cadherin. On the other side cells treated with cEXOs and TGFβ loss some of that epithelial morphology and the expression of E-cadherin and acquired N-cadherin expressed around cell adhesions.

To further test the expression of EMT markers, ELISA assays specific to E- and N-cadherin were done in cell lysates to detect proteins present in cell-cell adhesions. Figure 5.3b shows the concentration of both cadherins in cells before and after treatment with initial concentrations (day 0), marked with a dashed line, used as a baseline to compare to values after treatment. In the left graph, it can be observed that E-cadherin concentration decreases in all cells after treatment with the lowest concentration exhibited by cells treated with cEXOs followed by those treated with TGFβ. On the other side N-cadherin concentration increases in cells treated with cEXOs or with TGFβ. These results

align with the results shown in Figure 5.3a suggested that cEXOs induce EMT-like behavior in MCF-10A cells by reduced expression and disorganized localization of E-cadherin and increased expression of N-cadherin in cells treated with cEXOs. The unexpected decrease of both cadherins by control cells after treatment could be possibly due to the high confluency that cells reach at day 7 after treatment suggesting shorter treatment times for future experiments.

Previous evidence indicates that stimulus with physiological relevant concentrations (30 μg) of cEXOs for 9 hours induce a transient EMT-like behavior in MCF-10A cells[355]. With this in mind, several conditions were screened to induce permanent EMT-behavior in MCF-10A cells using more physiologically relevant cEXOs concentrations, shorter periods of treatment time, and lower initial cell confluency.

Several conditions were altered to optimize the experiment to induce EMT-like behavior in MCF-10A via cEXOs. Physiologically relevant conditions were implemented, including a lower concentration of cEXOs (50 μg), a higher concentration of TGFβ (10 ng/mL), around 85% confluency at day 0, and a cEXOs administration in 12 hours intervals for 60 hours. Figure 5.4 shows that under these conditions, a more homogenous monolayer without dome-like structures is achieved for all conditions with a higher number of cells treated with cEXOs and TGFβ.

Increased cell proliferation has been previously observed in cells treated with cEXOs as seen in chapter 3 and 4. E-cadherin (green) expression in cells treated with cEXOs or TGFβ is lower and less localized at the cell borders than in non-treated cells, as expected. In the case of N-cadherin (red), its expression is notably higher in cells treated with cEXOs or TGFβ than in control cells, and it is localized to the cell membrane

as expected and seen in Figure 5.3a. Together, these results suggest that treatment with cEXOs every 12 hours for 60 hours induces EMT-like behavior in MCF-10A cells indicated by a low and disorganized E-cadherin localization and high expression of N-cadherin around cell membranes.

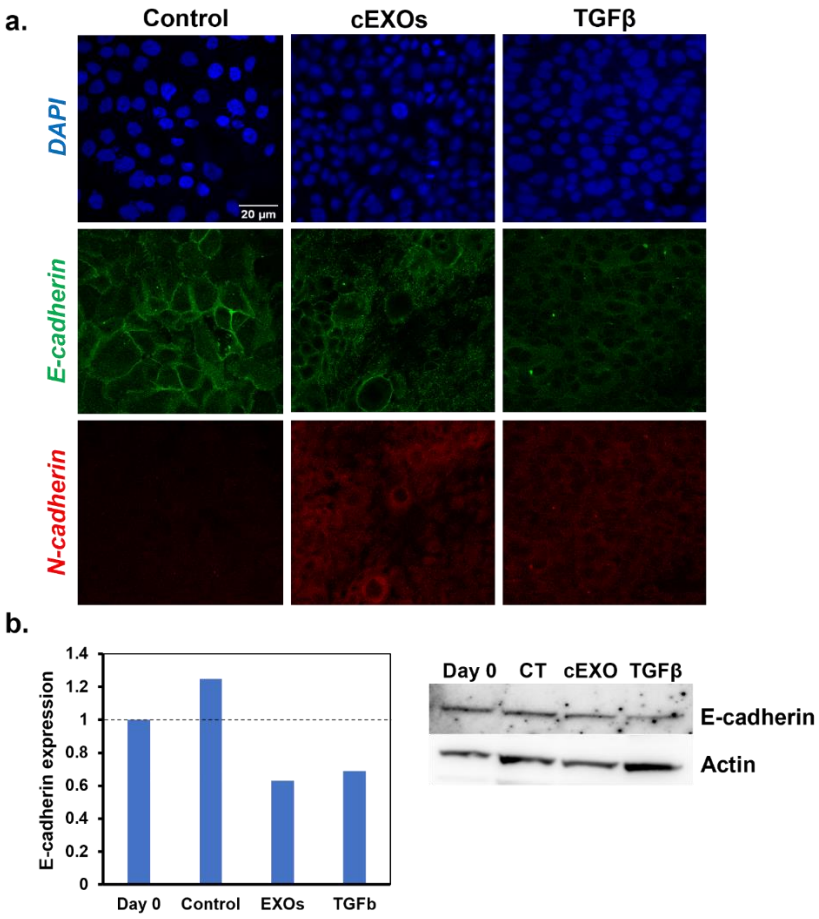

Figure 5.4. EMT markers in MCF10A cells treated with cEXOs for 60 hours. Immunofluorescence of E-cadherin (green), N-cadherin (red), and nuclei (blue) on MCF-10A monolayer with no treatment (left column), treated with 50 μg of cEXOs (middle column), or with 10 ng/mL TGFβ (right column) every 12 hours for 60 hours.

5.5.3. Organic electrochemical transistors (OECTs) to monitor cell barrier integrity

Epithelial cells form layers that naturally work as protective barriers by strictly controlling the flux of ions between cells. Tight junctions, cell-cell adhesions, regulate the ion flow between cells and their malfunctioning or deterioration is associated to

several disease states including cancer. The EMT process is characterized by the loss of tight junctions leading to a "leaky" cell barrier allowing the uncontrolled passage of ions. Electrical measurement of the epithelial cell layers electrical resistance (transepithelial resistance) is commonly used as a strategy to monitor tight junctions and epithelial barrier. Organic electrochemical transistors (OECTs) have been previously used for dual monitoring, optical and electrical, of epithelial barrier formation and integrity[352, 365, 366].

In the previous sections, we showed that MCF-10A cells treated with cEXOs for seven days, displayed an EMT-like behavior indicated by changes in morphology, loss of E-cadherin and gain of N-cadherin, via conventional biochemical methods like IF, ELISA, and western blot. Here, we will use OECTs to measure the transepithelial resistance of MCF-10A layer before and during cEXOs treatment to monitor the barrier integrity over time, as a measure of EMT. We hypothesize the ability of this system to detect disruption of barrier integrity, as a sign of EMT, sooner than IF as previously reported with the detection of nephrotoxicity due to cistplain[350]. To do so, OECTs were fabricated and operated as previously reported[365] and explained in the experimental section. The device consists of three terminals including two gold/Au (to improve the contact measurement) electrodes, source and drain, and a conducting polymer (PEDOT: PS) channel in between (Figure 5.5). Two polymer layers, a vapor deposited parylene C layer, to insulate the contacts and interconnects, and a PEDOT: PSS layer, were patterned at the same time by a peel-off process. In addition, a PDMS well was fixed on the device (Figure 5.5a) to enclose the seeded cells and cell growth medium.

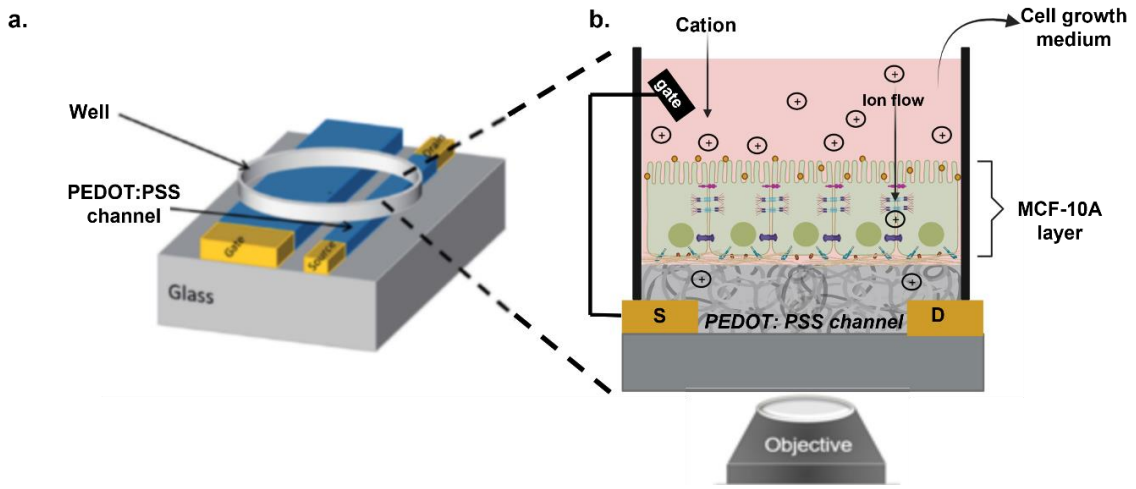

Figure 5.5. Schematic of OECT biosensor. a) The device consists of a PEDOT:PSS channel, gold source (S) and drain (D) electrodes, and a PEDOT:PSS gate patterned on a glass substrate. The MCF-10A cells cultured on the device along their growth medium are constrained by a PDMS well. b) Gate voltage is applied to the system causing flow of cations from the media, through the cell layer, into the PEDOT:PSS channel. This system allows simultaneous optical and electrical monitoring of cell layer integrity[365]. *Created with BioRender.com*.

Briefly, operation of OECTs involves application of a positive pulse voltage from the gate to the source electrode and the cell layer, acting as an ion flow barrier, reduces the passage of cations from the cell medium to the PEDOT:PSS channel (Figure 5.5b). That blockage of cations flow leads to slow dedoping of the channel and modifications in its current. The measurement of the PEDOT:PSS channel-current during this process is fitted to a gate square pulse to find a time constant (τ), which reveals the ability of the cell layer to block the flow of cations into the channel and quantifies the quality/integrity of the cell barrier. A healthy epithelial cell layer with intact tight junctions will cause a long time to dedope the PEDOT:PSS channel with cations, resulting in a large τ value. However, a small τ value is expected from an unhealthy and leaky cell barrier with loss of tight junctions, characteristic of cells that undergo EMT.

5.5.4. cEXOs induce loss of barrier integrity, as a marker of EMT, in MCF-10A cells

MCF-10A cells were seeded and attached to OECTs as shown in Figure 5.6a, day

0. As ~90% confluency was reached and a monolayer was formed (day 3), the cells were treated with 100 µg of cEXOs every other day for 7 days. Brightfield image in Figure 5.6a at the end of the experiment (day 10) shows a cell layer covering the surface of the device with absence of the cobblestone morphology, characteristics of epithelial cells. A positive pulse voltage of V_{GS} = 0.3 V was applied between the gate and the source and measurements of the transconductance, or modifications in the PEDOT:PSS channel current, were recorded and used to find the time constant, τ, for every time point. Figure 5.6b shows that τ increases from day 0 to 3 as expected since the cells are growing to confluency and starting to form a layer; as the layer forms (closer to day 3), τ is higher suggesting the formation of a tight layer and the slow dedoping of the channel.

cEXOs treatment begins on day 3 as the cells formed a monolayer and τ is at its highest point and mostly stable until day 6, indicating reduced cation flow through the cell layer leading to slow dedoping of the channel and indicating good barrier integrity. As EXOs treatment progresses, there is a notable decrease in τ value from day 6 to day 9 indicating faster dedoping of the channel and poor barrier integrity, characteristic of cells under EMT. These results suggest that cEXOs induce loss of barrier integrity in MCF-10A cells monolayers, a sign of EMT, and it is detectable at least 4 days after the beginning of treatment. *However, the validation of these results remains to be tested with experiment replicates and inclusion of positive and negative controls. This is just an initial preliminary set of data that shows early detection of changes in barrier integrity in MCF-10A treated with cEXOs, in a label-free manner.*

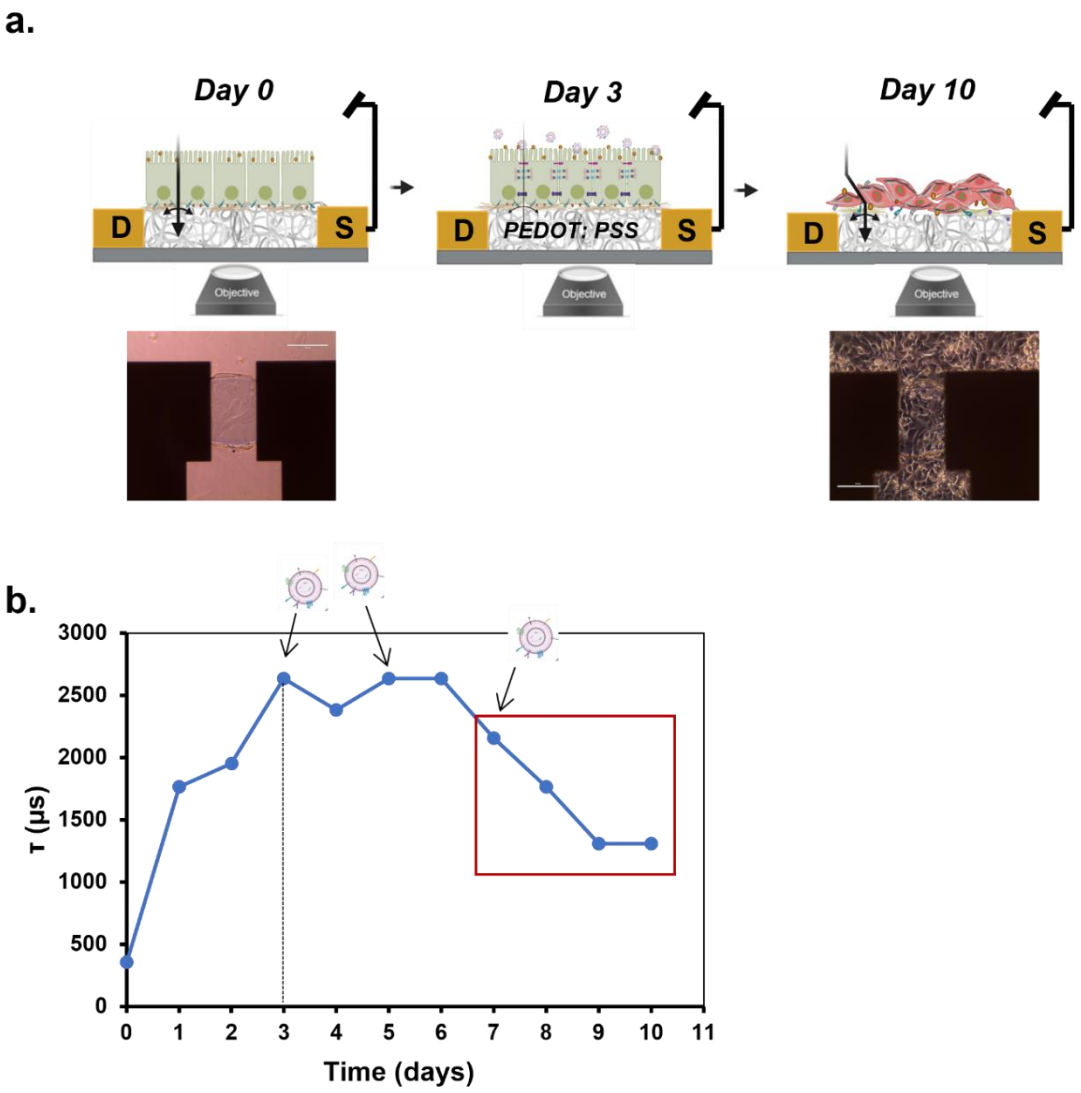

Figure 5.6. Electrical detection of decrease in barrier integrity of MCF-10A cells treated with cEXOs. a) schematic of electrical monitoring of MCF-10A cells forming a layer (day 0), in a tight layer with high barrier quality and at the beginning of treatment with cEXOs (day 3) and after 7 days of treatment, low barrier integrity and expected EMT (day 10). Brightfield images of cells on the device on day 0 and 10. *Created with BioRender.com*. b) time constant τ values derived from transconductance measurements indicating an increase in barrier integrity from day 0 to 3 as the monolayer forms, stable barrier integrity from day 3 to 6 with the beginning of cEXOs addition and decrease in barrier integrity starting from day 6 to day 9, at day 3-6 of cEXOs treatment.

5.6. Conclusions and future work

These preliminary results suggest that it is possible to induce an EMT-like behavior in non-tumorous breast epithelial cells, MCF-10A, with low concentrations and periodic applications of cEXOs derived from breast cancer cells, MD1-MB-231.

However, to confirm this, more experiments will be performed using different treatment times and more mesenchymal markers including smooth muscle actin, α-SMA, and vimentin. These EMT- associated changes including changes in cell morphology, f-actin reorganization, loss of endothelial and gain of mesenchymal markers, E-cadherin, and N-cadherin respectively, were detected using conventional methods like immunofluorescence, ELISA, and western blot.

Simultaneously, our collaborators at Cambridge University are working with the same cell system forming monolayers on the OECTs to electrically monitor tight junction (TJ) integrity to determine when TJ disruption happens, as a sign of loss of barrier integrity and EMT. Once the time at which TJ disruption takes place is known, EMT markers characterization will be repeated by IF, western blot, and ELISA. Those results will allow a comparation of both systems at the same time and treatment conditions and asses if the electrical system, using OECTs, can detect EMT-associated changes at faster times, which we expect based on previous evidence[350]. Lastly, since the OECTs are based on PEDOT: PSS, a low impedance and clear polymer, it will allow the recording of electrical characteristics of the cell monolayer while simultaneously collecting optical images of the monolayer in time-lapse mode. Therefore, this system facilitates precise correlation between the function and integrity of the cell monolayer (electrical characteristics) and the morphology of the cells forming the monolayer (optical characteristics).

CHAPTER 6

6. CONCLUSIONS AND OUTLOOK

Both subsets of cancer derived EVs, MVs and EXOs, have been recognize as modulators of communication between cancer cells and cells at the TME and at distal sites[66, 117, 272]. Evidence shows that transfer of information between cells, facilitated by EVs, leads to changes in recipient cells favoring tumorigenesis and cancer progression[3, 6, 78, 367]. Several aspects are involved in the exchange of EVs- associated oncogenic information between cells and understanding them is essential to develop strategies to hold back cancer progression influenced by EVs. For instance, several groups have examined the biogenesis and composition of EVs[1, 368], transfer of EVs[275, 296] and information between cells[74, 369], as well as the outcomes of EVs-cell interactions[10, 75, 370]. However, just a few studies have investigated the specific interactions between specific EVs-cell pairs[8, 115, 349]. This has created absence of information in an essential aspect of EVs-facilitated intercellular communication, how do EVs interact with the surface of the recipient cell to deliver their signals or cargo? Surface interactions are the first step at which EVs begin to influence the cell and its microenvironment[115]. Therefore, understanding them, the mediating factors, and finding strategies to stop them and subsequently, their malignant outcomes are strategies with great therapeutic value.

This information gap is partially due to the lack of tools to facilitate the study of EV-cell interactions including EVs binding to recipient cell and route for information delivery. To fulfill this need, this thesis work offers two biomimetic membrane models as tools to simplify the study of surface interactions between EVs and cells. Particularly, these systems facilitate the investigation of surface interactions between breast cancer

cells (MDA-MB-231) derived EVs and human primary ADSCs. However, their application is not limited to studying this EV-stromal cell pair since their versatility allows them to be tuned to investigate surface interactions for different types of EVs and cells. We chose to study ADSCs because they are important cell type in the TME and favor cancer progression by modulating angiogenesis, through secretion of growth factors and differentiating to new vasculature-forming cell types that promote tumor proliferation, like fibroblasts and myofibroblasts[6, 7, 41-43]. Additionally, MDA-MB-231 derived EVs have shown to further favor their contribution to disease progression by inducing ADSCs proangiogenic potential, indicated by upregulation of VEGF, and differentiation to pro-angiogenic and pro-invasive myofibroblasts[4-6]. The biogenesis[371, 372] and characteristics of this type of EVs[373] and their influence in ADSCs have been previously studied, yet the surface interactions leading to those outcomes and the strategies to stop them remain unknown. Towards that end, chapter 3 and 4 described a biomimetic EV and a ADSC membrane model, respectively, to investigate surface interactions between EVs and ADSCs. Our models are hybrid SLBs, which are the standard membrane system introduced in chapter 2 with incorporated membrane native components.

First, using the standard gold technique for EVs isolation, differential ultracentrifugation (dUC), effective isolation of EVs from breast cancer MDA-MB-231 cells was achieved. Differences in characterization aspects including size, appearance, and proteins specific to each EV subtype, indicated successful isolation of two different subpopulations, EXOs and MVs. A complete characterization of MVs and EXOs was done agreeing with the MISEV (Minimal Information for Studies of Extracellular

Vesicles) guidelines for EVs published work. Additionally, in the case of EXOs, a complete proteomics analysis is offered in this body of work, allowing further investigation of this EV subpopulation.

In the first part of this work, I offered the EVSB platform to offer the EVs surface components, solely, to ADSCs, facilitate interactions at that biointerface, and investigate their biological outcomes. EVs, EXOs and MVs, separately, ruptured upon interaction with PEGylated liposomes, successfully forming EXOs- and MVs-EVSBs. These EVSBs make good biomimetic *in vitro* models of EVs membrane since they preserve some of its natural features, including native components and its characteristic lateral fluidity; but did not retain any EVs cargo. Moreover, ADSCs were successfully cultured on the EVSBs; and using them as EVs membrane models, we showed that interactions between ADSCs and EVs surface led to enhanced cell adhesion and spreading, proliferation, viability, and proangiogenic potential, indicated by upregulated VEGF secretion, but did not induce myofibroblast differentiation. Most likely, myofibroblast differentiation is attributed to EVs cargo, but it remains to be tested. Due to the presence of membrane components and absence of EVs cargo in our EVSBs, we suggest that the biological outcomes observed in ADSCs were induced merely by EVs surface constituents and not by internal components. This observation indicates that as expected, our EVSB system allows the isolation of EVs surface interactions from others. Furthermore, the stronger enhancement of ADSCs adhesion, spreading, and VEGF upregulation by MVs-EVSB membrane compared to EXOs-EVSB is possibly due to their difference in size, and so in content/ surface area in the EVSBs.

The EVSB system presented here offers several advantages including i) the

exclusive decoupling of EVs surface components, ii) its tunability to be made from different type of EVs and to investigate their surface composition and/or their interactions with different types of cells, and iii) their planar geometry and versatility to be used with different characterization tools including TIRFM, FRAP, QCM-D, AFM, among others. Additionally, the development of EVSBs requires a low concentration of EVs compared to the amount needed for commonly done periodic treatments of cells with EVs for several days, which often requires the use of several EVs batches. This is a huge advantage given that isolation of EVs is a tedious and extensive process, sometimes challenging, with a final low yield of EVs. Furthermore, the adhesion and growth of ADSCs on EVSBs further corroborates the presence of EVs membrane components that mediate cell adhesion on the biomimetic membrane model, that otherwise is not favorable on standard SLBs. Therefore, our system makes one more strategy, along those in chapter 2, to modify SLBs composition and so, their nonfouling nature for their application as cell culture platforms. In fact, our EVSB model is the first EVs-derived SLB developed and used as a cell culture system[9].

To further investigate the specific interactions happening at the ADSCs plasma membrane interface with EVs, I offered the ASB system to facilitate the study of EVs binding, as the initial step for EVs to influence ADSCs and their microenvironment. The ASB showed preservation of lateral fluidity and integrin β1, native components of ADSCs plasma membrane, making a suitable biomimetic model of it. This model allowed the isolation of EVs (MVs and EXOs) binding, from EVs uptake, to ADSCs and its optical detection and real time monitoring and quantification using TIRFM. Particularly, the ASB-MEA system introduced in chapter 4, facilitated label-free electrical monitoring

of EXOs binding to ADSCs. Moreover, optical and electrical readouts showed that blocking integrin β1/CD29, in the ASB, using an anti-CD29 Ab led a significant decrease of EXOs binding to ASB. Analogously, the same strategy to block integrin β1 in live ADSCs, resulted in a slight increase in ADSCs proliferation and VEGF secretion, otherwise highly upregulated upon treatment with EXOs. Therefore, these results indicate that integrin β1 plays an important role in EVs binding to ADSCs and that CD29Ab is a potential strategy/ therapeutic to reduce it along its biological consequences. Although EXOs binding to ADSCs and its outcomes were significantly reduced using CD29Ab, some remaining binding was still observed, which suggests the participation of other proteins/ molecules in this interaction. Appendix 1, as a complement to chapter 4, explored the potential participation of HSPGs in EVs-ADSCs binding. It further corroborated the ability to recapitulate and optically monitor not just EXOs, but also MVs binding to ADSCs using the ASB system. Likewise, using the ASB as a drug-screening tool, heparin was found to successfully decrease MVs and EXOs binding to ADSCs. Likewise, treatment of live ADSCs with heparin resulted in no significant increase in VEGF secretion and cell proliferation upon interactions with EXOs, whereas cells in the absence of heparin showed upregulation of both processes. We hypothesize that heparin, as a free HS, interacted with EXOs and MVs blocking their subsequent interactions with ADSCs. Therefore, these results indicate that HSPGs along integrin β1 play mediating roles in EVs binding to ADSCs and that heparin and CD29Ab are two strategies with therapeutic value to decrease EVs binding, VEGF upregulation and cell proliferation in ADSCs. Together these outcomes indicate the drug-screening value of our ASB and ASB-MEA systems as tools to screen potential therapeutics to block EVs binding to cells

and decrease its associated malignant effects[11].

The ASB system presented here offers several advantages over the conventional techniques available to study EVs binding to cells like immunofluorescence[341] and optical tweezers[8]. The ASB is free from the dynamism of cells and several studies can be done with one batch of ADSCs, which are human primary stem cells and so, are not easily found and usually costly, very sensitive, and have a short number of passages before they lose their stemness. In addition, the composition of the ASB can be adjusted to using blebs from any type of mammalian cell to work as its biomimetic membrane model and to facilitate the study of EVs, from any type of cancer or disease advanced by EVs, binding to the desired cell. Lastly, the ASB offers the possibility to use several characterization tools to monitor EVs binding to cells including optical and label-free, electrical techniques.

To further examine the contributions of EVs to tumorigenesis and metastasis, we investigated the role of breast cancer derived EXOs on breast epithelial cells (MCF-10A). Treatment of epithelial cells with EXOs led to f-actin reorganization, decrease and delocalization of the epithelial protein E-cadherin, and the gain of the mesenchymal marker N-cadherin. These results indicate that EXOs induced EMT-like, a hallmark of cancer, behavior in breast epithelial cells, further corroborating the favoring role of EXOs in cancer progression. Using conventional techniques for EMT detection, ELISA, western blot, and immunofluorescence, those EMT associated changes with observed in epithelial cells after periodic treatments with EXOs for 60 hours. Future work in this project includes electrical monitoring of epithelial cells, periodically treated with EXOs, barrier integrity using OECTs. Loss of tight junctions and barrier integrity in epithelial cells is a

marker of EMT. Therefore, the time at which significant decrease of barrier integrity is sensed by electrical readouts suggests the time at which EMT is detected in epithelial cells. Using that stated time, EMT-like signs will be evaluated by conventional techniques to compare the detection of epithelial transformation using conventional vs. electrical means at the same time point. Based on previous research, we expect the electrical system to capture cell changes prior to conventional methods, showing then the potential of this PEDOT: PSS-OECT platform for early and label-free detection of EMT induced by breast cancer EXOs. Additionally, due to its transparency, this electrical platform also offers the option for simultaneous monitoring of EMT by optical and electrical means. Another possible avenue of research using this electrical system is the integration of an EXOs-EVSB (derived from any type of cancer EXO) with the PEDOT: PSS-OECT system as a cell culture platform for epithelial cells to electrically monitor the barrier integrity of the epithelial cell-monolayer as it is in constant interaction with EXOs surface. This will reduce the need for periodic EXOs dosage and potentially facilitate the detection of EMT-associated loss of barrier integrity induced by cancer EXOs, using any cancer EXOs-epithelial cell pair. In the same manner, using the same approach to make the ASB model, a biomimetic MCF-10A membrane model could be developed to identify the membrane components of MCF-10A facilitating EXOs binding and to investigate strategies to block it and the subsequent mesenchymal transition.

Although the results presented in this body of work contribute important insights for the understanding and study of EVs and ADSCs surface interactions, several aspects remain to be investigated, which open diverse avenues for research in the field. For instance, our EVSB system, as an *in vitro* model of EVs membrane has several

applications as a drug-screening tool. It will facilitate the investigation on the effect that existent chemotherapeutic agents have on the membrane of EVs and on the outcomes of interactions between cells and EVs. Analogously, it will aid to investigate the role that EVs membrane components play in drug resistance observed in several types of cancer derived EVs[374]. Besides favoring the study of existent chemotherapies, the development of new strategies with therapeutic potential to disarm EVs or to interrupt their surface interactions with cells, will be highly benefited by the EVSB model as a screening tool. Moreover, our EVSB could be used as a cell culture platform for different applications. For example, clinical evidence indicate that bone, lung, and liver are the most common sites for breast cancer metastasis[375-377]. Therefore, the use of EVSBs as cell culture platforms for bone, lung, and liver derived cells, will advance the understanding on the role that breast cancer EVs surface plays in cell behavior and subsequently, in metastasis. The versatility of the EVSB allows the composition to be modified for any other type of EV of interest. Therefore, this model is not limited to breast cancer but it allows the study of EVs surface influence in cell behavior for any type of cancer or disease advanced by EVs communication with cells, such as cardiovascular and metabolic [16], and neurodegenerative diseases [35]. Another research scenario is to explore and block the interactions of a particular EVs membrane protein with a desired type of cell. In this case, transfection of EVs generating cell leading to overexpression of the membrane protein in the cell, will result in overexpression of it in the EVSB as well, enabling a deeper investigation on the role of a specific EV membrane component on disease progression. Towards that end, the EXOs proteomic analysis offered in this work facilitates the identification of EXOs membrane components involved in particular diseases, and

biological and cellular pathways. Lastly, the study done with EVSB indicated the outcomes of the interactions between ADSCs and EVs surface, specifically. Therefore, the outcomes attributed to EVs cargo (possibly myofibroblast differentiation), and the mechanisms and places within the cell for cargo delivery are still unknown. Investigating these aspects will further contribute to the understanding of breast cancer progression favored by EVs and ADSCs communication and to further develop more target strategies to disable it.

Equivalently, the ASB system is not restricted to monitoring binding/blocking of EVs to ADSCs. Offering the same flexibility as the EVSB, this model can incorporate native material of different types of mammalian cell membrane and work as its *in vitro* model. This allows the monitoring, with the option to be label-free of binding and screening of binding blocking strategies for any EV- cell pair. The scope of this thesis was to offer a platform to facilitate the study of EVs-ADSCs binding and potential strategies to block it. Therefore, we were able to recapitulate binding, to monitor it optically and electrically, and to screen potential strategies to block it. However, we did not investigate EVs binding kinetics, but rather offered a system to do it as future work. We hypothesize that as investigating virus binding kinetics is essential for the discovery of novel receptors and development of vaccines[378], understanding EVs binding and fusion kinetics is imperative for the development of chemotherapies to inhibit EVs binding and decrease cancer progression. However, as of today, EVs binding kinetics is an unexplored topic that remains to be understood and the ASB platform presented here will facilitate its research. Additionally, using the ASB, several factors were screened as potential EVs fusion triggers including an acidic pH, increased levels of extracellular calcium, and

presence of hemagglutinin, but our attempts were unfruitful. Therefore, this avenue of research remains open to identify strategies to prompt EVs fusion or EVs uptake by ADSCs and delivery of their cargo.

The complete EXOs proteomics analysis offered here opens several avenues for future research in this field. For instance, integrin β1 and HSPGs were identified as two of the ADSCs membrane components modulating EVs binding, but their ligands in the surface of EXOs are still unknown. The proteomic analysis includes possible ligands for integrin β1 and HSPGs on the surface of EXOs, and this material will facilitate the identification of the specific molecules binding the integrin β1 and HSPGs present on ADSCs. Analogously, our collaborators in KAUST are working in a proteomics analysis of MDA-MB-231- derived MVs. This material will allow us to compare side to side the composition of MVs and EXOs from the same batch of cells to further corroborate the presence of two distinct EVs subpopulations. Additionally, it will offer the surface components of MVs to further investigate their ligands binding integrin β1 and HSPGs in the surface of ADSCs. On the other side, EVs binding to ADSCs was greatly reduced using CD29 Ab and heparin, but it was not completely inhibited, suggesting the participation of other molecules in the surface of ADSCs and of EVs in this process. Several groups offer proteomic analysis of ADSCs[327, 379] allowing the identification of membrane proteins potentially involved in EVs-ADSCs binding. Using those resources and the ASB as a drug/molecule-screening tool, the role of those proteins in EVs binding and strategies to block it can be further explored.

Conclusively, our EVSB and ASB offer flexibility to be modified and make biomimetic membrane models for different types of cells and EVs, compatibility with

scale-up and multiplexing, and the option to be label-free. These facilitate testing of multiple conditions while using just one batch of cells or EVs. Therefore, both platforms make great tools for drug screening and for the development of therapeutics to mitigate the effect of EVs on cancer, or on other diseases involving EVs, progression.

APPENDIX 1

1.HEPARIN BLOCKS BINDING OF ONCOGENIC EXTRACELLULAR VESICLES TO ADIPOSE DERIVED STEM CELLS

This material is complementary to chapter 4.

1. Introduction: Development of strategies that can block extracellular vesicles (EVs) binding and subsequent delivery of information from cancer to stromal cells is of great therapeutic value and importance. Heparan sulfate proteoglycans (HSPGs) have been recognized as mediating agents in binding of virus, peptide-nucleic acid complexes, and lipoproteins to the recipient cell surface[380-382]. In the same manner, previous studies have established that HSPGs, on the surface of EVs and recipient cells, act as receptors to facilitate EVs binding and transfer of information[383, 384].

Heparin, a heparan sulfate (HS) mimetic, has been shown to disrupt several particle-cell interactions mediated by HPSGs including: EVs binding and uptake[384], binding and infection of viruses,[385] including the novel SARS-CoV-2 to cells[386], and HSPG-fibronectin cell surface interactions[387]. Although it is a Food and Drug Administration (FDA) drug approved to treat blood clots, it purpose has been redirected and proposed as a potential therapeutic or prophylactic to COVID-19, the disease cause by the SARS-CoV-2 virus infection[386, 388, 389]; and as a therapy for multiple myeloma patients for its ability to decrease EXOs- cell interactions, in the form or Roneparstat (ClinicalTrials.gov identifier NCT01764880)[390].

Several HSPGs, as transmembrane proteins or GPI-anchored membrane proteins, are present on the surface of ADSCs[391, 392], and we hypothesize their important role as receptors mediating breast cancer EVs binding to the cell surface. Here, we test our

hypothesis assessing the ability of heparin, as an HS mimic, to block such interaction by competitive binding EVs and disabling their contact with HPSGs on the surface of ADSCs, as seen in leukemia virus[393] and glioblastoma derived EVs[384]. To do so, we used our ASB platform, as a model of human primary ADSCs plasma membrane, presented in chapter 4, as a tool to detect breast cancer EVs binding to ADSCs and to screen potential therapeutics to block it. In our previous work, we used this platform to detect binding of exosomes (EXOs) to ADSCs, the participation of integrin β1/CD29 in it, and the ability of blocking integrin β1 in the surface of ADSCs to decrease it. In this study, we use the ASB to detect binding of both subpopulations of EVs, EXOs and MV, and the ability of heparin to block it. Furthermore, we test the ability of heparin to decrease the malignant outcomes of EVs-ADSCs binding, upregulated VEGF secretion and cell proliferation, in an *in vitro* cell setting, to validate the results obtained using our ASB platform and the role of HSPGs in breast cancer EVs binding to ADSCs.

Therefore, this work further corroborates the therapeutic value of our ASB as a platform to screen drugs or biomolecules to block EVs binding to ADSCs along its biological outcomes. This value is not limited to just breast cancer EVs and ADSCs interactions, the versatility of our platform allows its application to study binding between different mammalian cells and EVs involved in cancer and other diseases for which progression is influenced by EVs[16, 274]. Lastly, the results obtained here along the previously reported ones establishing heparin ability to block interactions between EVs and cells[384, 390, 394], open an avenue to further study the therapeutic potential of heparin and its derivatives in such diseases.

2. Materials and Methods

Cell culture of Adipose-Derived Stem Cells (ADSCs) and human adenocarcinoma cells (MDA-MB-231 cells), isolation, characterization, fluorescence labeling of MDA-MB-231 derived EXOs and MVs, and formation and characterization of ASBs were done as previously reported in chapter 3 and 4[9]. Heparin sodium salt from porcine intestinal mucosa, (180 USP units/mg, (Sigma, St. Louis, MO)) was used for all experiments. The following experiments were adapted from chapter 4 using heparin:

2.1. Blocking binding of cEVs to ASB using heparin

To block non-specific binding, an ASB was incubated with 100 uL of 20% normal goat serum for 30 min followed by thoroughly washing with PBS. 100 µL of R18-labeled EVs, MVs and EXOs separately (previously incubated with 20 µg/mL heparin for 30 min at room temperature) were added and incubated with the well for 30 minutes to allow binding time. ASB was washed with PBS to rinse unbound EVs and images were captured using total internal reflection fluorescence microscopy (TIRFM).

2.2. Assessment of VEGF secretion by ADSCs

ADSCs were seeded at 150,000 cells/well on Millicell EZ-slides (Millipore). After reaching around 80% confluency, cells were changed to 2% FBS media, to slowdown cell proliferation, and incubated overnight. Six different treatment conditions were done, one per well, as follow: a negative control with no treatment (NT), treatment with 5.96 x 10^7 EVs/mL (EXOs and MVs independently), treatment with 5.96 x 10^7 EVs-Heparin/mL (EXOs and MVs independently previously treated with 20 µg/mL heparin for 30 min at RT), and treatment with 10 ng/mL of TGFβ. Every other day cell media was changed,

and each treatment was repeated. 100 µL of media from each well were sampled on day 0,2, and 5 and stored at -20°C for ELISA assay. As a measure of proangiogenic activity, VEGF secretion by ADSCs in all the mentioned conditions was assessed using a Human VEGF DuoSet ELISA kit (R&D systems) following the manufacturer's protocol. Three independent replicates of the experiment were performed.

3. Results and discussion

A convenient aspect of the ASB platform, presented in chapter 4, is that we can focus on EVs binding isolated from EVs uptake by cells and cargo delivery. Therefore, here, we use the ASB to screen the ability of heparin, as a HS mimic, to block binding of EXOs and MVs to ADSCs. To do so, breast cancer cells (MDA-MB-231) derived EVs, MVs and EXOs separately, were labeled with Octadecyl Rhodamine (R18) and incubated with an ASB, formed as previously described. Images of EVs bound to the ASB were captured by total internal reflection fluorescence microscopy (TIRFM) and displayed in Figure A.1. Both subpopulations of EVs, EXOs and MVs, bound to the ASB upon contact as seen in Figure A.1a and A.1d, respectively. Oppositely, neither EVs population formed a stable bound with a POPC/PEG2k-SLB, (Figure A1c and A1f) as expected since POPC/PEG2k-SLBs do not contain HSPGs or other adhesion molecules to mediate EVs binding. Heparin has shown to work as an exogenous HS, it binds to EVs and causes their aggregation, subsequently blocking their binding to the recipient cell[384]. To investigate the therapeutic potential of heparin to block breast cancer EVs binding to ASDCs, we used our ASB, as a model of ADSCs plasma membrane, and screened heparin ability to block EVs binding to it. To do so, the ASB was treated R18-labeled EXOs and MVs, previously incubated with 20 µg/ml heparin. Images in Figure A1b and A1e and data

presented in Figure A1g and A1h show that heparin significantly decreases binding of EXOs and MVs, respectively, to the ASB. These results suggest a mediating role of HSPGs in breast cancer EVs binding to ADSCs, such as previously reported for other cell types, and the therapeutic potential of heparin to decrease such binding [384, 395].

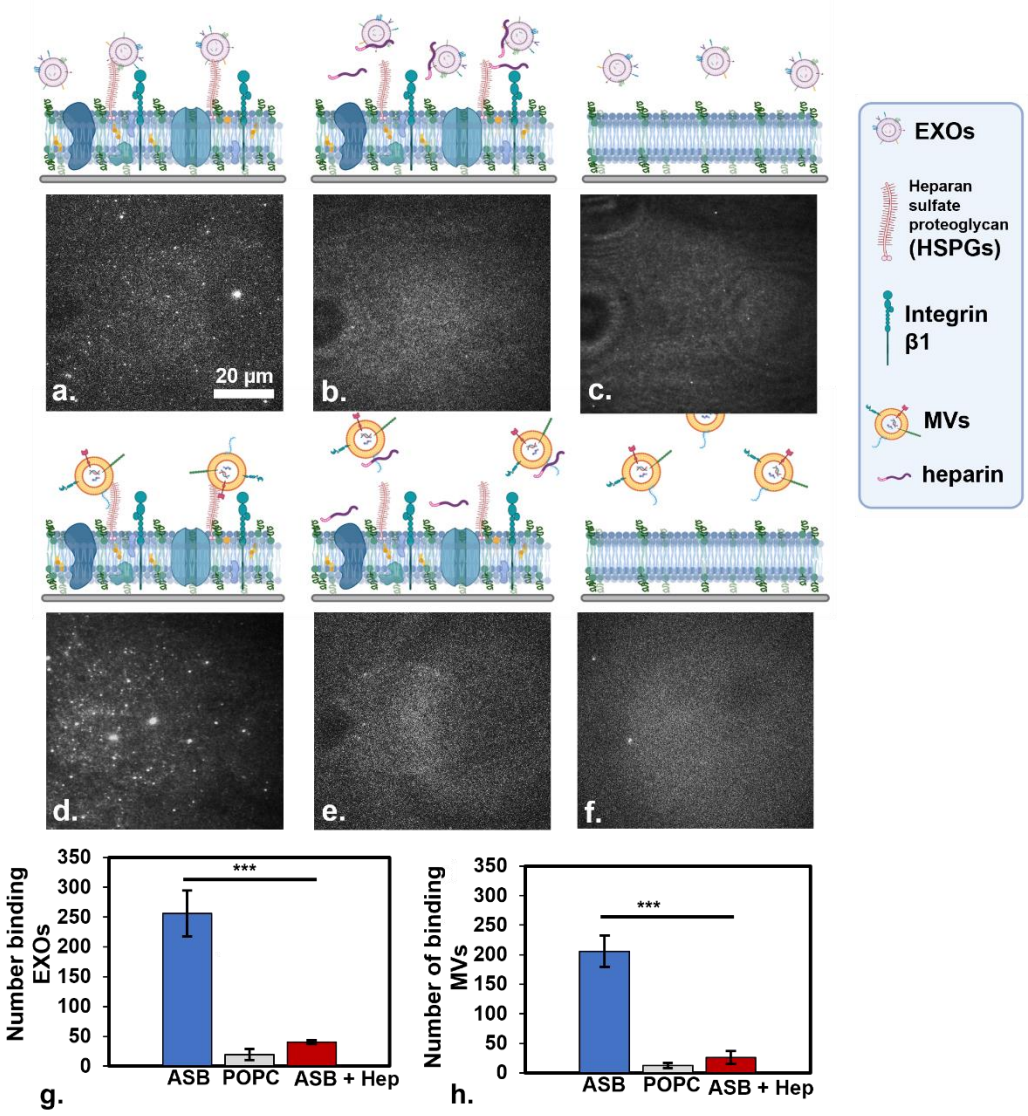

Figure A.1. Heparin blocks binding of EVs to ASB. Binding of EXOs to a) ASB, b) ASB treated EXOs + heparin, c) POPC/PEG-SLB. Binding of MVs to d) ASB, e) ASB treated with MVs + heparin, f) POPC/PEG2k SLB. Quantification of EXOs (g) and MVs (h) bound to ASBs, with and without heparin, and to POPC/PEG2k SLB after 30 minutes of incubation.

To further validate the results obtained using our ASB, we investigated the effect

of heparin in the biological outcomes of breast cancer EVs-ADSCs binding, upregulation of VEGF secretion and cell proliferation. To do so, we assessed total cell number and VEGF concentration secreted by cultured ADSCs treated with breast cancer EVs, EXOs and MVs, in the presence and absence of heparin treatment for 5 days. As seen in Figure 2a, six conditions were used in this experiment, as follows: non-treatment (NT), treatment with EXOs, treatment with EXOs previously incubated with heparin (Hep + EXOs), treatment with MVs, treatment with MVs previously incubated with heparin (Hep + MVs), and treatment with TGFβ. NT was implemented as a negative control and a baseline to compare the other conditions since ADSCs under no treatment are expected to secrete less VEGF than their treated counterparts, and TGFβ was used as a positive control because it has an effect of VEGF regulation and induction of proangiogenic activity[338, 340].

After 5 days of treatment, results displayed in Figure 2b show that ADSCs treated with EXOs, MVs, and TGFβ, secreted approximately twice the concentration of VEGF than NT cells, as previously seen. Conversely, cells treated with EXOs and MVs previously incubated with heparin (Hep + EXOs and Hep + MVs conditions), secreted less VEGF than those without heparin treatment, EXOs and MVs, and similar VEGF concentration than NT cells. In the same manner, after 5 days of treatment, the number of cells for EXOs-, MVs-, and TGFβ-treated ADSCs is higher than for NT cells. Interestingly, treatment EXOs and MVs previously incubated with heparin, led to a lower cell number than in the absence of heparin, and even than in NT cells (Figure A2c). These results suggest that treatment of ADSCs with EXOs and MVs lead to upregulation of VEGF secretion and cell proliferation, as previously reported, and that such outcomes are

decreased by heparin treatment. This observation further validates our results presented in Figure 1 and our hypothesis that HSPGs on the surface of ADSCs mediate breast cancer EVs binding and heparin is a strategy to block it.

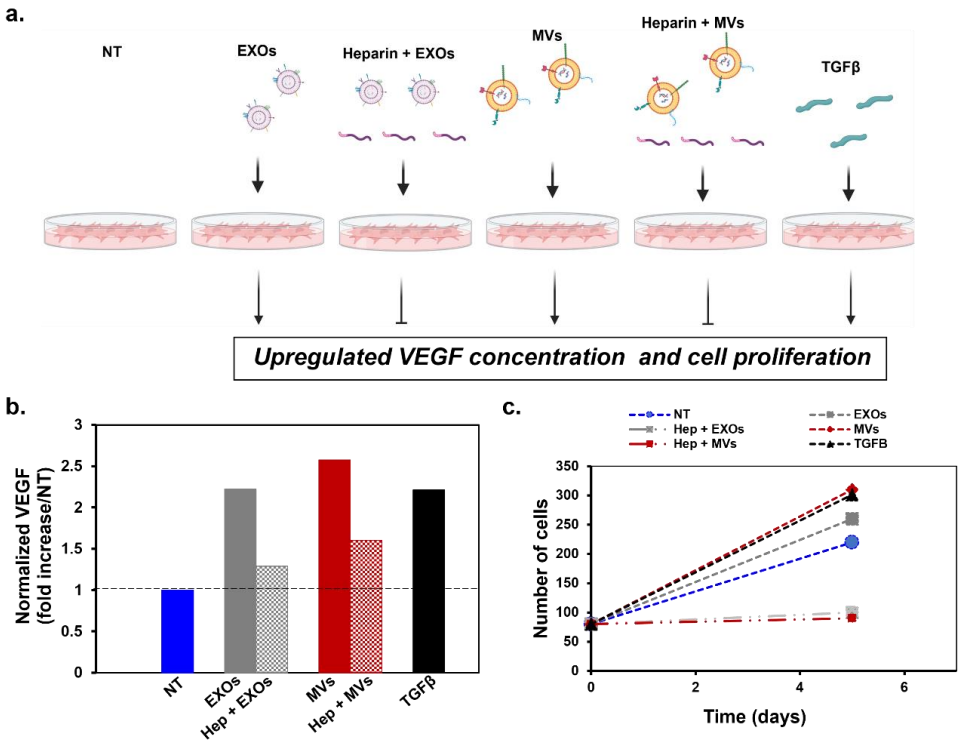

Figure A.2. Heparin decreases VEGF secretion and cell proliferation in ADSCs treated with breast cancer EVs. a) schematic of experiment to assess VEGF secretion and cell number of ADSCs treated with EVs in the presence and absence of heparin; conditions included ADSCs treatment with: no treatment (NT), EXOs, EXOs with heparin, MVs, MVs with heparin, and TGFβ. b) VEGF concentration secreted by ADSCs under all conditions mentioned in (a) normalized by the concentration of NT cells, on day 5 of treatment. c) Number of alive cells on day 5 of treatment for all conditions.

The low number of cells resultant on ADSCs treated with EVs previously incubated with heparin could be possible due to some cytotoxicity associated with heparin, as previously reported[396]. Different doses will be evaluated to find the optimal heparin dosage to inhibit breast cancer EVs binding to ADSCs and to decrease its outcomes, while avoiding damage of the cells. Note that treatment with the same concentration of both types of EVs, EXOs and MVs, had the same effect on ADSCs, upregulation of VEGF secretion

and cell proliferation, but the effect of MVs was slightly higher. This pattern was also observed in our previous work[9], and we believe that the characteristic bigger and consequently higher surface area of MVs compared to EXOs, could lead to MVs having a stronger effect than EXOs on ADSCs behavior.

4. Conclusions

Here, we utilized our ASB platform, introduced in chapter 4, to screen the potential of heparin, as an HS mimic, to block breast cancer EVs binding to ADSCs and decrease the outcomes associated with it. Using the ASB as a biomimetic model of human primary ADSCs, we detected MVs and EXOs binding using TIRFM and its blocking, indicated by a significant decrease in binding events, using heparin. Furthermore, heparin treatment led to a decrease in VEGF secretion and cell proliferation, otherwise upregulated in ADSCs treated with breast cancer EVs. These results suggest that heparin decreases breast cancer EVs binding to ADSCs and its associated outcomes and furthers validate our hypothesis that HSPGs on the surface of ADSCs play an important role in EVs-ADSCs interactions. Furthermore, we were able to verify one more time the value of our ASB, as a biomimetic model of human primary ASDCs, to detect binding of EVs and screen strategies to block in a cell-free manner without the challenges of culturing and maintaining human primary stem cells and conducting long and complicated cell experiments.

Lastly, we contributed to the field with one more example of heparin ability to disrupt EVs interactions with cells. The advantage of being an FDA-approved drug and the number of studies indicating its potential to disrupt HSPGs-mediating interactions,

has given heparin an increased popularity in the last years and several proposals to redirect its main purpose, from preventing and treating blood clots to become a COVID-19 and multiple myeloma therapeutic. Here, we show one more value of heparin, to disrupt breast cancer EVs binding to human primary ADSCs and reduce pro-angiogenic activity of ADSCs. Although the specific mechanisms used by heparin to achieve those outcomes are not explored here and remain unknown, we think it is possibly due to competitive binding of heparin to breast cancer EVs decreasing their availability to bind the HS chains in HSPGs on the surface of ADSCs, as previously seen in other types of cells and EVs[384, 394, 397] and viruses[398]. Therefore, this opens a new avenue of research to further explore heparin mechanism of action in breast cancer EVs-ADSCs binding and its potential use as a breast cancer therapeutic.

REFERENCES

1. Abels, E. R.; Breakefield, X. O., Introduction to Extracellular Vesicles: Biogenesis, RNA Cargo Selection, Content, Release, and Uptake. *Cell Mol Neurobiol* **2016,** *36* (3), 301-12 DOI: 10.1007/s10571-016-0366-z.

2. Muralidharan-Chari, V.; Clancy, J. W.; Sedgwick, A.; D'Souza-Schorey, C., Microvesicles: mediators of extracellular communication during cancer progression. *Journal of cell science* **2010,** *123* (Pt 10), 1603-1611 DOI: 10.1242/jcs.064386.

3. Becker, A.; Thakur, B. K.; Weiss, J. M.; Kim, H. S.; Peinado, H.; Lyden, D., Extracellular Vesicles in Cancer: Cell-to-Cell Mediators of Metastasis. *Cancer Cell* **2016,** *30* (6), 836-848 DOI: https://doi.org/10.1016/j.ccell.2016.10.009.

4. Song, Y. H.; Warncke, C.; Choi, S. J.; Choi, S.; Chiou, A. E.; Ling, L.; Liu, H. Y.; Daniel, S.; Antonyak, M. A.; Cerione, R. A.; Fischbach, C., Breast cancer-derived extracellular vesicles stimulate myofibroblast differentiation and pro-angiogenic behavior of adipose stem cells. *Matrix Biol* **2017,** *60-61*, 190-205 DOI: 10.1016/j.matbio.2016.11.008.

5. Ah Cho, J.; Park, H.; Hye Lim, E.; Lee, K. W., *Exosomes from breast cancer cells can convert adipose tissue-derived*. 2011; Vol. 40, p 130-8.

6. Chowdhury, R.; Webber, J. P.; Gurney, M.; Mason, M. D.; Tabi, Z.; Clayton, A., Cancer exosomes trigger mesenchymal stem cell differentiation into pro-angiogenic and pro-invasive myofibroblasts. *Oncotarget* **2014,** *6* (2), 715-731 DOI: 10.18632/oncotarget.2711.

7. Freese, K. E.; Kokai, L.; Edwards, R. P.; Philips, B. J.; Sheikh, M. A.; Kelley, J.; Comerci, J.; Marra, K. G.; Rubin, J. P.; Linkov, F., Adipose-Derived Stems Cells and Their Role in Human Cancer Development, Growth, Progression, and Metastasis: A Systematic Review. **2015,** *75* (7), 1161-1168 DOI: 10.1158/0008-5472.CAN-14-2744 %J Cancer Research.

8. Prada, I.; Amin, L.; Furlan, R.; Legname, G.; Verderio, C.; Cojoc, D., A new approach to follow a single extracellular vesicle—cell interaction using optical tweezers. *BioTechniques* **2016,** *60* (1), 35 DOI: 10.2144/000114371.

9. Uribe, J.; Liu, H.-Y.; Mohamed, Z.; Chiou, A. E.; Fischbach, C.; Daniel, S., Supported Membrane Platform to Assess Surface Interactions between Extracellular Vesicles and Stromal Cells. *ACS Biomaterials Science & Engineering* **2020,** *6* (7), 3945-3956 DOI: 10.1021/acsbiomaterials.0c00133.

10. Cui, Y.; Wang, D.; Xie, M., Tumor-Derived Extracellular Vesicles Promote Activation of Carcinoma-Associated Fibroblasts and Facilitate Invasion and Metastasis

of Ovarian Cancer by Carrying miR-630. *Frontiers in Cell and Developmental Biology* **2021,** *9* (1576), DOI: 10.3389/fcell.2021.652322.

11. Uribe, J.; Traberg, W. C.; Hama, A.; Druet, V.; Mohamed, Z.; Ooi, A.; Pappa, A.-M.; Huerta, M.; Inal, S.; Owens, R. M.; Daniel, S., Dual Mode Sensing of Binding and Blocking of Cancer Exosomes to Biomimetic Human Primary Stem Cell Surfaces. *ACS Biomaterials Science & Engineering* **2021**, DOI: 10.1021/acsbiomaterials.1c01056.

13. Heron, M.; Hoyert, D. L.; Murphy, S. L.; Xu, J.; Kochanek, K. D.; Tejada-Vera, B. J. N. V. S. R., National vital statistics reports. **2009,** *57* (14).

14. Liu, Q.; Zhang, H.; Jiang, X.; Qian, C.; Liu, Z.; Luo, D., Factors involved in cancer metastasis: a better understanding to "seed and soil" hypothesis. *Mol Cancer* **2017,** *16* (1), 176 DOI: 10.1186/s12943-017-0742-4.

15. van Niel, G.; D'Angelo, G.; Raposo, G., Shedding light on the cell biology of extracellular vesicles. *Nat Rev Mol Cell Biol* **2018,** *19* (4), 213-228 DOI: 10.1038/nrm.2017.125.

16. Lawson, C.; Vicencio, J. M.; Yellon, D. M.; Davidson, S. M., Microvesicles and exosomes: new players in metabolic and cardiovascular disease. **2016,** *228* (2), R57 DOI: 10.1530/joe-15-0201.

17. König, L.; Kasimir-Bauer, S.; Bittner, A.-K.; Hoffmann, O.; Wagner, B.; Santos Manvailer, L. F.; Kimmig, R.; Horn, P. A.; Rebmann, V., Elevated levels of extracellular vesicles are associated with therapy failure and disease progression in breast cancer patients undergoing neoadjuvant chemotherapy. *Oncoimmunology* **2017,** *7* (1), e1376153-e1376153 DOI: 10.1080/2162402X.2017.1376153.

18. Grange, C.; Tapparo, M.; Collino, F.; Vitillo, L.; Damasco, C.; Deregibus, M. C.; Tetta, C.; Bussolati, B.; Camussi, G., Microvesicles Released from Human Renal Cancer Stem Cells Stimulate Angiogenesis and Formation of Lung Premetastatic Niche. **2011,** *71* (15), 5346-5356 DOI: 10.1158/0008-5472.CAN-11-0241 %J Cancer Research.

19. Köppler, B.; Cohen, C.; Schlöndorff, D.; Mack, M., Differential mechanisms of microparticle transfer toB cells and monocytes: anti-inflammatory propertiesof microparticles. **2006,** *36* (3), 648-660 DOI: doi:10.1002/eji.200535435.

20. Antonyak, M. A.; Li, B.; Boroughs, L. K.; Johnson, J. L.; Druso, J. E.; Bryant, K. L.; Holowka, D. A.; Cerione, R. A., Cancer cell-derived microvesicles induce transformation by transferring tissue transglutaminase and fibronectin to recipient cells. **2011,** *108* (12), 4852-4857 DOI: 10.1073/pnas.1017667108 %J Proceedings of the National Academy of Sciences.

21. Kim, H.; Lee, S.; Shin, E.; Seong, K. M.; Jin, Y. W.; Youn, H.; Youn, B., The Emerging Roles of Exosomes as EMT Regulators in Cancer. *Cells* **2020,** *9* (4), DOI: 10.3390/cells9040861.

22. Rahman, M. A.; Barger, J. F.; Lovat, F.; Gao, M.; Otterson, G. A.; Nana-Sinkam, P., Lung cancer exosomes as drivers of epithelial mesenchymal transition. *Oncotarget* **2016,** *7* (34), 54852-54866 DOI: 10.18632/oncotarget.10243.

23. van Dommelen, S. M.; Fish, M.; Barendrecht, A. D.; Schiffelers, R. M.; Eniola-Adefeso, O.; Vader, P., Interaction of Extracellular Vesicles with Endothelial Cells Under Physiological Flow Conditions. In *Exosomes and Microvesicles: Methods and Protocols*, Hill, A. F., Ed. Springer New York: New York, NY, 2017; pp 205-213.

24. Xu, R.; Rai, A.; Chen, M.; Suwakulsiri, W.; Greening, D. W.; Simpson, R. J., Extracellular vesicles in cancer — implications for future improvements in cancer care. *Nature Reviews Clinical Oncology* **2018,** *15* (10), 617-638 DOI: 10.1038/s41571-018-0036-9.

25. Supported Lipid Bilayers. In *Wiley Encyclopedia of Chemical Biology*.

26. Richter, R. P.; Bérat, R.; Brisson, A. R., Formation of Solid-Supported Lipid Bilayers: An Integrated View. *Langmuir* **2006,** *22* (8), 3497-3505 DOI: 10.1021/la052687c.

27. Tamm, L. K.; McConnell, H. M., Supported phospholipid bilayers. *Biophysical Journal* **1985,** *47* (1), 105-113 DOI: https://doi.org/10.1016/S0006-3495(85)83882-0.

28. Crites, T. J.; Maddox, M.; Padhan, K.; Muller, J.; Eigsti, C.; Varma, R., Supported Lipid Bilayer Technology for the Study of Cellular Interfaces. *Curr Protoc Cell Biol* **2015,** *68*, 24.5.1-24.5.31 DOI: 10.1002/0471143030.cb2405s68.

29. Nordin, D.; Yarkoni, O.; Savinykh, N.; Donlon, L.; Frankel, D., Revealing the selective interactions of fibronectin with lipid bilayers. *Soft Matter* **2011,** *7* (22), 10666-10675 DOI: 10.1039/C1SM06291C.

30. Afanasenkau, D.; Offenhäusser, A., Positively Charged Supported Lipid Bilayers as a Biomimetic Platform for Neuronal Cell Culture. *Langmuir* **2012,** *28* (37), 13387-13394 DOI: 10.1021/la302500r.

31. Pautot, S.; Lee, H.; Isacoff, E. Y.; Groves, J. T., Neuronal synapse interaction reconstituted between live cells and supported lipid bilayers. *Nature Chemical Biology* **2005,** *1* (5), 283-289 DOI: 10.1038/nchembio737.

32. Vafaei, S.; Tabaei, S. R.; Cho, N.-J., Optimizing the Performance of Supported Lipid Bilayers as Cell Culture Platforms Based on Extracellular Matrix Functionalization. *ACS Omega* **2017,** *2* (6), 2395-2404 DOI: 10.1021/acsomega.7b00158.

33. Richards, M. J.; Hsia, C.-Y.; Singh, R. R.; Haider, H.; Kumpf, J.; Kawate, T.; Daniel, S., Membrane Protein Mobility and Orientation Preserved in Supported Bilayers Created Directly from Cell Plasma Membrane Blebs. *Langmuir* **2016,** *32* (12), 2963-2974 DOI: 10.1021/acs.langmuir.5b03415.

34. Liu, H.-Y.; Grant, H.; Hsu, H.-L.; Sorkin, R.; Bošković, F.; Wuite, G.; Daniel, S., *Supported Planar Mammalian Membranes as Models of in Vivo Cell Surface Architectures*. 2017; Vol. 9.

35. Lee, J. Y.; Kim, H.-S., Extracellular Vesicles in Neurodegenerative Diseases: A Double-Edged Sword. *Tissue engineering and regenerative medicine* **2017,** *14* (6), 667-678 DOI: 10.1007/s13770-017-0090-x.

36. Ryu, A.-R.; Kim, D. H.; Kim, E.; Lee, M. Y., The Potential Roles of Extracellular Vesicles in Cigarette Smoke-Associated Diseases %J Oxidative Medicine and Cellular Longevity. **2018,** *2018*, 8 DOI: 10.1155/2018/4692081.

37. Lee, D. H.; Giovannucci, E. L., The Obesity Paradox in Cancer: Epidemiologic Insights and Perspectives. *Current Nutrition Reports* **2019,** *8* (3), 175-181 DOI: 10.1007/s13668-019-00280-6.

38. Avgerinos, K. I.; Spyrou, N.; Mantzoros, C. S.; Dalamaga, M., Obesity and cancer risk: Emerging biological mechanisms and perspectives. *Metabolism* **2019,** *92*, 121-135 DOI: https://doi.org/10.1016/j.metabol.2018.11.001.

39. Castro-Oropeza, R.; Vazquez-Santillan, K.; Díaz-Gastelum, C.; Melendez-Zajgla, J.; Zampedri, C.; Ferat-Osorio, E.; Rodríguez-González, A.; Arriaga-Pizano, L.; Maldonado, V., Adipose-derived mesenchymal stem cells promote the malignant phenotype of cervical cancer. *Sci Rep* **2020,** *10* (1), 14205 DOI: 10.1038/s41598-020-69907-x.

40. Kolb, R.; Zhang, W., Obesity and Breast Cancer: A Case of Inflamed Adipose Tissue. *Cancers (Basel)* **2020,** *12* (6), 1686 DOI: 10.3390/cancers12061686.

41. Wang, M.; Zhao, J.; Zhang, L.; Wei, F.; Lian, Y.; Wu, Y.; Gong, Z.; Zhang, S.; Zhou, J.; Cao, K.; Li, X.; Xiong, W.; Li, G.; Zeng, Z.; Guo, C., Role of tumor microenvironment in tumorigenesis. *Journal of Cancer* **2017,** *8* (5), 761-773 DOI: 10.7150/jca.17648.

42. Desai, V. D.; Hsia, H. C.; Schwarzbauer, J. E., Reversible modulation of myofibroblast differentiation in adipose-derived mesenchymal stem cells. *PloS one* **2014,** *9* (1), e86865-e86865 DOI: 10.1371/journal.pone.0086865.

43. Otranto, M.; Sarrazy, V.; Bonté, F.; Hinz, B.; Gabbiani, G.; Desmoulière, A., The role of the myofibroblast in tumor stroma remodeling. *Cell adhesion & migration* **2012,** *6* (3), 203-219 DOI: 10.4161/cam.20377.

44. Chu, Y.; Wang, Y.; Peng, W.; Xu, L.; Liu, M.; Li, J.; Hu, X.; Li, Y.; Zuo, J.; Ye, Y., STAT3 activation by IL-6 from adipose-derived stem cells promotes endometrial carcinoma proliferation and metastasis. *Biochemical and Biophysical Research Communications* **2018,** *500* (3), 626-631 DOI: https://doi.org/10.1016/j.bbrc.2018.04.121.

45. Eterno, V.; Zambelli, A.; Pavesi, L.; Villani, L.; Zanini, V.; Petrolo, G.; Manera, S.; Tuscano, A.; Amato, A., Adipose-derived Mesenchymal Stem Cells (ASCs) may favour breast cancer recurrence via HGF/c-Met signaling. *Oncotarget* **2014,** *5* (3), 613-633 DOI: 10.18632/oncotarget.1359.

46. Wels, J.; Kaplan, R. N.; Rafii, S.; Lyden, D., Migratory neighbors and distant invaders: tumor-associated niche cells. *Genes Dev* **2008,** *22* (5), 559-74 DOI: 10.1101/gad.1636908.

47. Schweizer, R.; Tsuji, W.; Gorantla, V. S.; Marra, K. G.; Rubin, J. P.; Plock, J. A., The role of adipose-derived stem cells in breast cancer progression and metastasis. *Stem cells international* **2015,** *2015*, 120949-120949 DOI: 10.1155/2015/120949.

48. Scioli, M. G.; Storti, G.; D'Amico, F.; Gentile, P.; Kim, B.-S.; Cervelli, V.; Orlandi, A., Adipose-Derived Stem Cells in Cancer Progression: New Perspectives and Opportunities. *Int J Mol Sci* **2019,** *20* (13), 3296 DOI: 10.3390/ijms20133296.

49. Koellensperger, E.; Bonnert, L.-C.; Zoernig, I.; Marmé, F.; Sandmann, S.; Germann, G.; Gramley, F.; Leimer, U., The impact of human adipose tissue-derived stem cells on breast cancer cells: implications for cell-assisted lipotransfers in breast reconstruction. *Stem Cell Research & Therapy* **2017,** *8* (1), 121 DOI: 10.1186/s13287-017-0579-1.

50. Strong, A. L.; Strong, T. A.; Rhodes, L. V.; Semon, J. A.; Zhang, X.; Shi, Z.; Zhang, S.; Gimble, J. M.; Burow, M. E.; Bunnell, B. A., Obesity associated alterations in the biology of adipose stem cells mediate enhanced tumorigenesis by estrogen dependent pathways. *Breast Cancer Res* **2013,** *15* (5), R102 DOI: 10.1186/bcr3569.

51. Dirat, B.; Bochet, L.; Dabek, M.; Daviaud, D.; Dauvillier, S.; Majed, B.; Wang, Y. Y.; Meulle, A.; Salles, B.; Le Gonidec, S.; Garrido, I.; Escourrou, G.; Valet, P.; Muller, C., Cancer-associated adipocytes exhibit an activated phenotype and contribute to breast cancer invasion. *Cancer Res* **2011,** *71* (7), 2455-65 DOI: 10.1158/0008-5472.Can-10-3323.

52. Lewis, M. P.; Lygoe, K. A.; Nystrom, M. L.; Anderson, W. P.; Speight, P. M.; Marshall, J. F.; Thomas, G. J., Tumour-derived TGF-beta1 modulates myofibroblast differentiation and promotes HGF/SF-dependent invasion of squamous carcinoma cells. *British journal of cancer* **2004,** *90* (4), 822-832 DOI: 10.1038/sj.bjc.6601611.

53. Ringuette Goulet, C.; Bernard, G.; Tremblay, S.; Chabaud, S.; Bolduc, S.; Pouliot, F., Exosomes Induce Fibroblast Differentiation into Cancer-Associated Fibroblasts through TGFβ Signaling. *Molecular Cancer Research* **2018,** *16* (7), 1196-1204 DOI: 10.1158/1541-7786.Mcr-17-0784.

54. Shelke, G. V.; Yin, Y.; Jang, S. C.; Lässer, C.; Wennmalm, S.; Hoffmann, H. J.; Li, L.; Gho, Y. S.; Nilsson, J. A.; Lötvall, J., Endosomal signalling via exosome surface TGFβ-1. *Journal of extracellular vesicles* **2019,** *8* (1), 1650458-1650458 DOI: 10.1080/20013078.2019.1650458.

55. Scharenberg, M. A.; Pippenger, B. E.; Sack, R.; Zingg, D.; Ferralli, J.; Schenk, S.; Martin, I.; Chiquet-Ehrismann, R., TGF-β-induced differentiation into myofibroblasts involves specific regulation of two MKL1 isoforms. *Journal of Cell Science* **2014,** *127* (5), 1079-1091 DOI: 10.1242/jcs.142075.

56. García-Honduvilla, N.; Cifuentes, A.; Ortega, M. A.; Delgado, A.; González, S.; Bujan, J.; Alvarez-Mon, M., High Sensitivity of Human Adipose Stem Cells to Differentiate into Myofibroblasts in the Presence of C. aspersa Egg Extract. *Stem cells international* **2017,** *2017*, 9142493-9142493 DOI: 10.1155/2017/9142493.

57. Paggetti, J.; Haderk, F.; Seiffert, M.; Janji, B.; Distler, U.; Ammerlaan, W.; Kim, Y. J.; Adam, J.; Lichter, P.; Solary, E.; Berchem, G.; Moussay, E., Exosomes released by chronic lymphocytic leukemia cells induce the transition of stromal cells into cancer-associated fibroblasts. *Blood* **2015,** *126* (9), 1106-1117 DOI: 10.1182/blood-2014-12-618025.

58. Yáñez-Mó, M.; Siljander, P. R.; Andreu, Z.; Zavec, A. B.; Borràs, F. E.; Buzas, E. I.; Buzas, K.; Casal, E.; Cappello, F.; Carvalho, J.; Colás, E.; Cordeiro-da Silva, A.; Fais, S.; Falcon-Perez, J. M.; Ghobrial, I. M.; Giebel, B.; Gimona, M.; Graner, M.; Gursel, I.; Gursel, M.; Heegaard, N. H.; Hendrix, A.; Kierulf, P.; Kokubun, K.; Kosanovic, M.; Kralj-Iglic, V.; Krämer-Albers, E. M.; Laitinen, S.; Lässer, C.; Lener, T.; Ligeti, E.; Linē, A.; Lipps, G.; Llorente, A.; Lötvall, J.; Manček-Keber, M.; Marcilla, A.; Mittelbrunn, M.; Nazarenko, I.; Nolte-'t Hoen, E. N.; Nyman, T. A.; O'Driscoll, L.; Olivan, M.; Oliveira, C.; Pállinger, É.; Del Portillo, H. A.; Reventós, J.; Rigau, M.; Rohde, E.; Sammar, M.; Sánchez-Madrid, F.; Santarém, N.; Schallmoser, K.; Ostenfeld, M. S.; Stoorvogel, W.; Stukelj, R.; Van der Grein, S. G.; Vasconcelos, M. H.; Wauben, M. H.; De Wever, O., Biological properties of extracellular vesicles and their physiological functions. *J Extracell Vesicles* **2015,** *4*, 27066 DOI: 10.3402/jev.v4.27066.

59. Lin, J.; Li, J.; Huang, B.; Liu, J.; Chen, X.; Chen, X.-M.; Xu, Y.-M.; Huang, L.-F.; Wang, X.-Z., Exosomes: novel biomarkers for clinical diagnosis. *ScientificWorldJournal* **2015,** *2015*, 657086-657086 DOI: 10.1155/2015/657086.

60. Chen, J.; Xu, Y.; Lu, Y.; Xing, W., Isolation and Visible Detection of Tumor-Derived Exosomes from Plasma. *Analytical Chemistry* **2018,** *90* (24), 14207-14215 DOI: 10.1021/acs.analchem.8b03031.

61. Lowry, M. C.; Gallagher, W. M.; O'Driscoll, L., The Role of Exosomes in Breast Cancer. **2015,** *61* (12), 1457-1465 DOI: 10.1373/clinchem.2015.240028 %J Clinical Chemistry.

62. Zaborowski, M. P.; Balaj, L.; Breakefield, X. O.; Lai, C. P., Extracellular Vesicles: Composition, Biological Relevance, and Methods of Study. *Bioscience* **2015,** *65* (8), 783-797 DOI: 10.1093/biosci/biv084.

63. Raposo, G.; Stoorvogel, W., Extracellular vesicles: Exosomes, microvesicles, and friends. **2013,** *200* (4), 373-383 DOI: 10.1083/jcb.201211138 %J The Journal of Cell Biology.

64. Caivano, A.; Del Vecchio, L.; Musto, P., Do we need to distinguish exosomes from microvesicles in hematological malignancies? *Leukemia* **2017,** *31*, 2009 DOI: 10.1038/leu.2017.205.

65. Evans-Osses, I.; Reichembach, L. H.; Ramirez, M. I. J. P. R., Exosomes or microvesicles? Two kinds of extracellular vesicles with different routes to modify protozoan-host cell interaction. **2015,** *114* (10), 3567-3575 DOI: 10.1007/s00436-015-4659-9.

66. Lee, Y.; Wood, M. J. A.; EL Andaloussi, S., Exosomes and microvesicles: extracellular vesicles for genetic information transfer and gene therapy. *Human Molecular Genetics* **2012,** *21* (R1), R125-R134 DOI: 10.1093/hmg/dds317 %J Human Molecular Genetics.

67. Bremnes, R. M.; Dønnem, T.; Al-Saad, S.; Al-Shibli, K.; Andersen, S.; Sirera, R.; Camps, C.; Marinez, I.; Busund, L.-T., The Role of Tumor Stroma in Cancer Progression and Prognosis: Emphasis on Carcinoma-Associated Fibroblasts and Non-small Cell Lung Cancer. *Journal of Thoracic Oncology* **2011,** *6* (1), 209-217 DOI: https://doi.org/10.1097/JTO.0b013e3181f8a1bd.

68. Whiteside, T. L., The tumor microenvironment and its role in promoting tumor growth. *Oncogene* **2008,** *27* (45), 5904-12 DOI: 10.1038/onc.2008.271.

69. Sabol, R. A.; Giacomelli, P.; Beighley, A.; Bunnell, B. A., Adipose Stem Cells and Cancer: Concise Review. *STEM CELLS* **2019,** *37* (10), 1261-1266 DOI: 10.1002/stem.3050.

70. Peng, J.; Wang, W.; Hua, S.; Liu, L., Roles of Extracellular Vesicles in Metastatic Breast Cancer. *Breast Cancer (Auckl)* **2018,** *12*, 1178223418767666-1178223418767666 DOI: 10.1177/1178223418767666.

71. Peinado, H.; Alečković, M.; Lavotshkin, S.; Matei, I.; Costa-Silva, B.; Moreno-Bueno, G.; Hergueta-Redondo, M.; Williams, C.; García-Santos, G.; Ghajar, C. M.; Nitadori-Hoshino, A.; Hoffman, C.; Badal, K.; Garcia, B. A.; Callahan, M. K.; Yuan, J.; Martins, V. R.; Skog, J.; Kaplan, R. N.; Brady, M. S.; Wolchok, J. D.; Chapman, P. B.; Kang, Y.; Bromberg, J.; Lyden, D., Melanoma exosomes educate bone marrow progenitor cells toward a pro-metastatic phenotype through MET. *Nature Medicine* **2012,** *18* (6), 883-891 DOI: 10.1038/nm.2753.

72. Tkach, M.; Théry, C., Communication by Extracellular Vesicles: Where We Are and Where We Need to Go. *Cell* **2016,** *164* (6), 1226-1232 DOI: https://doi.org/10.1016/j.cell.2016.01.043.

73. Rontogianni, S.; Synadaki, E.; Li, B.; Liefaard, M. C.; Lips, E. H.; Wesseling, J.; Wu, W.; Altelaar, M., Proteomic profiling of extracellular vesicles allows for human breast cancer subtyping. *Communications Biology* **2019,** *2* (1), 325 DOI: 10.1038/s42003-019-0570-8.

74. Fang, J. H.; Zhang, Z. J.; Shang, L. R.; Luo, Y. W.; Lin, Y. F.; Yuan, Y.; Zhuang, S. M., Hepatoma cell-secreted exosomal microRNA-103 increases vascular permeability and promotes metastasis by targeting junction proteins. *Hepatology* **2018,** *68* (4), 1459-1475 DOI: 10.1002/hep.29920.

75. Umezu, T.; Tadokoro, H.; Azuma, K.; Yoshizawa, S.; Ohyashiki, K.; Ohyashiki, J. H., Exosomal miR-135b shed from hypoxic multiple myeloma cells enhances angiogenesis by targeting factor-inhibiting HIF-1. *Blood* **2014,** *124* (25), 3748-57 DOI: 10.1182/blood-2014-05-576116.

76. Melo, S. A.; Sugimoto, H.; O'Connell, J. T.; Kato, N.; Villanueva, A.; Vidal, A.; Qiu, L.; Vitkin, E.; Perelman, L. T.; Melo, C. A.; Lucci, A.; Ivan, C.; Calin, G. A.; Kalluri, R., Cancer exosomes perform cell-independent microRNA biogenesis and promote tumorigenesis. *Cancer cell* **2014,** *26* (5), 707-721 DOI: 10.1016/j.ccell.2014.09.005.

77. Feng, Q.; Zhang, C.; Lum, D.; Druso, J. E.; Blank, B.; Wilson, K. F.; Welm, A.; Antonyak, M. A.; Cerione, R. A., A class of extracellular vesicles from breast cancer cells activates VEGF receptors and tumour angiogenesis. *Nature Communications* **2017,** *8*, 14450 DOI: 10.1038/ncomms14450

https://www.nature.com/articles/ncomms14450#supplementary-information.

78. Conigliaro, A.; Cicchini, C., Exosome-Mediated Signaling in Epithelial to Mesenchymal Transition and Tumor Progression. *J Clin Med* **2018,** *8* (1), DOI: 10.3390/jcm8010026.

79. Fabbri, M.; Paone, A.; Calore, F.; Galli, R.; Gaudio, E.; Santhanam, R.; Lovat, F.; Fadda, P.; Mao, C.; Nuovo, G. J.; Zanesi, N.; Crawford, M.; Ozer, G. H.; Wernicke, D.; Alder, H.; Caligiuri, M. A.; Nana-Sinkam, P.; Perrotti, D.; Croce, C. M., MicroRNAs bind to Toll-like receptors to induce prometastatic inflammatory response. *Proceedings of the National Academy of Sciences* **2012,** *109* (31), E2110-E2116 DOI: 10.1073/pnas.1209414109.

80. DeNardo, D. G.; Johansson, M.; Coussens, L. M., Immune cells as mediators of solid tumor metastasis. *Cancer and Metastasis Reviews* **2008,** *27* (1), 11-18 DOI: 10.1007/s10555-007-9100-0.

81. Pang, W.; Su, J.; Wang, Y.; Feng, H.; Dai, X.; Yuan, Y.; Chen, X.; Yao, W., Pancreatic cancer-secreted miR-155 implicates in the conversion from normal fibroblasts to cancer-associated fibroblasts. *Cancer Science* **2015,** *106* (10), 1362-1369 DOI: https://doi.org/10.1111/cas.12747.

82. Rana, S.; Malinowska, K.; Zöller, M., Exosomal tumor microRNA modulates premetastatic organ cells. *Neoplasia* **2013,** *15* (3), 281-95 DOI: 10.1593/neo.122010.

83. Giusti, I.; Di Francesco, M.; D'Ascenzo, S.; Palmerini, M. G.; Macchiarelli, G.; Carta, G.; Dolo, V., Ovarian cancer-derived extracellular vesicles affect normal human fibroblast behavior. *Cancer Biology & Therapy* **2018,** *19* (8), 722-734 DOI: 10.1080/15384047.2018.1451286.

84. Moses, B. S.; Evans, R.; Slone, W. L.; Piktel, D.; Martinez, I.; Craig, M. D.; Gibson, L. F., Bone Marrow Microenvironment Niche Regulates miR-221/222 in Acute Lymphoblastic Leukemia. *Molecular Cancer Research* **2016,** *14* (10), 909-919 DOI: 10.1158/1541-7786.Mcr-15-0474.

85. Bliss, S. A.; Sinha, G.; Sandiford, O. A.; Williams, L. M.; Engelberth, D. J.; Guiro, K.; Isenalumhe, L. L.; Greco, S. J.; Ayer, S.; Bryan, M.; Kumar, R.; Ponzio, N. M.; Rameshwar, P., Mesenchymal Stem Cell–Derived Exosomes Stimulate Cycling Quiescence and Early Breast Cancer Dormancy in Bone Marrow. *Cancer Research* **2016,** *76* (19), 5832-5844 DOI: 10.1158/0008-5472.Can-16-1092.

86. Matsumoto, Y.; Kano, M.; Murakami, K.; Toyozumi, T.; Suito, H.; Takahashi, M.; Sekino, N.; Shiraishi, T.; Kamata, T.; Ryuzaki, T.; Hirasawa, S.; Kinoshita, K.; Matsubara, H., Tumor-derived exosomes influence the cell cycle and cell migration of human esophageal cancer cell lines. *Cancer Science* **2020,** *111* (12), 4348-4358 DOI: https://doi.org/10.1111/cas.14660.

87. Fujita, Y.; Yoshioka, Y.; Ochiya, T., Extracellular vesicle transfer of cancer pathogenic components. *Cancer Sci* **2016,** *107* (4), 385-90 DOI: 10.1111/cas.12896.

88. Auber, M.; Fröhlich, D.; Drechsel, O.; Karaulanov, E.; Krämer-Albers, E.-M., Serum-free media supplements carry miRNAs that co-purify with extracellular vesicles. *J Extracell Vesicles* **2019,** *8* (1), 1656042 DOI: 10.1080/20013078.2019.1656042.

89. Sidhom, K.; Obi, P. O.; Saleem, A., A Review of Exosomal Isolation Methods: Is Size Exclusion Chromatography the Best Option? *Int J Mol Sci* **2020,** *21* (18), 6466.

90. Lucchetti, D.; Fattorossi, A.; Sgambato, A., Extracellular Vesicles in Oncology: Progress and Pitfalls in the Methods of Isolation and Analysis. *Biotechnology Journal* **2019,** *14* (1), 1700716 DOI: https://doi.org/10.1002/biot.201700716.

91. Liu, C.; Zhao, J.; Tian, F.; Chang, J.; Zhang, W.; Sun, J., λ-DNA- and Aptamer-Mediated Sorting and Analysis of Extracellular Vesicles. *Journal of the American Chemical Society* **2019,** *141* (9), 3817-3821 DOI: 10.1021/jacs.9b00007.

92. Böing, A. N.; van der Pol, E.; Grootemaat, A. E.; Coumans, F. A. W.; Sturk, A.; Nieuwland, R., Single-step isolation of extracellular vesicles by size-exclusion chromatography. *J Extracell Vesicles* **2014,** *3* (1), 23430 DOI: 10.3402/jev.v3.23430.

93. Chiriacò, M. S.; Bianco, M.; Nigro, A.; Primiceri, E.; Ferrara, F.; Romano, A.; Quattrini, A.; Furlan, R.; Arima, V.; Maruccio, G., Lab-on-Chip for Exosomes and Microvesicles Detection and Characterization. *Sensors (Basel)* **2018,** *18* (10), DOI: 10.3390/s18103175.

94. Momen-Heravi, F., Isolation of Extracellular Vesicles by Ultracentrifugation. *Methods Mol Biol* **2017,** *1660*, 25-32 DOI: 10.1007/978-1-4939-7253-1_3.

95. Niu, Z.; Pang, R. T. K.; Liu, W.; Li, Q.; Cheng, R.; Yeung, W. S. B., Polymer-based precipitation preserves biological activities of extracellular vesicles from an endometrial cell line. *PLOS ONE* **2017,** *12* (10), e0186534 DOI: 10.1371/journal.pone.0186534.

96. Pedersen, K. W.; Kierulf, B.; Neurauter, A., Specific and Generic Isolation of Extracellular Vesicles with Magnetic Beads. *Methods Mol Biol* **2017,** *1660*, 65-87 DOI: 10.1007/978-1-4939-7253-1_7.

97. Serrano-Pertierra, E.; Oliveira-Rodríguez, M.; Matos, M.; Gutiérrez, G.; Moyano, A.; Salvador, M.; Rivas, M.; Blanco-López, M. C., Extracellular Vesicles: Current Analytical Techniques for Detection and Quantification. *Biomolecules* **2020,** *10* (6), 824 DOI: 10.3390/biom10060824.

98. Tauro, B. J.; Greening, D. W.; Mathias, R. A.; Ji, H.; Mathivanan, S.; Scott, A. M.; Simpson, R. J., Comparison of ultracentrifugation, density gradient separation, and immunoaffinity capture methods for isolating human colon cancer cell line LIM1863-derived exosomes. *Methods* **2012,** *56* (2), 293-304 DOI: https://doi.org/10.1016/j.ymeth.2012.01.002.

99. Gardiner, C.; Vizio, D. D.; Sahoo, S.; Théry, C.; Witwer, K. W.; Wauben, M.; Hill, A. F., Techniques used for the isolation and characterization of extracellular vesicles: results of a worldwide survey. *J Extracell Vesicles* **2016,** *5* (1), 32945 DOI: 10.3402/jev.v5.32945.

100. Kowal, E. J. K.; Ter-Ovanesyan, D.; Regev, A.; Church, G. M., Extracellular Vesicle Isolation and Analysis by Western Blotting. In *Extracellular Vesicles: Methods and Protocols*, Kuo, W. P.; Jia, S., Eds. Springer New York: New York, NY, 2017; pp 143-152.

101. Kowal, J.; Arras, G.; Colombo, M.; Jouve, M.; Morath, J. P.; Primdal-Bengtson, B.; Dingli, F.; Loew, D.; Tkach, M.; Théry, C., Proteomic comparison defines novel markers to characterize heterogeneous populations of extracellular vesicle subtypes. **2016,** *113* (8), E968-E977 DOI: 10.1073/pnas.1521230113 %J Proceedings of the National Academy of Sciences.

102. Amber Gonda, R. M., Janviere Kabagwira, Paul A. Vallejos and Nathan R. Wall Cellular-Defined Microenvironmental Internalization of Exosomes, Extracellular Vesicles and Their Importance in Human Health, Ana Gil De Bona and Jose Antonio Reales Calderon *IntechOpen* **2019**, DOI: DOI: 10.5772/intechopen.86020. .

103. Kaddour, H.; Panzner, T. D.; Welch, J. L.; Shouman, N.; Mohan, M.; Stapleton, J. T.; Okeoma, C. M., Electrostatic Surface Properties of Blood and Semen Extracellular Vesicles: Implications of Sialylation and HIV-Induced Changes on EV Internalization. *Viruses* **2020,** *12* (10), 1117.

104. Sharma, S.; Rasool, H. I.; Palanisamy, V.; Mathisen, C.; Schmidt, M.; Wong, D. T.; Gimzewski, J. K., Structural-Mechanical Characterization of Nanoparticle Exosomes in Human Saliva, Using Correlative AFM, FESEM, and Force Spectroscopy. *ACS Nano* **2010,** *4* (4), 1921-1926 DOI: 10.1021/nn901824n.

105. Rupert, D. L. M.; Claudio, V.; Lässer, C.; Bally, M., Methods for the physical characterization and quantification of extracellular vesicles in biological samples. *Biochimica et Biophysica Acta (BBA) - General Subjects* **2017,** *1861* (1, Part A), 3164-3179 DOI: https://doi.org/10.1016/j.bbagen.2016.07.028.

106. Welsh, J. A.; Holloway, J. A.; Wilkinson, J. S.; Englyst, N. A., Extracellular Vesicle Flow Cytometry Analysis and Standardization. *Frontiers in Cell and Developmental Biology* **2017,** *5* (78), DOI: 10.3389/fcell.2017.00078.

107. Gandham, S.; Su, X.; Wood, J.; Nocera, A. L.; Alli, S. C.; Milane, L.; Zimmerman, A.; Amiji, M.; Ivanov, A. R., Technologies and Standardization in Research on Extracellular Vesicles. *Trends in Biotechnology* **2020,** *38* (10), 1066-1098 DOI: https://doi.org/10.1016/j.tibtech.2020.05.012.

108. Midekessa, G.; Godakumara, K.; Ord, J.; Viil, J.; Lättekivi, F.; Dissanayake, K.; Kopanchuk, S.; Rinken, A.; Andronowska, A.; Bhattacharjee, S.; Rinken, T.; Fazeli, A., Zeta Potential of Extracellular Vesicles: Toward Understanding the Attributes that Determine Colloidal Stability. *ACS Omega* **2020,** *5* (27), 16701-16710 DOI: 10.1021/acsomega.0c01582.

109. Théry, C.; Witwer, K. W.; Aikawa, E.; Alcaraz, M. J.; Anderson, J. D.; Andriantsitohaina, R.; Antoniou, A.; Arab, T.; Archer, F.; Atkin-Smith, G. K.; Ayre, D. C.; Bach, J.-M.; Bachurski, D.; Baharvand, H.; Balaj, L.; Baldacchino, S.; Bauer, N. N.; Baxter, A. A.; Bebawy, M.; Beckham, C.; Bedina Zavec, A.; Benmoussa, A.; Berardi, A. C.; Bergese, P.; Bielska, E.; Blenkiron, C.; Bobis-Wozowicz, S.; Boilard, E.; Boireau, W.; Bongiovanni, A.; Borràs, F. E.; Bosch, S.; Boulanger, C. M.; Breakefield, X.; Breglio, A. M.; Brennan, M. Á.; Brigstock, D. R.; Brisson, A.; Broekman, M. L. D.; Bromberg, J. F.; Bryl-Górecka, P.; Buch, S.; Buck, A. H.; Burger, D.; Busatto, S.; Buschmann, D.; Bussolati, B.; Buzás, E. I.; Byrd, J. B.; Camussi, G.; Carter, D. R. F.; Caruso, S.; Chamley, L. W.; Chang, Y.-T.; Chen, C.; Chen, S.; Cheng, L.; Chin, A. R.; Clayton, A.; Clerici, S. P.; Cocks, A.; Cocucci, E.; Coffey, R. J.; Cordeiro-da-Silva, A.; Couch, Y.; Coumans, F. A. W.; Coyle, B.; Crescitelli, R.; Criado, M. F.; D'Souza-Schorey, C.; Das, S.; Datta Chaudhuri, A.; de Candia, P.; De Santana, E. F.; De Wever, O.; del Portillo, H. A.; Demaret, T.; Deville, S.; Devitt, A.; Dhondt, B.; Di Vizio, D.; Dieterich, L. C.; Dolo, V.; Dominguez Rubio, A. P.; Dominici, M.; Dourado, M. R.; Driedonks, T. A. P.; Duarte, F. V.; Duncan, H. M.; Eichenberger, R. M.; Ekström, K.; El Andaloussi, S.; Elie-Caille, C.; Erdbrügger, U.;

Falcón-Pérez, J. M.; Fatima, F.; Fish, J. E.; Flores-Bellver, M.; Försönits, A.; Frelet-Barrand, A.; Fricke, F.; Fuhrmann, G.; Gabrielsson, S.; Gámez-Valero, A.; Gardiner, C.; Gärtner, K.; Gaudin, R.; Gho, Y. S.; Giebel, B.; Gilbert, C.; Gimona, M.; Giusti, I.; Goberdhan, D. C. I.; Görgens, A.; Gorski, S. M.; Greening, D. W.; Gross, J. C.; Gualerzi, A.; Gupta, G. N.; Gustafson, D.; Handberg, A.; Haraszti, R. A.; Harrison, P.; Hegyesi, H.; Hendrix, A.; Hill, A. F.; Hochberg, F. H.; Hoffmann, K. F.; Holder, B.; Holthofer, H.; Hosseinkhani, B.; Hu, G.; Huang, Y.; Huber, V.; Hunt, S.; Ibrahim, A. G.-E.; Ikezu, T.; Inal, J. M.; Isin, M.; Ivanova, A.; Jackson, H. K.; Jacobsen, S.; Jay, S. M.; Jayachandran, M.; Jenster, G.; Jiang, L.; Johnson, S. M.; Jones, J. C.; Jong, A.; Jovanovic-Talisman, T.; Jung, S.; Kalluri, R.; Kano, S.-i.; Kaur, S.; Kawamura, Y.; Keller, E. T.; Khamari, D.; Khomyakova, E.; Khvorova, A.; Kierulf, P.; Kim, K. P.; Kislinger, T.; Klingeborn, M.; Klinke, D. J.; Kornek, M.; Kosanović, M. M.; Kovács, Á. F.; Krämer-Albers, E.-M.; Krasemann, S.; Krause, M.; Kurochkin, I. V.; Kusuma, G. D.; Kuypers, S.; Laitinen, S.; Langevin, S. M.; Languino, L. R.; Lannigan, J.; Lässer, C.; Laurent, L. C.; Lavieu, G.; Lázaro-Ibáñez, E.; Le Lay, S.; Lee, M.-S.; Lee, Y. X. F.; Lemos, D. S.; Lenassi, M.; Leszczynska, A.; Li, I. T. S.; Liao, K.; Libregts, S. F.; Ligeti, E.; Lim, R.; Lim, S. K.; Linē, A.; Linnemannstöns, K.; Llorente, A.; Lombard, C. A.; Lorenowicz, M. J.; Lörincz, Á. M.; Lötvall, J.; Lovett, J.; Lowry, M. C.; Loyer, X.; Lu, Q.; Lukomska, B.; Lunavat, T. R.; Maas, S. L. N.; Malhi, H.; Marcilla, A.; Mariani, J.; Mariscal, J.; Martens-Uzunova, E. S.; Martin-Jaular, L.; Martinez, M. C.; Martins, V. R.; Mathieu, M.; Mathivanan, S.; Maugeri, M.; McGinnis, L. K.; McVey, M. J.; Meckes, D. G.; Meehan, K. L.; Mertens, I.; Minciacchi, V. R.; Möller, A.; Møller Jørgensen, M.; Morales-Kastresana, A.; Morhayim, J.; Mullier, F.; Muraca, M.; Musante, L.; Mussack, V.; Muth, D. C.; Myburgh, K. H.; Najrana, T.; Nawaz, M.; Nazarenko, I.; Nejsum, P.; Neri, C.; Neri, T.; Nieuwland, R.; Nimrichter, L.; Nolan, J. P.; Nolte-'t Hoen, E. N. M.; Noren Hooten, N.; O'Driscoll, L.; O'Grady, T.; O'Loghlen, A.; Ochiya, T.; Olivier, M.; Ortiz, A.; Ortiz, L. A.; Osteikoetxea, X.; Østergaard, O.; Ostrowski, M.; Park, J.; Pegtel, D. M.; Peinado, H.; Perut, F.; Pfaffl, M. W.; Phinney, D. G.; Pieters, B. C. H.; Pink, R. C.; Pisetsky, D. S.; Pogge von Strandmann, E.; Polakovicova, I.; Poon, I. K. H.; Powell, B. H.; Prada, I.; Pulliam, L.; Quesenberry, P.; Radeghieri, A.; Raffai, R. L.; Raimondo, S.; Rak, J.; Ramirez, M. I.; Raposo, G.; Rayyan, M. S.; Regev-Rudzki, N.; Ricklefs, F. L.; Robbins, P. D.; Roberts, D. D.; Rodrigues, S. C.; Rohde, E.; Rome, S.; Rouschop, K. M. A.; Rughetti, A.; Russell, A. E.; Saá, P.; Sahoo, S.; Salas-Huenuleo, E.; Sánchez, C.; Saugstad, J. A.; Saul, M. J.; Schiffelers, R. M.; Schneider, R.; Schøyen, T. H.; Scott, A.; Shahaj, E.; Sharma, S.; Shatnyeva, O.; Shekari, F.; Shelke, G. V.; Shetty, A. K.; Shiba, K.; Siljander, P. R. M.; Silva, A. M.; Skowronek, A.; Snyder, O. L.; Soares, R. P.; Sódar, B. W.; Soekmadji, C.; Sotillo, J.; Stahl, P. D.; Stoorvogel, W.; Stott, S. L.; Strasser, E. F.; Swift, S.; Tahara, H.; Tewari, M.; Timms, K.; Tiwari, S.; Tixeira, R.; Tkach, M.; Toh, W. S.; Tomasini, R.; Torrecilhas, A. C.; Tosar, J. P.; Toxavidis, V.; Urbanelli, L.; Vader, P.; van Balkom, B. W. M.; van der Grein, S. G.; Van Deun, J.; van Herwijnen, M. J. C.; Van Keuren-Jensen, K.; van Niel, G.; van Royen, M. E.; van Wijnen, A. J.; Vasconcelos, M. H.; Vechetti, I. J.; Veit, T. D.; Vella, L. J.; Velot, É.; Verweij, F. J.; Vestad, B.; Viñas, J. L.; Visnovitz, T.; Vukman, K. V.; Wahlgren, J.; Watson, D. C.; Wauben, M. H. M.; Weaver, A.; Webber, J. P.; Weber, V.; Wehman, A. M.; Weiss, D. J.; Welsh, J. A.; Wendt, S.; Wheelock, A. M.; Wiener, Z.; Witte, L.;

Wolfram, J.; Xagorari, A.; Xander, P.; Xu, J.; Yan, X.; Yáñez-Mó, M.; Yin, H.; Yuana, Y.; Zappulli, V.; Zarubova, J.; Žėkas, V.; Zhang, J.-y.; Zhao, Z.; Zheng, L.; Zheutlin, A. R.; Zickler, A. M.; Zimmermann, P.; Zivkovic, A. M.; Zocco, D.; Zuba-Surma, E. K., Minimal information for studies of extracellular vesicles 2018 (MISEV2018): a position statement of the International Society for Extracellular Vesicles and update of the MISEV2014 guidelines. *J Extracell Vesicles* **2018,** *7* (1), 1535750 DOI: 10.1080/20013078.2018.1535750.

110. Buzás, E. I.; Tóth, E. Á.; Sódar, B. W.; Szabó-Taylor, K. É., Molecular interactions at the surface of extracellular vesicles. *Seminars in immunopathology* **2018,** *40* (5), 453-464 DOI: 10.1007/s00281-018-0682-0.

111. Lösche, W.; Scholz, T.; Temmler, U.; Oberle, V.; Claus, R. A., Platelet-derived microvesicles transfer tissue factor to monocytes but not to neutrophils. *Platelets* **2004,** *15* (2), 109-15 DOI: 10.1080/09537100310001649885.

112. Eken, C.; Gasser, O.; Zenhaeusern, G.; Oehri, I.; Hess, C.; Schifferli, J. A., Polymorphonuclear Neutrophil-Derived Ectosomes Interfere with the Maturation of Monocyte-Derived Dendritic Cells. **2008,** *180* (2), 817-824 DOI: 10.4049/jimmunol.180.2.817 %J The Journal of Immunology.

113. Kuravi, S. J.; Harrison, P.; Rainger, G. E.; Nash, G. B., Ability of Platelet-Derived Extracellular Vesicles to Promote Neutrophil-Endothelial Cell Interactions. *Inflammation* **2019,** *42* (1), 290-305 DOI: 10.1007/s10753-018-0893-5.

114. Rossaint, J.; Kühne, K.; Skupski, J.; Van Aken, H.; Looney, M. R.; Hidalgo, A.; Zarbock, A., Directed transport of neutrophil-derived extracellular vesicles enables platelet-mediated innate immune response. *Nature Communications* **2016,** *7* (1), 13464 DOI: 10.1038/ncomms13464.

115. French, K. C.; Antonyak, M. A.; Cerione, R. A., Extracellular vesicle docking at the cellular port: Extracellular vesicle binding and uptake. *Seminars in cell & developmental biology* **2017,** *67*, 48-55 DOI: 10.1016/j.semcdb.2017.01.002.

116. Wiklander, O. P. B.; Nordin, J. Z.; O'Loughlin, A.; Gustafsson, Y.; Corso, G.; Mäger, I.; Vader, P.; Lee, Y.; Sork, H.; Seow, Y.; Heldring, N.; Alvarez-Erviti, L.; Smith, C. I. E.; Le Blanc, K.; Macchiarini, P.; Jungebluth, P.; Wood, M. J. A.; Andaloussi, S. E., Extracellular vesicle in vivo biodistribution is determined by cell source, route of administration and targeting. *J Extracell Vesicles* **2015,** *4*, 26316-26316 DOI: 10.3402/jev.v4.26316.

117. Christianson, H. C.; Svensson, K. J.; Belting, M., Exosome and microvesicle mediated phene transfer in mammalian cells. *Seminars in Cancer Biology* **2014,** *28*, 31-38 DOI: https://doi.org/10.1016/j.semcancer.2014.04.007.

118. William, C. N.; Joseph, W. K.; John, Z. Q. L.; LuGuang, L., Stem cell-derived exosomes: a novel vector for tissue repair and diabetic therapy. *Journal of Molecular Endocrinology* **2017,** *59* (4), R155-R165 DOI: 10.1530/JME-17-0080.

119. Prada, I.; Meldolesi, J., Binding and Fusion of Extracellular Vesicles to the Plasma Membrane of Their Cell Targets. *International journal of molecular sciences* **2016,** *17* (8), 1296 DOI: 10.3390/ijms17081296.

120. Urbanelli, L.; Magini, A.; Buratta, S.; Brozzi, A.; Sagini, K.; Polchi, A.; Tancini, B.; Emiliani, C., Signaling pathways in exosomes biogenesis, secretion and fate. *Genes (Basel)* **2013,** *4* (2), 152-170 DOI: 10.3390/genes4020152.

121. Zech, D.; Rana, S.; Büchler, M. W.; Zöller, M., Tumor-exosomes and leukocyte activation: an ambivalent crosstalk. *Cell Commun Signal* **2012,** *10* (1), 37 DOI: 10.1186/1478-811x-10-37.

122. Brameshuber, M.; Schütz, G. J., Single Molecule Measurements in Membranes☆. In *Reference Module in Life Sciences*, Elsevier: 2017.

123. Johnson, S. J.; Bayerl, T. M.; McDermott, D. C.; Adam, G. W.; Rennie, A. R.; Thomas, R. K.; Sackmann, E., Structure of an adsorbed dimyristoylphosphatidylcholine bilayer measured with specular reflection of neutrons. *Biophysical Journal* **1991,** *59* (2), 289-294 DOI: https://doi.org/10.1016/S0006-3495(91)82222-6.

124. Khan, M. S.; Dosoky, N. S.; Williams, J. D., Engineering lipid bilayer membranes for protein studies. *Int J Mol Sci* **2013,** *14* (11), 21561-21597 DOI: 10.3390/ijms141121561.

125. Andersson, J.; Köper, I., Tethered and Polymer Supported Bilayer Lipid Membranes: Structure and Function. *Membranes (Basel)* **2016,** *6* (2), 30 DOI: 10.3390/membranes6020030.

126. Reich, C.; Andruzzi, L., Preparation of fluid tethered lipid bilayers on poly(ethylene glycol) by spin-coating. *Soft Matter* **2010,** *6* (3), 493-500 DOI: 10.1039/B917497D.

127. Goennenwein, S.; Tanaka, M.; Hu, B.; Moroder, L.; Sackmann, E., Functional incorporation of integrins into solid supported membranes on ultrathin films of cellulose: impact on adhesion. *Biophysical journal* **2003,** *85* (1), 646-655 DOI: 10.1016/S0006-3495(03)74508-1.

128. Elender, G.; Kühner, M.; Sackmann, E., Functionalisation of Si/SiO2 and glass surfaces with ultrathin dextran films and deposition of lipid bilayers. *Biosensors and Bioelectronics* **1996,** *11* (6), 565-577 DOI: https://doi.org/10.1016/0956-5663(96)83292-1.

129. Mashaghi, S.; van Oijen, A. M., A versatile approach to the generation of fluid supported lipid bilayers and its applications. *Biotechnol Bioeng* **2014,** *111* (10), 2076-81 DOI: 10.1002/bit.25273.

130. Ye, Q.; Konradi, R.; Textor, M.; Reimhult, E., Liposomes Tethered to Omega-Functional PEG Brushes and Induced Formation of PEG Brush Supported Planar Lipid Bilayers. *Langmuir* **2009,** *25* (23), 13534-13539 DOI: 10.1021/la902039g.

131. Wagner, M. L.; Tamm, L. K., Tethered Polymer-Supported Planar Lipid Bilayers for Reconstitution of Integral Membrane Proteins: Silane-Polyethyleneglycol-Lipid as a Cushion and Covalent Linker. *Biophysical Journal* **2000,** *79* (3), 1400-1414 DOI: https://doi.org/10.1016/S0006-3495(00)76392-2.

132. Hsia, C.-Y.; Jason Richards, M.; Daniel, S., *A review of traditional and emerging methods to characterize lipid-protein interactions in biological membranes*. 2015; Vol. 7.

133. Rigaud, J.-L.; Lévy, D., Reconstitution of Membrane Proteins into Liposomes. In *Methods in Enzymology*, Academic Press: 2003; Vol. 372, pp 65-86.

134. Mirbagheri, M.; Adibnia, V.; Hughes, B.; Waldman, S.; Banquy, X.; Hwang, D. K., Advanced cell culture platforms: A growing quest for emulating natural tissues. *Materials Horizons* **2018,** *6*, DOI: 10.1039/C8MH00803E.

135. Dustin, M. L., Supported bilayers at the vanguard of immune cell activation studies. *J Struct Biol* **2009,** *168* (1), 152-160 DOI: 10.1016/j.jsb.2009.05.007.

136. Thid, D.; Holm, K.; Eriksson, P. S.; Ekeroth, J.; Kasemo, B.; Gold, J., Supported phospholipid bilayers as a platform for neural progenitor cell culture. *Journal of Biomedical Materials Research Part A* **2008,** *84A* (4), 940-953 DOI: https://doi.org/10.1002/jbm.a.31358.

137. Hao, W.; Han, J.; Chu, Y.; Huang, L.; Sun, J.; Zhuang, Y.; Li, X.; Ma, H.; Chen, Y.; Dai, J., Lower fluidity of supported lipid bilayers promotes neuronal differentiation of neural stem cells by enhancing focal adhesion formation. *Biomaterials* **2018,** *161*, 106-116 DOI: https://doi.org/10.1016/j.biomaterials.2018.01.034.

138. González-García, C.; Moratal, D.; Oreffo, R. O. C.; Dalby, M. J.; Salmerón-Sánchez, M., Surface mobility regulates skeletal stem cell differentiation. *Integrative Biology* **2012,** *4* (5), 531-539 DOI: 10.1039/C2IB00139J.

139. Huth, M.; Hertrich, S.; Mezo, G.; Madarasz, E.; Nickel, B., Neural Stem Cell Spreading on Lipid Based Artificial Cell Surfaces, Characterized by Combined X-ray and Neutron Reflectometry. *Materials (Basel)* **2010,** *3* (11), 4994-5006 DOI: 10.3390/ma3114994.

140. Biswas, K. H.; Hartman, K. L.; Yu, C.-h.; Harrison, O. J.; Song, H.; Smith, A. W.; Huang, W. Y. C.; Lin, W.-C.; Guo, Z.; Padmanabhan, A.; Troyanovsky, S. M.; Dustin, M. L.; Shapiro, L.; Honig, B.; Zaidel-Bar, R.; Groves, J. T., E-cadherin junction formation involves an active kinetic nucleation process. *Proceedings of the National Academy of Sciences* **2015,** *112* (35), 10932-10937 DOI: 10.1073/pnas.1513775112.

141. Barker, S. L.; LaRocca, P. J., Method of production and control of a commercial tissue culture surface. *Journal of tissue culture methods* **1994,** *16* (3), 151-153 DOI: 10.1007/BF01540642.

142. Harrison, R. G., ON THE STEREOTROPISM OF EMBRYONIC CELLS. *Science* **1911,** *34* (870), 279-81 DOI: 10.1126/science.34.870.279.

143. Zeiger, A. S.; Hinton, B.; Van Vliet, K. J., Why the dish makes a difference: quantitative comparison of polystyrene culture surfaces. *Acta Biomater* **2013,** *9* (7), 7354-61 DOI: 10.1016/j.actbio.2013.02.035.

144. Altering bacteriological plastic petri dishes for tissue culture use. *Public Health Rep* **1966,** *81* (9), 843-4.

145. Lerman, M. J.; Lembong, J.; Muramoto, S.; Gillen, G.; Fisher, J. P., The Evolution of Polystyrene as a Cell Culture Material. *Tissue Eng Part B Rev* **2018,** *24* (5), 359-372 DOI: 10.1089/ten.TEB.2018.0056.

146. Hoffman, B. D., Chapter One - The Detection and Role of Molecular Tension in Focal Adhesion Dynamics. In *Progress in Molecular Biology and Translational Science*, Engler, A. J.; Kumar, S., Eds. Academic Press: 2014; Vol. 126, pp 3-24.

147. Warrick, J. W.; Murphy, W. L.; Beebe, D. J., Screening the cellular microenvironment: a role for microfluidics. *IEEE Rev Biomed Eng* **2008,** *1* (1), 75-93 DOI: 10.1109/RBME.2008.2008241.

148. Mazia, D.; Schatten, G.; Sale, W., Adhesion of cells to surfaces coated with polylysine. Applications to electron microscopy. *J Cell Biol* **1975,** *66* (1), 198-200 DOI: 10.1083/jcb.66.1.198.

149. Malindisa, S.; Joseph, J.; Ntwasa, M., Two-Dimensional (2D) and Three-Dimensional (3D) Cell Culturing in Drug Discovery. 2019.

150. Knobloch, J.; Suhendro, D. K.; Zieleniecki, J. L.; Shapter, J. G.; Köper, I., Membrane-drug interactions studied using model membrane systems. *Saudi J Biol Sci* **2015,** *22* (6), 714-718 DOI: 10.1016/j.sjbs.2015.03.007.

151. Huang, C.-J.; Chang, Y.-C., Construction of Cell–Extracellular Matrix Microenvironments by Conjugating ECM Proteins on Supported Lipid Bilayers. *Frontiers in Materials* **2019,** *6* (39), DOI: 10.3389/fmats.2019.00039.

152. Vafaei, S.; Tabaei, S. R.; Biswas, K. H.; Groves, J. T.; Cho, N. J., Dynamic Cellular Interactions with Extracellular Matrix Triggered by Biomechanical Tuning of Low-Rigidity, Supported Lipid Membranes. *Adv Healthc Mater* **2017,** *6* (10), DOI: 10.1002/adhm.201700243.

153. Kamaloo, E., *Supported lipid bilayer interactions with nanoparticles, peptides and polymers*. Worcester Polytechnic Institute: 2018.

154. Takai, Y.; Reed, M. L.; Burakoff, S. J.; Herrmann, S. H., Direct evidence for a receptor-ligand interaction between the T-cell surface antigen CD2 and lymphocyte-function-associated antigen 3. *Proc Natl Acad Sci U S A* **1987,** *84* (19), 6864-8 DOI: 10.1073/pnas.84.19.6864.

155. Grakoui, A.; Bromley, S. K.; Sumen, C.; Davis, M. M.; Shaw, A. S.; Allen, P. M.; Dustin, M. L., The Immunological Synapse: A Molecular Machine Controlling T Cell Activation. *Science* **1999,** *285* (5425), 221-227 DOI: 10.1126/science.285.5425.221.

156. Groves, J. T.; Dustin, M. L., Supported planar bilayers in studies on immune cell adhesion and communication. *Journal of Immunological Methods* **2003,** *278* (1), 19-32 DOI: https://doi.org/10.1016/S0022-1759(03)00193-5.

157. Orth, R. N.; Wu, M.; Holowka, D. A.; Craighead, H. G.; Baird, B. A., Mast Cell Activation on Patterned Lipid Bilayers of Subcellular Dimensions. *Langmuir* **2003,** *19* (5), 1599-1605 DOI: 10.1021/la026314c.

158. Glazier, R.; Salaita, K., Supported lipid bilayer platforms to probe cell mechanobiology. *Biochimica et Biophysica Acta (BBA) - Biomembranes* **2017,** *1859* (9, Part A), 1465-1482 DOI: https://doi.org/10.1016/j.bbamem.2017.05.005.

159. Verstappen, J. F. M.; Jin, J.; Koçer, G.; Haroon, M.; Jonkheijm, P.; Bakker, A. D.; Klein-Nulend, J.; Jaspers, R. T., RGD-functionalized supported lipid bilayers modulate pre-osteoblast adherence and promote osteogenic differentiation. *J Biomed Mater Res A* **2020,** *108* (4), 923-937 DOI: 10.1002/jbm.a.36870.

160. Wessels, L.; Elting, M. W.; Scimeca, D.; Weninger, K., Rapid Membrane Fusion of Individual Virus Particles with Supported Lipid Bilayers. *Biophysical Journal* **2007,** *93* (2), 526-538 DOI: https://doi.org/10.1529/biophysj.106.097485.

161. Costello, D. A.; Millet, J. K.; Hsia, C.-Y.; Whittaker, G. R.; Daniel, S., Single particle assay of coronavirus membrane fusion with proteinaceous receptor-embedded supported bilayers. *Biomaterials* **2013,** *34* (32), 7895-7904 DOI: https://doi.org/10.1016/j.biomaterials.2013.06.034.

162. Biswas, K. H.; Groves, J. T., Hybrid Live Cell–Supported Membrane Interfaces for Signaling Studies. *Annual Review of Biophysics* **2019,** *48* (1), 537-562 DOI: 10.1146/annurev-biophys-070317-033330.

163. Andersson, A.-S.; Glasmästar, K.; Sutherland, D.; Lidberg, U.; Kasemo, B., Cell adhesion on supported lipid bilayers. **2003,** *64A* (4), 622-629 DOI: doi:10.1002/jbm.a.10442.

164. Kam, L.; Boxer, S. G., Cell adhesion to protein-micropatterned-supported lipid bilayer membranes. **2001,** *55* (4), 487-495 DOI: doi:10.1002/1097-4636(20010615)55:4<487::AID-JBM1041>3.0.CO;2-7.

165. Castellana, E. T.; Cremer, P. S., Solid supported lipid bilayers: From biophysical studies to sensor design. *Surf Sci Rep* **2006,** *61* (10), 429-444 DOI: https://doi.org/10.1016/j.surfrep.2006.06.001.

166. Zhu, X.; Wang, Z.; Zhao, A.; Huang, N.; Chen, H.; Zhou, S.; Xie, X., Cell adhesion on supported lipid bilayers functionalized with RGD peptides monitored by using a quartz crystal microbalance with dissipation. *Colloids and Surfaces B: Biointerfaces* **2014,** *116*, 459-464 DOI: https://doi.org/10.1016/j.colsurfb.2014.01.032.

167. Svedhem, S.; Dahlborg, D.; Ekeroth, J.; Kelly, J.; Höök, F.; Gold, J., In Situ Peptide-Modified Supported Lipid Bilayers for Controlled Cell Attachment. *Langmuir* **2003,** *19* (17), 6730-6736 DOI: 10.1021/la034172w.

168. Glasmästar, K.; Larsson, C.; Höök, F.; Kasemo, B., Protein adsorption on supported phospholipid bilayers. *J Colloid Interface Sci* **2002,** *246* (1), 40-7 DOI: 10.1006/jcis.2001.8060.

169. Bechinger, B., Supported Lipid Bilayers. In *Encyclopedia of Biophysics*, Roberts, G. C. K., Ed. Springer Berlin Heidelberg: Berlin, Heidelberg, 2013; pp 2522-2528.

170. Kiessling, V.; Yang, S.-T.; Tamm, L. K., Chapter One - Supported Lipid Bilayers as Models for Studying Membrane Domains. In *Current Topics in Membranes*, Kenworthy, A. K., Ed. Academic Press: 2015; Vol. 75, pp 1-23.

171. Ollivon, M.; Lesieur, S.; Grabielle-Madelmont, C.; Paternostre, M. t., Vesicle reconstitution from lipid–detergent mixed micelles. *Biochimica et Biophysica Acta (BBA) - Biomembranes* **2000,** *1508* (1), 34-50 DOI: https://doi.org/10.1016/S0304-4157(00)00006-X.

172. Vacklin, H. P.; Tiberg, F.; Thomas, R. K., Formation of supported phospholipid bilayers via co-adsorption with β-d-dodecyl maltoside. *Biochimica et Biophysica Acta (BBA) - Biomembranes* **2005,** *1668* (1), 17-24 DOI: https://doi.org/10.1016/j.bbamem.2004.11.001.

173. Lind, T. K.; Cárdenas, M., Understanding the formation of supported lipid bilayers via vesicle fusion—A case that exemplifies the need for the complementary method approach (Review). *Biointerphases* **2016,** *11* (2), 020801 DOI: 10.1116/1.4944830.

174. Jackman, J. A.; Cho, N.-J., Supported Lipid Bilayer Formation: Beyond Vesicle Fusion. *Langmuir* **2020,** *36* (6), 1387-1400 DOI: 10.1021/acs.langmuir.9b03706.

175. Brian, A. A.; McConnell, H. M., Allogeneic stimulation of cytotoxic T cells by supported planar membranes. *Proc Natl Acad Sci U S A* **1984,** *81* (19), 6159-6163 DOI: 10.1073/pnas.81.19.6159.

176. Kalb, E.; Frey, S.; Tamm, L. K., Formation of supported planar bilayers by fusion of vesicles to supported phospholipid monolayers. *Biochimica et Biophysica Acta (BBA)*

- *Biomembranes* **1992,** *1103* (2), 307-316 DOI: https://doi.org/10.1016/0005-2736(92)90101-Q.

177. McConnell, H. M.; Watts, T. H.; Weis, R. M.; Brian, A. A., Supported planar membranes in studies of cell-cell recognition in the immune system. *Biochim Biophys Acta* **1986,** *864* (1), 95-106 DOI: 10.1016/0304-4157(86)90016-x.

178. Lin, C.-M.; Li, C.-S.; Sheng, Y.-J.; Wu, D. T.; Tsao, H.-K., Size-Dependent Properties of Small Unilamellar Vesicles Formed by Model Lipids. *Langmuir* **2012,** *28* (1), 689-700 DOI: 10.1021/la203755v.

179. Mayer, L. D.; Hope, M. J.; Cullis, P. R., Vesicles of variable sizes produced by a rapid extrusion procedure. *Biochim Biophys Acta* **1986,** *858* (1), 161-8 DOI: 10.1016/0005-2736(86)90302-0.

180. Barenholz, Y.; Gibbes, D.; Litman, B. J.; Goll, J.; Thompson, T. E.; Carlson, F. D., A simple method for the preparation of homogeneous phospholipid vesicles. *Biochemistry* **1977,** *16* (12), 2806-2810 DOI: 10.1021/bi00631a035.

181. Gains, N.; Hauser, H., Small unilamellar vesicles can be formed by changing the pH: is this one aspect of a more general phenomenon? *Journal of Membrane Science* **1985,** *22* (2), 225-234 DOI: https://doi.org/10.1016/S0376-7388(00)81282-X.

182. Hardy, G. J.; Nayak, R.; Zauscher, S., Model cell membranes: Techniques to form complex biomimetic supported lipid bilayers via vesicle fusion. *Curr Opin Colloid Interface Sci* **2013,** *18* (5), 448-458 DOI: 10.1016/j.cocis.2013.06.004.

183. Mingeot-Leclercq, M. P.; Deleu, M.; Brasseur, R.; Dufrêne, Y. F., Atomic force microscopy of supported lipid bilayers. *Nat Protoc* **2008,** *3* (10), 1654-9 DOI: 10.1038/nprot.2008.149.

184. Reimhult, E.; Höök, F.; Kasemo, B., Temperature dependence of formation of a supported phospholipid bilayer from vesicles on SiO2. *Phys Rev E Stat Nonlin Soft Matter Phys* **2002,** *66* (5 Pt 1), 051905 DOI: 10.1103/PhysRevE.66.051905.

185. Reimhult, E.; Höök, F.; Kasemo, B., Intact Vesicle Adsorption and Supported Biomembrane Formation from Vesicles in Solution: Influence of Surface Chemistry, Vesicle Size, Temperature, and Osmotic Pressure. *Langmuir* **2003,** *19* (5), 1681-1691 DOI: 10.1021/la0263920.

186. Berquand, A.; Mazeran, P.-E.; Pantigny, J.; Proux-Delrouyre, V.; Laval, J.-M.; Bourdillon, C., Two-Step Formation of Streptavidin-Supported Lipid Bilayers by PEG-Triggered Vesicle Fusion. Fluorescence and Atomic Force Microscopy Characterization. *Langmuir* **2003,** *19* (5), 1700-1707 DOI: 10.1021/la0260180.

187. Sanderson, J. M., Resolving the kinetics of lipid, protein and peptide diffusion in membranes. *Molecular Membrane Biology* **2012,** *29* (5), 118-143 DOI: 10.3109/09687688.2012.678018.

188. Aisenbrey, C.; Bertani, P.; Bechinger, B., Solid-State NMR Investigations of Membrane-Associated Antimicrobial Peptides. In *Antimicrobial Peptides: Methods and Protocols*, Giuliani, A.; Rinaldi, A. C., Eds. Humana Press: Totowa, NJ, 2010; pp 209-233.

189. Powers, L.; Clark, N. A., Preparation of large monodomain phospholipid bilayer smectic liquid crystals. *Proceedings of the National Academy of Sciences* **1975,** *72* (3), 840-843 DOI: 10.1073/pnas.72.3.840.

190. Hsia, C.-Y.; Chen, L.; Singh, R. R.; DeLisa, M. P.; Daniel, S., A Molecularly Complete Planar Bacterial Outer Membrane Platform. *Sci Rep* **2016,** *6*, 32715 DOI: 10.1038/srep32715

https://www.nature.com/articles/srep32715#supplementary-information.

191. Wong, J. Y.; Majewski, J.; Seitz, M.; Park, C. K.; Israelachvili, J. N.; Smith, G. S., Polymer-cushioned bilayers. I. A structural study of various preparation methods using neutron reflectometry. *Biophysical journal* **1999,** *77* (3), 1445-1457 DOI: 10.1016/S0006-3495(99)76992-4.

192. Schmidt, A.; Spinke, J.; Bayerl, T.; Sackmann, E.; Knoll, W., Streptavidin binding to biotinylated lipid layers on solid supports. A neutron reflection and surface plasmon optical study. *Biophysical journal* **1992,** *63* (5), 1385-1392 DOI: 10.1016/S0006-3495(92)81715-0.

193. Yu, C.-h.; Groves, J. T., Engineering supported membranes for cell biology. *Medical & Biological Engineering & Computing* **2010,** *48* (10), 955-963 DOI: 10.1007/s11517-010-0634-x.

194. Langmuir, I., The mechanism of the surface phenomena of flotation. *Transactions of the Faraday Society* **1920,** *15* (June), 62-74 DOI: 10.1039/TF9201500062.

195. Girard-Egrot, A. P.; Blum, L. J., Langmuir-Blodgett Technique for Synthesis of Biomimetic Lipid Membranes. In *Nanobiotechnology of Biomimetic Membranes*, Martin, D. K., Ed. Springer US: Boston, MA, 2007; pp 23-74.

196. Kurniawan, J.; Ventrici de Souza, J. F.; Dang, A. T.; Liu, G.-y.; Kuhl, T. L., Preparation and Characterization of Solid-Supported Lipid Bilayers Formed by Langmuir–Blodgett Deposition: A Tutorial. *Langmuir* **2018,** *34* (51), 15622-15639 DOI: 10.1021/acs.langmuir.8b03504.

197. Langmuir, I.; Schaefer, V. J., Activities of Urease and Pepsin Monolayers. *Journal of the American Chemical Society* **1938,** *60* (6), 1351-1360 DOI: 10.1021/ja01273a023.

198. El Kirat, K.; Morandat, S.; Dufrêne, Y. F., Nanoscale analysis of supported lipid bilayers using atomic force microscopy. *Biochimica et Biophysica Acta (BBA)* -

Biomembranes **2010,** *1798* (4), 750-765 DOI: https://doi.org/10.1016/j.bbamem.2009.07.026.

199. Daniel, S.; Chao, L., Supported Lipid Bilayer Electrophoresis for Separation and Analytical Studies of Cell Membrane Biomolecules. In *Interfaces and Interphases in Analytical Chemistry*, American Chemical Society: 2011; Vol. 1062, pp 99-121.

200. Tanaka, M.; Sackmann, E., Polymer-supported membranes as models of the cell surface. *Nature* **2005,** *437* (7059), 656-663 DOI: 10.1038/nature04164.

201. Wang, L.; Roth, J. S.; Han, X.; Evans, S. D., Photosynthetic Proteins in Supported Lipid Bilayers: Towards a Biokleptic Approach for Energy Capture. *Small* **2015,** *11* (27), 3306-18 DOI: 10.1002/smll.201403469.

202. Crane, J. M.; Kiessling, V.; Tamm, L. K., Measuring Lipid Asymmetry in Planar Supported Bilayers by Fluorescence Interference Contrast Microscopy. *Langmuir* **2005,** *21* (4), 1377-1388 DOI: 10.1021/la047654w.

203. Reimhult, E.; Baumann, M. K.; Kaufmann, S.; Kumar, K.; Spycher, P. R., Advances in nanopatterned and nanostructured supported lipid membranes and their applications. *Biotechnology and Genetic Engineering Reviews* **2010,** *27* (1), 185-216 DOI: 10.1080/02648725.2010.10648150.

204. Kiessling, V.; Tamm, L. K., Measuring distances in supported bilayers by fluorescence interference-contrast microscopy: polymer supports and SNARE proteins. *Biophys J* **2003,** *84* (1), 408-18 DOI: 10.1016/s0006-3495(03)74861-9.

205. Seitz, M.; Ter-Ovanesyan, E.; Hausch, M.; Park, C. K.; Zasadzinski, J. A.; Zentel, R.; Israelachvili, J. N., Formation of Tethered Supported Bilayers by Vesicle Fusion onto Lipopolymer Monolayers Promoted by Osmotic Stress. *Langmuir : the ACS journal of surfaces and colloids* **2000,** *16* (14), 6067-6070 DOI: 10.1021/la9915771.

206. Mennicke, U.; Salditt, T., Preparation of Solid-Supported Lipid Bilayers by Spin-Coating. *Langmuir* **2002,** *18* (21), 8172-8177 DOI: 10.1021/la025863f.

207. Pompeo, G.; Girasole, M.; Cricenti, A.; Cattaruzza, F.; Flamini, A.; Prosperi, T.; Generosi, J.; Congiu Castellano, A., AFM characterization of solid-supported lipid multilayers prepared by spin-coating. *Biochimica et Biophysica Acta (BBA) - Biomembranes* **2005,** *1712* (1), 29-36 DOI: https://doi.org/10.1016/j.bbamem.2005.03.007.

208. Honigmann, A.; Mueller, V.; Ta, H.; Schoenle, A.; Sezgin, E.; Hell, S. W.; Eggeling, C., Scanning STED-FCS reveals spatiotemporal heterogeneity of lipid interaction in the plasma membrane of living cells. *Nature Communications* **2014,** *5* (1), 5412 DOI: 10.1038/ncomms6412.

209. Honigmann, A.; van den Bogaart, G.; Iraheta, E.; Risselada, H. J.; Milovanovic, D.; Mueller, V.; Müllar, S.; Diederichsen, U.; Fasshauer, D.; Grubmüller, H.; Hell, S.

W.; Eggeling, C.; Kühnel, K.; Jahn, R., Phosphatidylinositol 4,5-bisphosphate clusters act as molecular beacons for vesicle recruitment. *Nat Struct Mol Biol* **2013,** *20* (6), 679-686 DOI: 10.1038/nsmb.2570.

210. Gillissen, J. J. J.; Tabaei, S. R.; Cho, N.-J., A phenomenological model of the solvent-assisted lipid bilayer formation method. *Physical Chemistry Chemical Physics* **2016,** *18* (35), 24157-24163 DOI: 10.1039/C6CP04816A.

211. Hohner, A. O.; David, M. P.; Rädler, J. O., Controlled solvent-exchange deposition of phospholipid membranes onto solid surfaces. *Biointerphases* **2010,** *5* (1), 1-8 DOI: 10.1116/1.3319326.

212. Tabaei, S. R.; Choi, J.-H.; Haw Zan, G.; Zhdanov, V. P.; Cho, N.-J., Solvent-Assisted Lipid Bilayer Formation on Silicon Dioxide and Gold. *Langmuir* **2014,** *30* (34), 10363-10373 DOI: 10.1021/la501534f.

213. Tabaei, S. R.; Jackman, J. A.; Kim, M.; Yorulmaz, S.; Vafaei, S.; Cho, N.-J., Biomembrane Fabrication by the Solvent-assisted Lipid Bilayer (SALB) Method. *J Vis Exp* **2015,** (106), 53073 DOI: 10.3791/53073.

214. Ferhan, A. R.; Yoon, B. K.; Park, S.; Sut, T. N.; Chin, H.; Park, J. H.; Jackman, J. A.; Cho, N.-J., Solvent-assisted preparation of supported lipid bilayers. *Nature Protocols* **2019,** *14* (7), 2091-2118 DOI: 10.1038/s41596-019-0174-2.

215. Griebenow, K.; Klibanov, A. M., On Protein Denaturation in Aqueous−Organic Mixtures but Not in Pure Organic Solvents. *Journal of the American Chemical Society* **1996,** *118* (47), 11695-11700 DOI: 10.1021/ja961869d.

216. Zeineldin, R.; Last, J. A.; Slade, A. L.; Ista, L. K.; Bisong, P.; O'Brien, M. J.; Brueck, S. R. J.; Sasaki, D. Y.; Lopez, G. P., Using Bicellar Mixtures To Form Supported and Suspended Lipid Bilayers on Silicon Chips. *Langmuir* **2006,** *22* (19), 8163-8168 DOI: 10.1021/la060817r.

217. Kolahdouzan, K.; Jackman, J. A.; Yoon, B. K.; Kim, M. C.; Johal, M. S.; Cho, N.-J., Optimizing the Formation of Supported Lipid Bilayers from Bicellar Mixtures. *Langmuir* **2017,** *33* (20), 5052-5064 DOI: 10.1021/acs.langmuir.7b00210.

218. Morigaki, K.; Kimura, S.; Okada, K.; Kawasaki, T.; Kawasaki, K., Formation of Substrate-Supported Membranes from Mixtures of Long- and Short-Chain Phospholipids. *Langmuir* **2012,** *28* (25), 9649-9655 DOI: 10.1021/la300696z.

219. Sut, T. N.; Park, S.; Choe, Y.; Cho, N.-J., Characterizing the Supported Lipid Membrane Formation from Cholesterol-Rich Bicelles. *Langmuir* **2019,** *35* (47), 15063-15070 DOI: 10.1021/acs.langmuir.9b02851.

220. Sundh, M.; Svedhem, S.; Sutherland, D. S., Influence of phase separating lipids on supported lipid bilayer formation at SiO2 surfaces. *Physical Chemistry Chemical Physics* **2010,** *12* (2), 453-460 DOI: 10.1039/B912598A.

221. Diller, A.; Loudet, C.; Aussenac, F.; Raffard, G.; Fournier, S.; Laguerre, M.; Grélard, A.; Opella, S. J.; Marassi, F. M.; Dufourc, E. J., Bicelles: A natural 'molecular goniometer' for structural, dynamical and topological studies of molecules in membranes. *Biochimie* **2009,** *91* (6), 744-751 DOI: 10.1016/j.biochi.2009.02.003.

222. Dürr, U. H. N.; Gildenberg, M.; Ramamoorthy, A., The magic of bicelles lights up membrane protein structure. *Chem Rev* **2012,** *112* (11), 6054-6074 DOI: 10.1021/cr300061w.

223. Loura, L. M. S.; Prieto, M., FRET in Membrane Biophysics: An Overview. *Front Physiol* **2011,** *2*, 82-82 DOI: 10.3389/fphys.2011.00082.

224. Silvius, J. R.; Nabi, I. R., Fluorescence-quenching and resonance energy transfer studies of lipid microdomains in model and biological membranes. *Mol Membr Biol* **2006,** *23* (1), 5-16 DOI: 10.1080/09687860500473002.

225. Oreopoulos, J.; Yip, C. M., Probing membrane order and topography in supported lipid bilayers by combined polarized total internal reflection fluorescence-atomic force microscopy. *Biophysical journal* **2009,** *96* (5), 1970-1984 DOI: 10.1016/j.bpj.2008.11.041.

226. Thompson, N. L.; Pearce, K. H.; Hsieh, H. V., Total internal reflection fluorescence microscopy: application to substrate-supported planar membranes. *Eur Biophys J* **1993,** *22* (5), 367-78 DOI: 10.1007/bf00213560.

227. Korlach, J.; Schwille, P.; Webb, W. W.; Feigenson, G. W., Characterization of lipid bilayer phases by confocal microscopy and fluorescence correlation spectroscopy. *Proceedings of the National Academy of Sciences* **1999,** *96* (15), 8461-8466 DOI: 10.1073/pnas.96.15.8461.

228. Bernchou, U.; Brewer, J.; Midtiby, H. S.; Ipsen, J. H.; Bagatolli, L. A.; Simonsen, A. C., Texture of Lipid Bilayer Domains. *Journal of the American Chemical Society* **2009,** *131* (40), 14130-14131 DOI: 10.1021/ja903375m.

229. Dufrêne, Y. F.; Lee, G. U., Advances in the characterization of supported lipid films with the atomic force microscope. *Biochimica et Biophysica Acta (BBA) - Biomembranes* **2000,** *1509* (1), 14-41 DOI: https://doi.org/10.1016/S0005-2736(00)00346-1.

230. Keller, C. A.; Kasemo, B., Surface specific kinetics of lipid vesicle adsorption measured with a quartz crystal microbalance. *Biophysical journal* **1998,** *75* (3), 1397-1402 DOI: 10.1016/S0006-3495(98)74057-3.

231. Rydell, G. E.; Dahlin, A. B.; Höök, F.; Larson, G., QCM-D studies of human norovirus VLPs binding to glycosphingolipids in supported lipid bilayers reveal strain-specific characteristics. *Glycobiology* **2009,** *19* (11), 1176-1184 DOI: 10.1093/glycob/cwp103.

232. Englebienne, P.; Hoonacker, A. V.; Verhas, M., Surface plasmon resonance: principles, methods and applications in biomedical sciences. *Spectroscopy* **2003,** *17*, 372913 DOI: 10.1155/2003/372913.

233. Parkkila, P.; Elderdfi, M.; Bunker, A.; Viitala, T., Biophysical Characterization of Supported Lipid Bilayers Using Parallel Dual-Wavelength Surface Plasmon Resonance and Quartz Crystal Microbalance Measurements. *Langmuir : the ACS journal of surfaces and colloids* **2018,** *34* (27), 8081-8091 DOI: 10.1021/acs.langmuir.8b01259.

234. Richter, R. P.; Brisson, A. R., Following the Formation of Supported Lipid Bilayers on Mica: A Study Combining AFM, QCM-D, and Ellipsometry. *Biophysical Journal* **2005,** *88* (5), 3422-3433 DOI: https://doi.org/10.1529/biophysj.104.053728.

235. Pincet, F.; Adrien, V.; Yang, R.; Delacotte, J.; Rothman, J. E.; Urbach, W.; Tareste, D., FRAP to Characterize Molecular Diffusion and Interaction in Various Membrane Environments. *PloS one* **2016,** *11* (7), e0158457-e0158457 DOI: 10.1371/journal.pone.0158457.

236. Macháň, R.; Hof, M., Lipid diffusion in planar membranes investigated by fluorescence correlation spectroscopy. *Biochimica et Biophysica Acta (BBA) - Biomembranes* **2010,** *1798* (7), 1377-1391 DOI: https://doi.org/10.1016/j.bbamem.2010.02.014.

237. Morandat, S.; Kirat, K. E. In *Exploring the Properties and Interactions of Supported Lipid Bilayers on the Nanoscale by Atomic Force Microscopy*, 2010.

238. Guo, H.; Xing, Q.; Huang, R.; Lee, D. W.; Su, R.; Qi, W.; He, Z., Real-Time QCM-D Monitoring of Deposition of Gold Nanorods on a Supported Lipid Bilayer as a Model Cell Membrane. *ACS Omega* **2019,** *4* (3), 6059-6067 DOI: 10.1021/acsomega.9b00287.

239. Costello, D. A.; Lee, D. W.; Drewes, J.; Vasquez, K. A.; Kisler, K.; Wiesner, U.; Pollack, L.; Whittaker, G. R.; Daniel, S., Influenza Virus-Membrane Fusion Triggered by Proton Uncaging for Single Particle Studies of Fusion Kinetics. *Analytical Chemistry* **2012,** *84* (20), 8480-8489 DOI: 10.1021/ac3006473.

240. Oreopoulos, J.; Yip, C. M., Combinatorial microscopy for the study of protein–membrane interactions in supported lipid bilayers: Order parameter measurements by combined polarized TIRFM/AFM. *J Struct Biol* **2009,** *168* (1), 21-36 DOI: https://doi.org/10.1016/j.jsb.2009.02.011.

241. Rose, M.; Hirmiz, N.; Moran-Mirabal, J. M.; Fradin, C., Lipid Diffusion in Supported Lipid Bilayers: A Comparison between Line-Scanning Fluorescence Correlation Spectroscopy and Single-Particle Tracking. *Membranes (Basel)* **2015,** *5* (4), 702-721 DOI: 10.3390/membranes5040702.

242. Khalili, A. A.; Ahmad, M. R., A Review of Cell Adhesion Studies for Biomedical and Biological Applications. *Int J Mol Sci* **2015,** *16* (8), 18149-18184 DOI: 10.3390/ijms160818149.

243. Borsig, L.; Läubli, H., Cell Adhesion During Tumorigenesis and Metastasis. In *Encyclopedia of Cancer (Third Edition)*, Boffetta, P.; Hainaut, P., Eds. Academic Press: Oxford, 2019; pp 307-314.

244. Blankenberg, S.; Barbaux, S.; Tiret, L., Adhesion molecules and atherosclerosis. *Atherosclerosis* **2003,** *170* (2), 191-203 DOI: https://doi.org/10.1016/S0021-9150(03)00097-2.

245. Janiszewska, M.; Primi, M. C.; Izard, T., Cell adhesion in cancer: Beyond the migration of single cells. *The Journal of biological chemistry* **2020,** *295* (8), 2495-2505 DOI: 10.1074/jbc.REV119.007759.

246. Merten, O.-W., Advances in cell culture: anchorage dependence. *Philos Trans R Soc Lond B Biol Sci* **2015,** *370* (1661), 20140040-20140040 DOI: 10.1098/rstb.2014.0040.

247. Bennett, M.; Cantini, M.; Reboud, J.; Cooper, J. M.; Roca-Cusachs, P.; Salmeron-Sanchez, M., Molecular clutch drives cell response to surface viscosity. *Proceedings of the National Academy of Sciences* **2018,** *115* (6), 1192-1197 DOI: 10.1073/pnas.1710653115.

248. Arnaout, M. A.; Mahalingam, B.; Xiong, J. P., Integrin structure, allostery, and bidirectional signaling. *Annu Rev Cell Dev Biol* **2005,** *21*, 381-410 DOI: 10.1146/annurev.cellbio.21.090704.151217.

249. Bellis, S. L., Advantages of RGD peptides for directing cell association with biomaterials. *Biomaterials* **2011,** *32* (18), 4205-4210 DOI: 10.1016/j.biomaterials.2011.02.029.

250. Ananthanarayanan, B.; Little, L.; Schaffer, D. V.; Healy, K. E.; Tirrell, M., Neural stem cell adhesion and proliferation on phospholipid bilayers functionalized with RGD peptides. *Biomaterials* **2010,** *31* (33), 8706-8715 DOI: 10.1016/j.biomaterials.2010.07.104.

251. Kilic, A.; Kok, F. N., Peptide-functionalized supported lipid bilayers to construct cell membrane mimicking interfaces. *Colloids and Surfaces B: Biointerfaces* **2019,** *176*, 18-26 DOI: https://doi.org/10.1016/j.colsurfb.2018.12.052.

252. Sandrin, L.; Coche-Guérente, L.; Bernstein, A.; Basit, H.; Labbé, P.; Dumy, P.; Boturyn, D., Cell adhesion through clustered ligand on fluid supported lipid bilayers. *Organic & Biomolecular Chemistry* **2010,** *8* (7), 1531-1534 DOI: 10.1039/B924523E.

253. Bérat, R.; Rémy-Zolghadry, M.; Gounou, C.; Manigand, C.; Tan, S.; Saltó, C.; Arenas, E.; Bordenave, L.; Brisson, A. R., Peptide-presenting two-dimensional protein

matrix on supported lipid bilayers: An efficient platform for cell adhesion. *Biointerphases* **2007,** *2* (4), 165-172 DOI: 10.1116/1.2821954.

254. Koçer, G.; Jonkheijm, P., Guiding hMSC Adhesion and Differentiation on Supported Lipid Bilayers. *Advanced Healthcare Materials* **2017,** *6* (3), 1600862 DOI: https://doi.org/10.1002/adhm.201600862.

255. Yam, J. W.; Tse, E. Y.; Ng, I. O., Role and significance of focal adhesion proteins in hepatocellular carcinoma. *J Gastroenterol Hepatol* **2009,** *24* (4), 520-30 DOI: 10.1111/j.1440-1746.2009.05813.x.

256. Satav, T.; Huskens, J.; Jonkheijm, P., Effects of Variations in Ligand Density on Cell Signaling. *Small* **2015,** *11* (39), 5184-5199 DOI: https://doi.org/10.1002/smll.201500747.

257. Kourouklis, A. P.; Lerum, R. V.; Bermudez, H., Cell adhesion mechanisms on laterally mobile polymer films. *Biomaterials* **2014,** *35* (17), 4827-4834 DOI: https://doi.org/10.1016/j.biomaterials.2014.02.052.

258. Sandrin, L.; Thakar, D.; Goyer, C.; Labbé, P.; Boturyn, D.; Coche-Guérente, L., Controlled surface density of RGD ligands for cell adhesion: evidence for ligand specificity by using QCM-D. *Journal of Materials Chemistry B* **2015,** *3* (27), 5577-5587 DOI: 10.1039/C5TB00420A.

259. Worsfold, O.; Voelcker, N. H.; Nishiya, T., Biosensing Using Lipid Bilayers Suspended on Porous Silicon. *Langmuir* **2006,** *22* (16), 7078-7083 DOI: 10.1021/la060121y.

260. Patel, R.; Santhosh, M.; Dash, J. K.; Karpoormath, R.; Jha, A.; Kwak, J.; Patel, M.; Kim, J. H., Ile-Lys-Val-ala-Val (IKVAV) peptide for neuronal tissue engineering. *Polymers for Advanced Technologies* **2019,** *30* (1), 4-12 DOI: https://doi.org/10.1002/pat.4442.

261. Wang, N., Cell Adhesion Molecules (CAMs). In *Encyclopedia of the Neurological Sciences (Second Edition)*, Aminoff, M. J.; Daroff, R. B., Eds. Academic Press: Oxford, 2014; pp 628-629.

262. Hartsock, A.; Nelson, W. J., Adherens and tight junctions: Structure, function and connections to the actin cytoskeleton. *Biochimica et Biophysica Acta (BBA) - Biomembranes* **2008,** *1778* (3), 660-669 DOI: https://doi.org/10.1016/j.bbamem.2007.07.012.

263. Evans, S. F.; Docheva, D.; Bernecker, A.; Colnot, C.; Richter, R. P.; Knothe Tate, M. L., Solid-supported lipid bilayers to drive stem cell fate and tissue architecture using periosteum derived progenitor cells. *Biomaterials* **2013,** *34* (8), 1878-1887 DOI: https://doi.org/10.1016/j.biomaterials.2012.09.024.

264. Ross, J. M., Chapter II. 1 - Cell-Extracellular Matrix Interactions. In *Frontiers in Tissue Engineering*, Patrick, C. W.; Mikos, A. G.; McIntire, L. V.; Langer, R. S., Eds. Pergamon: Oxford, 1998; pp 15-27.

265. Sainio, A.; Järveläinen, H., Extracellular matrix-cell interactions: Focus on therapeutic applications. *Cellular Signalling* **2020,** *66*, 109487 DOI: https://doi.org/10.1016/j.cellsig.2019.109487.

266. Huang, C.-J.; Cho, N.-J.; Hsu, C.-J.; Tseng, P.-Y.; Frank, C. W.; Chang, Y.-C., Type I Collagen-Functionalized Supported Lipid Bilayer as a Cell Culture Platform. *Biomacromolecules* **2010,** *11* (5), 1231-1240 DOI: 10.1021/bm901445r.

267. McDonald, J. A.; Kelley, D. G.; Broekelmann, T. J., Role of fibronectin in collagen deposition: Fab' to the gelatin-binding domain of fibronectin inhibits both fibronectin and collagen organization in fibroblast extracellular matrix. *Journal of Cell Biology* **1982,** *92* (2), 485-492 DOI: 10.1083/jcb.92.2.485.

268. Bagambisa, F. B.; Kappert, H. F.; Schilli, W., Cellular and molecular biological events at the implant interface. *Journal of Cranio-Maxillofacial Surgery* **1994,** *22* (1), 12-17 DOI: https://doi.org/10.1016/S1010-5182(05)80290-2.

269. Huang, C. J.; Tseng, P. Y.; Chang, Y. C., Effects of extracellular matrix protein functionalized fluid membrane on cell adhesion and matrix remodeling. *Biomaterials* **2010,** *31* (27), 7183-95 DOI: 10.1016/j.biomaterials.2010.05.076.

270. Huang, C.-J.; Tseng, P.-Y.; Chang, Y.-C., Effects of extracellular matrix protein functionalized fluid membrane on cell adhesion and matrix remodeling. *Biomaterials* **2010,** *31* (27), 7183-7195 DOI: https://doi.org/10.1016/j.biomaterials.2010.05.076.

271. Vafaei, S.; Tabaei, S. R.; Guneta, V.; Choong, C.; Cho, N.-J., Hybrid Biomimetic Interfaces Integrating Supported Lipid Bilayers with Decellularized Extracellular Matrix Components. *Langmuir* **2018,** *34* (11), 3507-3516 DOI: 10.1021/acs.langmuir.7b03265.

272. Paolicelli, R. C.; Bergamini, G.; Rajendran, L., Cell-to-cell Communication by Extracellular Vesicles: Focus on Microglia. *Neuroscience* **2019,** *405*, 148-157 DOI: https://doi.org/10.1016/j.neuroscience.2018.04.003.

273. Xie, C.; Ji, N.; Tang, Z.; Li, J.; Chen, Q., The role of extracellular vesicles from different origin in the microenvironment of head and neck cancers. *Molecular Cancer* **2019,** *18* (1), 83 DOI: 10.1186/s12943-019-0985-3.

274. Candelario, K. M.; Steindler, D. A., The role of extracellular vesicles in the progression of neurodegenerative disease and cancer. *Trends in molecular medicine* **2014,** *20* (7), 368-374 DOI: 10.1016/j.molmed.2014.04.003.

275. Escrevente, C.; Keller, S.; Altevogt, P.; Costa, J., Interaction and uptake of exosomes by ovarian cancer cells. *BMC cancer* **2011,** *11*, 108-108 DOI: 10.1186/1471-2407-11-108.

276. Rodrigues, M.; Fan, J.; Lyon, C.; Wan, M.; Hu, Y., Role of Extracellular Vesicles in Viral and Bacterial Infections: Pathogenesis, Diagnostics, and Therapeutics. *Theranostics* **2018,** *8* (10), 2709-2721 DOI: 10.7150/thno.20576.

277. Buzas, E. I.; György, B.; Nagy, G.; Falus, A.; Gay, S., Emerging role of extracellular vesicles in inflammatory diseases. *Nature Reviews Rheumatology* **2014,** *10*, 356 DOI: 10.1038/nrrheum.2014.19.

278. Gho, Y. S.; Lee, J., Special issue on the role of extracellular vesicles in human diseases. *Experimental & Molecular Medicine* **2019,** *51* (3), 34 DOI: 10.1038/s12276-019-0208-4.

279. Jindal, A., The effect of particle shape on cellular interaction and drug delivery applications of micro- and nanoparticles. *International Journal of Pharmaceutics* **2017,** *532*, DOI: 10.1016/j.ijpharm.2017.09.028.

280. Dasgupta, S.; Auth, T.; Gompper, G., Shape and Orientation Matter for the Cellular Uptake of Nonspherical Particles. *Nano Letters* **2014,** *14* (2), 687-693 DOI: 10.1021/nl403949h.

281. He, Y.; Park, K., Effects of the Microparticle Shape on Cellular Uptake. *Molecular pharmaceutics* **2016,** *13* (7), 2164-2171 DOI: 10.1021/acs.molpharmaceut.5b00992.

282. Théry, C.; Amigorena, S.; Raposo, G.; Clayton, A., Isolation and Characterization of Exosomes from Cell Culture Supernatants and Biological Fluids. *Curr Protoc Cell Biol* **2006,** *30* (1), 3.22.1-3.22.29 DOI: 10.1002/0471143030.cb0322s30.

283. Akagi, T.; Kato, K.; Kobayashi, M.; Kosaka, N.; Ochiya, T.; Ichiki, T., On-chip immunoelectrophoresis of extracellular vesicles released from human breast cancer cells. *PloS one* **2015,** *10* (4), e0123603-e0123603 DOI: 10.1371/journal.pone.0123603.

284. Zhang, H.; Freitas, D.; Kim, H. S.; Fabijanic, K.; Li, Z.; Chen, H.; Mark, M. T.; Molina, H.; Martin, A. B.; Bojmar, L.; Fang, J.; Rampersaud, S.; Hoshino, A.; Matei, I.; Kenific, C. M.; Nakajima, M.; Mutvei, A. P.; Sansone, P.; Buehring, W.; Wang, H.; Jimenez, J. P.; Cohen-Gould, L.; Paknejad, N.; Brendel, M.; Manova-Todorova, K.; Magalhães, A.; Ferreira, J. A.; Osório, H.; Silva, A. M.; Massey, A.; Cubillos-Ruiz, J. R.; Galletti, G.; Giannakakou, P.; Cuervo, A. M.; Blenis, J.; Schwartz, R.; Brady, M. S.; Peinado, H.; Bromberg, J.; Matsui, H.; Reis, C. A.; Lyden, D., Identification of distinct nanoparticles and subsets of extracellular vesicles by asymmetric flow field-flow fractionation. *Nature Cell Biology* **2018,** *20* (3), 332-343 DOI: 10.1038/s41556-018-0040-4.

285. Andreu, Z.; Yáñez-Mó, M., Tetraspanins in extracellular vesicle formation and function. *Frontiers in immunology* **2014,** *5*, 442-442 DOI: 10.3389/fimmu.2014.00442.

286. Subik, K.; Lee, J.-F.; Baxter, L.; Strzepek, T.; Costello, D.; Crowley, P.; Xing, L.; Hung, M.-C.; Bonfiglio, T.; Hicks, D. G.; Tang, P., The Expression Patterns of ER, PR, HER2, CK5/6, EGFR, Ki-67 and AR by Immunohistochemical Analysis in Breast Cancer Cell Lines. *Breast Cancer (Auckl)* **2010,** *4*, 35-41.

287. Ageberg, M.; Lindmark, A., Characterisation of the biosynthesis and processing of the neutrophil granule membrane protein CD63 in myeloid cells. *Clinical & Laboratory Haematology* **2003,** *25* (5), 297-306 DOI: 10.1046/j.1365-2257.2003.00541.x.

288. Lorente, G.; Syriani, E.; Morales, M., Actin filaments at the leading edge of cancer cells are characterized by a high mobile fraction and turnover regulation by profilin I. *PloS one* **2014,** *9* (1), e85817-e85817 DOI: 10.1371/journal.pone.0085817.

289. Muralidharan-Chari, V.; Clancy, J. W.; Sedgwick, A.; D'Souza-Schorey, C., Microvesicles: mediators of extracellular communication during cancer progression. **2010,** *123* (10), 1603-1611 DOI: 10.1242/jcs.064386 %J Journal of Cell Science.

290. Li, B.; Antonyak, M. A.; Zhang, J.; Cerione, R. A., RhoA triggers a specific signaling pathway that generates transforming microvesicles in cancer cells. *Oncogene* **2012,** *31* (45), 4740-4749 DOI: 10.1038/onc.2011.636.

291. Park, S. J.; Kim, J. M.; Kim, J.; Hur, J.; Park, S.; Kim, K.; Shin, H.-J.; Chwae, Y.-J., Molecular mechanisms of biogenesis of apoptotic exosome-like vesicles and their roles as damage-associated molecular patterns. *Proceedings of the National Academy of Sciences* **2018,** *115* (50), E11721-E11730 DOI: 10.1073/pnas.1811432115.

292. Hosseini-Beheshti, E.; Pham, S.; Adomat, H.; Li, N.; Tomlinson Guns, E. S., Exosomes as biomarker enriched microvesicles: characterization of exosomal proteins derived from a panel of prostate cell lines with distinct AR phenotypes. *Molecular & cellular proteomics : MCP* **2012,** *11* (10), 863-885 DOI: 10.1074/mcp.M111.014845.

293. Singh, R. R.; Sangani, A. S.; Daniel, S.; Koch, D. L., The combined hydrodynamic and thermodynamic effects of immobilized proteins on the diffusion of mobile transmembrane proteins. *Journal of Fluid Mechanics* **2019,** *877*, 648-681 DOI: 10.1017/jfm.2019.592.

294. Yoshioka, Y.; Konishi, Y.; Kosaka, N.; Katsuda, T.; Kato, T.; Ochiya, T., Comparative marker analysis of extracellular vesicles in different human cancer types. *J Extracell Vesicles* **2013,** *2*, 10.3402/jev.v2i0.20424 DOI: 10.3402/jev.v2i0.20424.

295. Stangl, S.; Gehrmann, M.; Riegger, J.; Kuhs, K.; Riederer, I.; Sievert, W.; Hube, K.; Mocikat, R.; Dressel, R.; Kremmer, E.; Pockley, A. G.; Friedrich, L.; Vigh, L.; Skerra, A.; Multhoff, G., Targeting membrane heat-shock protein 70 (Hsp70) on

tumors by cmHsp70.1 antibody. *Proc Natl Acad Sci U S A* **2011,** *108* (2), 733-738 DOI: 10.1073/pnas.1016065108.

296. Al-Nedawi, K.; Meehan, B.; Kerbel, R. S.; Allison, A. C.; Rak, J., Endothelial expression of autocrine VEGF upon the uptake of tumor-derived microvesicles containing oncogenic EGFR. *Proc Natl Acad Sci U S A* **2009,** *106* (10), 3794-3799 DOI: 10.1073/pnas.0804543106.

297. Wang, K.; Wang, K.; Li, W.; Huang, T.; Li, R.; Wang, D.; Shen, B.; Chen, X., Characterizing breast cancer xenograft epidermal growth factor receptor expression by using near-infrared optical imaging. *Acta radiologica (Stockholm, Sweden : 1987)* **2009,** *50* (10), 1095-1103 DOI: 10.3109/02841850903008800.

298. Costello, D. A.; Hsia, C.-Y.; Millet, J. K.; Porri, T.; Daniel, S., Membrane Fusion-Competent Virus-Like Proteoliposomes and Proteinaceous Supported Bilayers Made Directly from Cell Plasma Membranes. *Langmuir* **2013,** *29* (21), 6409-6419 DOI: 10.1021/la400861u.

299. Reimhult, E.; Kasemo, B.; Höök, F., Rupture Pathway of Phosphatidylcholine Liposomes on Silicon Dioxide. *International Journal of Molecular Sciences* **2009,** *10* (4), 1683-1696.

300. Fuhrmans, M.; Müller, M., Mechanisms of Vesicle Spreading on Surfaces: Coarse-Grained Simulations. *Langmuir* **2013,** *29* (13), 4335-4349 DOI: 10.1021/la400119e.

301. Chandler, E. M.; Seo, B. R.; Califano, J. P.; Andresen Eguiluz, R. C.; Lee, J. S.; Yoon, C. J.; Tims, D. T.; Wang, J. X.; Cheng, L.; Mohanan, S.; Buckley, M. R.; Cohen, I.; Nikitin, A. Y.; Williams, R. M.; Gourdon, D.; Reinhart-King, C. A.; Fischbach, C., Implanted adipose progenitor cells as physicochemical regulators of breast cancer. *Proceedings of the National Academy of Sciences* **2012,** *109* (25), 9786-9791 DOI: 10.1073/pnas.1121160109.

302. Heino, J., The collagen family members as cell adhesion proteins. **2007,** *29* (10), 1001-1010 DOI: doi:10.1002/bies.20636.

303. Plant, A. L.; Bhadriraju, K.; Spurlin, T. A.; Elliott, J. T., Cell response to matrix mechanics: Focus on collagen. *Biochimica et Biophysica Acta (BBA) - Molecular Cell Research* **2009,** *1793* (5), 893-902 DOI: https://doi.org/10.1016/j.bbamcr.2008.10.012.

304. Horzum, U.; Ozdil, B.; Pesen-Okvur, D., Step-by-step quantitative analysis of focal adhesions. *MethodsX* **2014,** *1*, 56-59 DOI: 10.1016/j.mex.2014.06.004.

305. Rao K, B.; Malathi, N.; Narashiman, S.; Rajan, S. T., Evaluation of myofibroblasts by expression of alpha smooth muscle actin: a marker in fibrosis, dysplasia and carcinoma. *J Clin Diagn Res* **2014,** *8* (4), ZC14-ZC17 DOI: 10.7860/JCDR/2014/7820.4231.

306. Ehrlich, H. P.; Allison, G. M.; Leggett, M., The myofibroblast, cadherin, alpha smooth muscle actin and the collagen effect. *Cell Biochem Funct* **2006,** *24* (1), 63-70 DOI: 10.1002/cbf.1188.

307. Ortiz, A., Extracellular vesicles in cancer progression. *Seminars in Cancer Biology* **2021**, DOI: https://doi.org/10.1016/j.semcancer.2021.05.032.

308. Peinado, H.; Alečković, M.; Lavotshkin, S.; Matei, I.; Costa-Silva, B.; Moreno-Bueno, G.; Hergueta-Redondo, M.; Williams, C.; García-Santos, G.; Ghajar, C.; Nitadori-Hoshino, A.; Hoffman, C.; Badal, K.; Garcia, B. A.; Callahan, M. K.; Yuan, J.; Martins, V. R.; Skog, J.; Kaplan, R. N.; Brady, M. S.; Wolchok, J. D.; Chapman, P. B.; Kang, Y.; Bromberg, J.; Lyden, D., Melanoma exosomes educate bone marrow progenitor cells toward a pro-metastatic phenotype through MET. *Nat Med* **2012,** *18* (6), 883-91 DOI: 10.1038/nm.2753.

309. Stranford, D. M.; Hung, M. E.; Gargus, E. S.; Shah, R. N.; Leonard, J. N., A Systematic Evaluation of Factors Affecting Extracellular Vesicle Uptake by Breast Cancer Cells. *Tissue engineering. Part A* **2017,** *23* (21-22), 1274-1282 DOI: 10.1089/ten.TEA.2017.0158.

310. Richter, R. P.; Him, J. L. K.; Brisson, A., Supported lipid membranes. *Materials Today* **2003,** *6* (11), 32-37 DOI: https://doi.org/10.1016/S1369-7021(03)01129-5.

311. Tamm, L. K.; Groves, J. T., Supported membranes in structural biology. *J Struct Biol* **2009,** *168* (1), 1-2 DOI: 10.1016/j.jsb.2009.07.016.

312. Wallert, M.; Nie, C.; Anilkumar, P.; Abbina, S.; Bhatia, S.; Ludwig, K.; Kizhakkedathu, J. N.; Haag, R.; Block, S., Mucin-Inspired, High Molecular Weight Virus Binding Inhibitors Show Biphasic Binding Behavior to Influenza A Viruses. *Small* **2020,** *16* (47), 2004635 DOI: https://doi.org/10.1002/smll.202004635.

313. Peerboom, N.; Schmidt, E.; Trybala, E.; Block, S.; Bergström, T.; Pace, H. P.; Bally, M., Cell Membrane Derived Platform To Study Virus Binding Kinetics and Diffusion with Single Particle Sensitivity. *ACS Infectious Diseases* **2018,** *4* (6), 944-953 DOI: 10.1021/acsinfecdis.7b00270.

314. Lee, D. W.; Hsu, H.-L.; Bacon, K. B.; Daniel, S., Image Restoration and Analysis of Influenza Virions Binding to Membrane Receptors Reveal Adhesion-Strengthening Kinetics. *PLOS ONE* **2016,** *11* (10), e0163437 DOI: 10.1371/journal.pone.0163437.

315. Nathan, L.; Daniel, S., Single Virion Tracking Microscopy for the Study of Virus Entry Processes in Live Cells and Biomimetic Platforms. *Adv Exp Med Biol* **2019,** *1215*, 13-43 DOI: 10.1007/978-3-030-14741-9_2.

316. Kunze, A.; Bally, M.; Höök, F.; Larson, G., Equilibrium-fluctuation-analysis of single liposome binding events reveals how cholesterol and Ca2+ modulate glycosphingolipid trans-interactions. *Sci Rep* **2013,** *3*, 1452-1452 DOI: 10.1038/srep01452.

317. Bally, M.; Graule, M.; Parra, F.; Larson, G.; Höök, F., A virus biosensor with single virus-particle sensitivity based on fluorescent vesicle labels and equilibrium fluctuation analysis. *Biointerphases* **2013,** *8* (1), 4 DOI: 10.1186/1559-4106-8-4.

318. Pappa, A.-M.; Liu, H.-Y.; Traberg-Christensen, W.; Thiburce, Q.; Savva, A.; Pavia, A.; Salleo, A.; Daniel, S.; Owens, R. M., Optical and Electronic Ion Channel Monitoring from Native Human Membranes. *ACS Nano* **2020,** *14* (10), 12538-12545 DOI: 10.1021/acsnano.0c01330.

319. Liu, H.-Y.; Pappa, A.-M.; Hidalgo, T. C.; Inal, S.; Owens, R. M.; Daniel, S., Biomembrane-based organic electronic devices for ligand–receptor binding studies. *Analytical and Bioanalytical Chemistry* **2020,** *412* (24), 6265-6273 DOI: 10.1007/s00216-020-02449-3.

320. Proctor, C. M.; Rivnay, J.; Malliaras, G. G., Understanding volumetric capacitance in conducting polymers. *Journal of Polymer Science Part B: Polymer Physics* **2016,** *54* (15), 1433-1436 DOI: https://doi.org/10.1002/polb.24038.

321. Atanasov, V.; Knorr, N.; Duran, R. S.; Ingebrandt, S.; Offenhäusser, A.; Knoll, W.; Köper, I., Membrane on a chip: a functional tethered lipid bilayer membrane on silicon oxide surfaces. *Biophysical journal* **2005,** *89* (3), 1780-1788 DOI: 10.1529/biophysj.105.061374.

322. Charras, G. T.; Coughlin, M.; Mitchison, T. J.; Mahadevan, L., Life and times of a cellular bleb. *Biophysical journal* **2008,** *94* (5), 1836-1853 DOI: 10.1529/biophysj.107.113605.

323. Burckhardt, C. J.; Greber, U. F., Virus movements on the plasma membrane support infection and transmission between cells. *PLoS Pathog* **2009,** *5* (11), e1000621-e1000621 DOI: 10.1371/journal.ppat.1000621.

324. Jan Akhunzada, M.; D'Autilia, F.; Chandramouli, B.; Bhattacharjee, N.; Catte, A.; Di Rienzo, R.; Cardarelli, F.; Brancato, G., Interplay between lipid lateral diffusion, dye concentration and membrane permeability unveiled by a combined spectroscopic and computational study of a model lipid bilayer. *Sci Rep* **2019,** *9* (1), 1508 DOI: 10.1038/s41598-018-37814-x.

325. Merminod, S.; Edison, J. R.; Fang, H.; Hagan, M. F.; Rogers, W. B., Avidity and surface mobility in multivalent ligand–receptor binding. *Nanoscale* **2021**, DOI: 10.1039/D1NR02083H.

326. Jung, H.; Robison, A. D.; Cremer, P. S., Multivalent ligand-receptor binding on supported lipid bilayers. *J Struct Biol* **2009,** *168* (1), 90-94 DOI: 10.1016/j.jsb.2009.05.010.

327. Alexander, M.-W.; Wasim, K., Cell Surface Markers on Adipose-Derived Stem Cells: A Systematic Review. *Current Stem Cell Research & Therapy* **2017,** *12* (6), 484-492 DOI: http://dx.doi.org/10.2174/1574888X11666160429122133.

328. Blandin, A.-F.; Renner, G.; Lehmann, M.; Lelong-Rebel, I.; Martin, S.; Dontenwill, M., β1 Integrins as Therapeutic Targets to Disrupt Hallmarks of Cancer. *Front Pharmacol* **2015,** *6*, 279-279 DOI: 10.3389/fphar.2015.00279.

329. Burry, R. W., Controls for immunocytochemistry: an update. *J Histochem Cytochem* **2011,** *59* (1), 6-12 DOI: 10.1369/jhc.2010.956920.

330. Morelli, A. E.; Larregina, A. T.; Shufesky, W. J.; Sullivan, M. L. G.; Stolz, D. B.; Papworth, G. D.; Zahorchak, A. F.; Logar, A. J.; Wang, Z.; Watkins, S. C.; Falo, L. D.; Thomson, A. W., Endocytosis, intracellular sorting, and processing of exosomes by dendritic cells. **2004,** *104* (10), 3257-3266 DOI: 10.1182/blood-2004-03-0824 %J Blood.

331. McKelvey, K. J.; Powell, K. L.; Ashton, A. W.; Morris, J. M.; McCracken, S. A., Exosomes: Mechanisms of Uptake. *Journal of circulating biomarkers* **2015,** *4*, 7-7 DOI: 10.5772/61186.

332. Liu, H.-Y.; Pappa, A.-M.; Pavia, A.; Pitsalidis, C.; Thiburce, Q.; Salleo, A.; Owens, R. M.; Daniel, S., Self-Assembly of Mammalian-Cell Membranes on Bioelectronic Devices with Functional Transmembrane Proteins. *Langmuir* **2020,** *36* (26), 7325-7331 DOI: 10.1021/acs.langmuir.0c00804.

333. Kawan, M.; Hidalgo, T. C.; Du, W.; Pappa, A.-M.; Owens, R. M.; McCulloch, I.; Inal, S., Monitoring supported lipid bilayers with n-type organic electrochemical transistors. *Materials Horizons* **2020,** *7* (9), 2348-2358 DOI: 10.1039/D0MH00548G.

334. Ohayon, D.; Pitsalidis, C.; Pappa, A.-M.; Hama, A.; Zhang, Y.; Gallais, L.; Owens, R. M., Laser Patterning of Self-Assembled Monolayers on PEDOT:PSS Films for Controlled Cell Adhesion. *Advanced Materials Interfaces* **2017,** *4* (16), 1700191 DOI: https://doi.org/10.1002/admi.201700191.

335. Dijk, G.; Rutz, A. L.; Malliaras, G. G., Stability of PEDOT:PSS-Coated Gold Electrodes in Cell Culture Conditions. *Advanced Materials Technologies* **2020,** *5* (3), 1900662 DOI: https://doi.org/10.1002/admt.201900662.

336. Zhang, Y.; Inal, S.; Hsia, C.-Y.; Ferro, M.; Ferro, M.; Daniel, S.; Owens, R. M., Supported Lipid Bilayer Assembly on PEDOT:PSS Films and Transistors. *Advanced Functional Materials* **2016,** *26* (40), 7304-7313 DOI: https://doi.org/10.1002/adfm.201602123.

337. Liu, H.-Y.; Chen, W.-L.; Ober, C. K.; Daniel, S., Biologically Complex Planar Cell Plasma Membranes Supported on Polyelectrolyte Cushions Enhance Transmembrane Protein Mobility and Retain Native Orientation. *Langmuir* **2018,** *34* (3), 1061-1072 DOI: 10.1021/acs.langmuir.7b02945.

338. Nakagawa, T.; Li, J. H.; Garcia, G.; Mu, W.; Piek, E.; Böttinger, E. P.; Chen, Y.; Zhu, H. J.; Kang, D. H.; Schreiner, G. F.; Lan, H. Y.; Johnson, R. J., TGF-beta

induces proangiogenic and antiangiogenic factors via parallel but distinct Smad pathways. *Kidney Int* **2004,** *66* (2), 605-13 DOI: 10.1111/j.1523-1755.2004.00780.x.

339. Rodríguez, T. M.; Saldías, A.; Irigo, M.; Zamora, J. V.; Perone, M. J.; Dewey, R. A., Effect of TGF-β1 Stimulation on the Secretome of Human Adipose-Derived Mesenchymal Stromal Cells. *Stem Cells Transl Med* **2015,** *4* (8), 894-898 DOI: 10.5966/sctm.2015-0012.

340. Jarad, M.; Kuczynski, E. A.; Morrison, J.; Viloria-Petit, A. M.; Coomber, B. L., Release of endothelial cell associated VEGFR2 during TGF-β modulated angiogenesis in vitro. *BMC Cell Biology* **2017,** *18* (1), 10 DOI: 10.1186/s12860-017-0127-y.

341. Mondal, A.; Ashiq, K. A.; Phulpagar, P.; Singh, D. K.; Shiras, A., Effective Visualization and Easy Tracking of Extracellular Vesicles in Glioma Cells. *Biological Procedures Online* **2019,** *21* (1), 4 DOI: 10.1186/s12575-019-0092-2.

342. Campos, J.; #xe3; Henrique, o.; Soares, R. P.; Ribeiro, K.; Cronemberger Andrade, A.; #xe9; Batista, W. L.; Torrecilhas, A. C., Extracellular Vesicles: Role in Inflammatory Responses and Potential Uses in Vaccination in Cancer and Infectious Diseases %J Journal of Immunology Research. **2015,** *2015*, 14 DOI: 10.1155/2015/832057.

343. Hughes, C. S.; Moggridge, S.; Müller, T.; Sorensen, P. H.; Morin, G. B.; Krijgsveld, J., Single-pot, solid-phase-enhanced sample preparation for proteomics experiments. *Nature Protocols* **2019,** *14* (1), 68-85 DOI: 10.1038/s41596-018-0082-x.

344. Evrard, S. M.; Lecce, L.; Michelis, K. C.; Nomura-Kitabayashi, A.; Pandey, G.; Purushothaman, K. R.; d'Escamard, V.; Li, J. R.; Hadri, L.; Fujitani, K.; Moreno, P. R.; Benard, L.; Rimmele, P.; Cohain, A.; Mecham, B.; Randolph, G. J.; Nabel, E. G.; Hajjar, R.; Fuster, V.; Boehm, M.; Kovacic, J. C., Endothelial to mesenchymal transition is common in atherosclerotic lesions and is associated with plaque instability. *Nature Communications* **2016,** *7* (1), 11853 DOI: 10.1038/ncomms11853.

345. Pastushenko, I.; Blanpain, C., EMT Transition States during Tumor Progression and Metastasis. *Trends Cell Biol* **2019,** *29* (3), 212-226 DOI: 10.1016/j.tcb.2018.12.001.

346. Galindo-Hernandez, O.; Serna-Marquez, N.; Castillo-Sanchez, R.; Salazar, E. P., Extracellular vesicles from MDA-MB-231 breast cancer cells stimulated with linoleic acid promote an EMT-like process in MCF10A cells. *Prostaglandins, Leukotrienes and Essential Fatty Acids* **2014,** *91* (6), 299-310 DOI: https://doi.org/10.1016/j.plefa.2014.09.002.

347. Greening, D. W.; Gopal, S. K.; Mathias, R. A.; Liu, L.; Sheng, J.; Zhu, H.-J.; Simpson, R. J., Emerging roles of exosomes during epithelial–mesenchymal transition and cancer progression. *Seminars in Cell & Developmental Biology* **2015,** *40*, 60-71 DOI: https://doi.org/10.1016/j.semcdb.2015.02.008.

348. Colombo, F.; Norton, E. G.; Cocucci, E., Microscopy approaches to study extracellular vesicles. *Biochimica et Biophysica Acta (BBA) - General Subjects* **2021,** *1865* (4), 129752 DOI: https://doi.org/10.1016/j.bbagen.2020.129752.

349. Ofir-Birin, Y.; Abou karam, P.; Rudik, A.; Giladi, T.; Porat, Z.; Regev-Rudzki, N., Monitoring Extracellular Vesicle Cargo Active Uptake by Imaging Flow Cytometry. **2018,** *9* (1011), DOI: 10.3389/fimmu.2018.01011.

350. Early Detection of Nephrotoxicity In Vitro Using a Transparent Conducting Polymer Device. *Applied In Vitro Toxicology* **2016,** *2* (1), 17-25 DOI: 10.1089/aivt.2015.0028.

351. Ramuz, M.; Hama, A.; Rivnay, J.; Leleux, P.; Owens, R. M., Monitoring of cell layer coverage and differentiation with the organic electrochemical transistor. *Journal of Materials Chemistry B* **2015,** *3* (29), 5971-5977 DOI: 10.1039/C5TB00922G.

352. Ramuz, M.; Margita, K.; Hama, A.; Leleux, P.; Rivnay, J.; Bazin, I.; Owens, R. M., Optimization of a Planar All-Polymer Transistor for Characterization of Barrier Tissue. *ChemPhysChem* **2015,** *16* (6), 1210-1216 DOI: https://doi.org/10.1002/cphc.201402878.

353. Khodagholy, D.; Gurfinkel, M.; Stavrinidou, E.; Leleux, P.; Herve, T.; Sanaur, S.; Malliaras, G. G., High speed and high density organic electrochemical transistor arrays. *Applied Physics Letters* **2011,** *99* (16), 163304 DOI: 10.1063/1.3652912.

354. DeFranco, J. A.; Schmidt, B. S.; Lipson, M.; Malliaras, G. G., Photolithographic patterning of organic electronic materials. *Organic Electronics* **2006,** *7* (1), 22-28 DOI: https://doi.org/10.1016/j.orgel.2005.10.002.

355. Galindo-Hernandez, O.; Gonzales-Vazquez, C.; Cortes-Reynosa, P.; Reyes-Uribe, E.; Chavez-Ocaña, S.; Reyes-Hernandez, O.; Sierra-Martinez, M.; Salazar, E. P., Extracellular vesicles from women with breast cancer promote an epithelial-mesenchymal transition-like process in mammary epithelial cells MCF10A. *Tumour Biol* **2015,** *36* (12), 9649-9659 DOI: 10.1007/s13277-015-3711-9.

356. Stull, M. A.; Pai, V.; Vomachka, A. J.; Marshall, A. M.; Jacob, G. A.; Horseman, N. D., Mammary gland homeostasis employs serotonergic regulation of epithelial tight junctions. *Proceedings of the National Academy of Sciences* **2007,** *104* (42), 16708-16713 DOI: 10.1073/pnas.0708136104.

357. Qu, Y.; Han, B.; Yu, Y.; Yao, W.; Bose, S.; Karlan, B. Y.; Giuliano, A. E.; Cui, X., Evaluation of MCF10A as a Reliable Model for Normal Human Mammary Epithelial Cells. *PLOS ONE* **2015,** *10* (7), e0131285 DOI: 10.1371/journal.pone.0131285.

358. Liu, X.; Yun, F.; Shi, L.; Li, Z. H.; Luo, N. R.; Jia, Y. F., Roles of Signaling Pathways in the Epithelial-Mesenchymal Transition in Cancer. *Asian Pac J Cancer Prev* **2015,** *16* (15), 6201-6 DOI: 10.7314/apjcp.2015.16.15.6201.

359. Xu, J.; Lamouille, S.; Derynck, R., TGF-beta-induced epithelial to mesenchymal transition. *Cell Res* **2009,** *19* (2), 156-72 DOI: 10.1038/cr.2009.5.

360. Vaquero, J.; Guedj, N.; Clapéron, A.; Nguyen Ho-Bouldoires, T. H.; Paradis, V.; Fouassier, L., Epithelial-mesenchymal transition in cholangiocarcinoma: From clinical evidence to regulatory networks. *J Hepatol* **2017,** *66* (2), 424-441 DOI: 10.1016/j.jhep.2016.09.010.

361. Ozawa, M.; Kobayashi, W., Cadherin Cytoplasmic Domains Inhibit the Cell Surface Localization of Endogenous E-Cadherin, Blocking Desmosome and Tight Junction Formation and Inducing Cell Dissociation. *PLOS ONE* **2014,** *9* (8), e105313 DOI: 10.1371/journal.pone.0105313.

362. Kinch, M. S.; Clark, G. J.; Der, C. J.; Burridge, K., Tyrosine phosphorylation regulates the adhesions of ras-transformed breast epithelia. *J Cell Biol* **1995,** *130* (2), 461-71 DOI: 10.1083/jcb.130.2.461.

363. Nakajima, S.; Doi, R.; Toyoda, E.; Tsuji, S.; Wada, M.; Koizumi, M.; Tulachan, S. S.; Ito, D.; Kami, K.; Mori, T.; Kawaguchi, Y.; Fujimoto, K.; Hosotani, R.; Imamura, M., N-Cadherin Expression and Epithelial-Mesenchymal Transition in Pancreatic Carcinoma. *Clinical Cancer Research* **2004,** *10* (12), 4125-4133 DOI: 10.1158/1078-0432.Ccr-0578-03.

364. Skog, J.; Würdinger, T.; van Rijn, S.; Meijer, D. H.; Gainche, L.; Sena-Esteves, M.; Curry, W. T., Jr.; Carter, B. S.; Krichevsky, A. M.; Breakefield, X. O., Glioblastoma microvesicles transport RNA and proteins that promote tumour growth and provide diagnostic biomarkers. *Nat Cell Biol* **2008,** *10* (12), 1470-6 DOI: 10.1038/ncb1800.

365. Ramuz, M.; Hama, A.; Huerta, M.; Rivnay, J.; Leleux, P.; Owens, R. M., Combined Optical and Electronic Sensing of Epithelial Cells Using Planar Organic Transistors. *Advanced Materials* **2014,** *26* (41), 7083-7090 DOI: https://doi.org/10.1002/adma.201401706.

366. Rivnay, J.; Ramuz, M.; Leleux, P.; Hama, A.; Huerta, M.; Owens, R. M., Organic electrochemical transistors for cell-based impedance sensing. *Applied Physics Letters* **2015,** *106* (4), 043301 DOI: 10.1063/1.4906872.

367. Abdouh, M.; Floris, M.; Gao, Z.-H.; Arena, V.; Arena, M.; Arena, G. O., Colorectal cancer-derived extracellular vesicles induce transformation of fibroblasts into colon carcinoma cells. *Journal of Experimental & Clinical Cancer Research* **2019,** *38* (1), 257 DOI: 10.1186/s13046-019-1248-2.

368. Bebelman, M. P.; Janssen, E.; Pegtel, D. M.; Crudden, C., The forces driving cancer extracellular vesicle secretion. *Neoplasia* **2021,** *23* (1), 149-157 DOI: 10.1016/j.neo.2020.11.011.

369. Mittelbrunn, M.; Gutiérrez-Vázquez, C.; Villarroya-Beltri, C.; González, S.; Sánchez-Cabo, F.; González, M. Á.; Bernad, A.; Sánchez-Madrid, F., Unidirectional

transfer of microRNA-loaded exosomes from T cells to antigen-presenting cells. *Nature communications* **2011,** *2*, 282-282 DOI: 10.1038/ncomms1285.

370. Montecalvo, A.; Larregina, A. T.; Shufesky, W. J.; Stolz, D. B.; Sullivan, M. L. G.; Karlsson, J. M.; Baty, C. J.; Gibson, G. A.; Erdos, G.; Wang, Z.; Milosevic, J.; Tkacheva, O. A.; Divito, S. J.; Jordan, R.; Lyons-Weiler, J.; Watkins, S. C.; Morelli, A. E., Mechanism of transfer of functional microRNAs between mouse dendritic cells via exosomes. *Blood* **2012,** *119* (3), 756-766 DOI: 10.1182/blood-2011-02-338004.

371. Garcia-Hernandez, A.; Leal-Orta, E.; Ramirez-Ricardo, J.; Cortes-Reynosa, P.; Thompson-Bonilla, R.; Salazar, E. P., Linoleic acid induces secretion of extracellular vesicles from MDA-MB-231 breast cancer cells that mediate cellular processes involved with angiogenesis in HUVECs. *Prostaglandins & Other Lipid Mediators* **2021,** *153*, 106519 DOI: https://doi.org/10.1016/j.prostaglandins.2020.106519.

372. Zha, Q. B.; Yao, Y. F.; Ren, Z. J.; Li, X. J.; Tang, J. H., Extracellular vesicles: An overview of biogenesis, function, and role in breast cancer. *Tumor Biology* **2017,** *39* (2), 1010428317691182 DOI: 10.1177/1010428317691182.

373. Green, T. M.; Alpaugh, M. L.; Barsky, S. H.; Rappa, G.; Lorico, A., Breast Cancer-Derived Extracellular Vesicles: Characterization and Contribution to the Metastatic Phenotype. *BioMed research international* **2015,** *2015*, 634865-634865 DOI: 10.1155/2015/634865.

374. Namee, N. M.; O'Driscoll, L., Extracellular vesicles and anti-cancer drug resistance. *Biochimica et Biophysica Acta (BBA) - Reviews on Cancer* **2018,** *1870* (2), 123-136 DOI: https://doi.org/10.1016/j.bbcan.2018.07.003.

375. Chen, M.-T.; Sun, H.-F.; Zhao, Y.; Fu, W.-Y.; Yang, L.-P.; Gao, S.-P.; Li, L.-D.; Jiang, H.-l.; Jin, W., Comparison of patterns and prognosis among distant metastatic breast cancer patients by age groups: a SEER population-based analysis. *Sci Rep* **2017,** *7* (1), 9254 DOI: 10.1038/s41598-017-10166-8.

376. Patanaphan, V.; Salazar, O. M.; Risco, R., Breast cancer: metastatic patterns and their prognosis. *South Med J* **1988,** *81* (9), 1109-12.

377. Kennecke, H.; Yerushalmi, R.; Woods, R.; Cheang, M. C. U.; Voduc, D.; Speers, C. H.; Nielsen, T. O.; Gelmon, K., Metastatic Behavior of Breast Cancer Subtypes. *Journal of Clinical Oncology* **2010,** *28* (20), 3271-3277 DOI: 10.1200/jco.2009.25.9820.

378. Jonsson, N.; Gullberg, M.; Israelsson, S.; Lindberg, A. M., A rapid and efficient method for studies of virus interaction at the host cell surface using enteroviruses and real-time PCR. *Virol J* **2009,** *6*, 217-217 DOI: 10.1186/1743-422X-6-217.

379. Camilleri, E. T.; Gustafson, M. P.; Dudakovic, A.; Riester, S. M.; Garces, C. G.; Paradise, C. R.; Takai, H.; Karperien, M.; Cool, S.; Sampen, H.-J. I.; Larson, A. N.; Qu, W.; Smith, J.; Dietz, A. B.; van Wijnen, A. J. J. S. C. R.; Therapy, Identification

and validation of multiple cell surface markers of clinical-grade adipose-derived mesenchymal stromal cells as novel release criteria for good manufacturing practice-compliant production. **2016,** *7* (1), 107 DOI: 10.1186/s13287-016-0370-8.

380. Belting, M., Heparan sulfate proteoglycan as a plasma membrane carrier. *Trends Biochem Sci* **2003,** *28* (3), 145-51 DOI: 10.1016/s0968-0004(03)00031-8.

381. Kreuger , J.; Spillmann , D.; Li , J.-p.; Lindahl , U., Interactions between heparan sulfate and proteins: the concept of specificity. *Journal of Cell Biology* **2006,** *174* (3), 323-327 DOI: 10.1083/jcb.200604035.

382. Christianson, H. C.; Belting, M., Heparan sulfate proteoglycan as a cell-surface endocytosis receptor. *Matrix Biology* **2014,** *35*, 51-55 DOI: https://doi.org/10.1016/j.matbio.2013.10.004.

383. Christianson, H. C.; Svensson, K. J.; van Kuppevelt, T. H.; Li, J.-P.; Belting, M., Cancer cell exosomes depend on cell-surface heparan sulfate proteoglycans for their internalization and functional activity. *Proc Natl Acad Sci U S A* **2013,** *110* (43), 17380-17385 DOI: 10.1073/pnas.1304266110.

384. Atai, N. A.; Balaj, L.; van Veen, H.; Breakefield, X. O.; Jarzyna, P. A.; Van Noorden, C. J. F.; Skog, J.; Maguire, C. A., Heparin blocks transfer of extracellular vesicles between donor and recipient cells. *J Neurooncol* **2013,** *115* (3), 343-351 DOI: 10.1007/s11060-013-1235-y.

385. Chung, C. S.; Hsiao, J. C.; Chang, Y. S.; Chang, W., A27L protein mediates vaccinia virus interaction with cell surface heparan sulfate. *J Virol* **1998,** *72* (2), 1577-85 DOI: 10.1128/jvi.72.2.1577-1585.1998.

386. Clausen, T. M.; Sandoval, D. R.; Spliid, C. B.; Pihl, J.; Perrett, H. R.; Painter, C. D.; Narayanan, A.; Majowicz, S. A.; Kwong, E. M.; McVicar, R. N.; Thacker, B. E.; Glass, C. A.; Yang, Z.; Torres, J. L.; Golden, G. J.; Bartels, P. L.; Porell, R. N.; Garretson, A. F.; Laubach, L.; Feldman, J.; Yin, X.; Pu, Y.; Hauser, B. M.; Caradonna, T. M.; Kellman, B. P.; Martino, C.; Gordts, P. L. S. M.; Chanda, S. K.; Schmidt, A. G.; Godula, K.; Leibel, S. L.; Jose, J.; Corbett, K. D.; Ward, A. B.; Carlin, A. F.; Esko, J. D., SARS-CoV-2 Infection Depends on Cellular Heparan Sulfate and ACE2. *Cell* **2020,** *183* (4), 1043-1057.e15 DOI: https://doi.org/10.1016/j.cell.2020.09.033.

387. Park, I.-S.; Han, M.; Rhie, J.-W.; Kim, S. H.; Jung, Y.; Kim, I. H.; Kim, S.-H., The correlation between human adipose-derived stem cells differentiation and cell adhesion mechanism. *Biomaterials* **2009,** *30* (36), 6835-6843 DOI: https://doi.org/10.1016/j.biomaterials.2009.08.057.

388. Al-Horani, R. A.; Kar, S.; Aliter, K. F., Potential Anti-COVID-19 Therapeutics that Block the Early Stage of the Viral Life Cycle: Structures, Mechanisms, and Clinical Trials. *Int J Mol Sci* **2020,** *21* (15), 5224.

389. Vianello, A.; Del Turco, S.; Babboni, S.; Silvestrini, B.; Ragusa, R.; Caselli, C.; Melani, L.; Fanucci, L.; Basta, G., The Fight against COVID-19 on the Multi-Protease Front and Surroundings: Could an Early Therapeutic Approach with Repositioning Drugs Prevent the Disease Severity? *Biomedicines* **2021,** *9* (7), 710.

390. Purushothaman, A.; Bandari, S. K.; Liu, J.; Mobley, J. A.; Brown, E. E.; Sanderson, R. D., Fibronectin on the Surface of Myeloma Cell-derived Exosomes Mediates Exosome-Cell Interactions. *J Biol Chem* **2016,** *291* (4), 1652-63 DOI: 10.1074/jbc.M115.686295.

391. Aust, L.; Devlin, B.; Foster, S. J.; Halvorsen, Y. D. C.; Hicok, K.; du Laney, T.; Sen, A.; Willingmyre, G. D.; Gimble, J. M., Yield of human adipose-derived adult stem cells from liposuction aspirates. *Cytotherapy* **2004,** *6* (1), 7-14 DOI: https://doi.org/10.1080/14653240310004539.

392. Ceccarelli, S.; Nodale, C.; Vescarelli, E.; Pontecorvi, P.; Manganelli, V.; Casella, G.; Onesti, M. G.; Sorice, M.; Romano, F.; Angeloni, A.; Marchese, C., Neuropilin 1 Mediates Keratinocyte Growth Factor Signaling in Adipose-Derived Stem Cells: Potential Involvement in Adipogenesis. *Stem Cells International* **2018,** *2018*, 1075156 DOI: 10.1155/2018/1075156.

393. Walker, S. J.; Pizzato, M.; Takeuchi, Y.; Devereux, S., Heparin binds to murine leukemia virus and inhibits Env-independent attachment and infection. *Journal of virology* **2002,** *76* (14), 6909-6918 DOI: 10.1128/jvi.76.14.6909-6918.2002.

394. Sento, S.; Sasabe, E.; Yamamoto, T., Application of a Persistent Heparin Treatment Inhibits the Malignant Potential of Oral Squamous Carcinoma Cells Induced by Tumor Cell-Derived Exosomes. *PLOS ONE* **2016,** *11* (2), e0148454 DOI: 10.1371/journal.pone.0148454.

395. Maguire, C. A.; Balaj, L.; Sivaraman, S.; Crommentuijn, M. H.; Ericsson, M.; Mincheva-Nilsson, L.; Baranov, V.; Gianni, D.; Tannous, B. A.; Sena-Esteves, M.; Breakefield, X. O.; Skog, J., Microvesicle-associated AAV vector as a novel gene delivery system. *Mol Ther* **2012,** *20* (5), 960-71 DOI: 10.1038/mt.2011.303.

396. Gurbuz, H. A.; Durukan, A. B.; Sevim, H.; Ergin, E.; Gurpinar, A.; Yorgancioglu, C., Heparin toxicity in cell culture: a critical link in translation of basic science to clinical practice. *Blood Coagul Fibrinolysis* **2013,** *24* (7), 742-5 DOI: 10.1097/MBC.0b013e3283629bbc.

397. Christianson, H. C.; Svensson, K. J.; van Kuppevelt, T. H.; Li, J.-P.; Belting, M., Cancer cell exosomes depend on cell-surface heparan sulfate proteoglycans for their internalization and functional activity. *Proceedings of the National Academy of Sciences* **2013,** *110* (43), 17380-17385 DOI: 10.1073/pnas.1304266110.

398. Mycroft-West, C. J.; Su, D.; Pagani, I.; Rudd, T. R.; Elli, S.; Guimond, S. E.; Miller, G.; Meneghetti, M. C. Z.; Nader, H. B.; Li, Y.; Nunes, Q. M.; Procter, P.; Mancini, N.; Clementi, M.; Forsyth, N. R.; Turnbull, J. E.; Guerrini, M.; Fernig, D.

G.; Vicenzi, E.; Yates, E. A.; Lima, M. A.; Skidmore, M. A., Heparin inhibits cellular invasion by SARS-CoV-2: structural dependence of the interaction of the surface protein (spike) S1 receptor binding domain with heparin. *bioRxiv* **2020**, 2020.04.28.066761 DOI: 10.1101/2020.04.28.066761.